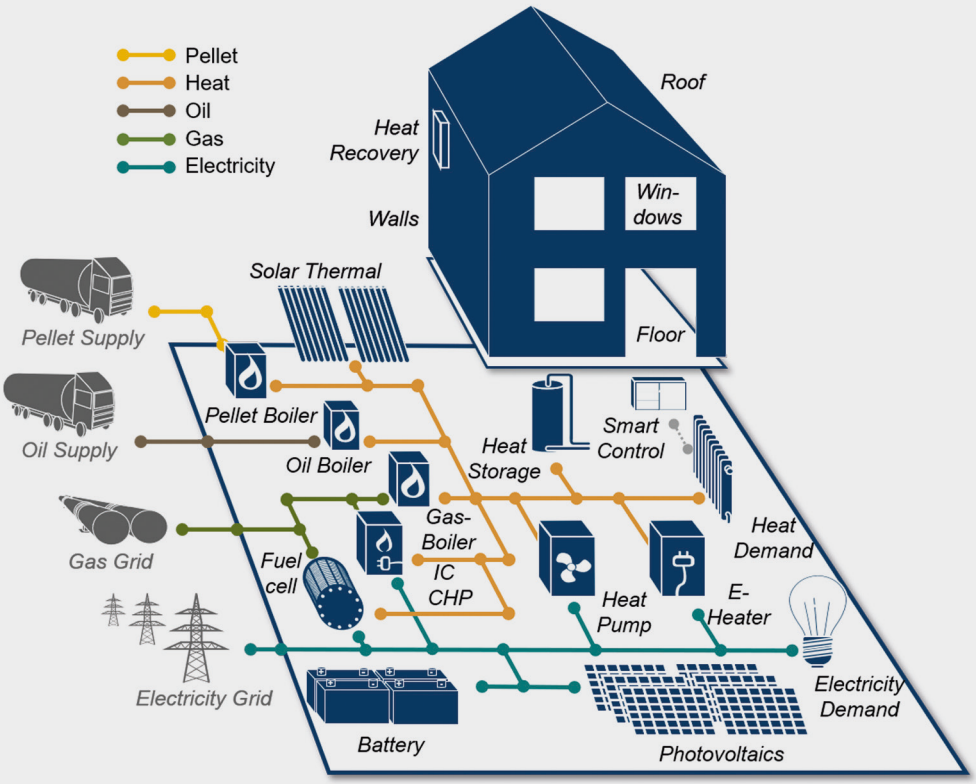

Future Grid Load of the Residential Building Sector

Leander Kotzur

Energie & Umwelt / Energy & Environment
Band / Volume 442
ISBN 978-3-95806-370-9

Mitglied der Helmholtz-Gemeinschaft

JÜLICH
Forschungszentrum

Schriften des Forschungszentrums Jülich
Reihe Energie & Umwelt / Energy & Environment Band / Volume 442

Forschungszentrum Jülich GmbH
Institut für Energie- und Klimaforschung
Elektrochemische Verfahrenstechnik (IEK-3)

Future Grid Load of the Residential Building Sector

Leander Kotzur

Schriften des Forschungszentrums Jülich
Reihe Energie & Umwelt / Energy & Environment Band / Volume 442

ISSN 1866-1793 ISBN 978-3-95806-370-9

Bibliografische Information der Deutschen Nationalbibliothek.
Die Deutsche Nationalbibliothek verzeichnet diese Publikation in der
Deutschen Nationalbibliografie; detaillierte Bibliografische Daten
sind im Internet über http://dnb.d-nb.de abrufbar.

Herausgeber und Vertrieb:	Forschungszentrum Jülich GmbH Zentralbibliothek, Verlag 52425 Jülich Tel.: +49 2461 61-5368 Fax: +49 2461 61-6103 zb-publikation@fz-juelich.de www.fz-juelich.de/zb
Umschlaggestaltung:	Grafische Medien, Forschungszentrum Jülich GmbH
Druck:	Grafische Medien, Forschungszentrum Jülich GmbH
Copyright:	Forschungszentrum Jülich 2018

Schriften des Forschungszentrums Jülich
Reihe Energie & Umwelt / Energy & Environment, Band / Volume 442

D 82 (Diss., RWTH Aachen University, 2018)

ISSN 1866-1793
ISBN 978-3-95806-370-9

Vollständig frei verfügbar über das Publikationsportal des Forschungszentrums Jülich (JuSER)
unter www.fz-juelich.de/zb/openaccess.

Abstract

The installation and operation of distributed energy resources in the form of photovoltaics, co-generation units, or batteries, and the electrification of the heat supply are seen as promising options to reduce greenhouse gas emissions of residential buildings. Nevertheless, their uptake significantly changes the interaction of the residential building stock with the electricity grid and the centralized supply infrastructure and questions their current design. Therefore, the objective of this work is to derive the future residential electricity grid load spatially and temporally resolved to define a decision basis for future grid and market designs.

In order to generally predict the future structure, design and operation of residential supply systems and efficiency measures, a Mixed-Integer Linear Program is introduced that minimizes the total annual energy supply cost of a single buildings since the technology adoption is mainly economically driven. The minimization of the greenhouse gas footprint can be added as second objective. The optimization model accounts for the temporal occupant activities, their related device usage, tolerated room temperature levels, limited roof capacities, or different levels of additional insulation. Since the variety of investment and operation options make the model computationally challenging, clustering based times series aggregation techniques are developed and introduced to reduce the complexity of the model. A novel aggregation algorithm based on Mixed-Integer Quadratic Programs is introduced to scale the technology adoption and operation from the single building perspective to a nationwide scope by creating a spatially resolved archetype building stock from Census data and building databases. 200 archetype buildings are concluded to sufficiently represent the diversity of building types in the different municipalities in Germany.

These archetype buildings are optimized for the weather years 2010 until 2015 and the results are validated to residential energy consumption value from public statistics, whereby the regional demand impact of different weather years is illustrated. Afterwards, a scenario frame for 2050 is defined and the buildings are optimized to reach a carbon neutral building stock with minimal cost. As result, at least 130 GW of photovoltaic are deployed and above 90 TWh/a of the generated electricity are used for self-consumption in the residential buildings. Nevertheless, the total demand for electricity significantly increases since 17 to 26 GW_{el} of heat pumps are installed to replace combustion boilers, while only 30 % of space heat are saved by refurbishment measures. The spatially resolved archetype building stock allows new insights: The urban areas can compensate the increasing electricity demand by efficient co-generation units, e.g. in form of fuel cells. Nevertheless, those are not cost efficient in the rural areas where the photovoltaic generation and the heat pump demand temporally disjoin, resulting in a doubling of the peak electricity load in the winter hours.

Kurzfassung

Zur Erreichung der Treibhausgasreduktionsziele im Haushaltssektor muss signifikant die Energieversorgungsstruktur der Wohngebäude verändert werden. Neben Einsparmaßnamen wird dabei vermehrt auf dezentrale Versorgungslösungen wie KWK-Anlagen, Photovoltaik und Batteriespeichersysteme zu Eigenversorgung gesetzt. Des Weiteren werden klassische Kessel durch Wärmepumpen ersetzt, welche im Rahmen der Sektorkopplung Raumwärme mit Hilfe erneuerbaren Stroms bereitstellen können. Dieser Wandel der Gebäudeversorgungsstruktur verändert signifikant die netzseitige Last der Wohngebäude und die Nachfrage nach zentraler Versorgungstechnologie. Daher ist das Ziel dieser Arbeit, die zukünftige Last der Wohngebäude zeitlich und räumlich aufgelöst abzuschätzen, um eine Grundlage für zukünftige Netzplanungen zu schaffen.

Dazu wird ein neues Bottom-Up Modell entwickelt, welches als Gemischt-Ganzzahliges Lineares Optimierungsprogramm konzipiert ist. Das Modell optimiert die Struktur und den Betrieb der Energieversorgung und den Einsatz möglicher Effizienzmaßnahmen einzelner Wohngebäude unter der Prämisse von Kosteneffizienz. Als weitere Zielfunktion kann die Minimierung der Treibhausgasemissionen hinzugefügt werden. Das Modell berücksichtigt das zeitliche Verhalten der Bewohner, die Benutzung von elektrischen Geräten, dynamische Temperaturtoleranzen in den Wohnräumen, limitierte Dachflächen für Solarinstallationen, sowie verschiedene Sanierungstiefen der jeweiligen Gebäudehüllen. Die große Anzahl an Entscheidungsvariablen und deren Interaktion machen das Modell rechenintensiv, weshalb Methoden zur Zeitreihenaggregation eingeführt werden, um die Komplexität des Modells zu reduzieren. Um die Ergebnisse der Einzelgebäude auf eine nationale Perspektive hoch zu skalieren, wird ein Aggregationsalgorithmus eingeführt, der mit Hilfe von quadratischen Optimierungen Typgebäude aus Zensusdaten und vorhanden Gebäudedatenbanken erstellt. Insgesamt ist festzustellen, dass 200 Typgebäude in der Lage sind die Vielfalt des Gebäudebestandes in Deutschland auf Gemeindeebene darzustellen.

Die Typgebäude werden mit dem Optimierungsmodell zunächst für die Jahre 2010 bis 2015 optimiert und die resultierende Endenergienachfrage wird mit den berichteten aggregierten Energienachfragen der Bundesregierung validiert. Zur Bestimmung der zukünftigen Last wird ein Szenario-Rahmen für den Wohngebäudesektor im Jahr 2050 definiert und ein kostenminimaler und klimaneutraler Gebäudebestand berechnet. Dabei werden über 130 GW Aufdach-Photovoltaik installiert, welche primär zum Eigenverbrauch von 90 TWh/a Photovoltaik-Strom innerhalb der Gebäude genutzt werden. Die absolute Stromnachfrage der Wohngebäude steigt signifikant an, da 17 bis 26 GW an elektrischer Wärmepumpenleistung installiert und betrieben werden. Sanierungsmaßnamen und Neubauten führen nur zu 30 % Einsparung bei der Raumwärme. Die räumliche Auflösung des Gebäudebestandes zeigt, dass die urbanen Gebiete die steigende Stromnachfrage durch effiziente KWK-Anlagen in Form von Brennstoffzellen kompensieren können. Diese sind jedoch nicht kosteneffizient in ländlichen Regionen. Dort fallen die Erzeugung des Photovoltaik-Stroms und die zusätzliche Stromnachfrage der Wärmepumpen zeitlich auseinander, sodass sich die Spitzennachfrage des Netzstroms im Winter verdoppelt.

Acknowledgement

Sincere, I am very grateful to Univ.-Prof. Dr.-Ing. Detlef Stolten for the initialization and supervision of this thesis. You gave me already during my recruitment interview the encouragement that I can succeed. Further, I am thankful that you provided me the freedom for developing new ideas while always focusing me on the final goal of my thesis. Moreover, I want to thank you for all the commenting in the last stage of my thesis and your patience regarding my poor English.

Further, I am thankful to Univ.-Prof. Dr.-Ing. Hermann-Josef Wagner for the co-supervision of this thesis. Your critical assessment and valuable feedback during the final stage of the thesis let me to the relevant conclusions.

I am thankful to Univ.-Prof. Dr.-Ing. Dr. rer. pol. habil. Michael Lauster for being the chairperson of the examination committee.

I want to thank Dr.-Ing. Martin Robinius as head of the Process and Systems Analysis department for keeping me motivated during the whole period of my thesis. You know what the right combination of pushing and caring is. You let grow my creativity without letting me loosen into it.

Dr.-Ing. Peter Markewitz, I want to thank you as head of the Stationary Energy Systems group for all the valuable input, the diverse feedback, and that you always had an open door regarding scientific and personal problems. You had a calming effect on me in times of high stress, and I was always aware that I could count on you when something got out of hand.

Further, I want to thank the persons I shared my office and the majority of my working time with: Especially, I want to mention Markus Reuß for the creative input in any time, and that you always brought my chaotic mind down-to-earth. Konstantinos Syranidis, I think your qualities as listener in combination with your sharp mind are unique. Severin Ryberg, I cannot imagine that it exist a person more helpful regarding IT-problems than you. Your input and the help with the workstations in the final stage of my thesis had a significant impact on the quality of my results. Lara Welder, I want to thank you for all the great conversations about the mathematical description of energy system models and your critical opinion, I always felt understood from you. Dilara Caglayan, I relied on your feedback, you enlightened every working day as my desk neighbor, and I will miss the spontaneous dance sessions in the office with you.

Further, I want to thank the whole Process and Systems Analysis Department for supporting me. It was a pleasure to work with Dr.-Ing. Thomas Grube, Dr.-Ing. Peter Stenzel, Dr.-Ing. Jochen Linßen, Dr.-Ing. Heidi Heinrichs, Dr. Patrick Kuckertz and Dr. Dr. Li Zhao. Further, I want to highlight the joy I had with my doctoral colleagues Yuan Wang, Peter Lopion, Timo Kannengießer, Simonas Cerniauskas and Philipp Heuser. The high level of collaboration was helpful and created a productive environment. Moreover, I want to thank all colleagues at the IEK-3, while I want to point out Anne Schroeders, Anke Clemens, Madita Kaul, Susanne Klatt, Wilma Fladung, Ann-Kathrin Steinke and Sandra Hoffmann. You were my stronghold against bureaucracy. Further, I want to acknowledge the support of Stefan Beer and Christopher Wood. Cheng Feng, Nils Becker, Nicolas Meerts and Fritz Röben, all your ground work helped me to finalize my thesis.

Gratitude is further owed to my colleagues at the Lawrence Berkeley National Lab who made my time in the bay area an unforgettable experience. I want to point out Gonçalo Ferreira Cardoso, the discussions with you about representative buildings were a key input for my thesis. Rahul Chopra, thank you for the organization of my visit. Miguel Heleno, I want to thank you for your vast feedback. Thomas Brouhard, I miss to crawl through the swimming pool with you under the Californian evening sun. Marie-Louise Arlt, thanks for your valuable feedback and the great debates about the benefits and drawbacks of competition in research. Holger Teichgräber, I enjoyed our discussions about time series aggregation and I want to thank you for the introduction to the research community in Stanford.

Last, I want to thank everyone who accompanied me also in my private life. Especially, I want to thank my family, Stefan Kotzur, Andrea Jarosch-Kotzur, Malte Kotzur, and Alexandra Kotzur, for your unconditional love, support, and counsel.

I devote this thesis to my grandfather Dr.-Ing. Joachim Kotzur who died on 15 June 2018.

Contents

List of Figures

List of Tables

Conventions

Throughout this thesis following conventions are used.

Proper names are italic.

EXPLANATION:
Informal excurses of a model or definition.

Formula conventions

The whole thesis is written in American English.

Nomenclature

General abbreviations

AB	Apartment Building
CAPEX	CAPital EXpenditure
CHP	Combined Heat and Power
COP	Coefficient of Performance
CRF	Capital Recovery Factor
DER	Distributed Energy Resources
ELP	Electric Load Profile
G	Terraced House
GHG	Greenhouse Gas
IC	Internal Combustion
LB	Lower Bound
LP	Linear Program
MFH	Multi-Family House
MILP	Mixed-Integer Linear Program
MINLP	Mixed-Integer Nonlinear Program
MPC	Model Predictive Control
MPP	Maximal Power Point
OPEX	OPerational EXpenditure
PE	Primary Energy
QIP	Quadratic Integer Program
QP	Quadratic Program
RMSE	Root Mean Squared Error
SFH	Single-Family House

SLP	Standard Load Profile
TH	Terraced House
UB	Upper Bound
WACC	Weighted Average Cost of Capital

Single Building Optimization - Variables and parameters

Δt	Duration of a single time step [h]
δ	Existence of a technology [-]
$\dot{E}$	Energy flow [kW]
$\dot{Q}$	Heat flow [kW]
η	Efficiency or quality grade [-]
γ	Greenhouse gas footprint [kg/kWh]
τ	Economic lifetime [a]
D	Scaling of a technology [kW(h)]
P	Power flow [kW]
SOC	State of charge [kWh]
T	Temperature [K]
x	Relative occupancy activity [-]

Single Building Optimization - Indices and abbreviations

ϵ	Energy or commodity type
λ	Discrete temperature level
amb	Ambient
com	Comfort
d	Index of the a general device or component
el	Electric
f	Index of the Transformer class
$inter$	Between typical periods
$intra$	Inside a typical period
L	Set of technology connections
n	Index of the Collector class
nom	Nominal
q	Index of the Source/Sink class
ret	Return

s	Index of the Storage class
sle	Sleeping
sup	Supply
t	Index of the discrete time step
th	Thermal
vac	Vacant

Archetype Building Aggregation - Variables and parameters

β	Archetype building occurrence
δ	Activator if archetype building has attribute expression
μ	Continuous attribute of the archetype building
ϕ	Fit function of the continuous attributes
d	Distribution of discrete attribute expressions
e	Prediction error between the data and their representation by archetype buildings
w	Weighting factor for a building attribute
y	Continuous attribute expressions of the node

Archetype Building Aggregation - Indices and abbreviations

b	Archetype building index
c	Continuous attribute index
m	Discrete attribute expressions
n	Node or municipality index
p	Categorical attribute index

Chapter 1

Introduction

1.1 Motivation and objective

In 2015, the residential building sector was directly emitting 10 % of the Greenhouse Gases (GHG) in Germany by the combustion of fossil fuels. Further, it was responsible for 12 % of the emissions due to the GHG footprint of its energy imports [AGEB, 2017; rwi, 2017; BMWi, 2016]. Those emissions need to be cut in order to reach the overall goal of net zero GHG emissions in the second half of this century [UN, 2015] and to minimize the impact of anthropogenic climate change [Solomon et al., 2009]. Therefore, the German federal government defined a target for a near GHG neutral building stock: The primary energy consumption of the heat demand in buildings shall be reduced 80 % from 2008 to 2050 [BRD, 2010]. The European Union introduced the concept of "Zero Energy Buildings" (ZEB) in the context of its energy performance of buildings directive [EU, 2010, 2012] with the goal to deploy GHG neutral buildings that compensate for their emissions by exporting on-site generated renewable energy [REHVA, 2011; Marszal et al., 2011].

While the objectives are clear, the optimal pathway to a GHG neutral building stock is uncertain: Every year new materials, methods and processes are invented which allow for future technological solutions that are from today's perspective not imaginable. Nevertheless, the majority of the technologies are not mature and it is uncertain how they will be integrated in a future energy system. This uncertainty unsettles utility providers [OCallaghan et al., 2014; Agnew and Dargusch, 2015] as well as governments [Rickerson et al., 2014]. Therefore, analyses are needed that are able to extrapolate from today's reality into the future, to predict technology development, their system integration and their cost distribution. They can lay the basis for decision makers to design incentives and markets to achieve a robust and

predictable transformation to a GHG neutral building stock.

Today's predictions for the building sector [McKenna et al., 2013; BMWi, 2015; Diefenbach et al., 2016; Beuth, 2017; BMWi, 2018] mainly focus on GHG reduction strategies for the heat demand. They conclude that significant energy saving potentials shall be accessed by increased refurbishment rates and the residual heat shall be supplied with renewable energy.

Nevertheless, in the realm of sector coupling [Robinius et al., 2017], the heat demand of the building sector cannot be regarded as any more isolated from the other energy system: Heat pumps are seen as a key option to efficiently provide space heat [IWES, 2015; UBA, 2017a]; and Combined Heat and Power (CHP) generation allows an efficient usage of the chemical energy carriers while providing flexibility to the grid [Lund et al., 2012]. Further, a trend towards an increased self-supply of residential buildings is recognizable: The rapidly falling prices of photovoltaics [ISE, 2015] and batteries [Nykvist and Nilsson, 2015] constitute the *grid parity* [Breyer and Gerlach, 2013], meaning that the levelized cost of self-generated electricity is below the retail electricity grid price.

Both trends, the changing heat supply and the increasing self-sufficiency of the buildings, will significantly change the future electricity grid load of the buildings and question the feasibility of the current grid infrastructure.

Therefore, new analysis are required that consider the adoption and operation of new supply technologies and efficiency measures spatially and temporally differentiated with the objective to locally evaluate the impact of the energy supply to the grid infrastructure. Thereby, they need to account for cost optimality, since the main motivations of building owners to adopt different supply technologies are savings or earnings from their installation [Balcombe et al., 2014]. This counts as well for efficiency measures or energy retrofits where the necessity of replacement or the financial profitability are the main activators for the adoption [Achtnicht and Madlener, 2014]. Although the assumption of sole financially optimal decision makers, referred to as *homo economicus*, underestimates social and attitudinal components influencing the technology adoption, it predicts well the rate of adoption and cumulative adoption [Robinson and Rai, 2015].

1.2 Structure

Consequently, the following questions shall be answered in this thesis:

1. What is the cost optimal combination of refurbishment and adoption of supply technologies for different residential buildings to achieve a carbon neutral building stock?
2. How can self-consumption contribute to this?
3. How does the changing supply structure temporally impact the electricity load?
4. What are regional differences in the technology adoption and the grid load?

Therefore, this work introduces a new model that predicts the cost optimal deployment and operation of energy assets for residential buildings in a high temporal and spatial resolution. Figure 1.1 embodies the basic idea and structure of this work.

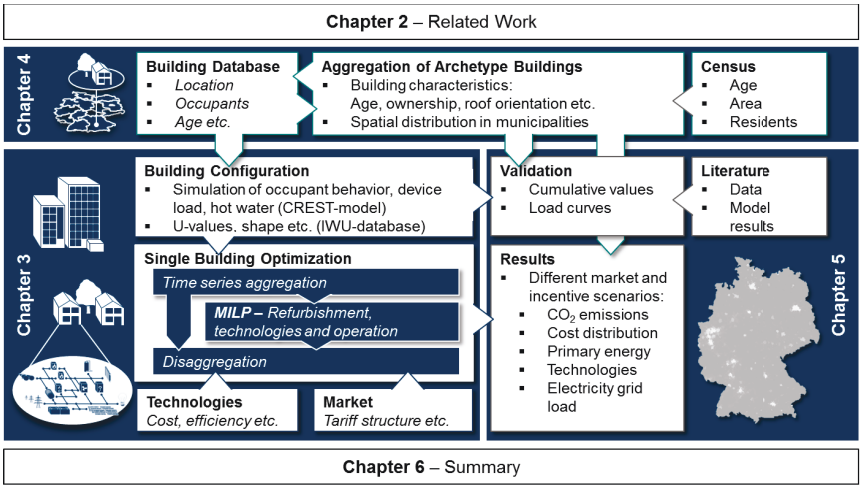

Figure 1.1: Overall workflow of the approach in the thesis and the different Chapters describing it.

Other analyses and models related to this work are discussed in Chapter 2. The discussion is separated into three categories: GHG reduction strategies for the residential building stock, potential assessment of self-sufficient residential energy supply, and cost optimal design of energy supply systems.

Based on this, a new optimization model for the residential energy supply is developed in Chapter 3. It accounts, e.g., for the temporal occupant behavior, their related device usage, tolerated room temperature levels, limited roof capacities or varying insulation materials. New times series aggregation methods are developed

and introduced to reduce the complexity of the model, since the variety of investment and operation options make it computationally challenging.

Chapter 4 introduces a novel aggregation algorithm to create a spatially resolved representative archetype building stock based on Census data. The relevant building parameters are introduced for Germany on the municipality level. The resulting stock is then extended with the construction and demolition of buildings to predict its development into the future.

In Chapter 5, first the model chain is validated, by optimizing the aggregated archetype buildings for the years 2010 until 2015 and comparing the resulting energy consumption with public available values. Afterwards, it is optimized for a scenario in 2050. Thereby, the cost optimal supply systems for the diversity of residential buildings are determined. Those are then adapted in different pathways to reach a GHG neutral building stock. The resulting change of the grid load is derived, discussed and compared to other literature.

Chapter 6 summarizes the results and draws the main conclusion.

Chapter 2

Related work

This chapter discusses existing research related to the environmental, technical and economical evaluation of residential buildings. It is structured as follows: Section 2.1 discusses the models and results of existing strategies for carbon dioxide reduction of the German residential building stock. Afterwards, research related to the trend towards self-sufficient energy supply of residential buildings are analyzed in Section 2.1. Section 2.3 examines existing models to determine cost optimal energy supply systems with the focus on buildings. The chapter closes with a discussion and summary of the related works in Section 2.4 and Section 2.5.

2.1 Strategies for greenhouse gas emission reduction

The residential sector was responsible for 26 % of the overall final energy consumption in Germany in 2015 with around 639 TWh/a (631 TWh/a [DESTATIS, 2017]; 636 TWh/a [rwi, 2017]; 639 TWh/a [AGEB, 2017]]. The majority of the energy was used for space heating with 483 TWh/a and hot water with 93 TWh/a. Other relevant demands are process heat, e.g., for cooking or washing with 38 TWh/a, refrigeration with 29 TWh/a and information and communication technology with 22 TWh/a. The demand for lighting and mechanical energy plays a tangential role with 10.75 and 4.6 TWh/a [rwi, 2017].

This demand structure also constitutes the GHG emissions caused by the residential building stock, as seen in Figure 2.1. The direct GHG emissions are generated by the burning of fossil gas or oil to meet the demand for space heating and hot water. The direct emissions due to process heating, e.g. by gas stoves, are negli-

gible. The majority of the residential GHG emissions are indirect emissions due to the district heating supply or imported electricity.

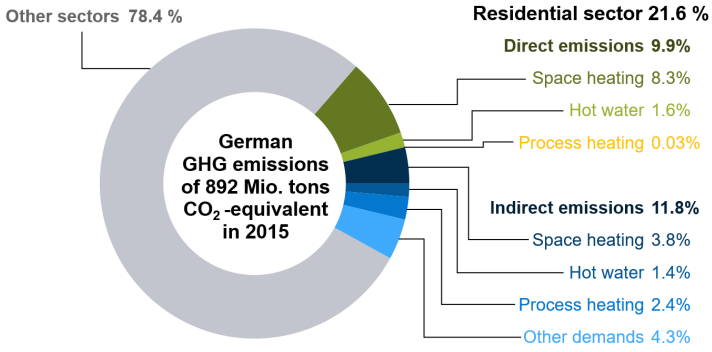

Figure 2.1: Share of the direct and indirect residential GHG emissions in 2015 of the total emissions in Germany. It includes the GHG footprint of the electricity imported from the grid, as well as the GHG emissions in the supply chains of gas or oil. The calculations are based on the data of [AGEB, 2017; rwi, 2017; BMWi, 2016].

In order to reduce these GHG emissions, different models have been proposed to develop strategies for the emission reduction or focusing on efficiency measures to reduce the final energy consumption. A general overview of such models can be found in Martinez Soto and Jentsch [2016], wherefore this section only presents the models and results relevant for Germany. The works are categorized to models considering only the building stock, and models that optimize all sectors and consider the building stock as part of it.

Sole building stock models

McKenna et al. [2013] proposed a framework to predict the development of the building stock and its related energy demand to 2050. The stock modeling dynamically considers demolition, construction, renovation rates and renovation depth as reduction indicators. A spatial separation of the stock development between old and new federal states is considered. The change of the energy demand of the buildings is statistically extrapolated from the historical development of the specific

residential final energy demand per living area. The results reveal that the historic refurbishment rate of 1 % has to be increased to 2 % to meet the primary energy demand reduction targets of 80 % from 2008 to 2050 by the German federal government.

In 2015, the *Federal Ministry for Economic Affairs and Energy (BMWi)* published an efficiency strategy for the whole German building stock, including buildings of the service and industry sectors [BMWi, 2015], developed by *Prognos* and *ifeu - Institut für Energie- und Umweltforschung Heidelberg*. The strategy mainly focuses on the heat supply of the buildings and defines a corridor between *efficiency* measures and the *renewable* share of the remaining energy supply to achieve an 80 % reduction target of the primary energy consumption from 2008 to 2050. The reduction of the final energy consumption is thereby in a range of 36 % to 54 % and the share of renewable energy supply between 57 % and 69 %. Heat pumps play a secondary role in both scenarios. Instead, biomass is considered as the main resource to provide renewable energy. The energy provided by district heating is decreasing in both scenarios. A cost analysis shows that the *efficiency* scenario results in higher costs for living and energy, although a higher biomass price is considered in the *renewable* scenario, caused by a higher demand. The interaction with the remaining energy system by sector coupling is only qualitatively discussed.

Diefenbach et al. [2016] introduced an analytical approach to determine strategies for reaching GHG emission targets in Germany for 2050, depending on the replacement rates of supply technologies and renovation rates of residential buildings. The building database behind this is from the *Institut für Wohnen und Umwelt (IWU)* [IWU, 2010]. Similar to McKenna et al. [2013], they find that an increase of the building renovation rate to at least 2 % is required to reach the GHG emission saving targets of 80 % to 95 % for 2050. The final energy demand for space heating will decrease from 567 TWh/a in 2009 to a value between 338 TWh/a to 363 TWh/a in 2050, depending on the time needed for increasing the renovation rate from 1 % to 2 %. Additionally, all newly installed heat supply systems need to be heat pumps, CHP units, biomass and solar systems after 2025, and no gas and oil boilers are allowed anymore. The basic scenario predicts a share of heat pumps of 59 % at the final heat supply in 2050. Natural gas boilers contribute only to 13 % of the heat supply and the remaining heat is provided by CHP units and district heating.

A techno-economic analysis of the future residential building stock is also performed by Sterchele et al. [2016]. They divide the residential building stock into nine archetype buildings derived from the *IWU* building database [IWU, 2010]. Those buildings are categorized by the age and the type of the buildings, e.g. single-family houses and multi-family houses. Further, Sterchele et al. [2016] consider four different renovation depths of such and rely on the different heat transfer coefficients, insulation thickness and building components. Stationary calculations are used to

evaluate building performance based on the *DIN V 18599* DIN [2016], which includes efficiency measures as well as the environmental evaluation of supply technologies. Although they consider historical refurbishment measures, the validation of the model with the final energy consumption for 2011 shows an overestimation of around 30 %. They conclude that this is constituted by the gap between the calculated demand of the standard and the real consumption behavior, which cannot be properly considered in a stationary calculation. Different future scenarios are defined for the building stock resulting in reductions of the final energy demand between 42 % and 73 % and reductions of the GHG emissions of 62 % to 82 %. No economic evaluation is performed for the aggregated building stock, which makes the numerous scenarios difficult to compare.

LOGIT MODEL:
A *logit* model is used to estimate the probability of a discrete or categorical output, e.g. buying a heat pump or a gas boiler, by a set of predictor variables, e.g. heat demand and supply temperature.

In 2018, the BMWi presented a set of scenarios for all sectors developed by the *Frauenhofer ISI*, *Consentenc GmbH* and the *ifeu* [BMWi, 2018]. While many different scenarios were developed, the review here focuses on the residential sector in the *Base* scenario. The technology adoption is modeled with the *Invert* tool developed at the Energy Economics Group in Vienna [Stadler et al., 2007; Kranzl et al., 2013; Müller, 2015]. It is a bottom-up model considering the evolution of a building stock and a technology adoption according to a nested logit model and the lifetime of the technologies. The model has a high degree of detail for the building technology adoption, but it is decoupled from the optimization of the overall energy system. Therefore, renovation rates are, e.g., extrinsically determined and steadily increase up to 3 % in 2050 for the *Base* scenario and result in a reduction of the final energy consumption of 58 % for space heating and hot water over all sectors. The largest share of heat still gets provided by natural gas. The demand for household appliances, lighting and refrigeration is separately modeled with the *FORECAST-residential* model from the *Frauenhofer ISI* [ISI, 2018] and is also based on a technology adoption considered with a logit model and probabilistic technology lifetimes. The base scenario predicts here a reduction of the residential electricity demand of 27 % from 2010 until 2050, mainly caused by the replacement with more efficient appliances.

Cross-sectoral optimization models

A collaboration between the *Fraunhofer IWES*, *Frauenhofer IBP* and the *ifeu* analyzed the future interaction between the renewable energies and the heat and trans-

port sector [IWES, 2015]. Therefore, they use a temporally resolved single node model for Germany, optimizing the energy supply for electricity, heat and transport. Although a building stock model is included, the reduction of the final energy demand for residential space heating is extrinsically reduced from 509 TWh/a in 2008 to 245.5 TWh/a in 2050. The results show that the remaining heat gets mainly supplied by heat pumps with 53 %, a large share by district heating with 24 % based on large-scale CHP and heat pumps, and 22 % by biomass. No fossil energy carrier is used anymore for residential heating since their usage is more cost efficient in the industry and mobility sectors. The study emphasizes the necessity for the reduction of the supply temperatures of the heating sector in order to improve the related heat pump performance.

A collaboration of the *Umweltbundesamt UBA* and the *Frauenhofer ISE* [UBA, 2017a] regularly publishes a strategy for a carbon neutral German building stock, including buildings of the residential and the service sectors. The building archetypes are also defined according to IWU [2010] and adapted with regional Census data [Bundesamt, 2011]. The stock model is integrated into the temporally resolved energy system optimization model REMod-D [Henning and Palzer, 2014; Palzer and Henning, 2014]. The reference scenarios define three different measure levels for the heating supply with a reduction of the final energy demand of 35 % to 60% resulting in GHG emission reductions of 82-84%. The remaining heat is supplied by a high share of heat pumps since chemical energy carriers, such as natural gas or biomass, are used more cost efficiently in the other energy sectors. An optimization of the whole model with renovation measures as unconstrained optimization variables leads to a sole reduction of final energy consumption for heating of the building stock by 24 % from 2008 to 2050. Instead, higher capacities of renewable energy are installed and lead to a cheaper overall energy system for the 80 % GHG reduction target. Still, an open question is how to reach 95 % GHG reduction or even a fully carbon neutral building sector, as the title of the report indicates.

While this is only an extraction of studies considering GHG reduction strategies of the building stock, it gives an overview of the considered solution space between energy savings and the change of the heat supply structure. The latter is dominated by a switch to heat pumps that can significantly impact the electricity grid load.

Further, the sole building stock models mainly focus on demand reduction and alternative energy supply carriers, but reduction targets can also be achieved by an energy export of the buildings according to the definition of nZEB [EU, 2009; REHVA, 2011] that compensates for their energy demand. Nevertheless, this is mainly possible by an electrical grid feed-in.

2.2 Grid impact of residential buildings and self-consumption

Besides the electrification of the heat supply, the electrical supply of residential buildings is dominated by a trend towards self-sufficient energy supply systems. In general it means the generation of electricity inside the building and the local consumption while only excess energy is exported to the grid. The desire of building owners to increase self-consumption is only minorly influenced by environmental goals. Instead, cost minimization is the main motivation to increase self-consumption [Balcombe et al., 2014]. The steady price drop of photovoltaic panels [ISE, 2015; IRENA, 2016] has the consequence that the levelized cost for electricity of on-roof photovoltaics (e.g., 23.9 ct/kWh in Germany 2016 [Lahnaoui et al., 2017]) are nowadays lower than the retail electricity prices for households in many countries (28.7 ct/kWh in Germany 2016 [Lahnaoui et al., 2017]), constituting the so-called *grid parity* [Breyer and Gerlach, 2013], which benefits the self-consumption of the produced electricity [Luthander et al., 2015; IEA, 2015].

This self-consumption can even be increased by the installation of batteries [Ratnam et al., 2015], which also had a significant price drop in recent years with learning rates between 12 to 16 % [Nykvist and Nilsson, 2015; Schmidt et al., 2017]. This results in a highly volatile market that ranges from prices above 2000 Euro/kWh to 530 Euro/kWh for residential battery systems, as seen in the Appendix A.3.2. Nevertheless, different studies [Khalilpour and Vassallo, 2015; Bracke et al., 2016; Vieira et al., 2017] show that sole photovoltaic battery systems are not economically feasible to reach an uninterrupted self-sufficient residential building supply. Therefore, a demand gap will remain that has to be supplied by the central energy systems. This gap is difficult to predict on an aggregated level since the uptake of the photovoltaic battery systems is expected to depend on the design of the electricity prices for residential buildings [Deutsch and Graichen, 2015; May and Neuhoff, 2016; Parag and Sovacool, 2016; Rickerson et al., 2014].

Therefore, different approaches exist for the model-based prediction of the uptake and impact of photovoltaic battery systems.

In 2014, the *Institut der deutschen Wirtschaft Köln (IW)* published together with the *Energiewirtschaftliches Institut an der Universität zu Köln (EWI)* a report [IW, 2014] about self-consumption of the residential sector, the industry sector, the service sector and the mobility sector. Besides photovoltaic battery systems, they also consider CHP systems together with heat storage systems. An assessment of the historic self-consumption rates indicates that it mainly existed in industry in the past and was negligible for the residential sector. They introduce a cost optimization model for the defined technologies and different actor types to predict the

potential for self-consumption under different market conditions in the future. The results show that the economic potential for residential self-consumption is around 115.6 TWh/a, if no levies or taxes are considered for self-consumption. The major part of the self-generated electricity gets provided by CHP units. This potential gets reduced to 0 TWh/a if all existing levies in Germany are considered for the self-consumed electricity.

Agora published in 2016 an article that derives the potential for photovoltaic storage systems in Germany [Prognos, 2016]. They define different archetypes for single and two family buildings, agriculture and food trade buildings. Based on those, they define different potential installation cases of photovoltaic and battery capacities. Self-consumption for heating appliances such as heat pumps is considered as well. Almost all considered cases are predicted to become economically feasible in the coming years due to the fast price reductions of photovoltaics and batteries. The analysis concludes that the economic potential for self-consumption is at 38.7 TWh/a in the considered residential buildings in 2035. 18.3 TWh/a of the energy is used for new heat applications such as heat pumps or warm water, indicating that self-generation can probably compensate for the increasing electricity demand for heating applications.

Schill et al. [2017] analyzed the macroeconomic effects of self-consumption by coupling different operation strategies of residential photovoltaic battery systems with the central electricity market model *DIETER* for the year 2035. 15 GWs of photovoltaic were assumed to be operated together with battery storage systems to reach self-sufficiency rates for single households between 40 % and 70 %. The total national energy systems cost increased for high self-sufficiency rates since redundant storage capacities are installed that are not necessarily required. A market-oriented operation of the batteries can reduce this, but is not able to fully compensate for the additional investment cost in the considered scenario.

Klingler [2017] developed a market diffusion model for photovoltaic battery systems respecting different consumer preferences and individual electricity consumption. The model is based on a techno-economic evaluation of the photovoltaic battery system and individual utility functions for their adoption. As such, an accumulated adoption of 760 thousand small scale photovoltaic battery systems is predicted until 2030 with a moderate battery capacity of 2 GWh. Nevertheless, the results indicate that at this time only the innovators and early adopters have installed photovoltaic battery systems while the majority and laggards would adopt the systems in the late 2030s and 2040s, which would substantially expand the overall potential until 2050. Klingler [2017] also points out that the model is highly sensitive to the assumed electricity and technology prices.

NUTS:
The abbreviation stands for the French *Nomenclature des Unités Territoriales Statistiques* and describes a geocode for subdivision of countries. While NUTS-0 starts with national states, higher levels disaggregate into subregions. For the case of Germany, NUTS-1 describes the 16 federal states, NUTS-2 a division into 39 Regions, and NUTS-3 the administrative boundaries of the 401 *Landkreise*. Higher levels of disaggregation are described by the *Local Administrative Unit (LAU)*, while LAU-2 represents the municipalities in Germany.

At the end of 2016, the *Frauenhofer ISI* published a report for the network development plan that predicts the spatial and temporal change of the electricity load in Germany until 2035 [ISI, 2016]. The *FORECAST*-model was used, which predicts the national energy demand for the residential, the service, the industry and the transport sectors. Based on those, the load is top-down distributed to NUTS-3 level based on, e.g., number of households or available income. The spatially resolved annual energy demand is validated with data from the transmission grid operators and is able to show a numerical fit of 90 %. Different scenarios for the penetration rate of heat pumps, electric vehicles and battery storage systems are defined until 2030. The scenarios show a small load reduction in a range of -6.7 % to 0 % from 2013 until 2030 since efficiency measures overcompensate for the additional electricity consumers. Still, the peak load is increasing in the winter evening hours, although system oriented load management is considered but not able to completely compensate for the additional demands. The outlook of the report concludes that a further load reduction would be expected until 2050 due to socio-structural development but the increasing demand of heat pumps and electric mobility dominates, wherefore an increase of the total electricity demand from 523 TWh/a in 2013 to 570 TWh/a in 2050 is expected. The results of the report are difficult to retrace, since no documentation of the data, e.g. behind the 2050 case, exists.

2.3 Optimal design of energy supply systems

Energy retrofits and self-consumption are mainly motivated by financial profitability [Balcombe et al., 2014; Achtnicht and Madlener, 2014]. Therefore, the following section analyzes models to determine cost optimal energy supply systems. Although this work focuses on residential building systems, the literature review here targets spatially and temporally resolved energy system design models in general, since related methods or approaches can be transferred. Passages of this section are based on two articles [Kotzur et al., 2018a,b] that were published in conjunction with this thesis.

In general, the determination of residential energy systems with minimal environmental and economical impact is a highly complex task: Energy supply and demand must be balanced in time, in space, and in energy form, and the increasing number of generation, storage, and load management and reduction options leads to extremely large solution spaces where identifying optimality in technology options, placement, sizing and operation can be daunting. The analytical solving of those optimization problems may not be feasible and requires instead the use of mathematical programs to identify the optimal solution [Baños et al., 2011].

Although Moore's Law held for most of the last few decades [Schaller, 1997], the computational tractability of these mathematical programs remains substantially limited [Leyffer et al., 2016]. The size of the input data directly influences the size of the related optimization problem, and with it the requirement for processing resources. The integration of renewable energy expands this challenge because the proper modeling of these technologies is only possible with increased resolution of the temporal framework [Poncelet et al., 2014; Stenzel et al., 2016; Pfenninger, 2017].

Therefore, a trade-off between the different complexities has to be made, as illustrated in Figure 2.2.

The scope and spatial resolution determines the **System Size**, which can be described by the scale of the overall technology network. It can either be influenced by the spatial resolution resulting in a high number of nodes [Samsatli and Samsatli, 2015; Samsatli et al., 2016; Pfenninger, 2017; Welder et al., 2017], or the dimensions of a single node regarding the different technology types and sectors [Palzer and Henning, 2014; Henning and Palzer, 2014], e.g. technical solutions for heating, cooling, electricity and chemical processes in a single node. To achieve these large-scale systems designs, primarily *Linear Programs (LP)* are used [Pfenninger, 2017; Schlachtberger et al., 2018], or *Mixed-Integer Linear Programs (MILP)* with a small amount of binary or integer variables [Mehleri et al., 2013; Harb et al., 2015; Samsatli and Samsatli, 2015; Samsatli et al., 2016; Kwon et al., 2016; Mashayekh et al., 2017; Welder et al., 2017].

The other factor directly affecting the scale and computational load of an optimization problem is the number of **Time Steps**, also sometimes referred to as time slices or snapshots. First, its cardinality is determined by the temporal resolution, e.g. if sub-minutely [Beck et al., 2016], sub-hourly [Appen et al., 2015; Lauinger et al., 2016], or hourly intervals are considered. Second, the observation periods can range from a number of typical days to time series over whole decades [Pfenninger, 2017]. The modeling of a hierarchical order of time grids [Yoza et al., 2014; Samsatli and Samsatli, 2015; Renaldi and Friedrich, 2017; Kotzur et al., 2018b] gains popularity since it allows the modeling of long observation periods without

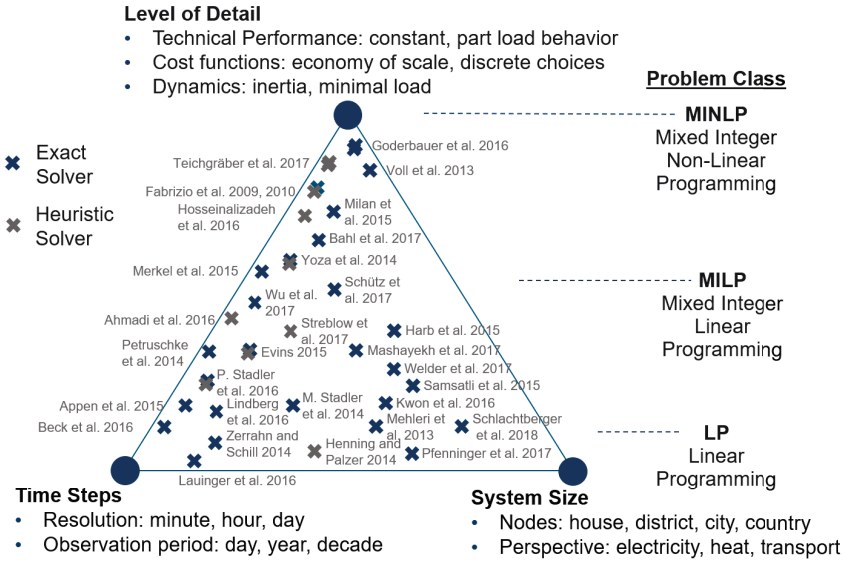

Figure 2.2: Illustration of the complexity dimensions, problem classes, and solving approaches in energy system design models and a qualitative classification of the selected models in the reviewed literature.

losing the information of short term time series fluctuations. The usage of time series aggregation can systematically reduce the temporal scale in advance and is analyzed in more detail in Kotzur et al. [2018a].

The overall allowable system scale is lately limited by the **Level of Detail** of the techno-economic models. Nonlinear performance functions, e.g. the part load efficiency of a fuel cell, determine a non-convex set of operation states, and with it a non-convex optimization problem, most often resulting in *Mixed-Integer Nonlinear Programs (MINLP)*. Although different approaches try to simplify them with piecewise linear operation states or iterative procedures incorporating discrete states [Goderbauer et al., 2016; Milan et al., 2015; Schütz et al., 2017b], this problem class is still computationally heavy, wherefore it can only be analyzed for small scale systems or small temporal observation periods. Minimal part load constraints can be defined with binary variables [Merkel et al., 2015], which is computationally tractable for hourly time series in a year, but also defines an additional binary variable for every technology and time step. Nevertheless, e.g., simple ramping constraints can be implemented continuously and linearly and do not significantly affect the computational load.

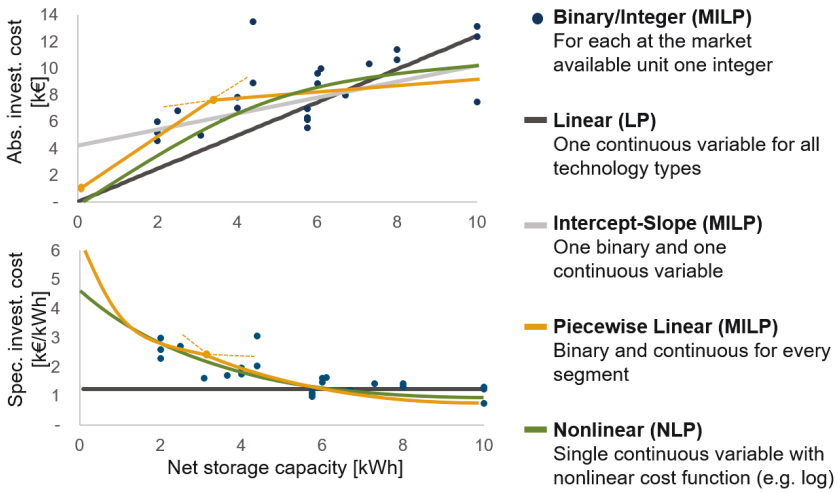

Figure 2.3: Comparison of different approaches to model the cost of certain technologies for the example of a residential battery.

Additional to the operational constraints of the systems, the choice and scaling of the technologies are challenging, as illustrated in Figure 2.3. The exact choice of technology units that are available on the market, including their related prices, would introduce many single binary or integer variables [Voll et al., 2013; Petruschke et al., 2014; Goderbauer et al., 2016; Bahl et al., 2017]. This is computationally challenging but closest to reality. National or global energy systems models do not require this degree of detail since they rely analytically on an abstract perspective of the system and model often the technology scaling with a continuous linear cost function [Henning and Palzer, 2014; Zerrahn and Schill, 2015; Ram et al., 2017; Schlachtberger et al., 2018]. Nevertheless, the consideration of, e.g., learning effects in macroeconomic models determines nonlinear cost curves, which have to be approximated with other approaches [Heuberger et al., 2017]. For the design of microgrids or building supply systems, it is common to approximate the technology cost with a cost share related to their existence (*Intercept*) and constant cost share related to their scale (*Slope*) [Stadler et al., 2014; Evins, 2015; Lindberg et al., 2016a; Stadler et al., 2016; Streblow and Ansorge, 2017] resulting in a MILP. The choice of efficiency measures, e.g. in the building envelope, are most often single binary variables [Stadler et al., 2014; Streblow and Ansorge, 2017; Schütz et al., 2017a; Wu et al., 2017]. While the Intercept-Slope approach is a good trade-off between complexity and accuracy, it still has high estimation errors for larger ranges of the technology scale. E.g., CHP units have a strong economy of

scale that state nonlinear cost functions. The exact modeling of such concave cost function would result for the case of cost minimization in a non-convex optimization problem. Therefore, global optimizer or non-exact metaheuristic approaches are required [Fabrizio et al., 2009]. Alternatively, piecewise linear approximations are popular [Milan et al., 2015; Merkel et al., 2015; Gabrielli et al., 2017; Elsido et al., 2017], which generate more binary variables but provide a sufficient degree of accuracy.

EXACT AND METAHEURISTIC SOLVER:
Exact solvers are an algorithm class that is able to *exactly* determine the global optimum for a given mathematical problem, or at least provide a solution with a measure indicating the theoretically maximal distance of it to the global optimum. *Metaheuristic* solvers are algorithms that search the solution space by a defined procedure to find sufficiently good solutions, often including stochastic sub-processes. They do not need as holistic information about the solutions space as exact solvers, but they cannot provide a measure of the global quality of the solution. Still, for combinatorial mathematical problems they can often provide good solutions with small computational effort.

While all these complexities limit the energy system models, different options for complexity reduction exist and gain popularity: Spatial aggregation can reduce the number of nodes in an energy system network [Mancarella, 2014], systematically simplifying the technology models by avoiding nonlinearities or discontinuities and the related non-convexity of the program Geidl and Andersson [2007]; Milan et al. [2015]. Temporal aggregation can reduce the cardinality of the input time steps and create typical periods representing the original input time series [Kotzur et al., 2018a,b].

The review of the models shows further that optimization problems solved with metaheuristics often rely on an operation simulation [Henning and Palzer, 2014; Ahmadi and Abdi, 2016; Hosseinalizadeh et al., 2016; Streblow and Ansorge, 2017] or an operation optimization [Stadler et al., 2016; Evins, 2015; Teichgräber et al., 2017] underneath, as illustrated in Figure 2.4. A reason is that heuristic solvers perform poorly with the scale of the overall problem size, wherefore it is preferred that only the technology structure and scale are chosen by the solver. The second reason is that simulation models are often developed first and it is decided as a second step to use the models for the purpose of a system design. For this purpose, heuristic solvers are advantageous since they can rely on a black-box system model.

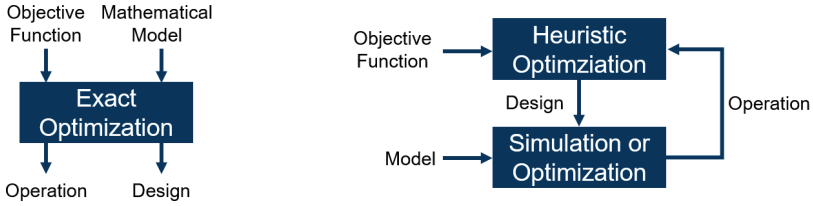

Figure 2.4: Comparison of optmization approaches for the design of energy systems.

2.4 Discussion

Different research areas related to this work were reviewed, ranging from GHG reduction strategies to the cost optimal energy system design. This section compares them and derives the open research gaps.

High renovation rate vs. cost optimality: The modeling of GHG reduction strategies for buildings is most often done with top-down models focusing on the energy demand for heating. Although a certain building stock is considered, it is extrinsically defined what measures are required to reach the reduction targets. Therefore, the majority of the studies concludes that an increase of the renovation rate from 1 % to at least 2 %, or even up to 3 %, is required to reach the GHG reduction targets in 2050, while reducing the final energy demand for heating in a broad range of 35 % to 73 %. Nevertheless, an unconstrained cross-sectoral optimization [UBA, 2017a] showed that smaller renovation rates are more cost efficient, resulting in an optimal final energy demand reduction for heating of 24 %. A similar tendency can be derived by the comparison of the two scenarios by BMWi [2015], where the costs of the *renewable energy* scenario were below the costs of the *efficiency* scenario.

Heat pumps or chemical energy carriers: The majority of the studies and scenarios expects that heat pumps will have the biggest share in the heat supply. Especially, the cross-sectoral optimization studies [IWES, 2015; UBA, 2017a] highlight that remaining chemical energy carriers, either fossil or synthetically produced, are more efficiently used in the industry and mobility sectors. Only the two studies commissioned by the BMWi consider that either biomass [BMWi, 2015] or natural gas [BMWi, 2018] has the biggest share. These contradictory predictions are partly determined by the different modeling approaches: Due to levies, electricity prices for end consumers are magnitudes higher than renewable generation costs, wherefore a bottom-up technology adoption model [Müller, 2015] avoids the instal-

lation of heat pumps and remains with gas boilers, although it is not optimal from a macroeconomic perspective [IWES, 2015; UBA, 2017a].

Self-consumption is sensitive to market design: Different studies try to predict the potential for self-consumption especially for photovoltaic battery systems. Nevertheless, the bottom-up models [IW, 2014; Prognos, 2016; Klingler, 2017] showed that it is highly dependent on the market design, e.g. if levies and taxes are considered for self-consumption or not. Depending on such, the potential for electric self-consumption in the residential sector ranges from 0 TWh/a to 115.6 TWh/a, including self-generation with CHP units [IW, 2014]. The upper bound would almost cover the whole residential electricity demand of 128 TWh/a in 2015. All in all, this makes the roll-out of highly self-sufficient supply systems a political decision.

Macroeconomic effects of self-consumption are diverse: Although self-consumption might be profitable from a building owner's perspective, it is open what type of self-consumption is cost optimal from a macro perspective. E.g., Schill et al. [2017] showed that redundant storage technologies increase the total system cost. Nevertheless, studies such as *The cellular Approach* [VDE, 2015] point out that decentralized produced electricity should also be decentrally consumed in order to achieve a robust system design. All in all, a compromise has to be determined regarding additional cost, robustness and acceptance of the resulting system.

Potential of Power-to-Heat for self-consumption: Only one study showed that a high potential for self-consumption especially exists for space and water heating [Prognos, 2016]. It covered almost 50 % of the overall potential for self-consumption. Nevertheless, the heat model was coarse and the whole of the residential building stock was not considered. It raises the question, how big the overall potential of self-consumption for heat pumps and electric heaters is; and if it will replace the demand for solar thermal. E.g., only the passive storage capacities of the German building stock are expected to have a storage capacity of 200 GWh [Kohlhepp and Hagenmeyer, 2017].

Bottom-up modeling more accurate than top-down: Bottom-up models are more popular for the self-consumption rate than top-down models, since it is mainly economically driven and can only be sufficiently evaluated with a temporally resolved model for single buildings. A comparison of models for GHG reduction strategies for heating in residential buildings showed additionally that bottom-up models are more accurate and less sensitive to the input variables [Martinez Soto and Jentsch, 2016]. Nevertheless, they are also more challenging in terms of parametrization. No bottom-up model was found that holistically considers cost optimal investment decisions into renovation measures together with an update of heat supply and decentral generation technologies for self-consumption from a building owner's perspective, although reinforcing effects of the different measures

are expected.

Variety of cost optimality models: In order to find good models for the cost optimal investment behavior into building energy supply systems and refurbishment measures, an analysis of existing decision models related to this topic was conducted. A variety of models exists already, a limited set of models includes renovation measures together with the supply system optimization [Stadler et al., 2014; Evins, 2015; Wu et al., 2017; Schütz et al., 2017a]. Further, a model that additionally incorporates the passive storage capacity of the buildings together with the constraining behavior of the occupants was not found. The identification of this gap is supported by the literature review of Bloess et al. [2018].

Cost optimal design is computationally challenging: The analysis of existing models revealed the computational limitations of mathematical programs for optimal energy system design. Since the majority of the reviewed models are just applied for a limited set of example buildings or application cases, computational inefficiencies are secondary. Nevertheless, for the purpose of a bottom-up model, computationally efficient programs are required because they need to be applied to many different building types in different locations. Therefore, a building optimization model would be needed that has a good compromise between computational load and accuracy.

Spatial resolution only rarely considered: The minority of the reviewed studies considered a spatial distribution of the building stock, although this would help to evaluate the future grid impact of self-consumption and the electrification of the heat demand. Only the study by ISI [2016] considers spatial effects in the uptake of heat pumps and battery technologies. Nevertheless, it is extrinsically prescribed and the technology operation centrally managed. This refers to a top-down model and constitutes high uncertainties in the input parameters, such as the heat demand [Martinez Soto and Jentsch, 2016].

In summary, it can be stated that a lack of bottom-up analyses exists that consider the cost optimal technology adoption of single building owners holistically, including supply and demand of heat and electricity together. Many models exist already for the cost optimal design and operation of such systems for single buildings, but do not allow the evaluation for a whole building stock. Nevertheless, this type of bottom-up approach is required to evaluate sufficiently the cross-sectoral effects of self-consumption together with the future residential heat demand and heat supply structure, since their combination and enforcing effects will determine together the final shape of the residential electricity demand. Therefore, this work aims at closing this gap.

2.5 Summary

This chapter introduced and discussed related works and studies to the energy demand and technology adoption of the residential building stock.

Section 2.1 discussed the models and results of existing strategies for carbon dioxide reduction of residential buildings in Germany. Mainly two options span a corridor of reduction strategies: Either the share of renewable energy in the residential energy supply has to be substantially raised or the renovation rate of the buildings has to increase from today's 1 % per year to a value between 2 % to 3 % to meet the German primary energy reduction target of 80 % from 2008 to 2050. Some studies indicated that the first strategy is more cost efficient, but the reference scenarios of the federal government consider the second strategy. Further, the review of cross-sectoral models revealed that the building stock should even reach higher goals since the remaining chemical energy carriers in the year 2050 are more cost efficiently used in the industry and mobility sectors.

Further, studies analyzing the trend towards self-sufficiency of residential buildings were reviewed in Section 2.2. It was revealed that the economic potential of self-sufficiency is mainly determined by the market design around the residential consumer. Hence, it is a political decision if a high share of self-sufficiency will arise. A big potential for self-consumption is expected for Power-to-Heat, but no study holistically evaluated its potential for the residential building stock.

In Section 2.3, existing models to determine cost optimal energy supply systems were compared. The conclusion could be drawn that already many models for the optimal design of single buildings exist. Nevertheless, their high computational load makes them not applicable to a whole building stock.

An integrated discussion of the reviewed literature was done in Section 2.4. Only one model was found that analyzes spatially and temporally resolved the load change due to a future technology adoption, but the adoption rates are extrinsically set and a centralized technology operation was considered. It was affirmed that no work exists that considers the cost optimal technology adoption and operation of single residential building owners bottom-up, simultaneously regarding the supply and demand for heat and electricity. Nevertheless, this is required in order to holistically evaluate the most cost efficient pathways to a GHG neutral building stock.

Chapter 3

Optimal residential energy supply

The following chapter introduces an optimization model that generically determines the cost optimal design and operation of energy supply and refurbishment measures in residential buildings. A flowchart of the whole model is illustrated in Figure 3.1. The shown numbers refer to the sections explaining the sub-models.

Section 3.1 introduces a profile generator that predicts the behavior of occupants in the building and derives the electricity load from appliances in the households, e.g. lights or stoves. The resulting profiles set the boundary conditions for the thermal comfort and electricity demand that has to be provided in a temporal resolution. Section 3.2 describes the thermal building model, which respects the optional refurbishment measures as well as the internal storage capacity of the building. The optimization framework is introduced in Section 3.3. It creates the superstructure of supply technology options for the building, while its generic formulation is adapted such that different supply temperatures of the heating system can be considered. Section 3.4 shows the integration of time series aggregation into the optimization model in order to keep it computationally tractable. The chapter closes with a discussion of the advantages and limitations of the whole building model in Section 3.5 and a summary in Section 3.6.

3.1 Residential electricity load

Residential electricity demand profiles for different buildings are required as a basis to predict the electricity load supplied by the grid and the building integrated supply technologies. In order to find sufficient profiles, Section 3.1.1 discusses the

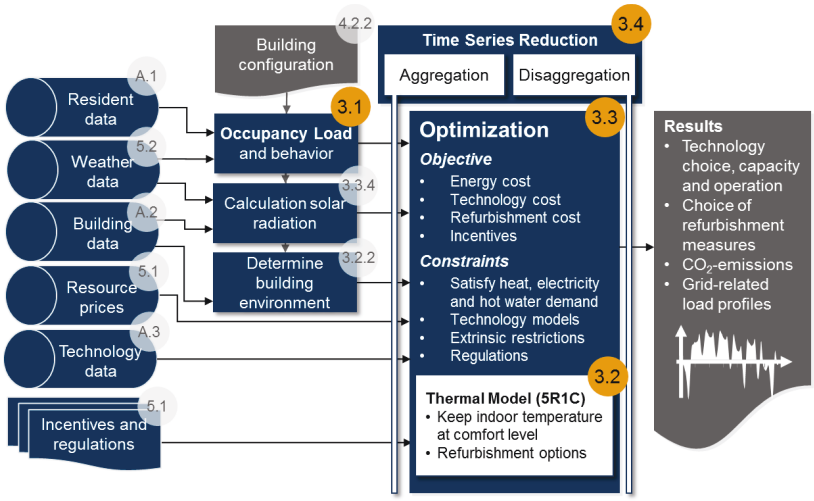

Figure 3.1: Work flow and structure of the single building optimization. The numbers in the *orange* bubbles refer to the related section numbers in this chapter. The *gray* bubbles relate to additional databases, parameters and submodels which are introduced in the appendix or the scenario definitions.

requirements of such for this work and analyzes the suitability of existing load models. Based on the discussion, a model is chosen and its new implementation and adaption to fit the scope of this work are shown in Section 3.1.2. Section 3.1.3 validates the resulting model.

3.1.1 Existing electricity load models

Since many different reference profiles or profile generators exist in the literature, first the requirements of the profiles for this work are defined to evaluate the suitability of the approaches:

- The shape and variance of the profiles on different temporal and spatial aggregation scales have to be correctly covered. They impact highly the prediction of self-consumption [Linssen et al., 2015; Stenzel et al., 2016; Beck et al., 2016] and with it the optimal investment and operation behavior, e.g. of battery storage systems [Ratnam et al., 2015].

- It should consist of different appliance loads in order to evaluate appliance-specific efficiency measures as well as demand side management potentials.

- Consistent profiles of the related occupancy behavior are needed to parametrize the heat load optimization later introduced, e.g. to respect internal heat gains or occupancy dependent thermostats.

- The load generator should be computationally efficient in order to calculate many different profiles for an increasing number of households.

Reference profiles

Probably the load profile most often considered is the Standard Load Profile - H0 [BDEW, 2011], which is a representative 15-min resolved electricity load for the residential sector. It consists of representative days differentiating between weekdays, Saturdays and Sundays, as well as winter, summer and transitional periods. An annual profile is created by chaining these days for a specific year and scaling them by a seasonal correction factor. The drawback of the resulting profile is that it does not cover the variance of a single household and makes it only suitable for an analysis of aggregated groups of households.

The VDI 4655 [VDI, 2008] introduces representative load profiles of single and multi-family houses for electricity, water and heating. It is based on measured load data with a 1-minute or 15-minute resolution that is aggregated to the most representative daily load shapes for weekday and weekend days and adapted to specific climate conditions. Although the load profiles are representative for a single building, they are not useful for describing the aggregated load of a whole building stock since the statistical balancing of fluctuating peak loads between different houses cannot be covered with a single profile.

A large residential load profile database is provided by Tjaden et al. [2015]. It consists of 74 electricity load profiles of residential buildings on a 1-second resolution for a whole year. The data set is synthetically generated based on two measured load data sets on different time resolutions. It is able to represent the load fluctuation for a single household on a high temporal resolution, as well as the fluctuation for a small district up to 74 buildings. Nevertheless, the devices laying behind the load and the related occupancy behavior is unknown. Therefore it is not suitable for this work. Still, it is especially useful for the validation of modeled load profiles.

Profile generators

Besides some exceptions [Paatero and Lund, 2006; Stokes, 2005], the majority of the reviewed bottom-up profile generators are based on the idea of a probabilistic occupant behavior model of which the appliance usage and their related loads are derived. The advantage of the probabilistic approach is that it creates good profiles for single buildings as well as for whole districts or building stocks.

An early approach of such a model was proposed by [Capasso et al., 1994], which derives the single occupancy behavior from a probability function with a Monte Carlo simulation. The motivation to develop the model is to extract the demand-side-management potential of the residential sector in Italy. Although the approach seems promising, the data behind it and the programmatic implementation are not available.

Two similar approaches were published by Widén and Wäckelgård [2010] and Richardson et al. [2010][Richardson et al., 2009, 2008]. They use a model that simulates first the activity of occupants with a Markov chain. The related transition probabilities are derived from time-of-use surveys, once for Sweden and once for Britain. The advantage of the model from [Richardson et al., 2010] is that its Excel-VBA implementation is open-source available as *CREST Demand Model* [CREST, 2017] and it has been further enhanced by McKenna and Thomson [2016] to incorporate hot water and heat demand besides the electricity load.

MARKOV CHAIN:
A Markov chain, named after the mathematician Andrei A. Markov, is ”a stochastic model describing a sequence of possible events in which the probability of each event depends only on the state attained in the previous event.” Source: https://en.oxforddictionaries.com/

An advanced profile generator for Germany was developed by Fischer et al. [2015], named *synPRO*. It is able to respect different household sizes as well as certain occupancy classes. It also generates stochastical occupancy behavior based on a time-of-use survey of Germany. Although the content-related suitability for this work is high, it is commercially distributed and the source code not publicly available, making it not applicable for this work.

The most sophisticated profile generator was developed by Pflugradt [2016]. It simulates the behavior based on the desire of the occupants and derives therefrom the load of the used appliances. It is able to generate profiles for occupants differing by, e.g., age, sex, sick days per year and their related differing desires. Yet, the degree of detail required to parametrize single households exceeds the scope of this work.

Additionally, its implementation as a *Windows* program makes it difficult to transfer it to different environments, such as *Linux*-based high performance computers.

All in all, the *CREST* [CREST, 2017] load generator is evaluated here as the most suitable since it has a high temporal resolution, differs between a variety of appliances and respects the stochastic load smoothing effects between different households. Further, it is available as open-source software, well-documented and provides a sufficient differentiation of the households by the number of occupants.

3.1.2 Extension of the *CREST* model

The overall idea of the *CREST* model developed by Richardson et al. [2010] can be summarized as follows: First, the model simulates the activity of the occupants in the household based on a Markov chain, either if they are active or not active. In case they are active, the generator determines what activity is performed based on a probability distribution, e.g. for cooking. Following on these specific activities, the use of the household owned appliance is triggered and their electrical load derived. The main inputs to the model are the probabilities of ownership of the different appliances, their electricity load, time-of-use surveys of the residents and weather data.

The evolution of the *CREST* load model by McKenna and Thomson [2016] is not required for this work since it mainly extends loads of the heating devices. Though the operation of the heating can be optimized and does not determine a strict final demand, such as e.g. the operation of a television. Therefore, this work incorporates instead a heat model integrated into the optimization model, introduced in Section 3.2.

The model received the following modifications and extensions to make it usable for this thesis:

- The Excel-implementation is replaced by an object-oriented Python module - *enerload* - in order to reach an automated workflow that is able to generically create load profiles [Becker, 2016].
- The occupancy model by Richardson et al. [2010] had a two-state activity approach (active/not active). Since the heat model also needs states like ”not active, but at home, e.g. sleeping” to provide thermal comfort, the four-state occupancy model from McKenna et al. [2015] is implemented.
- The model should be used for many different building types and household

combinations. Therefore, it is parallelized to produce annual time series for many different households at the same time [Röben, 2017].

- The original light load model was mainly based on light bulbs. Nevertheless, the EC Regulation No. 244/2009 [EU, 2009] banned those. The impact can already be identified in the change of the load profile. Therefore, the light model has been updated to a distribution of bulbs, halogen lamps and LED lamps, based on the values of UBA [2017a].
- The hot water demand can be extracted as an independent load profile in order to also supply it by other options than electric boilers.
- The model by Richardson et al. [2010] was not able to sufficiently cover the seasonal variations of the electricity load. Therefore, a correction factor has been introduced that varies the load depending on the position of the day in the year. Its derivation and description are found in A.1.2.

The model provides occupancy data on a 10-minute resolution and appliance load data on a 1-minute resolution. Since this level of detail would burst the optimization framework, the load profiles are downsampled either to a 15-minute or 60-minute resolution. In order to avoid smoothing effects due to averaging of the profiles [Stenzel et al., 2016][Kotzur et al., 2018a], the downsampling is done by choosing every N-th value instead of the average value.

The final workflow, including the sub-models, can be seen in Figure 3.2. On the left side are the considered databases listed. They are used to parametrize *n* different *Electrical Load Profile* (*ELP*) objects. A single ELP consists of an *Occupancy* object, an *Appliance* object and a *Light* object. The results of the *Occupancy* object define thereby the input to the *Appliance* and *Light* object. The different objects are given together to a manager module that simulates different *ELP* objects in parallel and collects, aggregates and downsamples the resulting load profiles.

3.1.3 Validation and parametrization

The resulting load model is validated by comparing it to the *Standard Load Profile (SLP)* for households [BDEW, 2011] as the most prominent representative profile in Germany. The second validation set is the residential measurement based building data from Tjaden et al. [2015], created at the *Hochschule für Technik und Wirtschaft Berlin (HTW)*.

In order to validate the profile generator, 1000 profiles for the year 2010 were created while the different household sizes were chosen such that they fit the overall

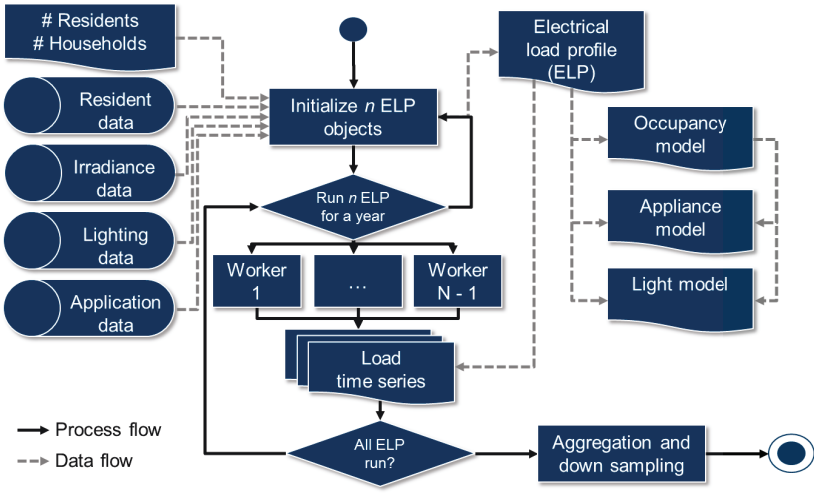

Figure 3.2: Workflow and structure of the *enerload* module, which is used to create the aggregated, annual profiles for *n* different households.

distribution of the household sizes in Germany, shown in Table 3.1. Based on those, an aggregated profile is created, which is scaled to the average annual demand of a single household of 3515 kWh per year in 2010 [BDEW, 2014]. This is done as well with the SLP and the aggregated profile based on the measured 74 data sets. The resulting profiles can be seen for three example days in Figure 3.3. The overall appliance loads are grouped into certain categories, such that the load share of the different appliance groups can be identified. Hot water and heating are here included in the profile since they are also included in the validation profiles. Nevertheless, for the later stock optimization, they are excluded and scaled separately since they are flexible and covered by the heat supply side.

Table 3.1: Distribution of household sizes in Germany based on the Census [Bundesamt, 2011].

Persons per household	**1**	**2**	**3**	**4**	**≥5**
Number in 1000	13961	12456	5455	3906	1793

A qualitative observation shows that the model is able to cover the main daily variation patterns appearing in the SLP and the average HTW profile. A systematic over- or underestimation at certain time periods is not recognizable. This is also

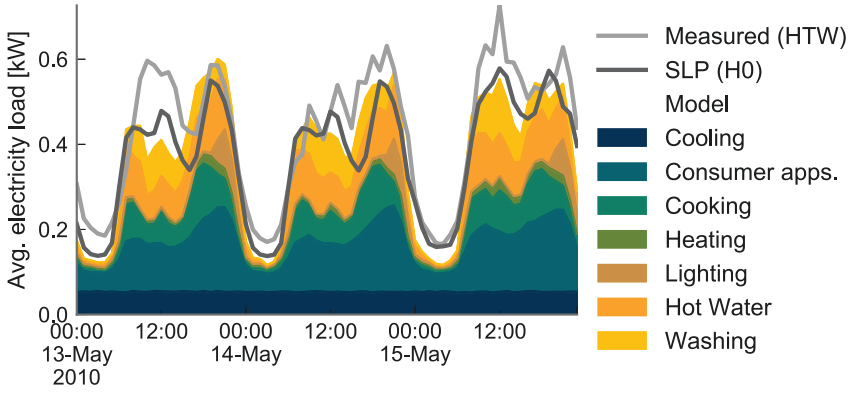

Figure 3.3: Example extraction of three days for the profile generated by 1000 runs of the load model, in comparison to the Standard Load Profile and an average profile of 74 measured residential buildings.

constituted by the integration of more efficient light bulbs since the model showed an overestimation of the cumulative electricity load in the evening hours with the original bulb loads. The numerical analysis supports the accuracy of the model: The Root-Mean-Squared-Error (RMSE) between the model and the SLP amounts to 7.06 %, between the model and the measured data 8.54 %, and between the measured data and the SLP 8.15 %. The distribution of the deviation between the three profiles can be found in A.1.3. Since the deviations of the model to the two validation profiles are in the same magnitude as the deviation between the two validation profiles themselves, it is concluded that the model describes the shape of the electricity load profiles on an aggregated level sufficiently.

An advantage of the load generator to the simple consideration of SLP or the measured data is that appliance loads or type loads can be identified: The load determined by cooling devices, e.g. a refrigerator, aggregates to a base load that is almost constant for the observation period. The consumer appliances, such as television, have a constant load share due to standby activities and a daily variation related to the occupancy activity, peaking in the evening. Electricity loads related to cooking, hot water, and washing are highly correlated to the activity patterns of the occupants and drop almost to zero at night. The lighting load peaks in the evening hours, apart from a small base load during the day.

Since the appliance data set is still based on statistics in Britain, the resulting load share of each device group is validated with German statistical data [BDEW, 2013].

The comparison is shown in Figure 3.4. Since it is not clearly defined which exact appliance is related to which group, the evaluation can only be qualitatively executed. A part of the electricity load in the statistical data is related to other loads (e.g., wellness, garden, etc.), which are not represented by the considered load generator. Instead, the model has a small share of electric heater loads, which are not present in the BDEW data, and a higher share of consumer applications. While washing and lighting have almost a perfect fit, the load required for cooling is a little bit higher in the statistical data (16.7% to 14.0%). A further deviation exists in the electricity required for hot water and cooking where the model based on the UK data has a higher share in the overall load. An explanation for this could be that in Germany a higher share of those are covered by gas boilers instead of electric heaters.

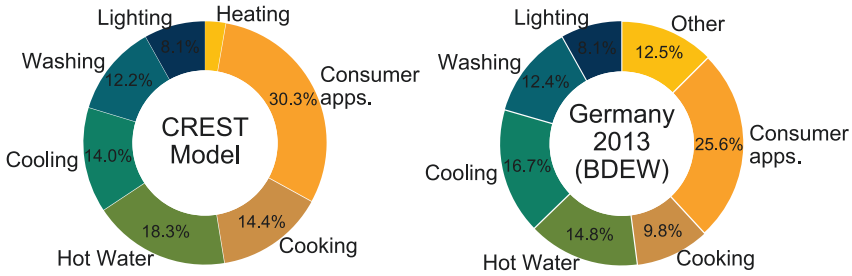

Figure 3.4: The distribution of the electrical device consumption of the considered load model for 1000 runs, in comparison to the distribution of the device consumption of households in Germany, 2013 [BDEW, 2013].

It is concluded that the deviations of the distribution of the device loads are in a tolerable range because of the uncertainty of the statistical data. Nevertheless, the integration of statistical data about the household device equipment in Germany could improve this in the future.

Another advantage of the model to the simple profiles is highlighted in Figure 3.5, which shows the duration curves of different load profiles on a log-log scale. While above only the profiles on an aggregated level are discussed, this figure also shows the duration curves of single generated household loads together with the single loads of the measured data. It clearly indicates how much higher the fluctuation of a single profile is in comparison to an aggregated load, and with it also the occurrence of peak loads. The model is able to cover this stochastic causality, which is, e.g., not

represented in the SLP. The duration curve of the SLP aligns somewhere between 100 and 1000 averaged profile runs of the model, indicating as expected that it is just sufficient to represent whole districts but not single households.

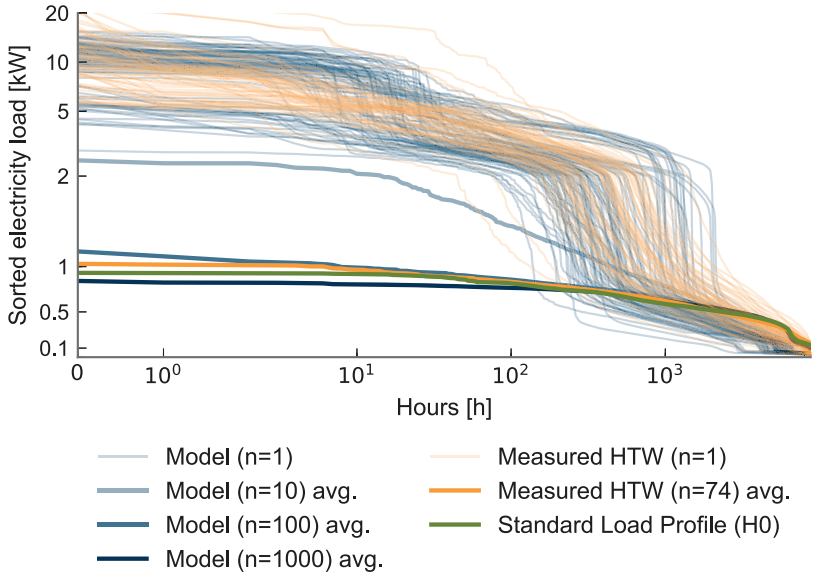

Figure 3.5: Duration curves of the electricity load of the model for different numbers of households (n), in comparison to the duration curve of the SLP and the average measured profile. All profiles are normalized to a typical electricity consumption of 3515 kWh/a.

All in all, the model fits all main requirements listed in Section 3.1.1.

3.2 Thermal building load

The second relevant energy demand is the residential heat load. In order to find good models predicting such, again Section 3.2.1 discusses the existing approaches in terms of their suitability for this thesis. Based on this, a model is chosen and extended to fit the scope of this work, shown in Section 3.2.2. Section 3.2.3 validates the resulting model for German archetype buildings.

3.2.1 Existing thermal building models

The most popular thermal building model is *EnergyPlus* [EnergyPlus, 2017] developed by *the National Renewable Energy Laboratory (NREL)* , which offers a large variety of functions and customization for building simulations in general. It has a high degree of detail and an integrated simulation algorithm. It provides a Functional Mock-up Interface (FMI) to integrate it into model chains such that it can be programmatically accessed. This is, e.g., done by Evins [2015] who iteratively calculates the heat load for different retrofit cases of a single building and attaches a supply system optimization behind. The drawback of this approach is that many different supply optimizations have to be calculated in order to find an optimal combination between retrofit and adaption of the supply system, which is computationally inefficient. Additionally, no exact statement can be given about the optimality of the results.

FUNCTIONAL MOCK-UP INTERFACE:
"Functional Mock-up Interface (FMI) is a tool independent standard to support both model exchange and co-simulation of dynamic models using a combination of XML-files and compiled C-code." Source: http://fmi-standard.org/

Wu et al. [2017] also incorporates a variation of *EnergyPlus* simulations into its supply system optimization. Nevertheless, it is no iterative procedure, instead, all retrofit options and the resulting demand profiles are calculated a priori and given as single investment options to the optimizer. Although the approach is quite interesting, one drawback could be that all cross combinations of retrofitting options have to be implemented as single binary options, e.g. change windows vs. change windows and change wall, constituting many binary variables in the optimization framework, which is computationally heavy. The second disadvantage is that the operation of the heating system is detached from the operation of the supply system. Therefore the heat storage capacity of the building cannot be considered.

These drawbacks would also apply for approaches with other simulation environments like *TrnSys* [TrnSys, 2018], which is, e.g., used in an iterative optimization by Diakaki et al. [2013], or the Modelica library *AixLib* developed by Müller et al. [2016]. Therefore, this work trades the accuracy of predicting the thermal load by those simulation environments to a lumped building model. It can be integrated into the overall mathematical program directly with the advantage of a better computational performance.

This type of lumped modeling of thermal building systems is state-of-the-art for Model Predictive Controls (MPC) or operation optimizations. Kossak and Stadler [2015], e.g., developed a 1R1C model in order to predict the heat load of a campus

building and clarify the importance to consider the thermal mass for an accurate model. Fux et al. [2014] compared different lumped parameter models from 1R1C, 2R1C, 3R2C up to 6R4C for the MPC of a six-story timber building in the Alps. De Rosa et al. [2014] even introduced a model that has an electrical analogy of 23R7C as an alternative model to *EnergyPlus* or *TrnSys* and validated it for different locations.

LUMPED MODEL:
A lumped model reduces the complex spatially distributed physical behavior of a system into a topology of discrete *lumps* (usually electrical circuit analogies) that approximate the original behavior. Those lumps can be given by the number of Resistances (R) and number of Capacities (C), comprising the models to xRxC equivalents.

Although a high order model is predicted to have more accurate results, they also have to be parametrized. An MPC is often able to parametrize itself with measured data. This would not be possible for the buildings in this work where many types are considered with a simplified parameter set. Further, Fux et al. [2014] predicted an RMSE of 0.68 °C between a measured room temperature and a room temperature predicted by a 1R1C model. This accuracy exceeds the accuracy required for this work because the uncertainty of the input parameters has a higher impact.

Nevertheless, in comparison to the MPC approaches, the mathematical program in this work has to account for two features:

1. Respecting investment decision into the building envelope simultaneously with the design optimization of the supply system.
2. Considering the thermal building mass together with the operation of the supply system.

In the context of a supply system design optimization, Ashouri et al. [2013] introduced a 1R1C model that respects the thermal building mass as storage to enable a more flexible operation of the heating system. Nevertheless, the parameters are defined as constants because no envelope optimization is considered.

On the other hand, Stadler et al. [2014] introduced the envelope optimization into the framework *DER-CAM* by creating different heat load profiles for different insulation measures. The mathematical program gets the level of freedom to choose between the profiles with different cost, similar to the approach of Wu et al. [2017].

Schütz et al. [2017a] combined these works and introduced a 5R1C model that

respects envelope investment decisions simultaneously with the thermal storage capacity of the building. It is based on the EN ISO 13799 [EN ISO, 2008]. The additional resistances are capable of respecting the solar and internal heat gains with a higher accuracy than a 1R1C model. Further, it is validated to the VDI 6007 [VDI, 2015] and shows a good alignment for the annual heat demands and the peak loads. Only the cooling demands are overestimated, which is not relevant for this work since they are not considered in the optimization.

3.2.2 Extension of the 5R1C model

The detailed description of the mathematical model itself is done by Schütz et al. [2017a]. Hence, this section only describes its extensions and integration into the overall model. Section 3.2.2 describes the configuration procedure of the model, sometimes also referred to as data enrichment tool. The integration of the thermal comfort zone of the occupants is described in Section 3.2.2.

Building configuration

The structure of the configuration of the model can be seen in Figure 3.6. Every building is defined by a set of input parameters that characterize it, e.g. the living area, the number of inhabitants or the construction year. These input parameters are used to get the relevant data that physically describes the building. The main data source for this is the building data from the *Institut für Wohnen und Umwelt (IWU)*, which states a representative building stock for Germany [IWU, 2010]. It includes non-refurbished and refurbished buildings for different types and construction years. In the framework of the *EPISCOPE* project [EPISCOPE, 2016], building types representing the building stock of other European countries have been made available as well and could be equivalently integrated into the model of this work.

The configuration can be done either by choosing one specific building type from which the shape, e.g. roof area, and the envelope fabric, e.g. the heat transfer coefficients of the walls, are derived. Alternatively, buildings can be parametrized by considering the most similar IWU-type building as the reference and then adapting the scale of the shape to the required scale. Thereby, the number of floors is fixed while the walls, floor area and roof area are scaled to the new reference area. The building types are illustrated further in Appendix A.2. The fabric depends on the building year, with the exceptional case that it has already been refurbished. In this case, the fabric standard of a construction date 40 years younger than the original

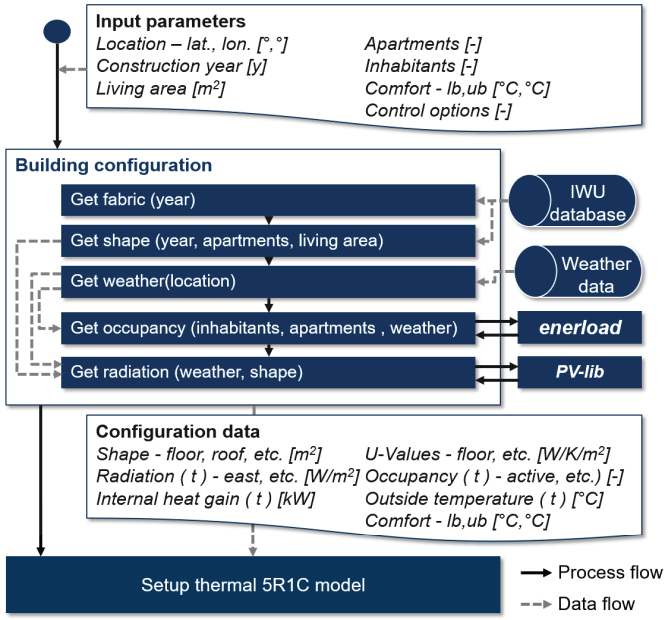

Figure 3.6: Workflow and structure of the *enerbuilding* configuration module, which is used to set up the thermal 5R1C model based on the building parameters of the IWU database and the occupancy data of the *enerload* module.

construction date is considered, which refers to the typical time of a refurbishment cycle [Beuth, 2015].

The weather data is derived from the DIN EN 12831 [DIN, 2014] by finding the closest location listed. Therefrom, the minimal design temperature is derived as well as the test reference region of the *Deutsche Wetter Dienst (DWD)* [DWD, 2012]. Alternatively, the weather data from COSMO rea-6 reanalysis data set [Bollmeyer et al., 2015] can be used for real years.

The weather data set is then first used in the *enerload* module (Section 3.1) together with the number of apartments and the number of inhabitants to calculate the occupancy behavior and appliance load. Since the internal heat gain has for refurbished buildings a significant impact on the effective energy demand [Elsland et al., 2014], it is dynamically calculated, while for active occupants an average heat gain of 150 W and for sleeping occupants an average heat gain of 100 W is assumed [VDI, 2012]. The internal heat gains from the appliances are derived from

their electricity load based on the appliance-specific values introduced by Degefa et al. [2015].

As a last configuration step, the radiation on the tilted areas, such as windows, has to be calculated since it is only provided as Direct Horizontal Irradiation (DHI) and Diffuse Horizontal Irradiation (DNI) by the test reference year [DWD, 2012]. Instead of the radiation model introduced in the work of Schütz et al. [2017a], this work uses the irradiance calculation included in the PV-lib [Andrews et al., 2014] and the integrated *Perez* model [Perez et al., 1987]. The so calculated time series and parameters are then given to the mathematical 5R1C program that describes the thermal behavior of the considered building.

Thermal comfort

A further extension is a new model for the thermal comfort of the occupants. Schütz et al. [2017a] provides only a lower bound for the required internal air temperature T_{air}, aligning with today's standards. This is sufficient to model the theoretical heat demand. Nevertheless, it is more realistic is to consider an indoor temperature with a night reduction or a shut-off of the heating system in case nobody is at home. It further constitutes a more volatile operation of the heating system.

The relevance of this temperature variation is highlighted by Marshall et al. [2016]. They conclude that in case the building is not fully occupied, a reduction of the internal temperature and partial spatial heating (zonal heating) can achieve similar savings as more expensive efficiency measures, like changing the wall insulation. Further, Oldewurtel et al. [2013] developed a Model Predictive Controller, which uses occupancy information in order to achieve a more energy efficient office building climate control. Although they clarify that the impact is highly dependent on the occupancy patterns, duration of vacancy etc., they conclude that savings up to 34% can be achieved. Additionally, they show that similar savings can already be achieved with a well-chosen fixed scheduling of the heating system.

To account for the indoor air temperature variation $T_{air,t}$ in every time step t, referred to as θ_{air} by Schütz et al. [2017a], the original equation from Schütz et al. [2017a] is replaced with the following constraints as lower bound:

$$\begin{aligned} T_{air,t} \geq \quad & +T^{com}_{air,lb} \\ & -\left(T^{com}_{air,lb} - T^{sle}_{air,lb}\right) x^{sle}_t \delta^{sle} \qquad \forall \quad t \\ & -\left(T^{com}_{air,lb} - T^{vac}_{air,lb}\right) x^{vac}_t \delta^{vac} \end{aligned} \tag{3.1}$$

$T^{com}_{air,lb}$ describes the lower bound (lb) of the comfortable air temperature and is basically the set point temperature defined by the occupants. For the default case, the same set point temperature of 21°C as in Marshall et al. [2016] is assumed.

This temperature can be reduced to $T^{sle}_{air,lb}$ in case the occupants are sleeping. This sleeping behavior is described by the time series x^{sle}_t which represents the share of occupants sleeping in ratio to all occupants living in the building at every time step t, calculated from the occupancy activity given by the *enerload* model. δ^{sle} describes the binary decision if a night reduction is integrated into the heating system. Equivalently, the time series x^{vac}_t describes the share of occupants that are not at home, or rather the relative vacancy of the building, and $T^{vac}_{air,lb}$ the minimal building temperature. The existence of an occupancy controller in the building is described by δ^{vac}.

The upper bound of the temperature $T^{com}_{air,ub}$ limits the heating operation and determines the cooling load in the summer period with the following constraint:

$$\begin{aligned} T_{air,k} \leq \quad & +T^{com}_{air,ub} \\ & -\left(T^{com}_{air,lb} - T^{vac}_{air,ub}\right) x^{vac}_t \delta^{vac} \quad \forall \quad t \end{aligned} \tag{3.2}$$

Thereby $T^{vac}_{air,ub}$ is the maximum temperature inside the building in case no occupant is present. The general upper bound for the temperature is set to 26°C.

Figure 3.7 illustrates the difference of the heat load in case a constant air temperature is set as a lower bound (*fix demand*) to the case when the temperature level is dynamically adapted to the occupancy behavior (*with control*). The second case is here illustrated for an ideal heating operation where the whole heating system is automatized, meaning that smart thermostats are integrated to the whole building. Since the majority of today's buildings do not own such controllers, its investment is later set as an optimization decision.

The operation tries to minimize the heat load with the consequence that the air temperature aligns with the lower bound of the air temperature, as introduced in equation 3.1. As expected, the air temperature of the smart control case directly correlates with the activity of the occupants. With it, not only the indoor air temperature fluctuates but also the building mass temperature has a higher variation, still damped by its thermal inertia. This inertia is highlighted in the period between 23:00 of the 16. February and 9:00 of the 17. February where the first order delay behavior is recognizable.

The lower bound of the air temperature is for the control case set higher (21 °C) than the overall lower bound of the air temperature for the fix demand case (20 °C).

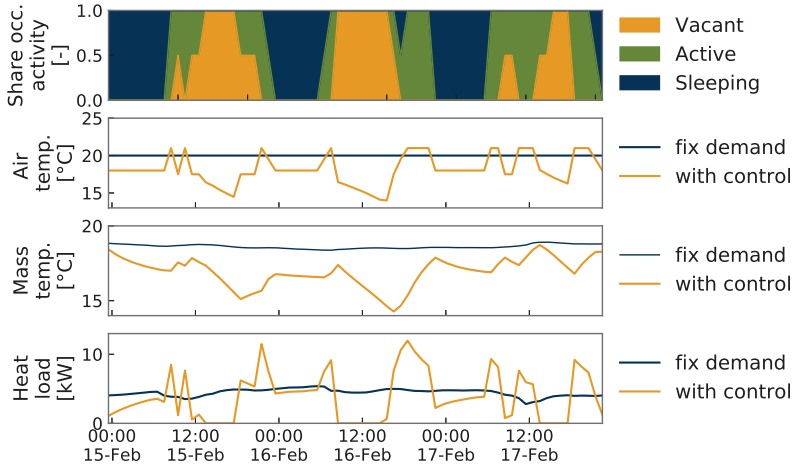

Figure 3.7: Example heating system operation and resulting air and mass temperatures depending on the occupancy activity.

Nevertheless, the resulting mass temperature of the control case is always below the mass temperature of the fix demand case. The reason is that a full up-heating of the mass is not required for the short time frames when occupants are active. The advantage is a reduced heat transfer to the environment and with it a reduced cumulative heat demand.

Nevertheless, this rapid heating and cooling of the air and thermal mass require a much more flexible operation of the heating system, shown in the resulting heat load profiles. This fluctuating operation would occur in a reduced manner in a real system in order to minimize degradation effects of, e.g., the valves. A reduction of the fluctuation would also be expected in the later overall system model incorporating the supply system optimization since the heating devices, e.g. the heat pump, will technically constrain the heat load. This does not apply for the here considered example.

3.2.3 Validation and parametrization

Although the model has already been validated for a single building by Schütz et al. [2017a], it is validated further for this work because the whole building configuration has been modified and extended.

The data set from the IWU building topology is used as the validation and parametrization set. It describes a national building stock by so-called reference or archetype buildings. Their creation is explained in Ballarini et al. [2014]. The data set consists of the technical envelope described by U-values etc. and shape values such as wall areas in different orientations. The reported heat capacity values c_m of 45 Wh/m^2/K of the IWU buildings are considered for the parametrization. These values are the same for all buildings. In reality, they would vary between the buildings because of the different materials and thicknesses used in the different constructions. Nevertheless, this inaccuracy is constituted by a lack of data.

These values are used to parametrize the introduced dynamic 5R1C heat load model where all buildings are considered to have a temperature tolerance of 20 °C to 26 °C and two occupants per apartment. The 5R1C model is once optimized with a *fix* lower bound of 20 °C, once with a *night reduction* to 18 °C and once with the introduced *occupancy* controller. The test reference year of Potsdam, Germany [DWD, 2012] is considered for the weather data. The resulting time series are summed up to an annual heat demand for every building type. These values are finally compared to the predicted annual heat demand of the *IWU* database.

The comparison of the resulting values can be seen in Figure 3.8. Although none of the 5R1C simulations do perfectly fit with the static calculated *IWU* values for all building types, the general trend of different specific heat loads for different building ages and types is represented. The reported annual heat demands of the *IWU* database in general align between the 5R1C model with a *fix* temperature with a RMSE of 6.82 kWh/(a m^2) as upper bound and the model with a *night reduction* with a RMSE 6.79 kWh/(a m^2) as lower bound. This matching is sufficiently good, since the *IWU* model just uses aggregated values like absolute numbers of heating days, correction factors for the night reduction, or absolute cumulative solar gains, while the 5R1C model simulates this all for every hour in a year.

The heat demand is reduced from the 5R1C simulation with a fix temperature to the 5R1C model with the occupancy controller between 15.5% and 19.2%. This is below the savings of 34% reported by Oldewurtel et al. [2013]. Nevertheless, their application focused also on an office building that is less frequently occupied than an residential building. Summarized, the potential of energy savings by such smart controllers are significant but the absolute saving potential especially for buildings with a low energy demand is limited.

The validation illustrates further the different heat demands of different building types and ages. Multi-family houses have in general smaller energy demands than single-family houses due to better area-to-volume ratios. Further, terraced single-family houses also have smaller energy demands than detached single-family houses, since less exterior walls transfer heat to the ambient air. The en-

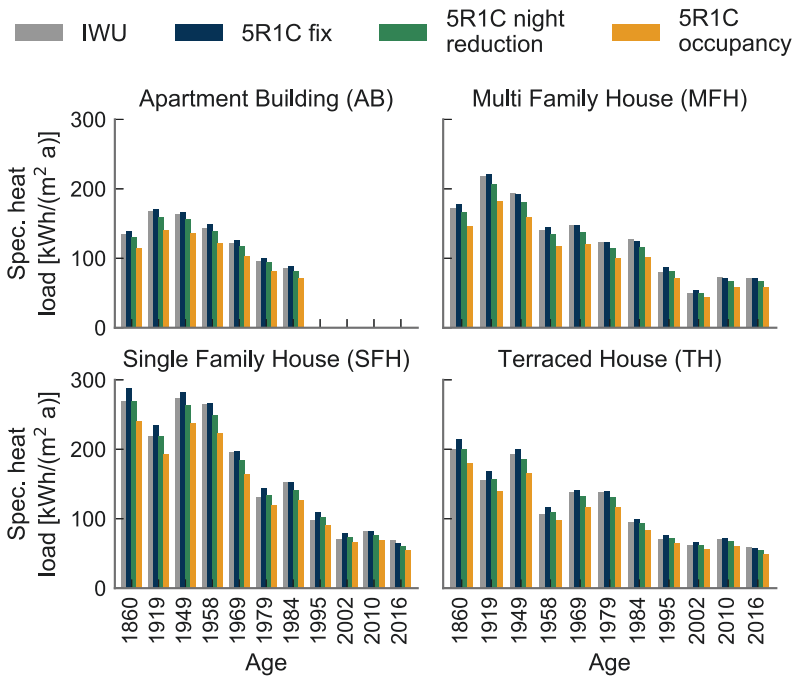

Figure 3.8: Comparison of the annual heat load provided by the IWU database to the heat load dynamically calculated with the considered 5R1C model. for a generic set of archetype buildings.

ergy demand is decreasing with newer construction years due to better insulation. Nevertheless, it is not strictly decreasing, which is constituted by different building shapes and orientations between the construction years. E.g. the increase of the energy demand between the 2002 and the 2010 single family house is constituted by less south oriented window areas in the newer building, resulting in less solar heat gains.

All in all, together with the validation of Schütz et al. [2017a], a sufficient accuracy of the optimization integrated heat model can be concluded.

3.3 Supply system optimization

The following section introduces the model generator *enercore* for building flexible different configurations of energy supply systems to satisfy the energy demand of the shown load models. As discussed in Section 2.3, the focus of the optimization model is its high performance because many different building types have to be optimized. Therefore, the investment costs of the technologies are approximated with a single binary and a single continuous decision variable. Section 3.3.1 introduces their integration to the overall cost function that gets minimized. The operation of the technology classes is kept continuous and linear, as shown in Section 3.3.2. The nonlinear behavior of the thermal components is separately modeled with a continuous linear approximation for different discretized supply temperature levels, described in Section 3.3.3. The generation of feed-in profiles for the photovoltaic and solar thermal collectors is introduced in Section 3.3.4 and Section 3.3.5. The final superstructure of the considered building model is summarized in Section 3.3.6.

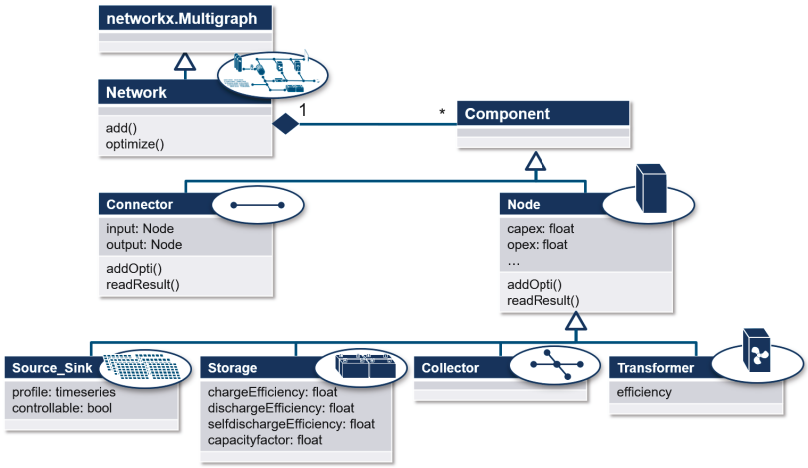

Figure 3.9: A simplified Class Diagram of the enercore.energysystem module defining the different technology classes and its association with the overall technology network.

The framework is an object-oriented Python package that introduces classes for different energy technology categories. Based on those, instances can be derived and parametrized to represent real energy system components. A network of them defines the overall superstructure of the energy supply system, which is optimized in terms of structure, scale and operation. Its programmatic implementation is il-

lustrated as a class diagram in Figure 3.9. It is set up in the Pyomo modeling environment [Hart et al., 2011].

3.3.1 Objective functions

Since a trade-off between the economic and the ecologic objectives shall be made, a multi-objective or multi-criteria optimization is required. For this work, either a linear scalarization or the ϵ-constraint approach [Haimes et al., 1971] can be used. Both approaches are able to consider two objectives (ω_1,ω_2) in a single objective environment. The linear scalarization adds the single objectives in a single function with different weightings. The ϵ-constraint approach solves both objectives once independently and then divides the solution space in between into a defined number of intervals which are independently optimized. One objective is set as a constraint and the other objective is optimized. This results in a Pareto front which can be used to evaluate the trade-off between the two goals. A more detailed description can be found, e.g., in Wu et al. [2017]; Schütz et al. [2017a].

In the following, the objectives are introduced, which are the annual energy cost, including the discounted investment, and the direct and indirect operation related CO_2 emissions. Life cycle related emissions due to manufacturing or disposal of technologies are not considered.

Annualized energy cost

The first objective function describes the annualized cost of the supply system considered. Therefore, for each technology d, the annualized costs are calculated with a capital recovery factor CRF_d, which considers the Weighted Average Cost of Capital $WACC_d$ and economic lifetime τ_d of the technology in years:

$$CRF_d = \frac{(1 - WACC_d)^{\tau_d} WACC_d}{(1 - WACC_d)^{\tau_d} - 1} \tag{3.3}$$

A simplified consideration of the economy of the scale is considered, as discussed in Section 2.3: The capital expenditures of each technology are divided into the existing related costs [eur] that only appear if the technology is installed, and specific costs [eur/kW] that are scale-dependent [Lindberg et al., 2016a]. Therefore, each technology has to be modeled by a binary variable δ_d that defines whether the component exists, and a continuous variable D_d that defines the installed capacity of the component. The full resulting technology specific annualized fixed cost can then be calculated with the existing related capital expenditure ($CAPEX_{exist}$), the

scaling-related capital expenditure ($CAPEX_{spec}$), and fixed operational expenditure ($OPEX_{fix,d}$) as follows:

$$\begin{aligned} c_{exist,d} &= CAPEX_{exist,d}\,(CRF_d + OPEX_{fix,d}) \\ c_{spec,d} &= CAPEX_{spec,d}\,(CRF_d + OPEX_{fix,d}) \end{aligned} \tag{3.4}$$

The costs, which vary with the operation of the system $c_{var,i,j,t}$, are related to the energy flows $\dot{E}_{i,j,t}$ between the technologies. Along with the scaling of the technologies D_d, the following objective function can be stated

$$\min \sum_d \left[c_{exist,d}\delta_d + c_{spec,d}D_d\right] + \sum_{(i,j)\in L}\sum_{t\in T} c_{var,i,j,t}\dot{E}_{i,j,t}\triangle t \tag{3.5}$$

which minimize the total annual energy cost.

Annual greenhouse gas emissions

The second objective is the minimization of the direct and indirect operational GHG emissions. Each energy flow $\dot{E}_{i,j,t}$ can have a defined GHG footprint $\gamma_{i,j,t}$ which is optionally time-variant. Based on this, the operational emissions are defined as follows:

$$min \sum_{(i,j)\in L}\sum_{t\in T} \gamma_{i,j,t}\dot{E}_{i,j,t}\triangle t \tag{3.6}$$

The introduced footprint is mainly used at the input energy flows of the network since the imported electricity or fuels constitute the operational GHG emissions.

3.3.2 Technology classes

The network of specific technologies is connected by energy flow variables $\dot{E}_{i,j,t}$ for every time step $t \in \{1, ..., N_t\}$. Each connection is therefore defined by an output technology i and input technology j and belongs to a connection set $(i, j) \in L$. Further, every connection belongs to an energy type $\epsilon((i, j))$. The energy flows of the connections are restricted by the technology models introduced.

The technology models establish the constraints of the system. They are divided into four classes, namely: *Source/Sinks, Collectors, Transformers* and *Storages*.

The *Source/Sink* class q represents input and output flows to the system, such as photovoltaic feed-in or electricity demand. It is essentially defined by a single equation:

$$\eta_{lb,q,t} D_q \leq \sum_{(q,j)\in L} \dot{E}_{q,j,t} + \sum_{(i,q)\in L} \dot{E}_{i,q,t} \leq \eta_{ub,q,t} D_q \quad \forall \quad t, q \tag{3.7}$$

where $\eta_{lb,q,t} D_q$ could be a certain demand that must at least be satisfied at time step t, or $\eta_{ub,q,t} D_q$ could be the maximum specific photovoltaic feed-in per. D_q is the scale of source or sink.

The *Collectors* class n can be seen as a hub in which all input energy flows must be equivalent to all output energy flows:

$$\sum_{(i,n)\in L} \dot{E}_{i,n,t} - \sum_{(n,j)\in L} \dot{E}_{n,j,t} = 0 \quad \forall \quad t, n \tag{3.8}$$

The *Transformer* class f represents technologies that transform the energy from one form to another. Examples include gas boilers, fuel cells or heat pumps. For the definition of those, the energy type (electricity, gas, etc.) ϵ is required. Further, a set of transformation paths $(\epsilon_{in}, \epsilon_{out}) \in P(f)$ is defined for every transformer. Thereby, every path has a defined transformation efficiency $\eta_{f,\epsilon_{in},\epsilon_{out}}$ from energy form ϵ_{in} in energy form ϵ_{out}. With those, the following equation can be stated for each *Transformer* in the system:

$$\eta_{f,\epsilon_{in},\epsilon_{out}} \sum_{(i,f)\in L|\epsilon_{in}((i,f))} \dot{E}_{i,f,t} = \sum_{(f,j)\in L|\epsilon_{out}((f,j))} \dot{E}_{f,j,t} \quad \forall \quad (\epsilon_{in}, \epsilon_{out}) \in P(f) \quad \forall \quad t, f \tag{3.9}$$

Basically, it states that all incoming energy flows of a certain energy type are in sum converted to a set of outgoing energy flows belonging to another energy type. E.g. for the case of a CHP unit, all incoming gas flows are converted with a fix efficiency to the sum of all outgoing electricity flows. The second path would be that the same gas flows are also converted to a set of outgoing heat flows.

Further, every Transformer f has an energy form ϵ_f that is limited by the Transformer capacity D_f, e.g. the generated electricity in case of a CHP unit:

$$\sum_{(i,f)\in L|\epsilon_f((i,f))} \dot{E}_{i,f,t} + \sum_{(f,j)\in L|\epsilon_f((f,j))} \dot{E}_{f,j,t} \leq D_f \quad \forall \quad t, f \tag{3.10}$$

The *Storage* class s is defined by an additional variable namely the State of Charge $SOC_{s,t}$ at every time step t. The Euler method is used to derive the state of charge

in the next time step $SOC_{s,t+1}$:

$$\begin{aligned} SOC_{s,t+1} = \quad & SOC_{s,t}(1-\eta_s^{self}\Delta t) \\ & +\eta_s^{char} \sum_{(i,s)\in L} \dot{E}_{i,s,t}\Delta t \\ & -\tfrac{1}{\eta_s^{dis}} \sum_{(s,j)\in L} \dot{E}_{s,j,t}\Delta t \end{aligned} \quad \forall \quad t,s \tag{3.11}$$

where $\dot{E}_{i,s,t}$ describes the charging flow with an efficiency of η_s^{char} and $\dot{E}_{s,j,t}$ the discharging flow with related efficiency η_s^{dis}. η_s^{self} defines the self-discharge of the storage and Δt the step length of a single time step. The state of charge at the beginning of the considered time frame $SOC_{s,1}$ is equal to the state of charge at the end of the time frame SOC_{s,N_t+1} by a so-called cyclic condition.

The design variable of the storage s is described by its maximal net capacity D_s and accordingly limits the state of charge:

$$SOC_{s,t} \leq D_s \quad \forall \quad t,s \tag{3.12}$$

The maximum charging and discharging flows are restricted by the capacity factor C_s as follows:

$$\sum_{(i,s)\in L} \dot{E}_{i,s,t} + \sum_{(s,j)\in L} \dot{E}_{s,j,t}\Delta t \leq C_s D_s \quad \forall \quad t,s \tag{3.13}$$

An additional constraint is required for all technologies to ensure that the existing related variable δ_d is activated in case the technology is installed. It is done by a so-called BigM Method [Bemporad and Morari, 1999], which restricts the scaling-dependent device variable D_d as follows:

$$\mathbf{M}\delta_d \geq D_d \tag{3.14}$$

The method is inspired by Stadler et al. [2014] and Lindberg et al. [2016a]. In order to minimize the computational load, the BigM should be chosen as small as possible [Bemporad and Morari, 1999], but big enough such that it is not restricting the solution space. Therefore, it is here set depending on the scale of the considered building, which determines the maximum scale of the technologies.

3.3.3 Heat supply model

Since *enercore* just defines the basis for flexible energy system models, some parts are extended such that they are able to cover the varying operation conditions in a

building. Especially the heat supply temperature has a high impact on the operation of certain technologies. Therefore, it is illustrated and integrated into the model in the following section for air source heat pumps, the heat storage and the building heat demand.

Impact of heat supply temperature

The literature review, shown in Section 2.1, revealed that heat pumps are seen as a key option to efficiently provide low-temperature heat for space heating by *pumping* ambient heat to the required temperature level with the help of electricity. As a reversely operated Carnot machine, their performance is dependent on the temperature level of the heat source, the ambient temperature T^{amb} for an air heat pump, and the heat sink, the supply temperature of the heating system T^{sup}.

Based on the Carnot cycle, their Coefficient of Performance CoP_k can be expressed as follows [Lauinger et al., 2016; Huchtemann, 2015; Zogg, 2009]

$$CoP_t = \frac{\dot{Q}_t}{P_{el,t}} = \eta_C \frac{T_t^{sup}}{T_t^{sup} - T_t^{amb}} \tag{3.15}$$

where $P_{el,t}$ is the electric power of the integrated compressor at every time step t, $\dot{Q}_k$ the provided heat, and η_C the quality grade of the heat pump system itself respecting the non-ideal operation of heat pumps due to temperature differences in the heat exchangers or electricity consumption of peripheral appliances.

Figure 3.10 illustrates the dependency of the CoP of the different temperature levels. It shows once the simplified Carnot efficiency introduced in Equation 3.15 with a quality grade of 40 % and validates it against manufacturer specifications and measured data of air source heat pumps. First, the high variance of the manufacturer specifications for the same operation conditions in yellow is observable, indicating the high performance range of different available heat pumps. The considered efficiency function aligns with the average of manufacture specifications for supply temperatures of 35 °C and an ambient temperature of 2 °C and adjusts in the lower range of the manufacturer specifications for an ambient temperature of 7 °C.

The measured performance data set is given for a variance of ambient temperature levels and a supply temperature of 55 °C. The model is able to cover the trend for reduced ambient temperatures and aligns again in the lower range of the reported performance values. The considered quality grade η_C of 40 % assumed is in comparison to the reported values rather conservative. Therefore, an increase

of the quality grade to 45 % could respect future efficiency improvements of the manufacturers.

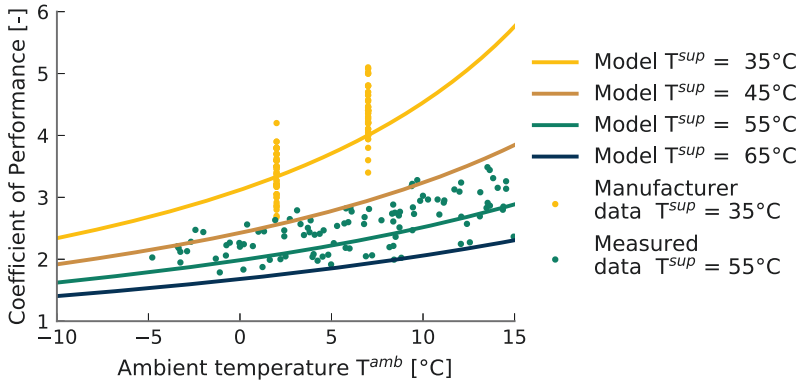

Figure 3.10: Coefficient of Performance for different outside air temperatures, different supply temperatures. The dots for a supply temperature of 35 °C are different manufacturer specifications, and the dots for a supply temperature of 55 °C are measured values based on ISE [2011] and Sterchele et al. [2016]. The lines are the efficiencies calculated with the Carnot efficiency and a quality grade of 0.4.

Considering an ambient temperature of 0 °C, the increase of the supply temperature from 45 to 55 °C reduces the CoP from 2.73 to 2.23 for the considered quality grade. For the same heat load, this would imply an increase in the electricity load of the heat pump by 22 %. Keeping in mind that the overall goal of the work is to predict the future grid related electricity load temporally resolved, such sensitivities are too big to be neglected.

Nevertheless, this is often done in energy system design models where the CoP is considered constant for the whole year [Ashouri et al., 2013; Evins, 2015; Wu et al., 2017; Mashayekh et al., 2017], which causes an overestimation of the CoP in winter and an underestimation in the summer. Lindberg et al. [2016b] solved this issue by considering a heat curve beforehand, depending on the heating system of the building. Such they get a CoP for every time step in the year before the optimization.

For the case of this work, no heat curve can be defined a priori, since the required heat load and related supply temperature depend on the occupancy activity, the storage operation, and the optimal refurbishment level, as introduced in Section 3.2. Therefore, the choice of the supply temperature should be an optimization variable,

since its intelligent operation can maximize the overall efficiency of the heating system. E.g., Huchtemann [2015] states that smart control, especially of the supply temperature, is able to save between 9.6 to 29% of the electrical load of a heat pump for the case of oversized heating systems. This would especially apply to refurbished buildings.

A direct formulation of the supply temperature as continuous optimization variable in 3.15 would constitute a nonlinear equation, which should be avoided. Therefore, an alternative formulation is required that is able to account for different supply temperature levels.

Besides the heat pump, the supply temperature is also relevant for the heat storage, since the usable heat of the storage SOC_t^{max} depends on the temperature gap between supply and return heat flow of the building. Wang et al. [2015] described the usable storage inventory as follows

$$SOC_t^{max} = \rho V_{st} c_{p,W} \left(T_t^{sup} - T_t^{ret}\right) \tag{3.16}$$

where V_{st} is the storage volume and T_t^{ret} the return temperature of the heating system. The additional temperature spreads of the heat exchangers considered by Wang et al. [2015] are excluded. In comparison to their system, the heat storage in this work is directly connected to the heating system.

Again, equivalent to the CoP description of the heat pump, a formulation of the supply temperature as variable T_t^{sup} would constitute a Nonlinear Program (NLP) in 3.16 since the storage volume V_{st} or rather the storage capacity is an optimization variable.

The last relevant component influenced by the supply temperature is the heat flow $Q_{sup,t}$ from the heating system to the building, which can be covered with certain temperature levels. Higher supply temperatures constitute higher possible heat loads since a better heat transfer is possible between the heating system, e.g. the radiators, and the building. In case that a linear heating curve is assumed for the building, the maximal possible heat load is qualitatively limited by the nominal design heat flow Q_{sup}^{nom}, the supply temperature T_t^{sup} and the indoor air temperature T_t^{air} as follows

$$Q_{sup,t} \leq Q_{sup}^{nom} \frac{T_t^{sup} - T_t^{air}}{T_{nom}^{sup} - T_t^{air}} \tag{3.17}$$

where T_{nom}^{sup} is the nominal design temperature.

The indoor temperature T^{air} is here assumed as a constant and conservatively assumed with the maximal tolerable air temperature inside the building.

It is referred to Huchtemann [2015] for more detailed models.

Supply temperature discretization

Since the impact of the supply temperature to the heat pump performance is significant but a correct mathematical integration would state an NLP, a discretization approach of the supply temperature is introduced. It is similar to the two-level heat storage model of Steen et al. [2015] but more generic and allows a more flexible storage operation. The concept is illustrated in Figure 3.11.

First, an order of temperature levels with $\lambda \in \Lambda$ are introduced for the supply temperature T_{λ}^{sup} that are considered in the mathematical program. They define possible operation conditions for the heating system. A higher number of levels constitutes a more precise model but simultaneously increases the size and computational load of it. The first temperature level is defined by the nominal supply temperature T_{λ}^{sup} at which as default the heat supply technologies feed-in to the system. These levels do not exist in parallel in a real system, instead, the real operation temperature is represented by combination or superposition of these introduced levels.

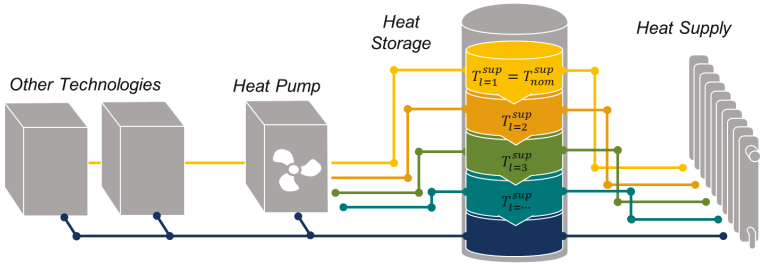

Figure 3.11: Illustration of the supply temperature discretization for the heat pump, the heat storage and the heat supply.

Based on the levels, the CoP of the heat pump, introduced in equation 3.15, can be calculated for every hour in the year and for all considered supply temperature levels T_{λ}^{sup}. With those the performance of the heat pump can be described for all time steps and temperature levels separately as:

$$Q_{hp,t,\lambda} = P_{el,t,\lambda}\eta_C \frac{T_{\lambda}^{sup}}{T_{\lambda}^{sup} - T_t^{amb}} \quad \forall \quad t, \lambda \tag{3.18}$$

Although the heat pump can operate at different levels in the same time frame, all technical constraints limiting the performance of the heat pump have still to hold for

the aggregated heat pump load such that:

$$Q_{hp}^{max} \geq \sum_{\lambda \in \Lambda} Q_{hp,t,\lambda} \quad \forall \quad t \tag{3.19}$$

In consequence, the heat pump can only operate at a single temperature level with the full load.

An equivalent formulation is made for the heat storage, which gets individual states of charges for the different temperature levels $SOC_{s,t,\lambda}$ and individual state equations, as defined in Equation 3.11.

Assuming a constant spread between the supply and the return temperature, the maximal state of charge has to hold for all states at the different temperature levels together:

$$SOC_{s}^{max} \geq \sum_{\lambda \in \Lambda} SOC_{s,t,\lambda} \tag{3.20}$$

The last equation that has to be adapted is the maximal heat supply for the different temperature levels. It can be stated equivalent to Equation 3.17 as follows:

$$Q_{sup}^{nom} \geq \sum_{\lambda \in \Lambda} Q_{sup,t,\lambda} \frac{T_{nom}^{sup} - T^{air}}{T_{\lambda}^{sup} - T^{air}} \quad \forall \quad t \tag{3.21}$$

A reduced supply temperature linearly reduces the possible heat transfer to the building.

All in all, this discretization allows continuous linear operation equations while respecting an adaption of the supply temperature to certain levels. Still, it is a simplification that partially deviates from the reality, as reported for a similar approach [Baeten et al., 2015]. E.g., the heat transfer inside the storage is neglected and ideal stratification is assumed. Nevertheless, it is an improvement to the consideration of a single supply temperature.

While in general a flexible number of temperature levels can be chosen, this work uses three equidistant distributed temperature levels. Those are derived from the maximal supply temperature of the building that states the maximum temperature level.

3.3.4 Photovoltaic performance model

For the planning and operation of photovoltaic panels, a performance model is needed to produce feed-in time series depending on the weather conditions, the

geo-location of the building and its roof orientation.

Therefore, this work developed and validated in collaboration with the *IEK-5, Forschungszentrum Jülich* a photovoltaic performance model, documented in the master thesis of Meerts [2016]. It is based on the *PV-Lib* [Andrews et al., 2014], which was developed at *Sandia Laboratories*. Different sub-models of the *PV-Lib* are compared and validated against three measured data sets at different locations in central Europe. The different model steps are illustrated in Figure 3.12.

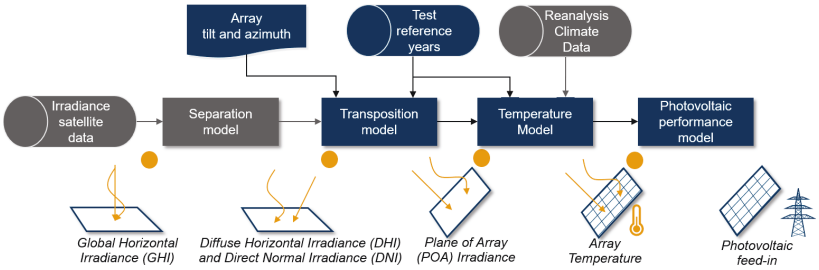

Figure 3.12: Sub-models and steps of the photovoltaic performance model. In blue are the steps considered in this thesis, while the gray boxes illustrate the additional steps performed in the master thesis of Meerts [2016].

The original model is based on measured Global Horizontal Irradiance (GHI) from satellite measurements and on reanalysis data for other climate parameters, such as the ambient temperature. Therefore, sub-models are required, e.g., to distinguish the GHI to direct and diffuse irradiance in order to validate the photovoltaic performance. This is not necessary for the final work since the test reference years [DWD, 2012] are used that independently provides already diffuse and direct irradiance data.

Next, transposition models are required for the calculation of the Plane Of Array (POA) irradiance from the horizontal irradiance. This can be straightforwardly performed for the direct irradiance by a simple trigonometric function. Also, the ground-reflected diffuse radiation can be isotropically calculated with the help of a ground albedo coefficient, where a value of 0.2 is considered [Kotak et al., 2015]. Nevertheless, the transposition of diffuse radiation from the sky to the tilted plane is not mature and many different models have been proposed for it. Their comparison is further illustrated in Meerts [2016], while it can be concluded that the Perez translation model [Perez et al., 1987] outperforms the others. The trial to develop a novel transposition model based on a Neural Network and different measurement data sets was not able to outperform the Perez model.

Afterwards, the module temperature can be calculated based on the irradiance, the ambient temperature and the wind speed. Again, different models are evaluated but no dominant one is found for the given data sets [Meerts, 2016]. Therefore, this work stays with the empirical Sandia Array Performance Model (SAPM) [King et al., 2004], which describes the thermal response with two coefficients for wind and irradiance, specific to the module type.

The array performance can be calculated with the irradiance data and the module temperature as the last step. Therefore, again the SAPM is used since it is widely validated and has good performance [Meerts, 2016]. It is semi-empirical and can reproduce the panel specific I-V curve based on five characteristic points, including the Maximal Power Point (MPP), for all operation conditions. The required coefficients are empirically determined for different arrays [King et al., 2016] and provided in a publicly available database.

In summary, a deviation between model and measurement of -3% to +2% results for the yearly yield for the whole model chain with the weather databases as input [Meerts, 2016]. The RMSE of the actual profile seem high with 35% and 47%, but this is mainly related to the high deviation between the measured irradiance data and the satellite irradiance data (OSI-SAF). This is not relevant for the model in this work since test reference year data is considered for the irradiance. Additionally, the performance model should only sufficiently predict the overall shape and yield of the photovoltaic feed-in but does not have to perfectly match historical data.

3.3.5 Solar thermal performance

The second solar-based energy generation unit is solar thermal. The calculation of the plane of array irradiance G_t^{poa} is the same as for the photovoltaic. Its performance, described by the area-specific heat generation q_t^{st}, is represented by the following polynomial function [Lindberg et al., 2016a; Rager, 2015]

$$q_t^{st} = c_0 G_t^{poa} - c_1 \left(T_t^{col} - T_t^{amb}\right) - c_2 \left(T_t^{col} - T_t^{amb}\right)^2 \tag{3.22}$$

where c_0, c_1 and c_2 are collector specific performance constants and T_t^{col} the collector temperature. The coefficients are here considered for collector number 1734 of the collector database of the *SPF Institut für Solartechnik* [SPF, 2017].

This work also optimistically assumes the collector temperature with 30 °C, equivalent to Lindberg et al. [2016a].

3.3.6 Superstructure of the building model

In this section, the overall technological superstructure is defined for a single building in the following section and illustrated in Figure 3.13.

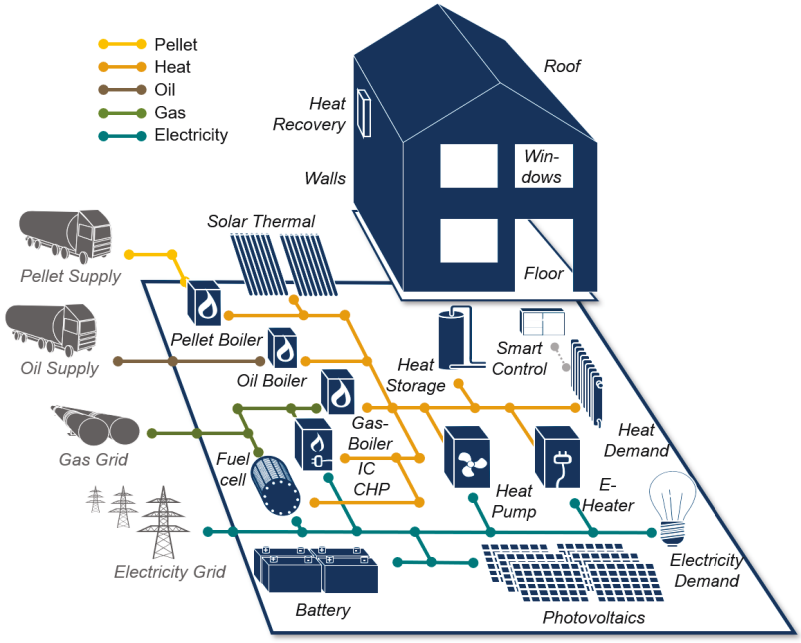

Figure 3.13: Illustration of the considered superstructure of the supply system and all potential refurbishment options for a single building.

The flexible energy imports from the electricity grid, the gas grid, and the pellet and oil supply are modeled as *Sources* without a limited import profile. The chemical energy carriers can be combusted in different *Transformers*, such as the pellet boiler, oil boiler and gas boiler with one-dimensional efficiencies. The gas can be further converted in a fuel cell or an internal combustion engine. The two co-generation units generate heat and electricity and are also modeled as *Transformers*. The electricity can be converted to heat with a simple electric heater as *Transformer*, or a heat pump described by the model in Section 3.3.3. Solar thermal and photovoltaic are *Sources* with time-dependent capacity factors, which are introduced in Section 3.3.4 and Section 3.3.5. Their installed capacity is limited by the roof area of the building. Electricity can be stored in a battery and heat can be stored in a

hot water tank, both modeled as *Storages*. The demands are modeled as *Sinks*. The hot water and electricity demand have fixed profiles, generated with the model introduced in Section 3.1. The heat demand is bound by the model introduced in Section 3.2.

The efficiency measures in the building itself can be the extension of the insulation of the outside walls, the roof, or the basement ceiling. Further, the windows can be replaced or a ventilation system with a heat recovery can be integrated. Moreover, the rooms can be equipped with an occupancy controller influencing the comfort temperature depending on the occupancy activity.

The detailed parametrization of the technologies and refurbishment measures depend on the scenario considered and are introduced in Chapter 5.

In conjunction with this work, 100% self-sufficient buildings [Kotzur et al., 2017; Röben, 2017] including technologies such as a reversible Solid Oxide Cell [Nguyen et al., 2013; Frank et al., 2018] and Liquid Organic Hydrogen Carrier [Eypasch et al., 2017; Teichmann et al., 2012] have also been evaluated. Although they were discarded for the case of the final thesis, it shows the flexibility and validity of the framework to easily include further technologies.

3.4 Time series aggregation and disaggregation

As discussed in Section 2.3, the considered optimization problems are challenging to solve because of the high temporal resolution and the range of design and operation options for the building energy supply. Clustering based time series aggregation is a promising approach to deal with this complexity. Therefore, two publications were created in conjunction with this thesis [Kotzur et al., 2018a,b]. The idea is to neglect redundant time series data and to reduce it to the relevant patterns. Such, the overall size of the optimization problem can be reduced.

3.4.1 Related work to time series aggregation

The first publication [Kotzur et al., 2018a] analyzes different algorithms and methods to reduce the data without losing the extreme periods relevant to the system design. The such aggregated time series are used for the design of three reference systems. The aggregation methods are open-source published at `https://github.com/FZJ-IEK3-VSA/tsam`.

The systems are first optimized in terms of design and operation with a full annual time series. The resulting designs and costs define the benchmark. Then, for all the considered systems different numbers of typical days are aggregated with different aggregation methods. These aggregated days are then also used to optimize the design of the systems.

For systems majorly relying on energy imports, it is shown that 12 typical days are sufficient to find system designs whose costs deviate less than 2% to the benchmark systems' costs. The smallest deviations are achieved with typical days aggregated by a *k-medoids* clustering algorithm.

For a system mainly relying on fluctuating renewable energies and seasonal storage, no sufficient number of typical days or even typical weeks is found to reach a good system design. This is related to the description of independent typical periods, which are not able to exchange energy in between.

Therefore, the second publication [Kotzur et al., 2018b] introduces a novel state formulation that is able to account for storage inventories between aggregated typical days. Such, it is possible to also model seasonal storage with aggregated time series. With this new formulation also for the renewable based system a design could be found with 12 typical days, which is similar to the design of the benchmark system.

3.4.2 Model reformulation

Accordingly, the model in this work also considers time series aggregation with the new storage formulation. The aggregation is performed with a *hierarchical* clustering. The resulting clusters are represented by their *medoids* while the day with the minimum temperature and the day with the maximal peak load are extrinsically added as potential cluster *medoids*.

A few adaptions have to be made to the model introduced in Section 3.3 in order to integrate typical periods. First, all time steps previously described with a single index t get replaced by a two-dimensional index consisting of the time step inside a typical period g and the typical period index k. Additionally, the objective function and the storage equations have to be rewritten.

Adaption of the objective function

The objective functions get an additional parameter that weights the occurrence of a typical period inside the observation frame. This occurrence is represented by the scale of the related cluster $|C_k|$ and is integrated into the cost function from Equation 3.5 as follows:

$$\min \sum_{d} [c_{exist,d}\delta_d + c_{spec,d}D_d] + \sum_{(i,j)\in L}\sum_{k\in K}|C_k|\sum_{g\in G} c_{var,i,j,g,k}\dot{E}_{i,j,g,k}\triangle t \tag{3.23}$$

Equivalently, the GHG emission function from Equation 3.6 is adapted:

$$min \sum_{(i,j)\in L}\sum_{k\in K}|C_k|\sum_{g\in G}\gamma_{i,j,g,k}\dot{E}_{i,j,g,k}\triangle t \tag{3.24}$$

Adaption of the storage equations

The other equation set that has to be modified are the storage equations in order to respect inter-period states and inter-period energy exchange. For the advanced derivation, it is referred to Kotzur et al. [2018b]. Here, just the resulting equation set is presented, which replaces the equations introduced in 3.11 and 3.12.

The intra-period states of charge $SOC^{intra}_{s,k,g}$ are equivalent to Equation 3.11 defined as follows:

$$\begin{aligned} SOC^{intra}_{s,k,g+1} = \quad & SOC^{intra}_{s,k,g}(1-\eta^{self}_s\Delta t) \\ & +\Delta t\left[\eta^{char}_s\dot{E}^{char}_{s,k,g} - \frac{\dot{E}^{dis}_{s,k,g}}{\eta^{dis}_s}\right] \qquad \forall \quad g,k \\ SOC^{intra}_{s,k,1} = \quad & 0 \qquad \forall \quad k \end{aligned} \tag{3.25}$$

The inter period states $SOC^{inter}_{s,i}$ are formulated for all original periods i while $k = f(i)$ is a look up table that relates every original period i to its representing typical period k:

$$\begin{aligned} SOC^{inter}_{s,i+1} = \quad & SOC^{inter}_{s,i}(1-\eta^{self}_s\Delta t)^{N_g} + SOC^{intra}_{s,k=f(i),N_g+1} \qquad \forall \quad i \\ SOC^{inter}_{s,N_i+1} = \quad & SOC^{inter}_{s,1} \end{aligned} \tag{3.26}$$

The superposition of the two states $SOC^{inter}_{s,i} + SOC^{intra}_{s,k=f(i),g}$ describes then the overall state of charge of the storage.

In order to reduce the equation set given by the limitations of the state of charge in Equation 3.12, two auxiliary variables are introduced: $SOC^{intra}_{s,k,max}$ is the maximum state of charge within the typical period k and $SOC^{intra}_{s,k,min}$ is the minimal state of charge. They restrict the intra-period state of charge as follows:

$$\begin{array}{rcll} SOC^{intra}_{s,k,g} & \leq & SOC^{intra}_{s,k,max} & \forall \quad g,k \\ SOC^{intra}_{s,k,g} & \geq & SOC^{intra}_{s,k,min} & \forall \quad g,k \end{array} \tag{3.27}$$

The state of charge for the entire sequence of typical periods is then further limited to the maximal and minimal state of charge:

$$\begin{array}{rcll} SOC^{inter}_{s,i} + SOC^{intra}_{s,k=f(i),max} & \leq & D_s & \forall \quad i \\ SOC^{inter}_{s,i}(1-\eta^{self}_s \Delta t)^{N_g} + SOC^{intra}_{s,k,min} & \geq & 0 & \forall \quad i \end{array} \tag{3.28}$$

This reformulation allows the optimization of the *enercore* model together with time series aggregation.

3.4.3 Time series disaggregation

Although time series aggregation is promising, it still has a drawback: If a system design is derived based on the reduced time series data, no guarantee can be given that the resulting system design is also feasible and optimal for the full time series.

Therefore, either new aggregation methods are required, or validation optimizations with the full time series have to be performed, as done by Bahl et al. [2017]. They introduce a method which iteratively determines structure and design with aggregated time series data and validates it for feasibility with an operation optimization for the full time series.

Since this work describes all technologies by an existing related binary variable δ_d and a scale related continuous variable D_d, an even more simple approach can be chosen:

1. A structure and design optimization based on 12 aggregated typical periods is performed. This constitutes the problem class of a MILP.
2. Based on the results, all technology choices described by the binary variables δ_d are fixed by defining the binary variables as constants. This also counts for the refurbishment decisions.

3. An optimization with the full time series is performed while the operation and the technology scaling D_d are optimized. Since they are just described by continuous variables, a simple LP results.

The overall procedure is shown in Figure 3.14. The first advantage of the approach is that with a small computational load a feasible design of the energy system can be achieved. Second, a more accurate temporally disaggregated representation of the system operation results, constituting also a more accurate grid load.

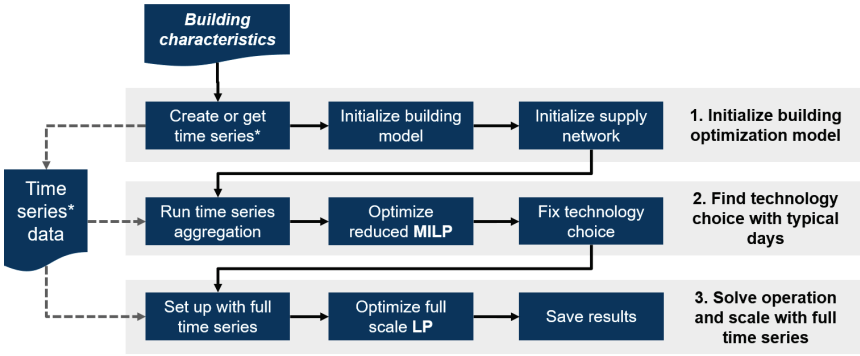

Figure 3.14: Two-level workflow of the building optimization, running once a model with an aggregated time series and afterwards with the full time series data. Time series data * are in this context the electricity load, internal heat gains, occupancy activity, photovoltaic feed-in, solar thermal feed-in, solar heat gains and the ambient temperature.

3.5 Discussion

The following section discusses the limitations and strengths of the single building optimization. Although the aggregated electricity profiles from Section 3.1 align with the validation data for Germany, the specific energy demands of single appliances deviate from the German data. In consequence, the analysis of the load change due to the integration of more efficient appliances would not be possible with a sufficient accuracy. Therefore, this work conservatively assumes that the future appliance load stays the same as today. As a future outlook, German time-usage-survey and statistics about the appliance equipment in German households could be included together with predictions of higher electrical appliance efficiencies.

Further, the model is able to differentiate between different household size and

their different demands for electricity and hot water. It is able to respect the variety of households with different cumulative electricity demands due to their different appliance equipment. The pieces of appliance equipment are randomly chosen and meet the aggregated distributions. Nevertheless, those differences are not altered by the socioeconomic background of the households, although this is the significant descriptor to determine the demand variation [Druckman and Jackson, 2008; Elnakat et al., 2016]. Still, the required data to model this effect is not publicly available. Thus, it is excluded in the model.

The techno-economic descriptions of the cost and operation of the technologies are simplified. The operation of the supply system is based on continuous variables and linear equations. In consequence, no part-load behavior or limitations, e.g. of the fuel cells, are considered. Nevertheless, its integration would introduce binary variables for every considered time step, which would magnify the overall computational load. Equivalently, the cost functions of the supply technologies are simply modeled with an existing related binary variable and a single continuous variable. Although this is an improvement to a sole continuous formulation, the cost function still has to be fitted to a certain technology scale. In consequence, the estimated cost will deviate outside the fitted range, which could lead to wrong investment decisions. This could have an impact since many different building scales are considered with varying scales of required supply systems. A solution would be a piecewise linear formulation of the cost function, as done by Milan et al. [2015]; Gabrielli et al. [2017]. Nevertheless, this would as well result in a more complex and computationally more challenging optimization problem.

A key strength is that the model can be automatically applied to all buildings given by the *EPISCOPE* database, including refurbished and non-refurbished building types for different construction years and sizes across Europe, although this work focuses on the German building stock. It is able to represent the high load variance of single households, as well as their smoothing for larger aggregations of households. Together, this allows for the later bottom-up modeling of a diverse building stock with a precise prediction of the energy demands and their temporal fluctuation.

In general, the model has a holistic perspective of residential buildings and is able to consider synergies between different solutions, e.g. demand-side measures are simultaneously considered with supply-side measures, or the operation of the heating system is optimized together with the operation of the electricity system. The latter has especially a high relevance for the case that Power-to-Heat technologies are considered, such as heat pumps or electric heaters. They can be flexibly operated, e.g. to maximize the self-consumption of photovoltaic electricity.

Further, a stochastic occupancy model temporally defining the demand for electric

device usage and thermal comfort is combined with a deterministic optimization of the whole supply and heating system. This enables the assessment of the maximal flexibility given by the building stock, without limiting the comfort level of residential occupants. The heat model especially has a high accuracy since it is able to dynamically consider the supply temperature and the thermal storage capacity of the building. On the other hand, current standards and the majority of models only rely on inelastic energy demands, calculated with a constant comfort temperature level.

Lastly, the model incorporates a complex set of decision variables, making it almost impossible to solve for a time resolution of 8760 hours. Nevertheless, the efficient integration of time series aggregation guarantees a high computational performance, which is required for applying it to the diversity of a whole building stock. In this context, two novel methods were introduced: A storage formulation based on a superposition of system states that allows the modeling of seasonal storage with time series aggregation, and a two-level optimization scheme that guarantees a feasible system design also for the full time series.

In summary, the model is novel in terms of its accuracy and holistic view of single building optimizations with the presumption of having a lean computational load. This is required because it will be applied to a regionally resolved building stock consisting of many different building types for different future scenarios.

3.6 Summary

This chapter proposed a design and operation optimization model for single residential buildings, implemented as a Mixed-Integer Linear Program. The objective of the optimization is to minimize the GHG emissions and the annual energy cost of a single building.

First, an occupancy simulation was introduced in order to determine the demand for electricity and thermal comfort in a building in Section 3.1. The resulting profiles are able to sufficiently incorporate the high variance of single residential load profiles, as well as respect the stochastic smoothing for the case that an agglomeration of households is considered.

Section 3.2 extends a thermal model for predicting the space heating demand of the building. The thermal model itself is part of the supply system optimization. It is able to account for the thermal building mass for a flexible supply system operation. Further, potential refurbishment measures are part of the solution space, such as the addition of wall or roof insulation, the replacement of windows, or the integra-

tion of smart thermostats. Additionally, a workflow was developed that can flexibly parametrize the model by a building database to consider the different shapes and envelope fabrics of different building types.

In Section 3.3, the supply system model was set up with a generic energy system framework whose formulation is adapted to better integrate the heating supply systems. The framework is object-oriented and standardizes the mathematical description of different technologies to different technology classes. While this leaves, in general, open which supply technologies are considered, a superstructure of the relevant residential supply technologies was defined for this work.

All in all, the combinatorial consideration of demand-side measures together with supply-side measures states a complex mathematical program that is computationally heavy. In order to keep the program tractable for many different building types and scenarios, time series aggregation was introduced in Section 3.4 to reduce the complexity of the model. Therefore, different clustering methods were compared and the most suitable is chosen. Additionally, a novel description of storage states is introduced which allows for an energy exchange between different typical periods. Lastly, a novel two-level optimization approach was introduced which significantly reduces the accuracy losses due to the time series aggregation.

The discussion in Section 3.5 concluded that the single building model has a holistic perspective of energetic measures in residential buildings. Nevertheless, its degree of detail is adapted to the requirement of having a lean computational load and the data available.

Chapter 4

Aggregation of an archetype building stock

The following chapter introduces a novel algorithm to aggregate a spatially resolved representative building stock which is used to scale the results of single building optimizations to a nationwide perspective. Therefore, the first Section 4.1 introduces existing approaches to model a building stock for energy performance analysis. Section 4.2 discusses the relevant attributes to describe the energy performance of a building. Afterwards, a novel aggregation algorithm is introduced in Section 4.3 which determines building archetypes to represent the distribution of building types on the municipality level. Section 4.4 illustrates and validates the algorithm for the case of Germany. The chapter closes with a discussion in Section 4.5 and a summary in Section 4.6.

4.1 Existing definitions of building archetypes

The representation of a building stock by a set of archetype buildings is widespread in the realm of modeling strategies for carbon dioxide emission reductions, as discussed in Section 2.1. Existing archetype building databases and approaches to create such databases are introduced in the following section.

In 2010, the *European Union* introduced the Energy Performance of Buildings Directive [EU, 2012]. It prescribes the analysis of the cost optimality of the national regulations for a minimum efficiency standard in the building stock at this time. The analysis should be performed based on a set of representative reference buildings.

In this context, [Corgnati et al., 2013] introduced different pathways to determine representative reference buildings for the analysis of cost optimal refurbishment measures:

1. *Example reference buildings* based on expert assumptions and studies. Those are manually defined to represent a group of buildings in case no statistical data are available and the parameters are based on the creator's best knowledge.

2. *Real reference buildings* that are the most common buildings of a certain category of buildings. Those have high accuracy, but their aggregation is data-intensive since a large data set of existing buildings is required that can be clustered to certain building classes.

3. *Theoretical reference buildings* that represent statistical data of a certain building stock by a composite of attributes, but do not have to exist as such in reality.

Although the pathways would be independently imaginable, Corgnati et al. [2013] concluded that in reality most often a mixture of the pathways is chosen due to different data available.

The most popular archetype database for the German residential building stock is provided by the *Institute für Wohnen und Umwelt* and has been under steady development since 1990 [IWU, 2005, 2010]. It is derived from real example buildings as well as statistical data about the nationwide building stock itself. It categorizes the stock into classes differing by construction year and scale. Each class is represented by a typical building, which is described with technical values such as the U-values of the wall and roof, or the area and orientation of windows. It is mainly used for static calculations and analysis of the energy saving potentials by changing or adding the insulation in different building classes. The data and method are available open-source, constituting the high popularity of the database. Further, this stock description has been extended to other European countries in the framework of the *EPISCOPE* project [EPISCOPE, 2016].

The *Department of Energy (DOE)* also introduced a set of archetype buildings for the residential sector [Hendron and Engebrecht, 2010] and the service sector [Torcellini et al., 2008] in the USA, referred to as benchmark or prototype buildings. These building definitions are under steady development by different national labs and are used for energy performance analysis as well. An advantage to the German *IWU* database is that additional time series data is provided for the different building types, e.g. including electricity, hot water, cooling or heating demand for

typical days in different climate zones. Therefore, these profiles and data can easily be used for dynamic models of energy supply systems, incorporating electricity supply and storage technologies.

Mata et al. [2014] proposed an analytical methodology to aggregate archetype building stocks for France, Germany, Spain, and the UK, based on publicly available data. The steps include:

1. a *segmentation* based on different categories, such as construction year or type,
2. a technical *characterization*, e.g. the thermal transmittance as input values for energy performance models,
3. and a *quantification* to scale them up to a nationwide level.

The data considered for Germany mainly relies on the introduced *IWU* database. The aggregated archetype buildings are then used to parameterize an energy performance model to predict the space heating, hot water and electricity demands on a nationwide level. Such calculated final energy demand shows a deviation from -4% to + 2% to the statistic values of the residential final energy demand in the countries.

The aggregation to archetype buildings is also widespread in the context of urban energy models: Cerezo et al. [2015] and Sokol et al. [2017] introduced methods to estimate unknown attributes of the proposed archetype buildings, such as comfort temperature levels, based on a probability distribution. The approach can make use of measured energy data in different buildings, e.g. annual or monthly gas demand, and fits the uncertain attributes to it. Although the resulting model has high accuracy, it is computationally intensive since many different simulations are performed and a highly resolved measured energy demand data set is required, which is not available for the whole of Germany.

Further, Fazlollahi et al. [2014] and Fonseca and Schlueter [2015] use k-means clustering methods to group similar buildings to urban areas. The location of the buildings and spatially resolved statistical attributes describe them. The clustered buildings are then accumulated to different zones in the analyzed district. The advantage of the clustering is that the simulation models or optimization models can be applied to the zones instead of the single buildings, reducing the number of variables and computational load of the related models.

Sandberg et al. [2016] introduces a stock model with the focus to dynamically predict construction, demolition and renovation rates in different European Countries.

It does not rely on single archetype buildings; instead, it describes top-down the whole building stock by statistical values, also related to attributes such as population development. Although it provides useful data for prediction of age structures in the building stock, the approach alone is not suitable for the modeling of the energy performance.

In summary, many different approaches for the aggregation and segmentation of archetype buildings have already been introduced. Nevertheless, none of the studies aggregate a nationwide archetype building stock that is spatially resolved and can be used to predict detailed temporally and spatially resolved energy performance analysis. Further, it can be concluded that the quality of the descriptions of the archetype buildings is highly dependent on the availability of data, making the generalization of the approaches challenging.

4.2 Relevant building attributes

In order to determine the required data for a sufficient building aggregation for Germany, this section discusses the relevant attributes for describing the energy performance of a building. It starts with a general description of attribute categories in Section 4.2.1 and introduces the data sets that are available for Germany in Section 4.2.2.

4.2.1 General attribute categories

As starting point, the relevant attributes to perform an energy analysis need to be introduced to describe the archetype buildings.

Depending on the focus of the analysis, different categorizations of the attributes are imaginable. Table 4.1 exposes the categories found in the literature and the nomenclature considered in this thesis.

In general, four categories are emphasized in the literature: The *Form* describes the physical exterior shape of the building, including orientation, wall, and roof areas. The *Envelope* characterizes the physical properties of materials used in the building. The technologies installed in the buildings to satisfy thermal comfort and other demands are grouped in the category *System*. The *Operation* summarizes all extrinsic conditions determining the system operation such as weather or occupancy behavior.

Table 4.1: Attribute categorization for energy performance models.

DOE [Torcellini et al., 2008]	Corgnati et al. [2013]	Mata et al. [2014]	This work	Examples
Form	Form	Building type	Form	Area, number of floors, orientation
Fabric	Envelope	Construction year	Envelope	U-values, window transparency, thermal capacity
Equipment	System	Heating system	System	Heat technology, efficiencies, photovoltaic capacity
Program	Operation	Climate zone	Operation	Location, comfort level, occupancy
-	-	-	Adoption	Ownership, interest rate

Further, this work also models the cost optimal technology adoption of the different buildings, in addition to the energy performance of the status quo. Therefore, the category *Adoption* summarizes all attributes referring to the investment capabilities of the building owner.

4.2.2 Considered attributes for the aggregation

The categories discussed define a general framework to segment buildings, but the required attributes depend on the model and the data availability. E.g., the envelope could be described by materials with exact heat conductivities and thicknesses, just heat transfer coefficients, or by the construction year of the building from which these values are derived.

The attributes considered for the aggregation procedure of this thesis are oriented towards the introduced model in Chapter 3 and the data especially provided by the Census [Bundesamt, 2011]. Figure 4.1 shows the aggregated Census data for Germany. It is dominated by above 12.3 million single-family houses and 6.3 multi-family houses, while buildings with more than 12 apartments have with 0.21 million a small share at the total building number. The majority of the SFH are detached, constituting an overall small proportion of terraced and semi-detached buildings.

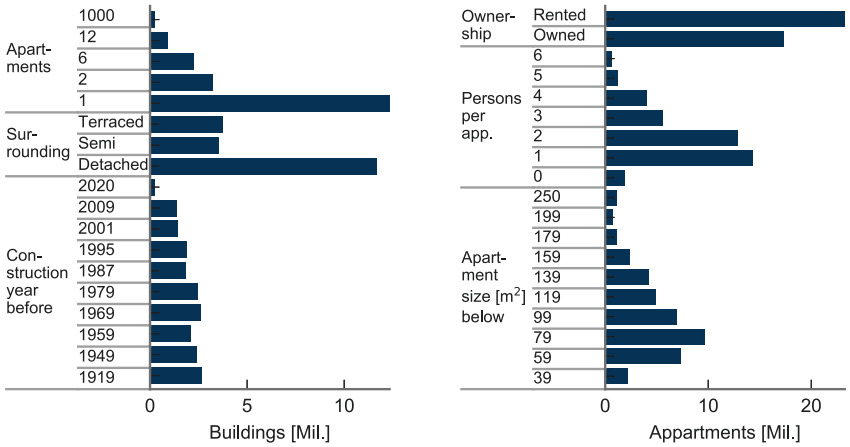

Figure 4.1: Attribute distribution of the German building stock based on the Census [Bundesamt, 2011].

The relative amount of buildings for construction years after 1995 seems relative low but it is explained by the shorter observation intervals. Therefore, an almost uniform distribution of constructions per year is recognizable for the period after 1949. Nevertheless, this is differing for the various building sizes but not identifiable on an aggregated level. 23.2 million of the 40.5 million apartments are rented, while one- and two-person households dominate with together 27.1 million households. Those also constitute the peak of apartment sizes at compact living areas 59 to 79 m^2 per household, while the bigger single-family houses spread over a higher bandwidth.

All these distributions are also available on an absolute scale for the municipalities in Germany and state the data basis for the considered archetype aggregation, as shown in Figure 4.2. Nevertheless, some additional values are required. Therefore, the following section introduces their derivation and the specific consideration of the Census data.

Form attributes

The **building orientation** is expressed by the azimuth angle and is relevant for the solar irradiance on roof and walls. Although it could be considered continuously, it

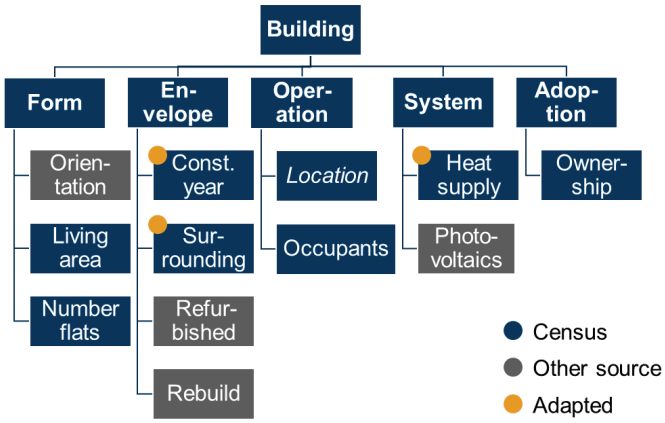

Figure 4.2: Structure of the considered attributes relevant for the building energy supply.

is categorically modeled to reduce the number of variants. New approaches use satellite image recognition [Mainzer et al., 2017] to determine the roof shapes, even including shadowing effects such as *Google Sunroof*, which is provided by *EON* [EON, 2018]. Nevertheless, no available data sets about the roof orientation were found on a German-wide municipality level. Therefore, a uniform distribution is assumed for all municipalities, similar to the approach of Mainzer et al. [2014].

The **living area** per flat and the **number of flats** per building determine the size and type of the building. The data is directly provided by the Census on the municipality level [Bundesamt, 2011]. The exact building shapes are then derived from the IWU-type buildings, as introduced in Section 3.2.2.

Envelope attributes

The **construction year** or age of a building is also provided for different intervals on the municipality level [Bundesamt, 2011]. Nevertheless, the intervals do not align with the intervals of the IWU data [IWU, 2010], wherefore they are adapted. A uniform distribution of constructions per year is assumed for every provided interval of construction years. The constructions per year are then superimposed and adjusted to the intervals of the IWU data. The constructions' years characterize the physical properties of the building envelope, given by the IWU database.

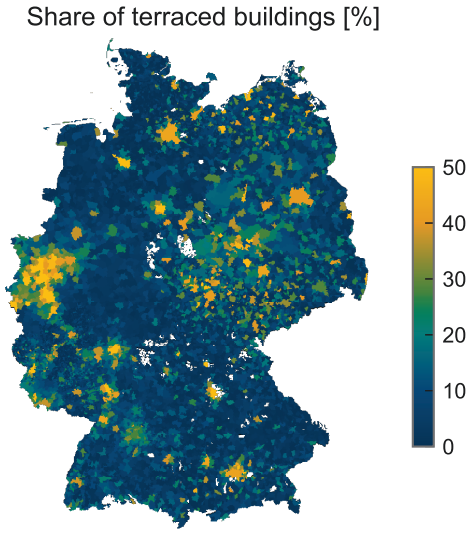

Figure 4.3: Relative share of terraced buildings in the different municipalities in Germany [Bundesamt, 2011], an example of the spatial distribution of the different considered building attributes.

The **surrounding** of the buildings is provided by the segments *detached, semi-detached, terraced* and *other* from the Census data [Bundesamt, 2011]. Since a sufficient energetic evaluation can just be performed with the first three categories, the segment *other* is assumed to be *semi-detached* as well. This constitutes the smallest error in case the buildings related given in the category *other* are *detached* or *terraced*, since *semi-detached* states the mean category. Further, the distributions of the three categories fit with the adaption to the distributions of the highly spatially resolved GIS analysis performed by Hartmann et al. [2016]. The spatial distribution, e.g. of the share of *terraced* buildings, is illustrated in Figure 4.3, highlighting their main appearance in urban areas.

Since the building stock shall be extrapolated into the future, new constructions are additionally integrated by **rebuilding** existing buildings. The data is derived from the *Regionaldatenbank*, which has provided statistics about new constructions in the different municipalities since 2008 [GENESIS, 2018]. Based on those, a municipality specific mean construction rate is derived for the years 2008 till 2015, which is then extrapolated until the year 2050. The amount of newly constructed build-

ings is limited by the number of buildings that are already constructed until the year 1987. Their integration will be further discussed and visualized in Section 4.5.1.

Operation attributes

The **location** of the buildings is determined by fitting their appearance to the centroid of the municipalities. The location is continuously modeled and described by the longitude and latitude. The resulting location determines the climate conditions and weather time series for the energy performance modeling of the archetype building. The results are later uniformly distributed over the municipalities.

The number of **occupants per flat** determines the occupancy behavior with their related demand for thermal comfort, hot water and their usage of electrical appliances in the building. It is directly extracted from the Census data set [Bundesamt, 2011]. The distribution of vacant apartments is added as attribute expression with zero occupants.

System attributes

The existing **heat supply** technology is derived from a combination of the Census data [Bundesamt, 2011] and a study that provides data about the heat supply on the federal state level [BDEW, 2015]. The spatially resolved data basis is given by the Census data, which differentiates between district heating, CHP supply, central heating, single-story heating and apartment heating units. While district heating and CHP supply can be directly used in the model, the other categories need to be further subdivided by the category specific heating technology distribution given by BDEW [2015] to gas boilers, oil boilers, pellet boilers and heat pumps.

Existing **photovoltaic** installations are derived from the *EEG-Anlagenregister* [Energymap, 2015], which is a collection of renewable energy plants that are regulated by the EEG and registered until 2015. The above 1.5 million data entries are filtered for rooftop photovoltaics below 250 kW, which are then assigned to the different municipalities. No spatially resolved data for solar thermal collector installations were found.

Adoption attribute

To capture different investment behavior, the type of **ownership** of the building is considered as well. It is differentiated between buildings where the occupants are also the owner of the building and buildings which are rented. The required data is provided for the apartments by the Census Bundesamt [2011].

4.3 Aggregation algorithm

The previously introduced spatially resolved attribute distributions need to be aggregated to a limited set of archetype buildings to evaluate them energetically.

Thereby, two challenges arise: First, the buildings are described by a mixture of categorical and continuous attributes. Approaches exist to deal with this type of aggregation class, such as the mixture of *k-means* and *k-modes* clustering, referred to as *k-prototypes* [Huang, 1998]. Nevertheless, they would rely on a data set consisting of real buildings which should be clustered and can then be represented, e.g. by its medoid. This does not apply to the case of the previously introduced data sets since only statistics of building attributes are provided and no real instances of buildings. Therefore, a new aggregation methodology is required.

The related mathematical problem formulation of representing the data by a limited set of archetype buildings is introduced in Section 4.3.1. The applied solving algorithm is then derived in Section 4.3.2.

4.3.1 Mathematical problem formulation

Each categorical attribute $p \in P$ has a set of discrete expressions $m \in M(p)$. E.g., the attribute heating system has the expressions oil boiler or gas boiler. Every node $n \in N$, in our case the municipalities, has a distribution $d_{n,m,p}$ of these attributes' expressions, e.g. the number of oil boilers in a municipality. Further, every node has a set of continuous attributes $c \in C$ on a cardinal scale with the value $y_{n,c}$, in our case the longitude and latitude of every municipality.

These attributes shall be represented by a limited set of archetype buildings $b \in B$. These archetype buildings occur $\beta_{b,n}$ times in every node n, represented by the whole variable set $\boldsymbol{\beta}$. This occurrence can be defined either as an integer variable or as a continuous variable for a relaxed approach. The categorical expressions

that describe the buildings are defined by the binary variable $\delta_{b,p,m}$, which is one if the building-attribute p expresses as m and zero otherwise. They belong to the set $\boldsymbol{\delta}$. The continuous expressions of the buildings are described as $\mu_{c,b}$, belonging to the variable set $\boldsymbol{\mu}$.

Additionally, weighting factors w_p and w_c are considered to weight the categorical and cardinal attributes according to their relevance for the energy performance analysis.

In order to fit the archetype buildings to the data, a prediction error is defined, describing the deviation between the statistical data and the archetype buildings representing such. For the case of the continuous attributes, it is expressed as follows:

$$e_c = \sum_{n \in N} \sum_{c \in C} w_c \left| d_{n,c} - \sum_{b \in B} \beta_{b,n} \varphi_c \left(y_{c,n}, \mu_{c,b} \right) \right| \tag{4.1}$$

$d_{n,c}$ is thereby the given number of buildings in every node n for every continuous attribute c, e.g. the absolute number of buildings in a municipality given by the Census. $y_{c,n}$ is the expression of the continuous attribute in the node, e.g. the longitude of the centroid of a municipality. This number has to be represented by the archetype building types $\beta_{b,n}$ located at the node. The distance between the continuous attribute expression of the archetype building $\mu_{c,b}$ and the expression in the node $y_{c,n}$ is evaluated by the fit function φ_c, which is one in case of identical attributes and zero if they have the maximal distance. The overall absolute error would converge to zero, if all buildings belonging to the municipality $\beta_{b,n}$ would have a perfect fit $\varphi_c \left(y_{c,n}, \mu_{c,b} \right)$ of one. The distance metric of the expressions is described by the following distance function:

$$\varphi_c \left(y_{c,n}, \mu_{c,b} \right) = 1 - \left[\frac{y_{c,n} - \mu_{c,b}}{\max_{n \in N} y_{c,n} - \min_{n \in N} y_{c,n}} \right]^2 \tag{4.2}$$

The error equation 4.1 together with the distance function 4.2 alone would state a special form of k-means clustering [Jain, 2010].

Nevertheless, the overall error is also determined by the fit of the categorical attribute distributions with the following equivalent error function:

$$e_p = \sum_{n \in N} \sum_{p \in P} w_p \sum_{m \in M(p)} \left| d_{n,m,p} - \sum_{b \in B} \beta_{b,n} \delta_{b,p,m} \right| \tag{4.3}$$

The categorical fit function is in this case simply expressed by a binary variable $\delta_{b,p,m}$, which is one if the archetype building has the categorical expression m and is zero otherwise. The goal is to fit the number of buildings $d_{n,m,p}$ in the node n with the categorical expression m.

Additionally, a constraint is required that defines that every archetype building can only have a single categorical expression of the related attribute p:

$$\sum_{m \in M(p)} \delta_{b,p,m} = 1 \quad \forall \quad b \in B, p \in P \tag{4.4}$$

E.g., the building can only be detached, semi-detached, or terraced, but not multiple categories simultaneously.

Lastly, a hard constraint is introduced that the number of buildings in every node b_n has to be represented by an equivalent number of archetype buildings:

$$b_n = \sum_{b \in B} \beta_{b,n} \quad \forall \quad n \in N \tag{4.5}$$

Overall, the cumulative error expressions 4.1 and 4.3 shall be minimized while holding the constraints 4.4 and 4.5. This defines the following mathematical problem $P(\boldsymbol{\beta}, \boldsymbol{\delta}, \boldsymbol{\mu})$ to determine the best representative set of archetype buildings:

$$\begin{aligned} \min_{\beta,\delta,\mu} \quad & \sum_{n \in N} \sum_{c \in C} w_c \left| d_{n,c} - \sum_{b \in B} \beta_{b,n} \varphi_c \left(y_{c,n}, \mu_{c,b} \right) \right| \\ & + \sum_{p \in P} w_p \sum_{m \in M(p)} \left| d_{n,m,p} - \sum_{b \in B} \beta_{b,n} \delta_{b,p,m} \right| \\ \text{s. t.} \quad & \sum_{m \in M(p)} \delta_{b,p,m} = 1 \quad \forall \quad b \in B, p \in P, \\ & b_n = \sum_{b \in B} \beta_{b,n} \quad \forall \quad n \in N, \\ & \beta \in \mathbb{Z}^{\geq 0}, \mu \in \mathbb{R}, \delta \in \{0, 1\}, \end{aligned} \tag{4.6}$$

It is nonlinear, combines binary with continuous variables, and has non-derivable elements, such as the absolute evaluation of the error term. All in all, it determines a Mixed-Integer Nonlinear Program (MINLP) that is challenging to solve for a global optimal solution for a large set of nodes and attributes.

4.3.2 Solving algorithm

Since a direct determination of the global optimal solution is almost impossible, an alternative approach is required to find optimal sets of archetype buildings: First, the absolute expressions in the objective function in Equation 4.6 are simplified to a quadratic measure to get a derivable objective term. Second, a novel greedy

algorithm is introduced with the goal to determine a locally optimal solution. It is inspired by the concept of an expectation-maximization algorithm, whereto Lloyd's k-means clustering algorithm [Lloyd, 1982; Jain, 2010] and the k-prototypes algorithm [Huang, 1998] belong as well.

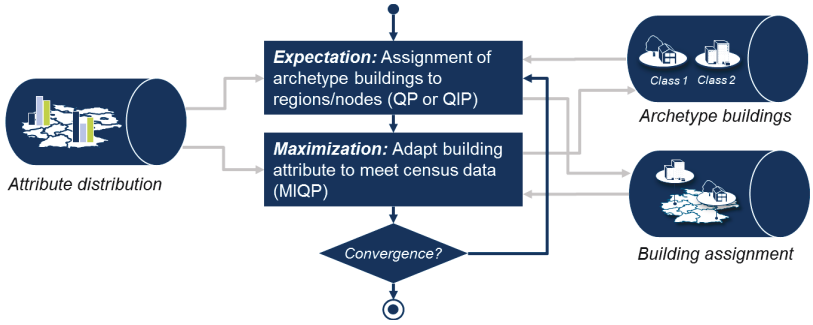

Figure 4.4: Structure of the developed algorithm to determine a spatially distributed archetype building stock.

The idea is to describe the assignment of the archetype buildings to the different nodes $\beta_{b,n}$ as the expectation step, with the objective to get in every municipality a representation of the attribute distributions by the most likely archetype buildings. Nevertheless, the attributes of the archetype buildings themselves are unknown wherefore their estimation $\mu_{c,b}, \delta_{b,p,m}$ is defined as the maximization step, illustrated in Figure 4.4. It results in two sub-problems that can be iteratively solved.

Therefore, the problem is restructured as follows:

1. Problem as expectation step: Fix the attributes of the archetype buildings as $\boldsymbol{\mu} = \hat{\boldsymbol{\mu}}$ and $\boldsymbol{\delta} = \hat{\boldsymbol{\delta}}$ and solve $P_1 = P(\boldsymbol{\beta}, \hat{\boldsymbol{\delta}}, \hat{\boldsymbol{\mu}})$ to determine the building assignment β. The problem is described as follows:

$$\begin{aligned} \min_{\beta} \quad & \sum_{n \in N} \sum_{c \in C} w_c \left[d_{n,c} - \sum_{b \in B} \beta_{b,n} \varphi_c \left(y_{c,n}, \hat{\mu}_{c,b} \right) \right]^2 \\ & + \sum_{p \in P} w_p \sum_{m \in M(p)} \left[d_{n,m,p} - \sum_{b \in B} \beta_{b,n} \hat{\delta}_{b,p,m} \right]^2 \\ \text{s. t.} \quad & b_n = \sum_{b \in B} \beta_{b,n} \quad \forall \quad n \in N, \\ & \beta \in \mathbb{Z}^{\geq 0} \end{aligned} \tag{4.7}$$

This states a Quadratic Integer Program (QIP). A relaxed version with many different buildings per node could be formulated with continuous variables for the num-

ber of buildings $\beta \in \mathbb{R}_{\geq 0}$ and would result in a Quadratic Program (QP) that can be solved with low computation load.

2. Problem as maximization step: Fix the assignment of the archetype buildings $\boldsymbol{\beta} = \hat{\boldsymbol{\beta}}$ and solve $P_2 = P(\hat{\boldsymbol{\beta}}, \boldsymbol{\delta}, \boldsymbol{\mu})$ to determine the new archetype building attributes $\boldsymbol{\delta}$ and $\mu_{c,b}$. The mathematical problem is stated as follows:

$$\begin{aligned} \min_{\delta,\mu} \quad & \sum_{n\in N}\sum_{c\in C} w_c \left(d_{n,c} - \sum_{b\in B} \hat{\beta}_{b,n} \varphi_c \left(y_{c,n}, \mu_{c,b} \right) \right)^2 \\ & + \sum_{p\in P} w_p \sum_{m\in M(p)} \left(d_{n,m,p} - \sum_{b\in B} \hat{\beta}_{b,n} \delta_{b,p,m} \right)^2 \\ \text{s. t.} \quad & \sum_{m\in M(p)} \delta_{b,p,m} = 1 \quad \forall \quad b \in B, p \in P, \\ & \mu \in \mathbb{R}, \delta \in \{0,1\}, \end{aligned} \tag{4.8}$$

This would state a large-scale Mixed-Integer Quadratic Program (MIQP). Nevertheless, its structure allows it to be decomposed into different sub-problems for each continuous attribute c and categorical attribute p. Their cumulative optimal solution states also the overall optimal solution.

For the categorical attributes $\boldsymbol{\delta}$ the following sub-QIPs are stated and deterministically solved:

$$\begin{aligned} \min_{\delta} \quad & \sum_{n\in N}\sum_{m\in M(p)} \left(d_{n,m,p} - \sum_{b\in B} \hat{\beta}_{b,n} \delta_{b,p,m} \right)^2 \\ \text{s. t.} \quad & \sum_{m\in M(p)} \delta_{b,p,m} = 1 \quad \forall \quad b \in B, \qquad \forall \quad p \in P \\ & \delta \in \{0,1\}, \end{aligned} \tag{4.9}$$

The continuous attributes $\boldsymbol{\mu}$ on the other hand can be directly calculated as follows:

$$\mu_{c,b} = \frac{\sum_{n\in N}\sum_{b\in B} \hat{\beta}_{b,n} y_{c,n}}{\sum_{n\in N}\sum_{b\in B} \hat{\beta}_{b,n}} \quad \forall \quad c \in C \tag{4.10}$$

The step is equivalent to the maximization step of the k-means algorithm [Huang, 1998].

The building assignment problem and the attribute adaption problem are iteratively solved until a convergence criterion is met, which can be either a minimal change

of the objective function value of the overall problem, or a maximal number of iterations.

The **overall algorithm** is given as follows:

1. Choose an initial set of random building attributes $\hat{\boldsymbol{\delta}}^0$ and $\hat{\boldsymbol{\mu}}^0$, and solve $P_1 = P(\boldsymbol{\beta}, \hat{\boldsymbol{\delta}}^{\mathbf{0}}, \hat{\boldsymbol{\mu}}^{\mathbf{0}})$ to obtain the building assignment $\hat{\boldsymbol{\beta}}^0$. Set the iterator to $t = 0$.
2. Solve $P_2^t = P(\hat{\boldsymbol{\beta}}^{\boldsymbol{t}}, \boldsymbol{\delta}, \boldsymbol{\mu})$ to obtain the building attributes $\hat{\boldsymbol{\delta}}^{t+1}$ and $\hat{\boldsymbol{\mu}}^{t+1}$.
3. Solve $P_1^t = P(\boldsymbol{\beta}, \hat{\boldsymbol{\delta}}^{\boldsymbol{t+1}}, \hat{\boldsymbol{\mu}}^{\boldsymbol{t+1}})$ to obtain the building assignment $\hat{\boldsymbol{\beta}}^{t+1}$.
4. If a convergence criterion is met, e.g $\left|P_1^t - P_1^{t-1}\right| \leq \epsilon$ or $t = t_{max}$, stop. Otherwise set $t = t + 1$ and go to 2.

In general, it is observed that the sequence of $P^t(\beta, \delta, \mu)$ is strictly decreasing to a minimum value which will be shown in the next section at the example of the considered attribute set for the German municipalities.

4.4 Validation aggregation algorithm

The following section applies the novel algorithm to the data set introduced in Section 4.2.2.

The initial guess of the archetype building attributes, the start solutions for the algorithm, are derived from the archetype buildings provided by the IWU database, while missing parameters are randomly generated, e.g. the number of persons living in an apartment. The iteration limit of the algorithm is set to four. The algorithm is applied once to different predefined numbers of archetype buildings with a single initial attribute guess. Additional information such as the weightings are found and discussed in the Appendix B.2.

The resulting objective function evaluations, defined by the cumulative squared error, are illustrated for the different iteration steps and an increasing number of archetype buildings in Figure 4.5 for a uniform weighting of the attributes. The visualization of the error on the linear scale reveals a high gap between the solution of the first iteration step and the second iteration step, reducing the error measure by a factor of 5 to 20. This illustrates the high improvement of the first attribute adaption of the building archetypes to fit the overall Census data. It is valuable since the first archetype buildings are initialized by the IWU database that defined the state-of-the-art representative archetype buildings in Germany.

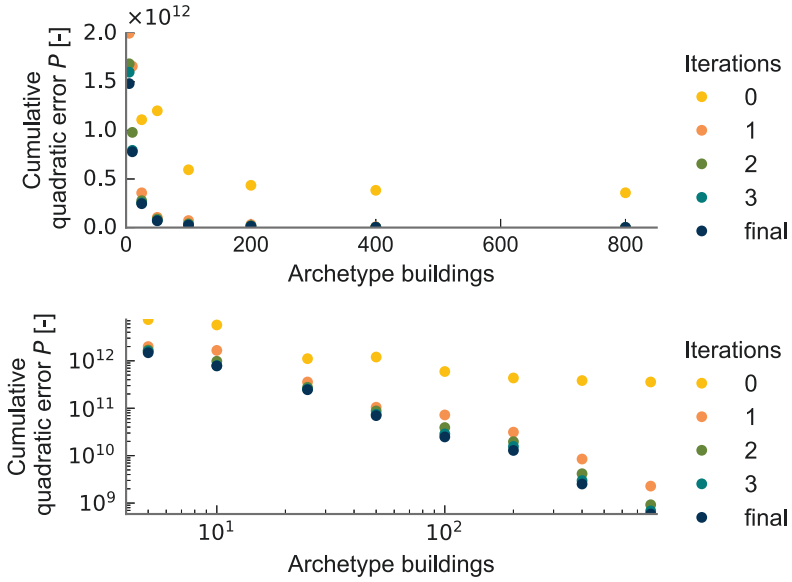

Figure 4.5: Objective function value as the squared error between the attributes estimated with archetype buildings and the given distributions on the municipality level, for different iteration steps and numbers of archetype buildings - top on an absolute scale and bottom on a logarithmic scale.

The following iteration steps constitute smaller improvements that become marginal from the third to the final iteration step. It embodies the statement that the algorithm is converging to a minimum value. Although it is probably only a local minimum, it states a high improvement to the initial guess of archetype buildings.

As expected, an increasing number of archetype buildings reduces the overall error measure and allows a more accurate representation of the Census data. While no improvement is observable between 50 and 800 archetype buildings on the linear scale, the logarithmic scale reveals that with an increasing number of archetype buildings the error gets reduced with an almost constant gradient. Therefore, an exponential decay function would describe best the accuracy improvement with an increasing number of archetype buildings, highlighting the convergence to an error close to zero for a sufficient number of archetype buildings. For the considered application case, it should at the latest converge to zero with 18 million archetype buildings, representing the full set of existing residential buildings in Germany.

Further, it is noticeable that for a high number of archetype buildings the initial solution error stays on a given offset and does not decrease with an increasing number of archetype buildings. It is mainly related to the choice of the initial set of archetype buildings derived from the IWU database: It is just based on 55 archetype buildings that are repetitively initialized for higher numbers of archetype buildings, except for the randomly chosen attributes, such as longitude or latitude. Therefore, an increasing number of initial guesses does not significantly increase the diversity of attribute combinations. Although this leads to a limited accuracy gain for the initial archetype guess for high numbers of archetype buildings, this drawback is compensated with every attribute adaption step for higher iteration numbers.

Since the evaluation of the absolute value of the overall error measure is inconclusive, the fitting of the different attributes for different numbers of archetype buildings is further illustrated in Figure 4.6 for the final iteration step. It is defined as the cumulative deviation of the representation of an attribute expression m for every region in ratio to the total attribute manifestations for the whole of Germany:

$$f(p,m) = \frac{\sum_{n \in N} d_{n,m,p} - \left| d_{n,m,p} - \sum_{b \in B} \beta_{b,n} \delta_{b,p,m} \right|}{\sum_{n \in N} d_{n,m,p}} \quad \forall \quad p, m \tag{4.11}$$

The figure shows that for some of the attribute expressions, already a small number of archetype buildings is able to represent them sufficiently, such as single-family houses with a single apartment or energy supply with gas boilers. These are attribute expressions that often occur in the original data set. Therefore, they are represented first by the archetype buildings to reduce the overall error. Nevertheless, attributes such as a CHP, heat pump supply, or apartments with a living area smaller than 39 m^2 rarely occur in the Census set. Therefore, the algorithm has a secondary priority to represent them and focuses instead on building attributes that exist more often. E.g., no archetype building was created with a heat pump supply for 5, 25 and 50 archetype buildings because the overall share of heat pump supply in Germany is below 2 %. Thus, it would not be efficient to sacrifice an additional archetype building.

For 800 archetype buildings, 50 of the 55 attribute expression fits lay above a value of 90%. Only rarely occurring attributes, such as a construction year above 2009, are still not well represented. Nevertheless, often occurring attribute expressions (45 of 55) are already fitted above 80 % for 200 archetype buildings, such as the different orientations, the building surroundings, or the number of persons.

The majority of attribute expressions get strictly better fitted with an increasing number of archetype buildings. Nevertheless, some attribute fits are first reduced and then increased again wherefore two explanations are possible: First, the algorithm converges only to a local optimum wherefore the different initial guesses could con-

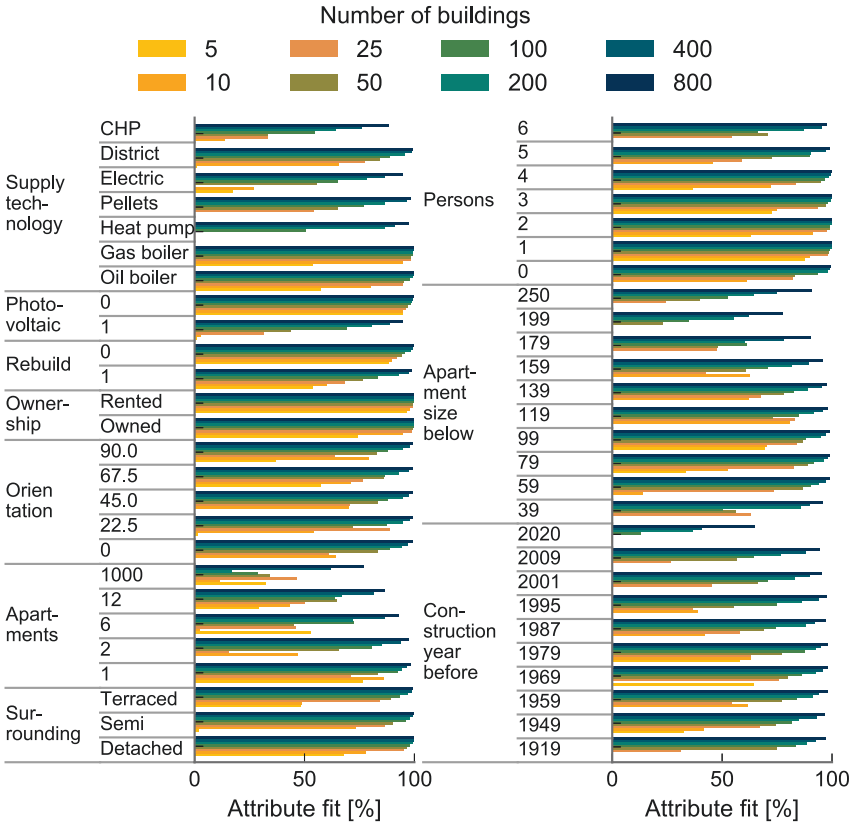

Figure 4.6: Relative fit of all categorical attribute expressions for different numbers of archetype buildings in Germany.

stitute different local minima which are suboptimal on a global evaluation. Second, a trade-off to the other attribute fits is made, and it could be more efficient to sacrifice the accuracy of one attribute to the accuracy of others. The second explanation is more likely since it is supported by the visualization of the total quadratic error, which is strictly decreasing with an increasing number of archetype buildings, shown in Figure 4.5.

In general, this is to clarify that a fit below 100 % does not imply that the expression is highly under-represented on the aggregated level: While an overestimation

of an attribute in one region and an underestimation in the other regions constitute a reduced fit, they could add up and compensate for each other out on an aggregated nationwide level, which is visualized in detail in Appendix B.2. The relative fit for Germany is shown in Table 4.2. It is defined by the total number of attribute expressions that are fitted in ratio to the total number of attribute expressions of the input data. Already with a small number of 25 archetype buildings, 90.4 % of the attribute diversity can be met on a nationwide scale. For 800 archetype buildings, an aggregated fit of even 99.5 % is reached.

Table 4.2: Relative fitting of the German-wide attribute distributions for a varying number of archetype buildings.

Archetype buildings	5	10	25	50	100	200	400	800
Aggregated fit [%]	54.3	81.4	90.4	93.9	96.2	98.2	98.9	99.5

The fitting of the continuous attributes, the latitude and longitude, is qualitatively illustrated in Figure 4.7 with their exact placement in Germany. For the case of 5 to 25 archetype buildings, all buildings are primarily located in the center of Germany. The reason is that building archetypes are mainly used to represent the diversity of categorical attribute combinations that are spatially distributed over Germany. E.g., a single-family house from 1960 with a four-person family and gas boiler supply manifests as an archetype building that represents this building type in Kiel as well as in Munich. For higher numbers of archetype buildings from 100 to 800, the geospatial location of the archetype buildings is spreading since similar categorical building types can be instantiated multiple times. In the case of 800 archetype buildings, it is even observable that in urban areas more archetype buildings are located to represent such.

Additionally, obstacles exist where building archetypes are located outside Germany. This happens because Germany has a non-convex shape: For the case that an archetype building represents buildings in municipalities whose line connection lays partially outside of Germany, the archetype building is also placed outside of Germany.

Nevertheless, the placement of archetype buildings at the borders of Germany is still avoided, which is typical for an aggregation algorithm and would appear as well for a conventional clustering approach. It is further illustrated in Figure 4.8 that introduces the local assignment of example archetype buildings selected from the set of 800 archetype buildings. The locations of the archetype buildings are the centroids of the buildings they represent. Since these clusters are spatially spread over different municipalities, the centroid is not placed at a municipality at

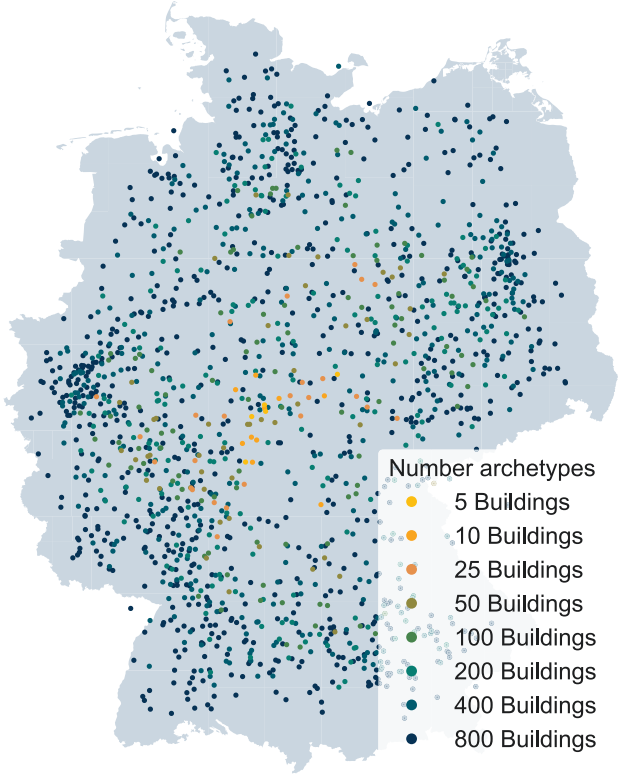

Figure 4.7: Geographical location of different numbers of archetype buildings in the final iteration step.

the border.

Further, it is recognizable that the areas and the amounts that are represented differ between the different archetypes: While an archetype building supplied with heat pumps must represent buildings over a large area, archetype single-family houses supplied by gas boilers have a definite local assignment area. The reason is that more archetype buildings with gas boilers are selected since also more buildings with gas boilers exist in reality. Therefore, the algorithm chooses for them a higher spatial separation to minimize the overall error, while accepting higher geospatial errors for the buildings with heat pumps.

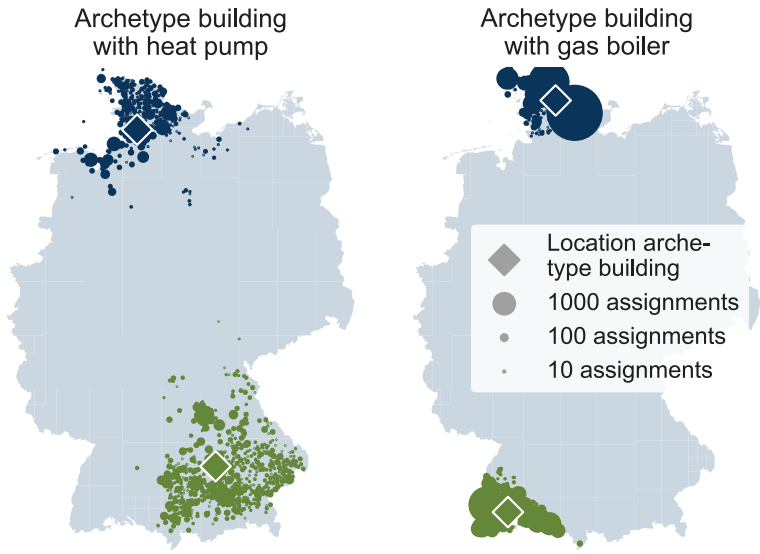

Figure 4.8: Location of the most northern (blue) and most southern (green) single-family house archetype with heat pump supply (left) and gas boiler supply (right) of the set of 800 archetype buildings, and their assignment to the different municipalities.

This illustrates the advantage of a numerical aggregation of archetype buildings since it can reasonably balance the different aggregation errors on multiple dimensions.

The explicit local assignment has the advantage of a high spatial resolution that is especially relevant for the consideration of local weather conditions. Nevertheless, in consequence, some municipalities are dominated by the representation of a few archetype buildings whose energy performance will dominate the energy performance prediction of the building stock in the whole region. If one of these archetype buildings is exceptional, e.g. regarding its stochastic occupancy behavior, it can lead to high spatial obstacles of the aggregated energy performance analysis. Therefore it could make sense for future works to trade-off the spatial accuracy to a higher diversity of building archetypes that represent a single municipality.

4.5 Discussion

The following section discusses the advantages and drawbacks of the such aggregated building stock. Section 4.5.1 analyzes the quality of the introduced and considered attributes as well as attributes that were consciously excluded. The strength and limitations of the aggregation algorithm are discussed in Section 4.5.2.

4.5.1 Further building attributes

A prerequisite for this work is the availability of the Census data [Bundesamt, 2011] in such a high spatial resolution. It allows a precise consideration of many building attributes that are relevant for an energy performance analysis.

Nevertheless, some parameters are further relevant for energy performance but not available on such a granular resolution. These attributes are heuristically derived after the aggregation.

Wood **fireplaces** have an increasing role in the heat supply of the residential sector. Nevertheless, no accurate data are available. The *Verband Deutscher Ingenieure* (VDI) assumes 12 to 15 million fireplaces with an overall heat capacity of 150 to 200 GW. Logs or, in general, instead firewood are their main fuel with a share of 75 TWh in 2014[VDI, 2015], approximately resulting in 430 full load hours per fireplace. It is assumed that they mainly occur in larger apartments, wherefore every flat with a living area bigger than 100 m^2 is set with a fireplace, resulting in 14.4 million fireplaces in total.

Also for the case of **hot water** supply no spatial data were found. Instead, the hot water generation by electric boilers is derived with a binomial distribution of 16.4 %, representing the share of end energy demand for electrically generated hot water in Germany in 2014 [BMWi, 2016]. Otherwise, the hot water is supplied with the same technology as the spatial heat.

The envelope is also dependent on the case that the building has already been **refurbished**. No spatially resolved data were available for providing such information. Nevertheless, a study done by IWU [IWU, 2018] provides data about the share of already performed refurbishment measures for different building ages. For each archetype building, a binary sample is chosen based on the probability that this building class has already been refurbished.

Further, a **refurbishment rate** is required to extrapolate the envelope refurbish-

ment activities to the future. While current energetic refurbishment rates lay around 1.1 % of the buildings per year [UBA, 2017b], the cosmetic refurbishment rates, e.g. repainting of facades, plus the energetic refurbishment measures, exceed 2 % per year[IWU, 2010]. Further, the BMWi considers an increase of the energetic refurbishment to above 2 % in the next decades for their *Base* scenario [BMWi, 2018]. While in this work the decision if an energetic refurbishment is intrinsically performed given by the cost optimization model introduced in Section 3.2, the cost for the energetic refurbishment measures are dependent on the case if the building was in the refurbishment cycle. The rate of this cycle is also assumed to be the 2 % [IWU, 2010] annually of the whole building stock, which relates to the sum of the current energetic and cosmetic refurbishment rates. The other buildings can also choose refurbishment measures, but with increased costs. Only a few buildings are assumed to be under a preservation order: Refurbishment measures are deactivated for 20% of the MFHs before 1950, 10% of the SFHs before 1950, and 5% of all buildings between 1950 and 1994 [UBA, 2017a]. The resulting share of the buildings with the construction years and the conditions for future refurbishment measures are illustrated in Figure 4.9.

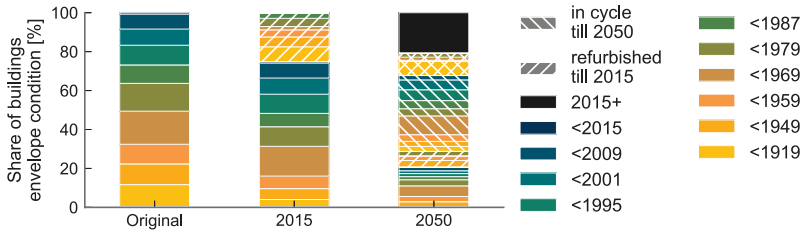

Figure 4.9: Original share of different building construction years at the whole residential building stock. Further, the percentage of buildings is illustrated that were already refurbished in 2015, and that will be in the refurbishment cycle until 2050, plus the new constructions until 2050.

Socio-structural changes such as a change of the specific living space or the population are not considered because of various reasons, as elaborated in Appendix B.1. Instead, the population and building structure are considered as constant while this work focuses on the impact of a changing energy supply structure.

4.5.2 Strengths and limitations of the aggregation

The novel algorithm to aggregate the archetype buildings is the first method that can aggregate a building stock on the granularity of municipalities in Germany. It has

the advantage that it can flexibly derive different numbers of archetype buildings, depending on the available computational resources and the accuracy wanted. Its numerical adaption of the archetype buildings to meet the statistical Census data guarantees a high accuracy of the representation. Further, its regional assignment of the archetype buildings allows spatially resolved energy performance analysis and the determination of the impact of building energy supply on central infrastructures, such as gas or electricity grids.

During the creation of the algorithm, it was alternatively considered to derive as a first step a set of 18 million real building samples from the Census data, e.g. by a Monte Carlo simulation. These could then have been used for classical cluster analysis, e.g. by the k-prototype algorithm. Hence, correlation coefficients between the different attributes would have been required, which are not available for Germany. This problem is avoided by introducing the aggregation algorithm since it directly chooses building archetypes that can represent as many of the attributes in different municipalities, intrinsically respecting the correlations inside the Census data.

Nevertheless, in case exact building samples are available, it would still be recommended to use conventional cluster algorithms. The fitting of archetype buildings to meet attribute distributions, as in this work, has the drawback that theoretical building configurations are created that meet the distribution values but can significantly deviate from real building instances. Therefore, a qualitative post-analysis of the resulting archetypes is required, or the solution space for potential attribute configurations needs to be constrained.

Although the algorithm simplifies the problem of the aggregation of archetype buildings, it stays computationally heavy. This is related to the large data set of the 11,339 municipalities, which are all considered simultaneously for the aggregation. For each municipality, a number of attribute distributions shall be met by a different set of archetype buildings. For the case that 1,000 archetype buildings should be assigned to 11,339 municipalities [Bundesamt, 2011], a Quadratic Program (QP) is stated that has 11.339 million variables. The algorithm runs into memory limitation of a workstation with 512 GB RAM and *Gurobi* as quadratic program solver for this amount of archetype buildings. Alternatively, the attribute distributions given on the level of the NUTS-3 regions could be considered instead of the municipality level. This would significantly reduce the computational load. Nevertheless, it would also cause an accuracy reduction on the single building level since unique building archetypes are not recognizable on higher regional aggregation levels. Instead, the aggregation of 800 archetype buildings showed clear spatial representation areas of single archetype buildings. For such high numbers, Germany should be spatially divided a priori, e.g. to federal states, where independent archetype buildings are aggregated still for the data on the municipality level. This would break down the

overall problems to many different sub-aggregation problems that could be solved in parallel with less memory allocation, constituting higher numbers of buildings that could be aggregated with the same computational resources. Nevertheless, such a high resolution is not required for the scope of this thesis and the maximum number of 800 archetype buildings is sufficient to illustrate the algorithm introduced and to represent the building stock on an aggregated national scale.

As an outlook for future extensions, the generic formulation of the algorithm allows the flexible integration of further relevant attributes for the residential buildings stock in case of available data. Especially, the more accurate distributions of rooftop orientations or the socio-economic background of the occupants and building owners would be valuable for more detailed analysis.

Further, the algorithm should be transferred to other energy sectors to derive spatially distributed sector specific representatives. Examples are the service sector including commercial buildings, or also representative fueling stations, whose detailed models could be upscaled to a nationwide perspective while respecting the spatially varying conditions to supply them. Together, the resulting representatives could then be integrated into a cross-sectoral spatially resolved bottom-up model that respects the individual economic entities.

4.6 Summary

This chapter introduced a spatially resolved data set to describe the German residential building stock and a novel algorithm to derive archetype buildings to represent it.

Section 4.1 discussed existing building archetype databases and methodological approaches to derive such. It was concluded that none of the methods reviewed could derive archetype buildings that represent the building stock spatially resolved on a nationwide scale.

The relevant attributes to describe an archetype building for energy performance analysis were introduced in Section 4.2. While most attributes could be based on existing definitions of archetype buildings, an additional category for attributes related to the technology adoption behavior of building owners was proposed. Further, the building attributes required for the analysis in this thesis were introduced for the German municipalities, mainly relying on Census data.

In Section 4.3, a mathematical model was stated with the objective to derive

archetype buildings to represent the different building attributes on the municipality level with a minimal error. Due to the size and the discontinuities of the model, it was concluded that it is not solvable with existing algorithms. Therefore, a novel algorithm was proposed that divides the overall problem into two sub-problems that are iteratively solved.

The novel algorithm was applied and validated in Section 4.4. It was shown that the algorithm intrinsically makes a trade-off between the errors occurring in such an aggregation for the different relevant attributes. Further, it was illustrated that the overall error measure gets reduced with an exponential decay function with an increasing number of buildings. Therefore, only a limited accuracy gain results for a high number of archetype buildings. E.g., the aggregated attribute fit on a nationwide scale just improved from 98.2 % to 99.5 % from 200 to 800 archetype buildings.

Section 4.5 discussed the strengths and limitations of the novel aggregation algorithm and explained the integration of further building attributes.

Chapter 5

Energy supply scenarios for the German residential building stock

This chapter applies the single building optimization introduced in Chapter 3 to the archetype buildings aggregated in Chapter 4 for different scenarios.

First, all techno-economic assumptions are introduced for the year 2015 and 2050 in Section 5.1. They define the input for the different scenarios. Second, the the *Reference* scenario is introduced in Section 5.2. It states the status quo of the residential energy supply and validates the model to national energy demand statistics. Further, the impact of considering a varying number of archetype buildings and the consideration of different weather years is analyzed. Section 5.3 presents the cost minimal residential energy supply structure for the year 2050 and analyzes the value of different technologies for the overall energy supply, the impact of an increased refurbishment rate and the sensitivity to the considered gas price. The objective function is extended in Section 5.3.5 by adding the goal to minimize the GHG emissions. Thereby, different pathways are introduced to reach a carbon neutral residential building stock. Section 5.4 discusses the results and contextualizes them to the existing literature. The chapter closes with a summary in Section 5.4. The different scenario cases and sensitivity analysis are illustrated in Figure 5.1.

5.1 Techno-economic assumptions

The main input assumptions to parametrize the optimization models are introduced in the following section, e.g. residential energy prices and efficiencies of the dif-

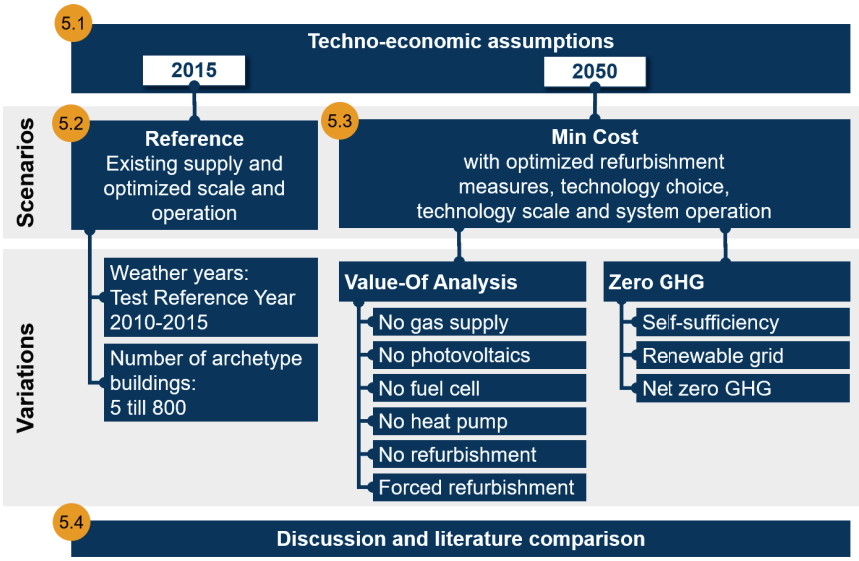

Figure 5.1: Considered supply scenarios for the German residential building stock with their objective and related sensitivity analysis.

ferent technologies. Section 5.1.1 defines the parameters for the year 2015, while Section 5.1.2 extends and adapts them to the year 2050.

5.1.1 Assumptions for 2015

In order to achieve a valid comparison of today's residential energy supply to the changes in the future, a valid scenario framework is introduced that represents today's cost and operation parameters of the residential energy supply systems.

The considered economic parameters for the supply technologies are illustrated in table 5.1 while their detailed derivation is discussed in Appendix A.3. The structure of the investment cost is oriented at the cost model introduced in Section 3.3. It is differentiated between the fixed investment costs that occur in case of installation, and the specific investment costs that are added and are related to the scale of the installations.

In summary, gas boilers and oil boilers are the heat generation technologies with the smallest investment, besides a simple electric heater. The pellet boiler and the heat

Table 5.1: Assumed economic parameters of the energy supply technologies for the *Reference* scenario.

Technology	CAPEX fix	CAPEX specific	OPEX %CAPEX/a	Lifetime a	Source
Gas boiler	2800 Euro	100 Euro/kW$_{th}$	1.5	20	Appendix A.3.5
Oil boiler	2800 Euro	100 Euro/kW$_{th}$	1.5	20	Appendix A.3.5
Pellet boiler	10000 Euro	300 Euro/kW$_{th}$	3.0	20	Appendix A.3.9
Heat pump	5000 Euro	600 Euro/kW$_{th}$	2.0	20	Appendix A.3.4
Heat storage	800 Euro	1200 Euro/m^3	0.0	25	Appendix A.3.7
Photovoltaic	1000 Euro	1400 Euro/kW$_{el}$	1.0	20	Appendix A.3.1
IC CHP	15000 Euro	1000 Euro/kW$_{el}$	7.0	15	Appendix A.3.6
Solar thermal	4000 Euro	350 Euro/m^2	1.0	20	Appendix A.3.8
Electric heater	0 Euro	60 Euro/kW$_{th}$	2.0	30	[Lindberg et al., 2016a]

pumps are more expensive. Their comparison shows that the heat pump is cheaper for small scales while the pellet boiler has a better economy of scale. It is further to highlight that the technologies do not exclude each other and can be installed as combinatorial systems. Therefore, the costs, e.g. of the heat pump, are related to their sole investment, while peripheral components such as peak boilers or heat storage systems are independently considered. The Internal Combustion (IC) CHP unit has a strong economy of scale, making it expensive for small scale applications. The fireplace has no investment cost because its installation is extrinsically given, as discussed in Section 4.5.1. Photovoltaic and solar thermal collectors share the available rooftop areas. Batteries and fuel cells have a negligible market share today, wherefore their costs are introduced later for the 2050 case.

Although the model allows for modeling different interest rates for different building types to respect the different investment behavior of the building owners [Schleich et al., 2016], it is here simplified to a single interest rate of 3 %. It lays between the 2 to 5% considered in the literature [Klingler, 2017; Lahnaoui et al., 2017; Lauinger et al., 2016; Lindberg et al., 2016a; Schütz et al., 2017a].

The energy and resource prices are illustrated in Table 5.2. The majority of the prices are derived from the study *Energieeffizienzstrategie Gebäude* [BMWi, 2015; prognos, 2015], which was created by *prognos*, *IWU* and *ifeu*. Their assumptions define the basic scenario framework for this thesis and rely themselves on the *Energiereferenzprognose* [EWI, 2014]. The majority of the resource prices assumed in the study align with the energy prices observed for 2016 [Bundesnetzagentur, 2017; BMWi, 2018]. Nevertheless, the assumed gas price overshoots the observed price of 2016 by more than 1 ct/kWh wherefore it is adapted in this work to the val-

ues reported for 2016 by the Bundesnetzagentur [2017].

The GHG footprint includes the emissions of the previous conversion processes, such as in the extraction of fuels, or the GHG emissions of the German power plant mix.

Table 5.2: Assumed residential energy prices including taxes, levies, and network charges based on *Energieeffizienzstrategie Gebäude* [EWI, 2014; prognos, 2015; BMWi, 2015] while missing parameters are derived from Lindberg et al. [2016b]; KWKG [2016]; EEG [2017]. The gas price is corrected to the observed gas prices in 2016 [Bundesnetzagentur, 2017]. The GHG footprint and primary energy factors (PE) are taken from prognos [2015]. FiT refers to Feed-in Tariff.

Technology -	OPEX-var Euro/kWh	OPEX-fix Euro/a	GHG kg/kWh	PE kWh/kWh	Comment -
Electricity supply	0.246	170	0.525	1.8	0.292 Euro/kWh for 3700 kWh/a
Gas supply	0.065	0	0.250	1.1	
Oil supply	0.064	0	0.320	1.1	
Pellet supply	0.060	0	0.014	0.2	
Heat pump tariff	0.190	70	0.525	1.8	
FiT CHP	-0.08	0	0.000	2.8	for less than 50 kWel
FiT PV	-0.108	0	0.000	1.8	
District heating	0.074	327	0.270	0.7	0.096 Euro/kWh for 15.000 kWh/a
Log supply	0.050	0	0.000	0.2	

Further, the price structure is modified from a sole energy price (Euro/kWh) structure to a combination of a flat price (Euro/a) and an energy price (Euro/kWh). This is relevant because the savings due to self-consumption, e.g. of photovoltaic electricity, would get overestimated with a sole energy price. Additionally, this structure respects that the specific wholesale prices decrease with larger energy consumptions rates [Bundesnetzagentur, 2017]. Further, the modeling of a flat price and a sole energy price respects, e.g. for district heating, the cost of the connection, which would be otherwise underestimated.

The technical performance of the technologies is summarized in Table 5.3. The efficiencies are given for the Lower Heating Value (LHV) of gas, oil or pellets. The

electrical and thermal CHP efficiencies are defined for a fixed operation ratio and cannot be varied in between. The values are chosen such that the different age structures of the technologies are respected, e.g. an efficiency is assumed for the gas boiler that refers to the efficiency of condensing boilers, while for the oil boiler a lower efficiency is considered that is related to older boiler technologies.

Table 5.3: Summary of the main technical parameters of the energy supply technologies

Technology	Efficiency	Comment and *Reference*
Gas boiler	0.96	Condensing boiler [Henning and Palzer, 2014]
Oil boiler	0.84	[UBA, 2017b]
Pellet boiler	0.9	[Lindberg et al., 2016a]
Heat pump	dynamic	Section 3.3.3 quality grade of 0.4
Heat storage	0.99	charge [Lindberg et al., 2016a]
	0.99	discharge
	0.6%/h	self-discharge [Schütz et al., 2015]
Photovoltaic	0.15%	based on Hanwha HSL 60 S [King et al., 2016] with 7 m^2/kWp
IC CHP	0.6	thermal [ASUE, 2015]
	0.25	electric [ASUE, 2015]
Electric heater	0.98	[UBA, 2017b]
Solar thermal	dynamic	Section 3.3.5
Fireplace	0.83	[UBA, 2017b; Olsberg, 2018]

The comfort temperature inside the buildings is assumed with a value of 21 °C in case occupants are active at home. The night reduction temperature is set for all buildings to 18 °C.

5.1.2 Assumptions for 2050

The techno-economic assumptions for the future energy supply until 2050 are introduced in the following section. While many parameters are estimated to stay in a similar magnitude as in the *Reference* case in Section 5.1.1, this section describes only the assumptions that are changing for the case of 2050. All prices and costs are provided as real prices in 2015.

While no major changes are expected for conventional heat generators, further learning rates and cost reductions are considered for photovoltaic and electrochemical technologies, as shown in Table 5.4. Their detailed derivation and discussion is done as well in the Appendix A.3.

Table 5.4: Change and addition of economic parameters of the energy supply technologies for the year 2050.

Technology	CAPEX fix	CAPEX specific	OPEX %CAPEX/a	Lifetime a	Source
Photovoltaic	1000 Euro	650 Euro/kW$_{el}$	1.0	20	Appendix A.3.1
Battery	1000 Euro	300 Euro/kWh	2.0	15	Appendix A.3.2
Fuel cell	4000 Euro	1500 Euro/kW$_{el}$	3.0	15	Appendix A.3.3

The technical assumptions for 2050 are shown in Table 5.5. The efficiency of the heat pumps is expected to increase further in the future [Willem et al., 2017], wherefore this work assumes an increase of the quality grade to 0.45, which is the upper bound of today's systems as shown in Section 3.3.3. The photovoltaic efficiency is assumed to increase to a value of 30 %, which is discussed in detail in Appendix A.3.1. Primarily, this impacts the space coverage on the rooftop and increases the photovoltaic potential that can be installed. The technical parameters of the batteries are derived from a prediction until 2050 [Elsner and Sauer, 2015], but some of today's residential storage systems already achieve similar efficiencies [Kairies et al., 2016].

Table 5.5: Summary of the main technical parameters of the energy supply technologies for 2050.

Technology	Efficiency	Comment and *Reference*
Heat pump	dynamic	Section 3.3.3 quality grade of 0.45
Photovoltaic	0.3	average 2050 [ISE, 2015] with 3.5 m^2/kWp
Battery	0.95	charge [Elsner and Sauer, 2015]
	0.95	discharge [Elsner and Sauer, 2015]
	0.01%/h	self-discharge [Elsner and Sauer, 2015]
	0.5 kW/kWh	capacity factor
Fuel cell	0.33	thermal Appendix A.3.3
	0.52	electric Appendix A.3.3

The electrical efficiency of the fuel cell is assumed with 52 % and positions itself between the efficiency that can be achieved from Solid Oxide Fuel Cell (SOFC) systems and the efficiency of the Proton Exchange Membrane Fuel Cells (PEMFC), as discussed in detail in Appendix A.3.3. A fully flexible operation is assumed for the year 2050. The efficiencies are considered to be the same for natural gas, biogas or as well potential hydrogen as alternative fuels [Peters et al., 2016].

The energy prices for 2050 are shown in Table 5.6 and are relying as well on the *Energieeffizienzstrategie Gebäude* [BMWi, 2015; prognos, 2015] and *Energiereferenzprognose* [EWI, 2014]. The *Energiereferenzprognose* considers a carbon price of 76 Euro/ton for the year 2050, which, e.g., increases the gas price by 1.9 ct/kWh.

Table 5.6: Assumed energy prices, GHG footprints and primary energy factors (PE) based on the *Energieeffizienzstrategie Gebäude* [EWI, 2014; prognos, 2015; BMWi, 2015] for 2050.

Technology -	OPEX-var Euro/kWh	OPEX-fix Euro/a	GHG kg/kWh	PE kWh/kWh	Comment -
Electricity supply	0.220	170	0.122	0.4	0.266 Euro/kWh for 3700 kWh/a
Gas supply	0.096	0	0.250	1.1	
Bio-methane	0.138	0	0.014	0.2	
Oil supply	0.124	0	0.320	1.1	
Pellet supply	0.080	0	0.014	0.2	
HP Tarif	0.190	70	0.122	0.4	
FiTCHP	-0.010	0	0.000	0.4	
FiTPV	-0.010	0	0.000	0.4	
District heating	0.085	327	0.144	0.5	0.107 Euro/kWh for 15000 kWh/a
Log supply	0.065	0	0.000	0.2	

Further, a bio-methane purchase is integrated with a price of 13.8 ct/kWh, which can be either a synthetic gas or biogas. Since no sufficient predictions for bio-methane prices in 2050 are found, its price is derived from the production cost of bio-methane for the feed-in into the gas grid of 7.5 ct/kWh in 2013 [Bundesnetzagentur, 2014], plus the surcharge for grid fees, tax etc. This surcharge is considered to be 6.3 ct/kWh, which is the difference between the gas market price of 3.3 ct/kWh and the residential gas price of 9.6 ct/kWh in 2050 [EWI, 2014]. All in all, it results in a price of 13.8 ct/kWh for the bio-methane, which is significantly above the fossil

gas price.

No values for future feed-in tariffs were found. Therefore, the feed-in is only marginally subsided since it is highly dependent on the future market environment. A marginal value of 0.01 eur/kWh is chosen in order to guarantee that photovoltaic generation is not curtailed and is instead fed-in to the grid.

The cost and energetic impact of the refurbishment measures for the opaque building envelope are shown in Table 5.7.

Table 5.7: Techno-economic assumptions for the insulation measures of a single building. The two measure levels are derived from Schütz et al. [2017a] while the exact cost and lambda are taken from BMVBS [2012].(* thickness equivalent. ** only capital expenditures related to energetic measures.)

Component	Measure -	Thickness* m	Lambda W/m/K	CAPEX Euro/m^2	CAPEX energy ** Euro/m^2
Wall	Base	0.15	0.035	124.0	51.5
	Future	0.22	0.035	140.9	68.5
Roof	Base	0.24	0.035	237.6	53.0
	Future	0.36	0.035	270.0	79.6
Floor	Base	0.08	0.035	51.7	-

All measures are additional layers to the existing envelope of the building. The costs are average values taken from a survey about subsided refurbishment measures in Germany [BMVBS, 2012]. They differ between the whole CAPEX of a refurbishment measure and the sole additional CAPEX of energy efficiency measures if the building would have been refurbished anyway, as discussed in Section 4.5.1. The costs are related to the exterior surface area of the building component. Two levels of potential insulation measures are considered and differ by the thickness of the insulation layer, referred to as *Base* and *Future*.

The costs of replacing the windows and the changing solar and thermal transmittance of the different window types are shown in Table 5.8 and rely on [BMVBS, 2012] as well. The costs are specific to the window area of the building. Again, it is differentiated between the two levels *Base* and *Future*.

All envelope measures have a lifetime of 40 years with zero operational costs.

Table 5.8: Techno-economic assumptions for the windows. The transmittance are based on [Schütz et al., 2017a] and the cost based on [BMVBS, 2012]

Measure	Solar transmittance -	Thermal transmittance W/m^2/K	CAPEX Euro/m^2
Base	0.575	1.1	313
Future	0.5	0.7	361.5

Additional to the conventional refurbishment measures at the envelope of the building, a heat recovery for the ventilation is assumed with a specific investment of 65 Euro/m^2 per living area, a lifetime of 25 years and operational cost of 4% per year BMVBS [2012] in ratio to the original investment. If integrated, 80% of the heat losses due to ventilation get recovered.

Lastly, an occupancy controller can be installed that reduces the comfort temperature in case of vacant occupants, as discussed in Section 3.2. Based on the cost of Controme [2018], they are assumed with a fixed investment of 1000 Euro for the central system controller and 3 Euro/m^2 per living area for the different thermostats in the rooms, including their installation costs. A lifetime of 15 years is assumed.

5.2 *Reference* scenario

The overall model consisting of the single building optimization (Chapter 3) of aggregated and spatially assigned residential archetype buildings (Chapter 4) is applied and validated in the following section. Therefore, the techno-economic assumptions for 2015 from Section 5.1.1 are used. The choice of the technologies are predefined by the archetype definition discussed in Chapter 4, but the technology scale and operation are optimized such that the building specific energy demands are met. It defines the *Reference* state of the residential energy supply, which is used as a benchmark for the future scenarios.

Since the energy demands of the single building model are already validated, this chapter focuses on the overall residential energy consumption on a nationwide level. First, Section 5.2.1 shows the impact of choosing different numbers of archetype buildings on the resulting final energy demand and concludes a sufficient number of archetype buildings for further scenarios. The effect of different weather years on the model performance is compared in Section 5.2.2. Additionally,

Section 5.2.3 illustrates the spatial differences of specific energy costs and GHG footprints due to the different building types and supply technologies in Germany.

5.2.1 Impact of the number of archetype buildings

This section analyzes the impact of a varying number of archetype buildings on the prediction accuracy of the aggregated nationwide residential energy demand. Therefore, the different numbers of aggregated archetype buildings that are introduced in Section 4.4 are independently optimized for the *Reference* scenario and then multiplied with their appearance in Germany. Each building is optimized with a single occupancy profile.

The resulting final energy demands are aggregated to different energy carriers and illustrated in Figure 5.2. They are validated against the final energy demand provided by AGEB [2017] that are themselves calculated by a top-down approach to estimate the aggregated energy demands for all sectors, mainly relying on consumption data provided by the energy suppliers.

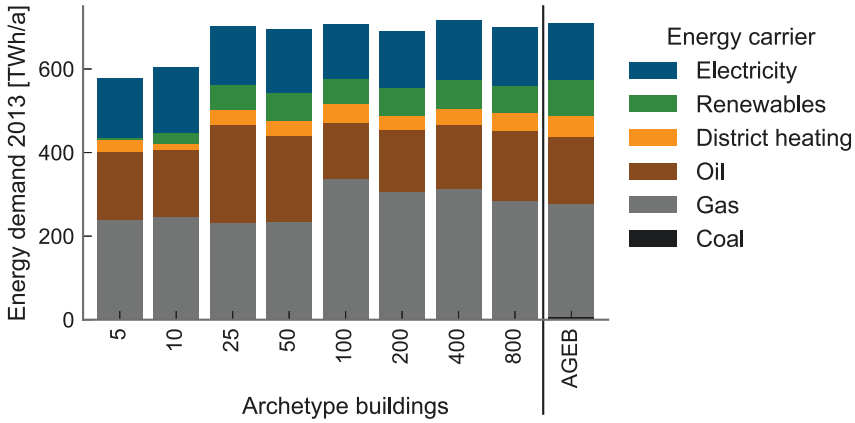

Figure 5.2: Final residential energy demand predicted for different numbers of archetype buildings.

The dominant energy carriers for the residential sector are gas, oil and electricity with 268, 162 and 136 TWh/a per year [AGEB, 2017]. The demand for renewable energy or district heating is secondary with 84 and 51 TWh/a per year. As seen in Figure 5.2, the model is able to roughly predict with five to ten archetype buildings

the demand of the three dominant energy carriers, but the appearance of minor energy supply carriers is not sufficiently included. This improves with an increasing number of archetype buildings while the best fit can be achieved with 800 buildings, the highest number considered. The resulting demands of 64.8 TWh/a for renewables and 44 TWh/a for district heating are still an underestimation. This deviation is constituted by the aggregation, which tries to capture the most appearing archetype buildings and neglects rarely occurring building types. Nevertheless, these missing energy demands for renewables and district heating are compensated by gas and oil demands, which are slightly overestimated with 286 and 165 TWh/a. This compensation effect appears already for 25 archetype buildings wherefore all cases between 25 and 800 archetype buildings predict the total final energy demand in a similar magnitude as the AGEB [2017]. Above 200 archetype buildings the share of the different energy carriers also aligns well with the structure of the AGEB [2017].

The prediction with 50 archetype buildings overestimates the demand for oil with 27.4 % and underestimates the demand for gas by 17.1 %, while 100 archetype buildings on the contrary overestimate the gas demand by 25.5 % and underestimate the oil demand by 16.1 %. This switch shows a drawback of the aggregation: Some archetype buildings appear often and have therefore a high impact on the overall energy load. If the majority of the buildings supplied, e.g., with gas boilers have a construction year before 1960 while the more modern buildings are supplied with oil, an overestimation of the gas demand and an underestimation of the oil demand results, although the absolute number of the different boiler types is well represented. This can change for a different number of archetype buildings since the input values rely on attribute distributions, which have to be met on an aggregated perspective, while the correlation between the attributes are with few archetype buildings not well respected. Nevertheless, this effect is reduced with an increasing number of archetype buildings since single archetypes represent attribute distributions on a more granular level. In consequence the spatial differences, e.g. of construction years, are better fitted and intrinsic correlations of the input data are represented with a higher accuracy.

The temporal prediction of the resulting electricity load is validated in Figure 5.4. It shows the sorted load curves predicted with different numbers of archetype buildings together with the sorted load curve of the Standard Load Profile (SLP)[BDEW, 2011], scaled by the electricity demand of the residential sector in 2013 [AGEB, 2017]. It is observed that for a small number of archetype buildings the peak demand gets overestimated since statistical balancing effects between different households cannot be sufficiently expressed, resulting in an RMSE of 3.66 GW between the SLP and the prediction with 10 archetype buildings. This deviation could be either reduced by optimizing every building with different occupancy profiles, or by increasing the number of archetype buildings: For already 200 buildings the RMSE decreases to a value of 1.33 GW.

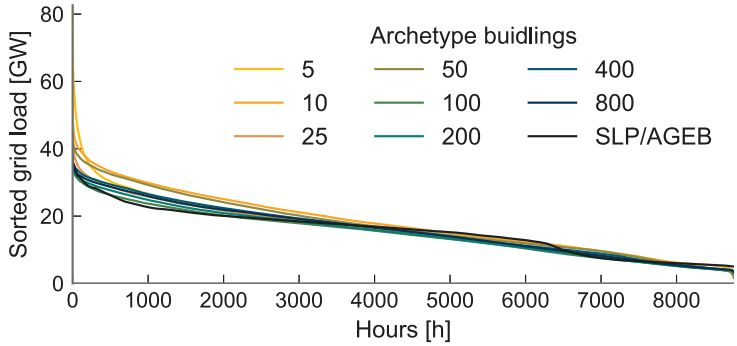

Figure 5.3: Sorted aggregated electricity load for different numbers of archetype buildings in comparison to the sorted electricity load based on the SLP [BDEW, 2011] scaled with the residential electricity demand in 2013 [AGEB, 2017].

The computational load of optimizing the *Reference* energy supply of the increasing number of archetype buildings is shown in Table 5.9. Obviously, the runtime increases with a higher number of archetype buildings. Nevertheless, from 5 to 50 buildings, the relative increase of the runtime is below the relative increase of the building number, since more threads can be used in parallel to optimize the buildings. Above 100 archetype buildings, the runtime proportionally increases with number of archetype buildings since the maximum number of threads is used: 200 archetype buildings have a runtime of 45 minutes while 800 buildings run 181 minutes.

Table 5.9: Runtime of the *Reference* scenario for a varying number of archetype buildings while using 100 threads in parallel on a workstation with two Intel(R) Xeon(R) Platinum 8180 CPUs and 512 GB RAM.

Number of buildings	5	10	25	50	100	200	400	800
Runtime [min]	2.2	2.6	4.6	8.3	21.0	45.3	89.6	181.0

Therefore, it first seems reasonable to consider the highest number of archetype buildings for the further scenarios and sensitivity analysis since a runtime of three hours would be acceptable. Nevertheless, the *Reference* optimization has a rather low computational load in comparison to the future scenarios because the system configurations are predefined and additional refurbishment measures are not considered. In consequence, all binary decision variables that will make the further scenarios more challenging to solve are not yet included .

Instead, this work assumes 200 archetype buildings as a sufficient trade-off between accuracy and computational load since they already capture the main diversity of the energy carriers and the statistical balancing effects between the buildings.

5.2.2 Impact of different weather years

The following section evaluates the impact of different weather years on the energy demand of the buildings. While the majority of the national energy performance analysis relies on degree days, this work uses the highly temporally and spatially resolved COSMO rea-6 reanalysis weather data [Bollmeyer et al., 2015]. Hourly values are considered that are provided for 880x856 grid points spanning over Europe. Every archetype building gets the weather data assigned from the grid point that is closest to its location.

The resulting final energy demand for different weather years is illustrated in Figure 5.4 for 200 archetype buildings and validated again to the final energy demand values provided by AGEB [2017]. According to AGEB [2017], the total residential energy demand varies from 743 TWh in 2010 as maximum to 608 TWh for 2014 as minimum.

For all different weather years, the systematic overestimation of gas demand and underestimation of district heating demand is observed, as already discussed in the previous section. Nevertheless, the relative deviation differs between the years. While the total final energy demand fits well for 2010 with an underestimation of below 2%, the deviation increases in the year 2011 up to 7.4 %. It reduces again to 2.8 % in the year 2013 while it has in 2014 again a value of 5.8 %. The differences are mainly constituted by the different demands for all energy carriers used to supply the space heat, while the electricity demands stay almost constant for the periods.

Figure 5.5 shows the spatial distribution of the final energy demand averaged for all the considered weather years. It clusters in the cities as expected. Additionally, the relative changes of the final energy demand for the different weather years are illustrated for the different municipalities. The overall magnitudes of differences align with the differences shown in Figure 5.4. Nevertheless, it is clearly recognizable that different weather years impact the annual energy demand spatially differently: While the year 2010 was generally a cold year, in northern Germany the final energy demand is even 17% above the average while in south-west Germany it is only 11 % higher than the average. This is the opposite in 2013: Southern Germany's energy demand lays 9 % above the regional average, while northern Germany just

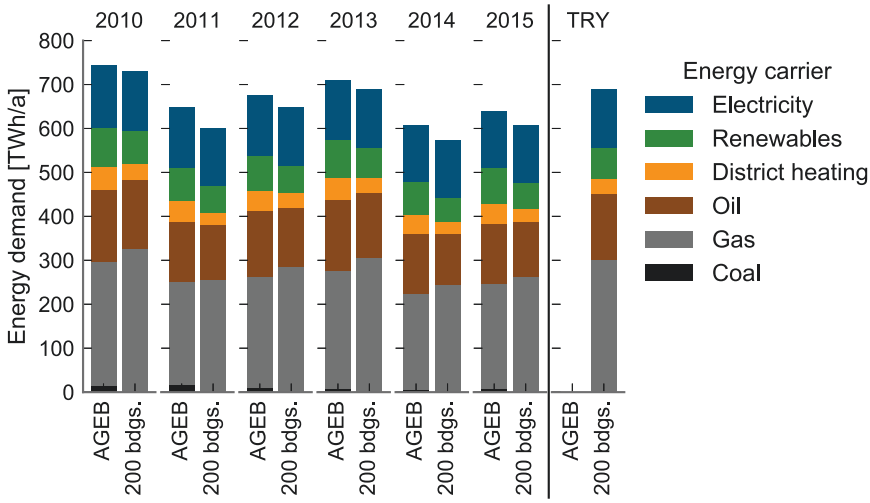

Figure 5.4: Final energy demand for different weather years predicted with 200 archetype buildings and compared to the values reported by the AGEB [2017]. The energy demands for Test *Reference* Year (TRY) are just calculated with the model.

lies 5 % above the average.

In 2014, no significant differences due to the geo-position are observed. Nevertheless, it becomes clear that the cities are less sensitive to the weather patterns (11.5 % below the average in 2014) than the rural areas (13.5 % below the average in 2014). The reason is that the relative share of energy demand for space heating to the overall energy demand is in the cities smaller than in the rural areas, reducing the relative impact of weather years on the total energy demand.

The energy demand determined by the weather data of the *Test Reference Year* (TRY) [DWD, 2012] aligns almost to 100 % with the average energy demand for the considered weather years in northern Germany. On the contrary, in the south it is up to 20 % higher than the average. Nevertheless, this work will rely on the TRY data for the further scenarios since many standards for the design and evaluation of building energy systems depend on it as well. Additionally, the prediction of the energy demand with the TRY is higher than the average prediction with the real weather years. This can compensate for the relative underestimation to the final energy demand in comparison to the AGEB [2017].

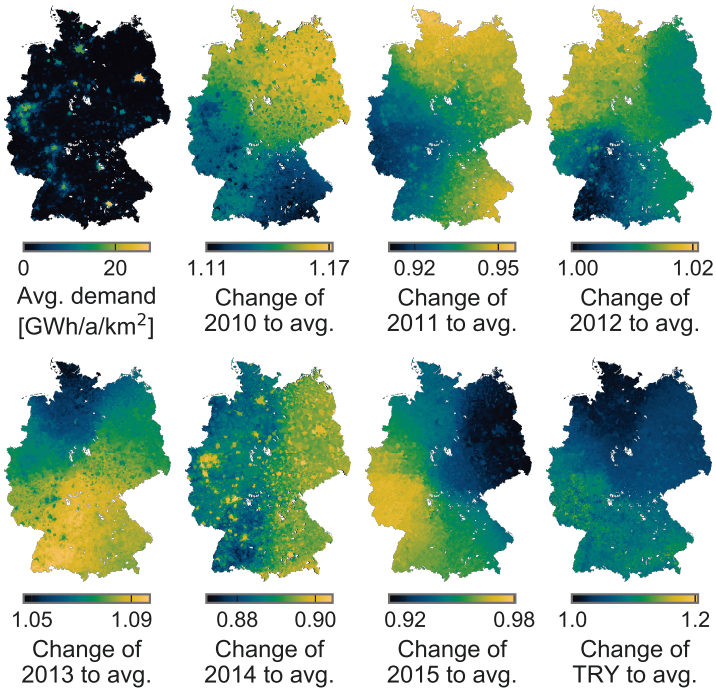

Figure 5.5: Spatial distribution of the final energy demand, averaged for the considered years 2010 until 2015, and the relative regional deviation from the average value.

All in all, the magnitudes of the spatial energy demand deviations due to different regional weather patterns are in a similar range as the deviations of the model to the validation set. Therefore, it can be concluded that a sufficient accuracy is given by the model, especially because previous works most often just worked with single weather locations or even only degree days.

Further, the analysis illustrates that the novel spatially resolved approach is able to identify local extreme weather patterns. While it was shown here only for the aggregated annual demand, the model also predicts the temporal demand of the energy carriers in all municipalities and can be used for the identification of local peak demands that are relevant for infrastructure design.

5.2.3 Spatial distribution of energy demand, cost and GHG footprints

The impact of the different regional energy demands of the residential buildings on the cost and GHG footprints are discussed in the following section for the case of 200 archetype buildings and the weather year 2013. The results are still based on the assumptions made in Section 5.1.1.

Figure 5.6 illustrates the demand for electricity, other energy carriers (oil, gas, district heating and renewables), and the GHG footprints specific to the available living area in the buildings. First, it is clearly recognizable that the demand for electricity specific to the living area is higher in the rural areas, which itself is constituted by the higher density of occupants per living area. A reverse effect is observed for the other energy carriers: They are mainly constituted by the demand for space heating and are with around 120 kWh/(m^2 a) significantly lower in the urban area than in the rural areas with 160 kWh/(m^2 a) due to lower surface-area-to-volume ratios and a lower share of detached buildings.

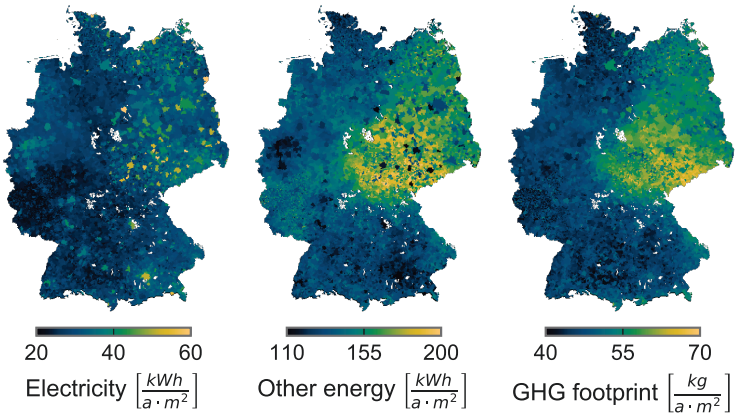

Figure 5.6: Spatial distribution of the final energy demand for electricity, the final energy demand for other energy carriers and the GHG emission equivalents specific to the living area in the *Reference* scenario.

Further, it is observed that the specific energy demand in the rural areas of the new federal states is with up to 200 kWh/(m^2 a) significant higher than in the rural areas of the old federal states of Germany. Since the building stock in east Germany is older, also the materials used in the envelope of the buildings have a worse energetic performance, resulting in a higher overall energy demand.

This also impacts the specific GHG footprints, which are almost 30 % higher in the new federal states in comparison to the old federal states, peaking in the south-east with a GHG equivalent of 70 kg/(m^2 a), including the GHG footprint of the electricity demand. Clear differences between rural and urban areas cannot be identified anymore since the spatially opposing effects of the specific electricity and space heating demand compensate for each other.

The resulting operational energy costs, mainly the cost due to the energy carrier import, are visualized in Figure 5.7.

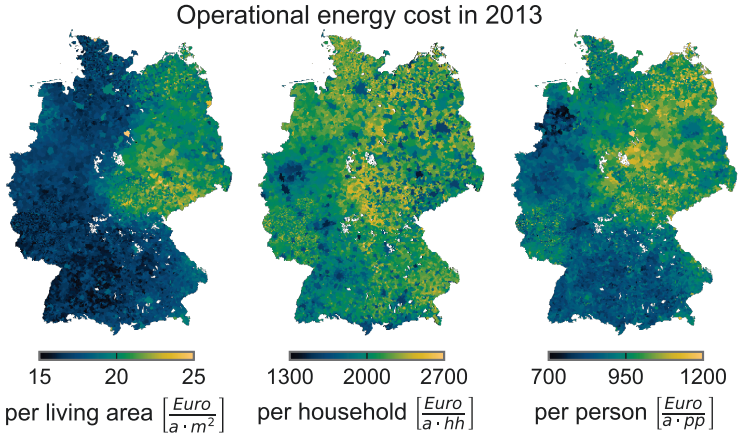

Figure 5.7: Spatial distribution of the operational energy cost per living area, per household and per person in the *Reference* scenario.

The energy costs per living area are in the new federal states higher than in the old federal states, equivalent to the GHG emissions. Yet, no significant difference between eastern and western Germany is recognized for the case of the energy cost per household since the specific living areas per household are smaller in eastern Germany, compensating for the higher area specific energy demands. Instead, a significant difference between the rural areas with 1400 Euro/a and the urban areas with above 2000 Euro/a per household is recognizable. The urban areas have significantly smaller living areas and lower specific energy demands for space heating. Additionally, the number of occupants per household is lower in the urban areas wherefore also the electricity demand is smaller. The visualization of the energy cost per persons reveals that especially the rural areas in eastern Germany have high specific energy costs. The reason is that a small number of occupants per household are living in buildings with a high specific demand for space heating.

The differences between the old federal states and the new federal states need to be evaluated with caution: The new federal states have higher refurbishment rates [IWU, 2018], although a uniform refurbishment rate for the whole of Germany is considered in this work. Further, regional differences of electricity and gas prices are not included and could affect the regional energy prices besides the energy demand itself.

Nevertheless, the section shows that the model is able to transfer the regional differences of the building and occupancy structure into the techno-economic evaluation of the regional energy supply.

5.3 *Min Cost* scenario in 2050

In order to predict the change of the supply structure in the future, the overall model is applied to 200 archetype buildings for the techno-economic assumptions in 2050, which are defined in 5.1.2. It is implied that the building owners have a technology adoption that minimizes their cost. This scenario is referred to as *Min Cost*. The results define the overall state that the residential energy supply system is converging to if the assumed energy prices of the *Energiereferenzprognose* and the techno-economic assumptions for the technologies will arise and no further incentives are given by the regulators. The demand for the usage of electrical devices, hot water demand and thermal comfort level will stay the same as today, as discussed in Chapter 3.

The choice, scale, and operation of the considered energy supply technologies are optimized together with the heating system and potential refurbishment measures. The cost for envelope refurbishment measures differs between buildings that are in the refurbishment cycle and buildings that are not, as discussed in Section 4.5.1.

The results are shown and discussed in Section 5.3.1 for the aggregated nationwide perspective. Section 5.3.2 points out the regional and building specific differences of the supply structure and the different usage of the central infrastructure. The value of different technologies for the energy supply or the impact of higher refurbishment rates are analyzed in Section 5.3.3. The section reveals further the sensitivities of the model.

5.3.1 Nationwide analysis

The following section provides a techno-economic analysis of the *Min Cost* scenario on a nationwide scale. Therefore, the overall structure of the total residential annual expenditures for the resulting energy supply are illustrated in Figure 5.8. These annual costs can also be referred to as cost of comfort, which integrates all costs that are related to residential electrical device usage, hot water demand and thermal comfort.

The annual costs amount to 65 billion Euro per year for the whole residential sector in Germany, or 1603 Euro per year per household. More than 53 % of the costs are still caused by energy imports of gas and electricity. The other expenditures are related to investments in the supply structure or energetic refurbishment measures, as visualized in Figure 5.9. To realize the technology portfolio, an overall investment of 382.3 billion Euro is needed. The biggest share are the photovoltaics

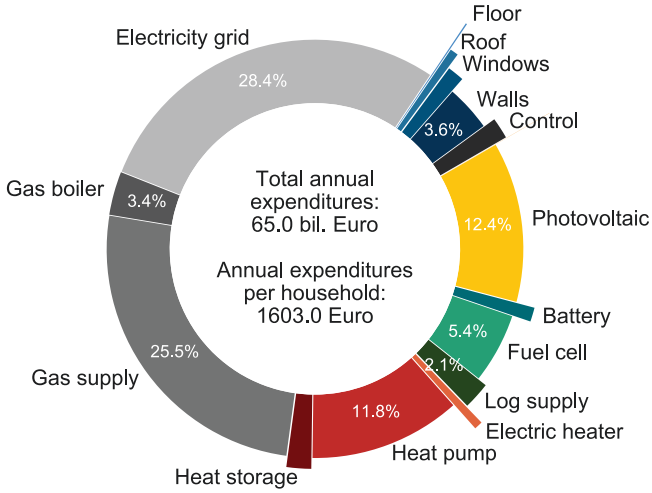

Figure 5.8: Composition of the total annual costs over the whole of Germany for the *Min Cost* scenario in 2050.

with 12.4 % and a total investment of 104.6 billion Euro, which is high by keeping in mind that cost reductions are assumed and no investment incentive is given to build photovoltaics for grid feed-in.

The second highest investment are the heat pumps with 88 billion Euro and a share of the annual cost of 11.8 %, indicating that they are the main supplier of space heat. Fuel cells are the chosen flexible co-generation option and amount to 5.4 % of the annual costs, while ICT CHP units are not chosen at all. Although the ICT CHP have a better economy of scale than the fuel cells, this is not sufficient to compensate for the higher efficiency of the fuel cell, which is relevant since an increase of the gas price is assumed for the scenario. The heat storage systems make out 1.9 % of the annual costs and have a total investment of 21.8 billion Euro. The investment of the batteries is significantly lower with 6.9 billion Euro, amounting to 1 % of the annual costs. The log supply for the fireplaces amounts to 2.1 % while the electric heaters have a minor share. District heating, oil boilers and pellet boilers are not chosen in the solution since they are not competitive in comparison to the heat pumps or gas boilers.

The share of solar thermal is negligible with an investment below 0.1 billion Euro, illustrating that its deployment is not cost optimal in the scenario. In consequence, the photovoltaics do not have to compete with other technologies and can be freely

deployed to the available rooftop areas.

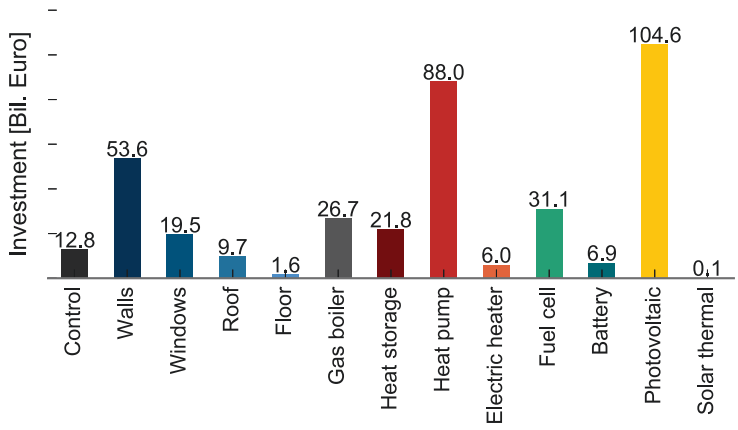

Figure 5.9: Total investments into the different measures in the residential buildings for the *Min Cost* scenario in 2050.

The refurbishment measures together account only for 7 % of the annual costs while more than half of them are determined by the walls. The occupancy control systems have a relatively high share with 1.6 %, followed by the windows and the roofs. A reason for the relatively small cost share of the efficiency measures is that mainly those are chosen that are in the refurbishment cycle anyway and do not account for high additional energetic costs. Further, the long lifetime of the refurbishment measures determines small capital recovery factors. In consequence, the total investment is relatively higher than the share of the annual costs indicate: The energetic cost for the refurbishment of the walls, e.g., amount to 53.6 billion Euro in total.

The resulting cumulative energy flows between the different technologies are illustrated in Figure 5.10 for the aggregated level of the whole of Germany. While no changes are considered for the electricity and hot water demand with 113 and 76 TWh/a, the space heating gets reduced to 310 TWh/a in comparison to the 449 TWh/a in the *Reference* scenario. The largest share of space heating gets supplied by the heat pumps with 225 TWh/a, while the gas boilers supply 66 TWh/a. The electric heaters also still generate 40 TWh/a, followed by the fuel cell with 34 TWh/a. The fireplace has only a minor share while the production by solar thermal is negligible. The usage of the heat storage increases by magnitudes in comparison to the *Reference* scenario and discharges 51 TWh/a.

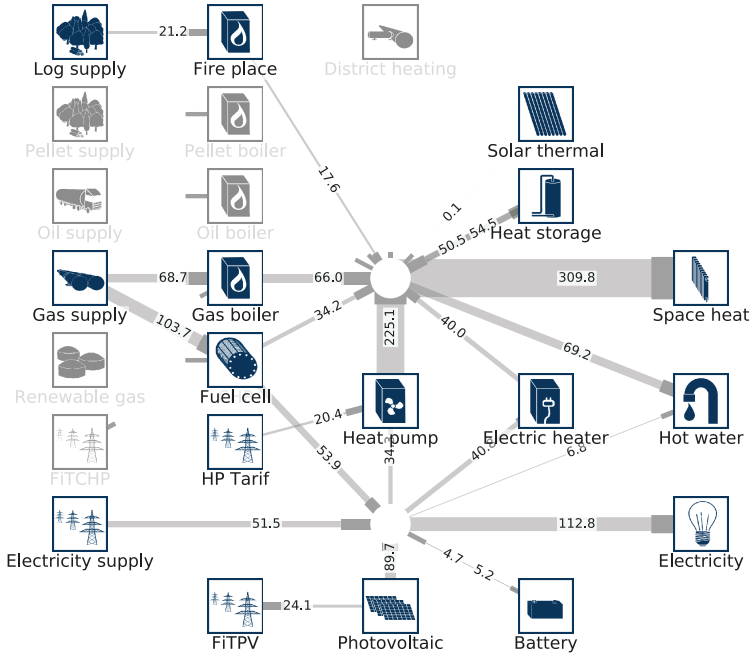

Figure 5.10: Annual energy flows in TWh between the different technologies aggregated for the whole of Germany for the *Min Cost* scenario

The electricity produced for self-consumption adds up by 89.7 TWh/a from photovoltaics and 53.9 TWh from the fuel cell. Only 24.1 TWh/a of the photovoltaic electricity is fed-in to the grid due to the marginal incentive of 0.01 Euro/kWh. No electricity generated by the fuel cell is fed-in to the grid since the incentive is too small to recover the fuel costs. The majority of self-produced electricity is used in the flexible generators, such as heat pumps with 34.3 TWh/a and electric heaters with 40.8 TWh/a. Only the remaining electricity is used for inelastic hot water generation or electrical devices. The residual electricity is imported from the grid with 51.5 TWh/a for the inelastic device demand and 20.4 TWh/a for the heat pumps, which is in sum less than the amount of the self-generated electricity used inside the buildings.

The resulting electricity grid exchange, defined by the electricity imported for the heat pump, the conventional electricity demand, and the photovoltaic feed-in is illustrated in Figure 5.11. For comparison purposes, the grid exchange of the *Refer-*

ence scenario is shown as well. The aggregated electricity load of the *Reference* scenario is dominated by the occupant activities in the morning and the evening. A small variation between winter and summer appears. The overall load peaks in the evening hours during winter with 36.4 GW. This aggregated load significantly changes for the *Min Cost* scenario: During the summer the load demand is reduced to values below 10 GW, also for the evening hours, while during the day high feed-in rates of the photovoltaic occur with up to 43.1 GW, exceeding the peak demand of the *Reference* scenario. The impact of the photovoltaic gets reduced during the winter but still reduces the load at noon for most days. The evening hours in winter are still the peak times with a load up to 32.3 GW for the Min *Cost scenario*, which is in a similar magnitude as the *Reference* scenario.

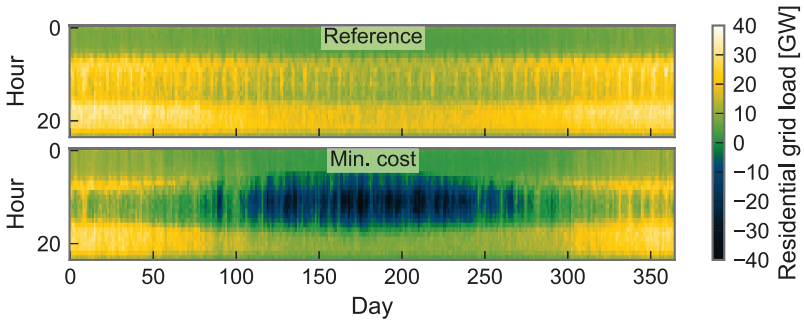

Figure 5.11: Aggregated grid exchange of the national residential building stock for the *Reference* and the *Min Cost* scenario.

Since the heat supply significantly affects the electricity load, the different operation patterns of the relevant heat generators and the demand for space heating are visualized in Figure 5.12. Obviously, the heat demand is dominated by the winter days. It peaks with 114.4 GW_{th} in winter morning hours when the night reduction gets deactivated, people wake up, and the heating system heats the building up to comfort temperature level. The load is then reduced during the day due to vacant occupants and solar heat gains. An opposite effect is observed in transient seasons during spring when the heat supply correlates more to the solar irradiance. The heat pump operation has in those periods a strong correlation with photovoltaic feed-in in order to increase the residential self-consumption. It uses then the thermal capacity of the building to heat it up during the day. This is not possible in winter, since the heat pump is most operated under full load without a remaining flexibility, resulting in total with 3790 full load hours with a thermal peak load of 59.4 GW. Instead, the gas boiler is used as a peak boiler at the morning and evening hours in winter with a peak load of 30.2 GW and 2181 full load hours. The electric heater is entirely correlated to the photovoltaic and is primarily used in summer for hot water gen-

eration, since the heat pumps cannot guarantee the high temperatures to supply hot water. Fireplaces are only operated in cold winter days with a stochastic profile correlated to the occupant activities and peak in the evening hours. Fuel cells are operated supplementary to the photovoltaic generation as flexible generators for self-consumption. In many winter days all of them are operated entirely in full load for the whole day. The produced heat of the fuel cells has only a minor share of the total heat supply with 8 GW peak and 4253 full load hours. Nevertheless, the resulting electricity generation has a peak of 12.7 GW and significantly decreases the electricity demand from the grid.

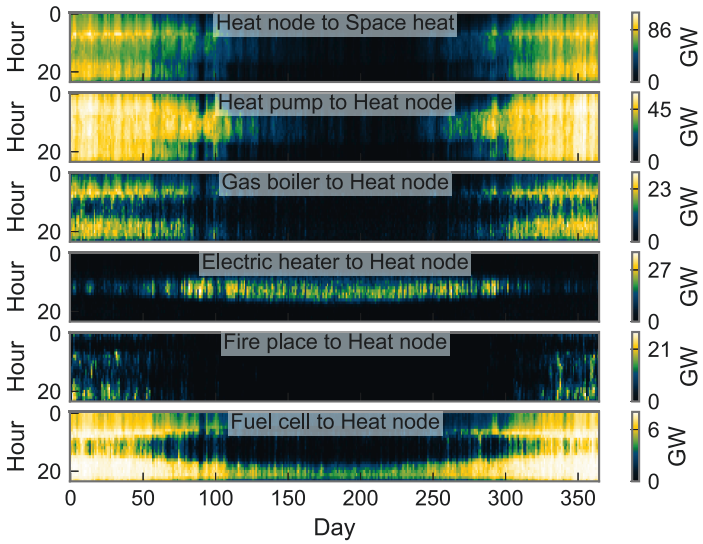

Figure 5.12: Heat flows of the relevant heat generators to the heat node and the connected demand for space heating for Germany in the *Min Cost* scenario in 2050.

In order to evaluate the role of the storage systems in the energy supply, Figure 5.13 illustrates their state of charge. The usage of the 16.9 GWh batteries is clearly correlated with the photovoltaic generation by charging the batteries during the day and discharging them in the evening hours when the electricity demand by the occupants increases. They reach their peak state shortly before sunset in the summer months. The available capacities are excessively used and this daily cycle is recognizable almost for the whole year, except for a few winter days when no photovoltaic generation exists. The maximal state of charge of the heat storage systems is, with 138 GWh, significantly higher than the maximal state of charge of the batteries. They also have a daily pattern that reaches the peak state of charge in the evening

hours of the transient months, constituted by a charging of the photovoltaic operated electric heater. In the winter days, it gets slowly charged during the night and is then discharged in the morning hours to meet the peak demand for hot water and space heating.

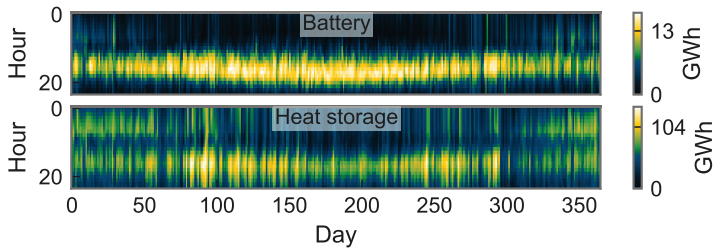

Figure 5.13: Aggregated state of charge of the battery and the heat storage for Germany in the *Min Cost* scenario in 2050.

The accumulated installed capacities of the different technologies are shown together with the maximal aggregated load in Table 5.10, which was already partially introduced in the paragraphs before. It is striking that the aggregated peak load is below the installed capacity for all technologies. One would expect that a cost minimal system results in a design where the technology capacity is just able to reach the technology peak load. Instead over-capacities are installed. The main reason for solar thermal and photovoltaic over-capacities is that their operation is highly depending on the solar irradiance. Their peak load is defined for optimal solar irradiance conditions that do not occur simultaneously for all installed capacities since they have different geo-positions or different installation angles.

The reason for the over-capacities of the other technologies is also related to the bottom-up approach: Every household with its different heat and electricity demand optimizes itself. Therefore, cheap technologies such as the gas boiler or the electric heater are designed to balance the different heat, hot water and electricity profiles. In consequence, these capacities are required at different times in different buildings and locations. Thus, a sole aggregated perspective would underestimate the required technology capacities: The total installed capacity of the electric heater is almost by a factor of three bigger than its aggregated peak load. The heat storage capacity is around 50% higher than the maximal aggregated state of charge and the gas boiler capacity is 20% higher than its aggregated peak load. Cost intensive technologies such as heat pumps or fuel cells are often operated at full load. In consequence, the probability that all buildings operate them at full load at the same time is high. Therefore, their aggregated peak load is almost the same as the installed capacity.

Table 5.10: Maximal load and installed capacities of the significant technologies for Germany in the *Min Cost* scenario in 2050.

	Unit	Max. load/ generation	Installed capacity
Photovoltaic	GW_{el}	80.66	133.40
Solar thermal	GW_{th}	0.15	0.21
Gas boiler	GW_{th}	30.24	36.63
Heat pump	GW_{th}	59.40	60.40
Electric heater	GW_{th}	36.29	99.65
Fuel cell	GW_{el}	12.68	12.69
Heat storage	GWh_{th}	138.18	215.60
Battery	GWh_{el}	16.72	16.90

5.3.2 Diversity of the energy supply

While the previous section discusses the results of the *Min Cost* scenario on a nationwide scale, the following section presents the results and characteristics for different regions and buildings.

The overall results are aggregated from the optimal system design of the different archetype buildings, whose cost structure is illustrated in Figure 5.14. The total annual cost of the buildings is scaled by the number of households in the buildings to show different sizes of buildings on a similar scale. In order to expose patterns between the buildings, they are manually clustered to four groups based on their resulting supply system. The Single Family Houses (SFHs) are differentiated between those with and those without heat pumps. The Multi Family Houses (MFHs) are distinguished between those with and without fuel cells, while the group without fuel cells is much smaller than the group with fuel cells.

In general, the only technology that is chosen for almost all buildings is rooftop photovoltaic. With the small cost of the photovoltaic panels and the high electricity price, they occur in the cost optimal solution for various scales but independent on the roof orientation of the building.

Except for one SFH that has a completely self-sufficient electricity supply, no other SFH has a fuel cell installed. Since the demand profile of a single-family house is highly volatile, the achievable full load hours for self-sufficient electricity supply are too small that a fuel cell would become economically feasible. Further, the required capacities of the fuel cell would be small, increasing the specific cost due to missing

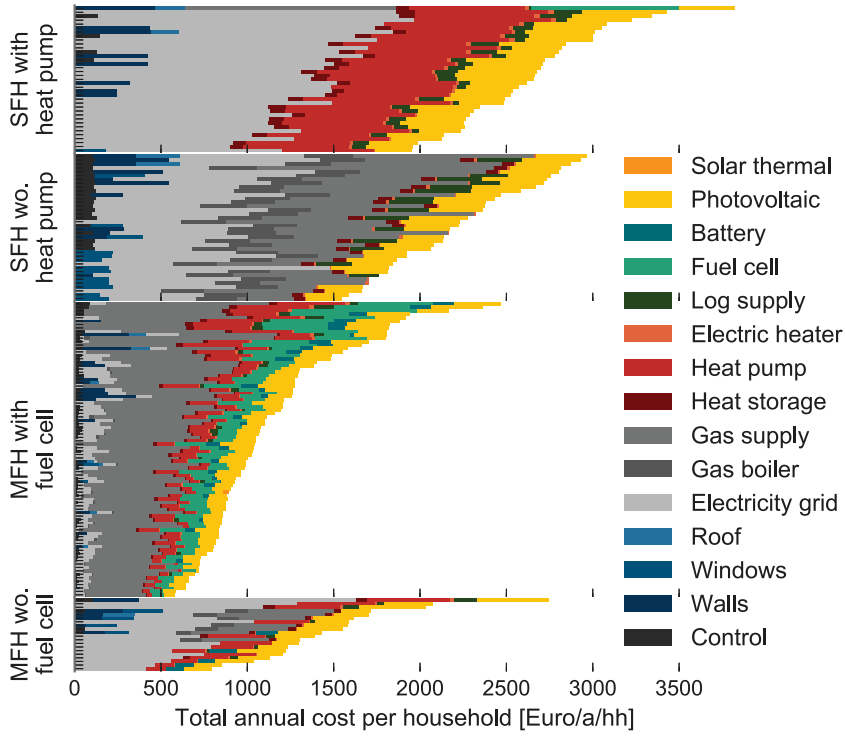

Figure 5.14: Cost composition of the different archetype buildings for the *Min Cost* scenario in 2050. They are grouped by Single-Family House (SFH) with and without (wo.) heatpumps and Multi-Family Houses (MFH) with and without (wo.) fuel cells.

the economy of scale.

Moreover, it is striking that the occupancy controllers are primarily installed in SFHs with gas boilers. The building cluster with gas boilers is dominated by compact buildings where only a few rooms need to be equipped with the thermostats, constituting small investment costs. Moreover, the heat capacity of those buildings is small and constitutes limited thermal inertia. This is beneficial for the occupancy controller since the building can cool down and heat up faster in case of vacant occupants.

All MFHs with a fuel cell have an additional heat pump installed. The cheap self-supply with electricity benefits electrical heat generation. Some of the MFHs add

a battery system to increase the share of the photovoltaic electricity that can be self-consumed.

Although over 60 % of the buildings are in the refurbishment cycle, only 33% of the shown buildings add insulation to the walls and 7% refurbish their roof. Nevertheless, 39% of the archetype buildings get equipped with the occupancy controller, stating that it is in general the most cost effective efficiency measure.

The different full load hours and capacities of the technologies in the different archetype buildings are shown in Figure 5.15. The scale of the dots indicate how often the archetype buildings are assigned in total in Germany. In general, it can be seen that although photovoltaics are installed in all buildings, the achievable full load hours vary from 683 to 1025 depending on the roof orientation and the location of the archetype building.

The highest full load hours are, with around 5000, achieved by the fuel cell. It is observed that a bigger fuel cell capacity correlates with higher achievable full load hours. This is mainly related to the occupancy profiles in the buildings where bigger buildings have, due to statistical balancing effects, flatter profiles that can be covered with higher self-generation rates. Opposing effects are observed for the peak generators, such as the gas boiler with around 2000 full load hours and the electric heater with below 1000 full load hours: The bigger the installed capacities are, the smaller are the achievable full load hours. For the heat pump no such effect is observed. It is operated with between 3000 to 4000 full load hours for small capacities as well as for big capacities.

The distribution of scales and full load hours indicates that the heat pumps significantly rely on a peak boiler, since their scaling to the maximal heat load would be more expensive. Nevertheless, it is open which peak boiler is chosen in the model. For a few full load hours, the electric heater is more cost effective while for many peak load hours an investment into a gas boiler could be advantageous. From a central infrastructure perspective, both options bear an intrinsic economic issue since they need the layout of an infrastructure that will be used in its maximal capacity only for a few hours.

Due to the assignment of the archetype buildings to the municipalities, the different system designs of the archetype buildings also constitute different loads and cost compositions in the municipalities, as illustrated in Figure 5.16. While this cost structure is available for all regions, here only the total annual costs for Köln, an example of an urban region, in comparison to Heimbach, an example of a rural region, are illustrated. The main energy carrier for the energy supply in the urban region is gas and counts for 36.6 % of the annual costs. It is mainly used for self-generation in fuel cells, which amount to 8.4 % of the annual costs. Therefore, imported elec-

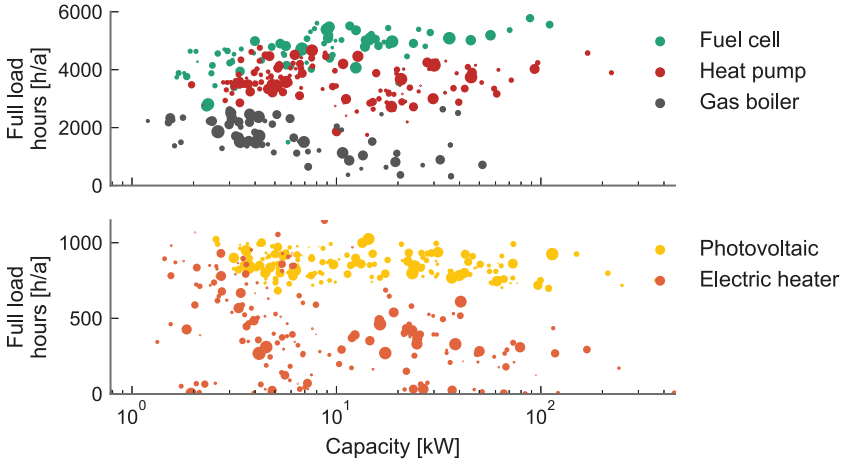

Figure 5.15: Full load hours and capacity of the installed technologies in the different archetype buildings for the *Min Cost* scenario in 2050. The size of the scatter is related to the overall appearance of the archetypes in Germany.

tricity has in the urban region only a share of 18.2 % of the total costs. This is different in the rural region, where the costs for the fuel cells are negligible and the only self-consumed electricity is generated by photovoltaics. In consequence, the majority of electricity is purchased from the grid and amounts to 36.4 % of the annual costs. This difference indicates a structural problem of distributed flexible generation: Co-generation units have in general a strong economy of scale and are not competitive in regions with small energy demand densities. In consequence, those regions will still rely more on an energy import by the electricity grid.

Similar to the results of the *Reference* scenario, the energy costs per household in the urban region are with 1243 Euro/a much smaller than in the rural regions with 2010 Euro/a. This is still mainly constituted by the different specific energy demands due to the different building structures, as already shown in the *Reference* scenario in Section 5.2.3. Nevertheless, it is noteworthy that the uptake of the distributed energy resources, mainly of fuel cells and photovoltaics, does not significantly distort the distribution of residential energy costs from the status today with significant higher costs in the rural areas. The reason is that self-consumption of cheap photovoltaic electricity exists in small scales in the urban areas. Additionally, the co-generation units have a better economy of scale in the urban areas.

The spatial differences of the technology installations are further clarified in Figure

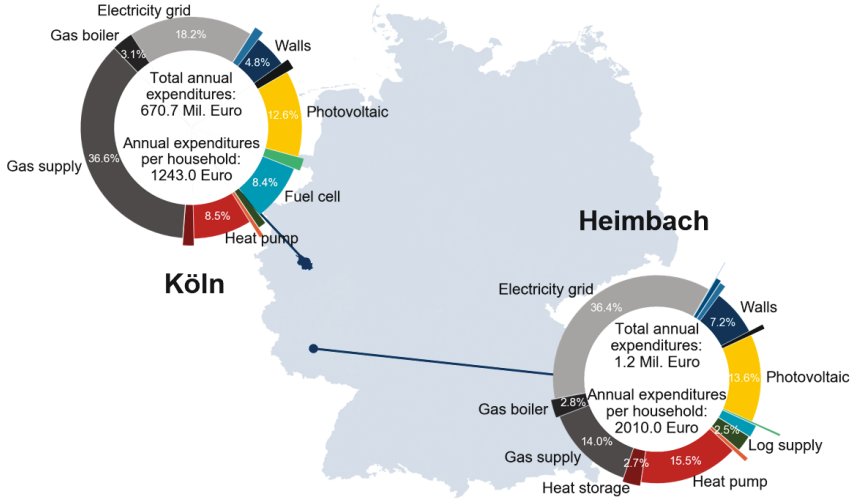

Figure 5.16: Illustration of the composition of the annual costs for Köln and Heimbach in the *Min Cost* scenario.

5.17, illustrating the capacities installed per household in the different regions. The installed thermal capacities of the heat pumps range from 0 to 4 kW thermal per household. The highest heat pump capacities are installed in the rural region of the old federal states: The demand for space heating per household is there the highest since these regions are dominated by large SFHs. The rural areas in the old federal states have smaller heat pump capacities or even none installed at all. The reason is that a sole gas boiler with lower investments can be more cost effective for the small SFHs in this region. The smallest capacities are installed in the rural areas since also the specific heat demand per household is low in the MFHs.

Similar regional trends as for the heat pumps are also observed for the photovoltaics: Large buildings constitute large roof areas that are available for photovoltaic installations up to 6.6 kW per household. Further, the number of occupants per household and the heat pump capacities are higher in the rural areas wherefore the potential for self-consumed electricity is higher. The photovoltaic installations in the urban regions decrease instead to 2.2 kW per household.

The fuel cell has an opposing trend compared to the photovoltaic and the heat pump. It is mainly installed in urban areas with up to 0.5 kW electric per household.

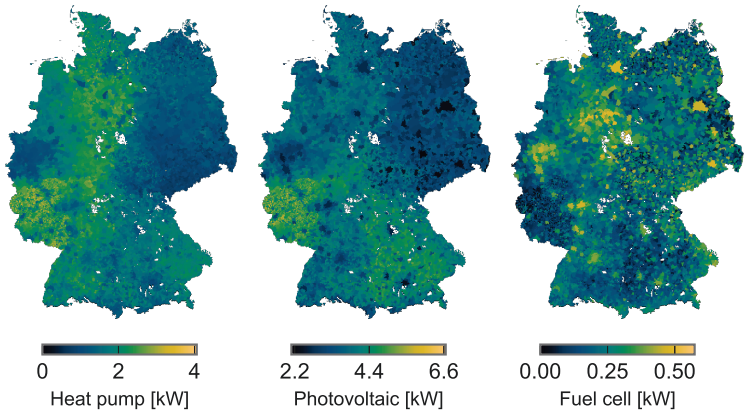

Figure 5.17: Regional technology installations per household for the *Min Cost* scenario.

There, sufficient full load hours can be reached with the high electric and thermal demands of the multi-family houses.

Although the capacities of the other technologies also vary between the regions, the three technologies introduced cause the major changes to the grid load, as illustrated in Figure 5.18. As expected, the majority of the regions reduce their annual electricity demand with the help of self-generation by photovoltaics and fuel cells. Nevertheless, regional differences are high: While urban areas are able to reduce their electricity demand by 60 %, some rural areas even increase their electricity demand. The high photovoltaic installation in the rural areas is not sufficient to compensate for the increased electricity demand by heat pumps. This effect intensifies for the case of the peak load: Almost no photovoltaic feed-in exists in the winter days, while the heat pumps are being operated full load. Therefore, regions characterized by large SFHs double their peak load. This is different for the urban areas that even reduce their peak load because the fuel cells exceed the electrical capacity of the heat pumps and are synchronously operated. Equivalent regional trends are observed for the feed-in: The rural areas feed up to 40 % of the original electricity demand into the grid, while the urban areas have only small feed-in rates of 10 %.

Striking are the high demands in Rhineland-Palatinate and Saarland. It is partially explained by the structure of the municipalities: The municipality boundaries are in this region relatively small and do not have any MFHs included. In consequence,

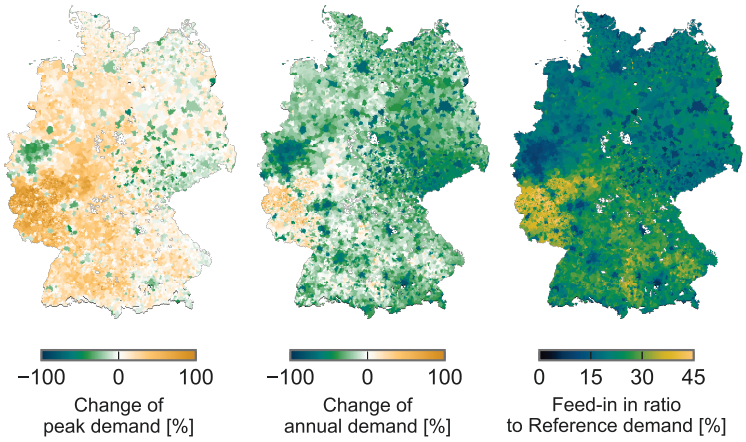

Figure 5.18: Spatial change of the peak electricity demand and the change of the cumulative positive demand from the *Reference* scenario to the *Min Cost* scenario. Further, the amount of electricity feed-in to the grid in the *Min Cost* scenario is shown in ratio to the cumulative electricity demand in the *Reference* scenario.

no fuel cells are installed that would be available to reduce the peak load in the winter months. Instead, rather high heat pump capacities supply space heating for the SFHs, constituting an increase of the demand.

The reason that it stands out that strongly from the other rural areas is also constituted by the model approach: Single archetype buildings are overrepresented in different municipalities for a coarse resolution of 200 archetype buildings. If on of those single buildings is highly sensitive to the scenario frame and its change of the supply structure stands out in comparison to the change of the other archetype buildings, the changing grid load is overestimated for the set of municipalities that it is representing. This obstacle is further clarified in Appendix B.3.

Still, in summary, the results indicate that the change of the energy supply in the rural areas is more challenging with respect to the electricity grid operation than the changes in the urban areas. The demand for electric heat generation is higher due to a larger heat demand per household, the photovoltaic generation is not able to reduce the electricity demand in the winter hours, and fuel operated flexible self-generation is more expensive to compensate for the increasing demand of the electricity.

5.3.3 Value of analysis

The following section provides an analysis of the sensitivities of selected technologies on the *Min Cost* result. Again, 200 archetype buildings are optimized but parts of the technologies are excluded or forced into the solution space in order to evaluate the robustness of the *Min Cost* scenario.

Figure 5.19 illustrates the resulting cost composition of the different cases that were considered for the analysis. Gas supply, fuel cell, photovoltaic, heat pump and refurbishment measures are each excluded from the solution space and optimized, and then compared to the original *Min Cost* scenario with all technologies available. The increase of the total systems costs can be interpreted as *Value Of* the integration of a certain technology. As an additional case, the full package of refurbishment measures are enforced for all buildings that are in the refurbishment cycle in order to reach lower demands for space heating. The total investment, the energy flows and the installed capacities are found in the Appendix C.3.

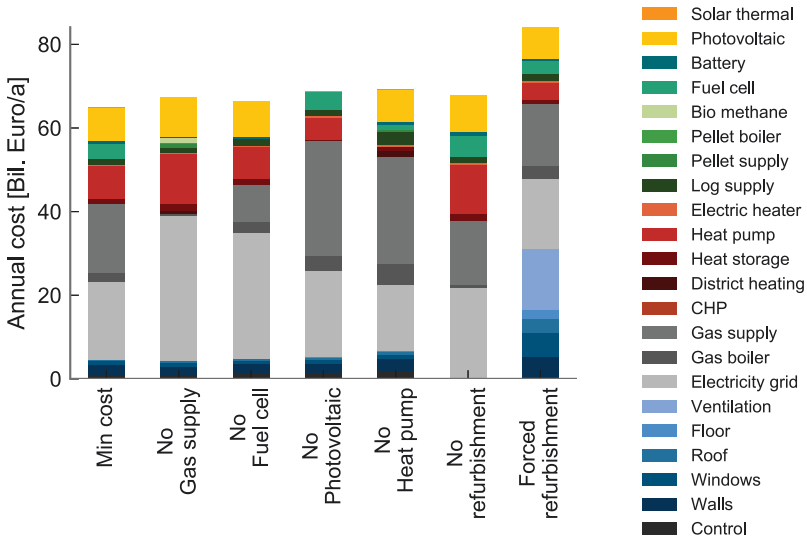

Figure 5.19: Annual cost of the *Min Cost* scenario and the resulting aggregated system cost if the solution space is constrained.

In the case that the fossil gas supply is excluded from the solution space, the electricity purchase doubles while no fuel cells are installed anymore. The bio-methane

or another renewable fuel are too expensive in the considered scenario to replace the fossil gas in the fuel cells and to compete with a an electricity import from the grid. Instead, higher capacities of photovoltaics are integrated into the solution with up to 160.3 GW. Further, the aggregated cost for heat pumps increases by 38 % since their share of the heat supply increases. While the *Min Cost* solution did not include district heating or pellet boilers, they are used in small scales for the case that fossil gas is excluded. 8.67 TWh/a of the fossil gas are compensated for with more expensive bio-methane, which is burned in 5.12 GW of gas boilers. The amount of occupancy controllers is also reduced without fossil gas. The reason is that the heat pump is intensively used during the day in order to use photovoltaic electricity while heating up the building. Nevertheless, the occupancy controller lowers the comfort temperature especially during the day when the occupants are working. These two temporally opposing effects reduce the value of an occupancy controller for the buildings supplied with heat pumps.

The structural changes to the *Min Cost* scenario are rather small for the case that the fuel cell is excluded from the solution space: The net electricity import increases as in the previous scenario and compensates for the missing self-generation, but the photovoltaic capacities just increase from 133.4 GW to 142.3 GW, while the heat pump capacities stay in a similar magnitude. This is different to the previous case and indicates that the value of further photovoltaic capacities is mainly correlated to higher heat pump capacities and not to smaller fuel cell capacities. It is noticeable that the fuel cell capacities are not replaced with IC CHP capacities, indicating that those are not cost effective at all in the considered scenario. The battery capacities are reduced from 16.9 GWh to 12.8 GWh, although the photovoltaic capacity is increasing. This implies that their operation partially complements the fuel cell operation.

Significant shifts and cost increases are recognizable in the case that the photovoltaic is excluded: While the electricity purchase only increases from 71.9 TWh/a to 80.9 TWh/a, the gas import almost doubles from 172.5 TWh/a to 285.7 TWh/a. High gas boiler capacities compensate for the reduction of the heat pump capacities from 60.4 to 46.9 GW_{th}. This indicates the enforcing effect between the heat pump and the photovoltaic, which is economically advantageous in case self-consumption with photovoltaics is available. No battery capacities are installed, supporting the statement that their main economic driver for installation is the photovoltaic, although they are also partially used to increase the self-consumption with fuel cell electricity.

In the case that the heat pump is excluded from the solution space, the amount of gas increases by 113.2 TWh/a while the electricity demand gets only reduced by 13.5 TWh/a. Further, the investment in refurbishment measures increases by 30 %, dominated by more occupancy controller and more wall insulation, and vice

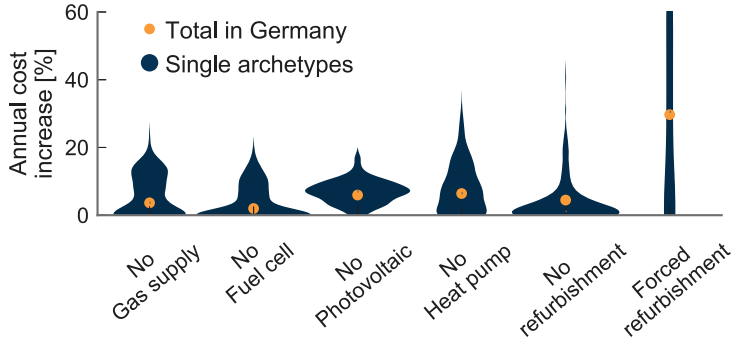

Figure 5.20: Annual cost increase for the case that certain technologies are excluded or added to the solution space in the *Min Cost* for 2050. The change is once shown for the total aggregated cost and once for the single archetype buildings.

versa, indicating that especially cheap heat produced by the heat pumps lowers the motivation to invest in efficiency measures. Also the fire wood supply increases from 21.2 TWh/a to 51.44 TWh/a, since it is a cheaper fuel than fossil gas in the scenario. Remarkable is the reduced investment in fuel cells, cutting their capacity from 12.7 to 5.1 GW_{el}. It illustrates that major fuel cell capacities are built to supply the heat pumps with electricity.

The exclusion of refurbishment measures from the solution space constitutes an increased investment in heat pumps and a reduced investment in gas boilers. This is surprising, since an enforcing effect between the heat pump and refurbishment measures could be expected because the refurbishment measures decrease the required supply temperature in the building, and vice versa, increasing the efficiency of heat pumps. Nevertheless, the economic effects dominate: The heat pumps have higher investment costs than the gas boilers, while on the other hand the energy cost for the gas supply is higher. In consequence, heat pumps are favored in the case of high heat demands and their deployment increases for the case of no refurbishment.

The reverse effect occurs for the forced refurbishment case: Installed heat pump capacities are reduced while gas boiler capacities increase. The overall demand for gas and electricity is reduced since the space heat demand drops to 209.1 TWh/a, in comparison to the 309.8 TWh/a in the *Min Cost* scenario and the 449 TWh/a in the *Reference* scenario. Nevertheless, the demand reduction is not able to compensate for the high cost of the refurbishment measures, resulting in an overall cost

increase of 29.7 %. In particular, ventilation systems with heat recovery amount for almost half of the efficiency measure costs. Ventilation systems do not benefit from the refurbishment cycle since their integration cost into the building is mostly independent of any outside renovation measures. Further noticeable is that the amount of occupancy control systems drops: If the heat demand is reduced anyway, additional measures by temporally reducing the inner air temperature have a minor effect, making the occupancy controller economically unfavorable.

It is striking that the aggregated cost gain is moderate for all considered cases, except for the forced refurbishment case. This indicates that the prediction of the total cost is robust and not sensitive to the available technologies in the future. Though, this robustness just accounts for an aggregated German-wide level, as illustrated in Figure 5.20. The figure shows the cost increase in total and the distribution of the cost increase of the single buildings. While the total cost in Germany just increases by 3.65 % for the case that no fossil gas supply is available, one of the building types has 22.9 % higher energy costs, while some other buildings are not affected at all, since they were also not supplied with gas for the *Min Cost* scenario. Similar effects are observed for the other sensitivity analyses: The sensitivities for single buildings are high, but the cost of the aggregated result is robust.

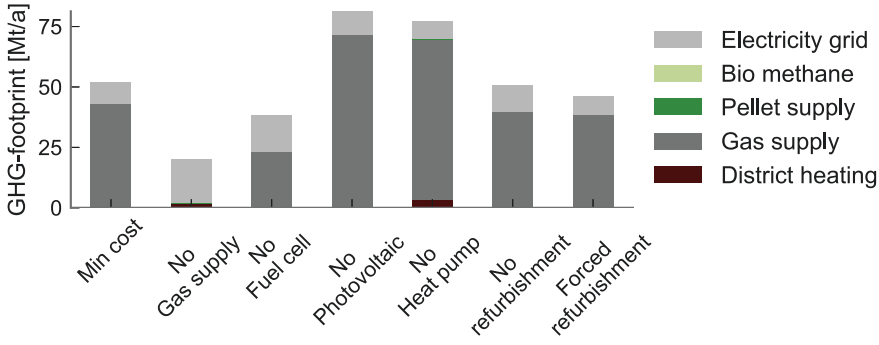

Figure 5.21: GHG footprint of the *Min Cost* scenario and the resulting aggregated GHG footprints if the solution space is constrained.

This robustness does not count for the resulting GHG footprints, which are illustrated in Figure 5.21. The smallest GHG footprints are given by the case without fossil gas supply, reducing the GHG emission equivalent from 51.9 Mt/a in the *Min Cost* scenario to 19.9 Mt/a. Also the exclusion of the fuel cell reduces the GHG footprints, since the specific GHG footprint of the electricity generated by fuel cells is below the GHG footprint of the electricity purchased from the grid. For the cases without photovoltaics and without heat pumps, the GHG footprints increase up to

81.3 Mt/a and 76.0 Mt/a since no carbon neutral electricity can be self-consumed and no efficient heat production is available.

The exclusion and the enforcement of refurbishment measures both constitute a small reduction of the GHG footprint to 50.8 Mt/a and 45.1 Mt/a. The first is related to the switch to more heat pumps, while the second is related to a reduced energy demand for space heating in general. The latter reduction is much smaller than expected because many buildings switch to gas boilers. This indicates a potential rebound effect that might occur in the future: The reduced demand for space heating lowers the economic incentive to invest in efficient but expensive heat supply technologies.

The impact on the electricity grid of the different cases is further illustrated in Figure 5.22. It shows the sorted grid load for the *Reference* scenario, the *Min Cost* scenario, and all related sensitivity analysis. The highest peak load occurs if the gas supply is completely excluded from the solution. No significant gas boiler capacities are able to satisfy the peak heat demand, and no fuel cells can diminish the additional the electricity load of the heat pumps: In consequence, the peak load almost doubles to 55.9 GW in comparison to the *Min Cost* scenario with 32.3 GW. The second highest demand is reached if no fuel cell is included and the peak load increases by 14.6 GW relative to the *Min Cost* scenario. It shows the importance of a decentral flexible electricity generation in order to compensate for the increased electricity demand by the heat pumps. As to be expected, the case without heat pumps has the lowest peak load with 25.7 GW.

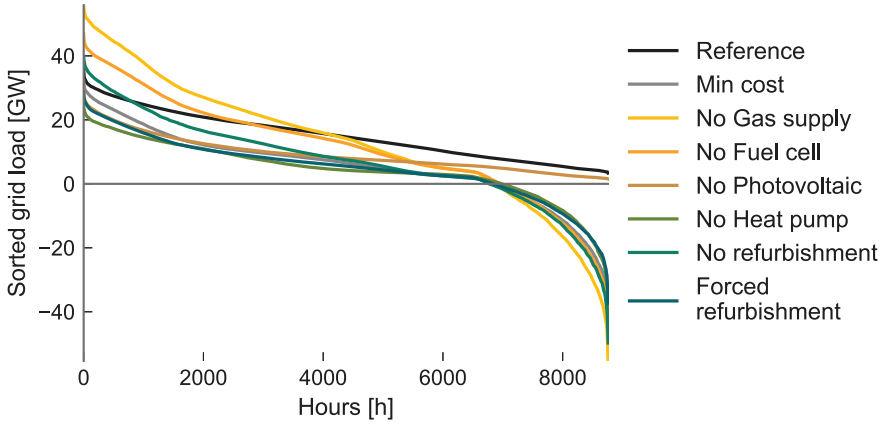

Figure 5.22: Sorted grid load of the *Min Cost* scenario and the grid load if the solution space is constrained.

The amount of photovoltaic feed-in is for all cases that include photovoltaics in a similar range. The maximal feed-in is reached with 55.4 GW for the no gas supply case, although the single buildings have the constraint to limit the feed-in to 50 % of their maximal capacity.

5.3.4 Sensitivity of the gas price

The chosen technologies significantly depend on the assumptions of the technology cost and the energy prices. Therefore, this section illustrates their deployment sensitivity by varying the gas price and optimizing the 200 archetype buildings to minimal cost for the scenario in 2050. The oil price is varied simultaneously and bio-methane is excluded from the solution in order to analyze the sole effect of the chemical energy carrier price on the system designs.

The composition of the resulting annual system cost for the different gas prices are shown in Figure 5.23.

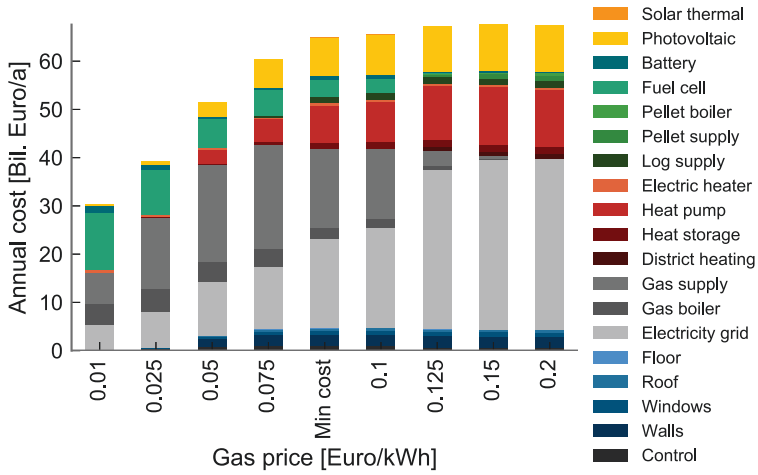

Figure 5.23: Annual cost of the *Min Cost* scenario and the resulting aggregated annual system cost for different considered gas prices.

The total annual residential energy costs are significantly reduced in comparison to the Min Cost scenario for small gas prices. For the extreme case of a gas price of 0.01 Euro/kWh, no refurbishment options are chosen and no significant photo-

voltaic capacities are installed. Large fuel cell capacities of 33 GW_{el} and gas boiler capacities of 125 GW_{th} cover the major parts of the electricity and heat demand. The installed capacities of batteries almost double to 32 GWh in comparison to the *Min Cost* scenario to maximize the self-consumption of the fuel cells. A similar supply structure is observed for a gas price of 0.025 Euro/kWh while the gas cost get a larger share at the total annual energy cost and the installed photovoltaic installations increase from 3.7 GW to 9.2 GW. This illustrates that for such a cheap self-production of electricity, the photovoltaic is only competitive in small buildings where the fuel cells are still too expensive, and instead a good roof orientation and solar irradiation exists.

For the case of a gas price of 0.05 Euro/kWh, the first heat pump capacities are getting installed with up to 28 GW_{th}. Nevertheless, they are secondary in comparison to the gas boiler capacities of 110 GW_{th}. The price of 0.05 Euro/kWh is in a similar range as the gas prices today and explains the small share of heat pumps at the current heat generator market. A higher deployment of heat pumps only results for scenarios with higher gas prices.

Thus, the system converges for gas prices from 0.075 to 0.1 Euro/kWh to the overall system design of the *Min Cost* scenario with significant higher photovoltaic installations and heat pump installations.

For gas prices above, the installed fuel cell capacities are reduced while the heat pump capacities and the photovoltaic capacities increase. The fuel cell capacities are zero for a gas price of 0.15 Euro/kWh and no gas boiler is installed for a gas price of 0.2 Euro/kWh. Instead, the heat pump and the photovoltaic converge to a maximum value of 83 GW_{th} and 163.4 GW. This shift significantly increases the demand for electricity from the grid which doubles almost to the *Min Cost* scenario for high gas prices since no more fuel cells are used for self-consumption, as shown in detail in Appendix C.4. Further, small pellet boiler capacities of 4 GW_{th} are installed in large buildings as peak boiler.

The resulting aggregated GHG footprints are shown in Table 5.11 for the cost minimal system designs depending on the different gas prices.

Table 5.11: Aggregated GHG footprint [Mt/a] of the residential building stock in for the *Reference* and the *Min Cost* scenario and for the cases with a varying gas.

	Reference	*Min Cost*	Gas price [Euro-ct/kWh]							
			1	2.5	5	7.5	10	12.5	15	20
GHG [Mt/a]	202	52	162	150	105	78	46	25	21	20

A clear trend of reduced GHG emissions at higher gas prices is observed since the system switches more to renewable energies and to grid electricity which has a lower GHG footprint than the self-generated electricity of the fuel cells in the scenario for 2050. Since the the *Min Cost* scenario just achieves a GHG reduction of 75% to the Reference scenario, the next section analyzes further pathways to reduce GHG emissions.

5.3.5 Zero GHG emissions

Since the *Min Cost* scenario just reached a reduction of the residential GHG footprint to 51.9 Mt/a, this section introduces the further system evolution that would be required to reach a carbon neutral building stock, i.e. a GHG footprint of zero.

Therefore, the *Min Cost* scenario in the previous Section 5.3.1 is extended with a second objective: The minimization of the GHG footprint. It is done by modifying the single objective function, introduced in Section 3.3.1, to a multi-objective function that includes the cost and the GHG footprint. A simple linear scalarization approach is used that weights the different objectives. Here, the costs are always weighted with one while the GHG emissions start with a weight of zero and are higher weighted iteratively in order to reach the goal of a GHG neutral building stock. The chosen buildings and the cost assumptions stay the same as in the *Min Cost* scenario from Section 5.3. The goal is to define the cost minimal supply structure to reach a GHG neutral building stock.

Thereby, different pathways towards reducing the GHG footprint are imaginable. The following three target cases are introduced:

1. The **Self-sufficiency** case is defined fully equivalent to the *Min Cost* scenario. The imported electricity from the grid has a GHG footprint of 122 g/kWh and only marginal incentives are given to feed electricity into the grid. In consequence, the only option to further reduce the GHG footprint are efficiency measures or self-supply with renewable energy.
2. The **Net zero emission** case is following the goal of the European Union of net Zero Emission Buildings. The imported electricity also still has a GHG footprint of 122 g/kWh as in the *Min Cost* case, but the feed-in has equivalent negative emissions of 122 g/kWh. In consequence, the building stock has an incentive to generate more on-site electricity and can become GHG neutral by compensating for its demand via an electricity feed-in.
3. The **Renewable grid** case assumes that the central electricity supply will become 100 % renewable, constituting a GHG footprint of 0 g/kWh. In conse-

quence, the buildings only have to switch completely from fossil resources to a full electrification or more expensive renewable fuels.

The pathways to reach the three cases of GHG neutral building stock are introduced for an aggregated perspective in Section 5.3.5. Section 5.3.5 discusses then the final cases in between as well as their impact on the electricity grid.

Pathways to reach GHG neutrality

The objective of minimizing the GHG emissions is achieved by weighting them in the objective function. The annual costs are kept with a constant weighting of one, while the GHG emissions are weighted by a price, distorting the cost optimal systems towards a more GHG friendly solution. A strict constraint to the GHG emissions is avoided since the results are determined by independent optimizations of different buildings. Thereby, different buildings have different GHG avoidance costs. In order to reach an aggregated efficient pathway, the different GHG avoidance measures are globally accessed by increasing the relative GHG prices.

The results for the annual cost and the resulting GHG emissions are shown in Figure 5.24.

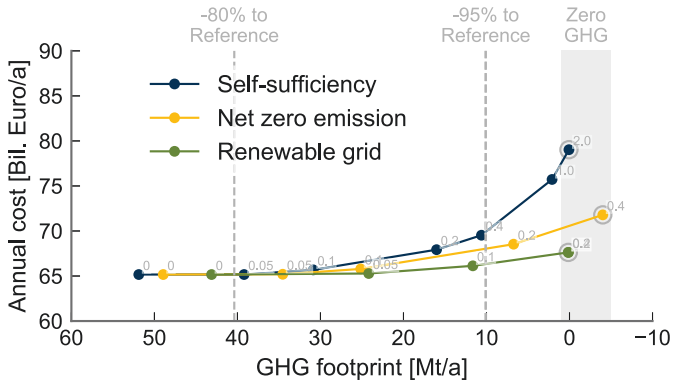

Figure 5.24: Pareto front between residential costs and GHG emissions for the three pathways to reach a GHG neutral building stock for the *Min Cost* scenario in 2050. The gray numbers define the weighting of the GHG emissions in Euro/kg.

All paths start at the same annual cost level of 65 Bil. Euro/a, which is equivalent

to the cost of the *Min Cost*. Also the system design is the same between the three cases and the *Min Cost* for a weighting of the GHG emissions by zero. Nevertheless, the GHG emissions are at different levels, since they are differently assumed between the different pathways: The *Self-sufficiency* pathway starts with the highest emissions of 51.9 Mt/a, fully equivalent to the *Min Cost* scenario, while the *Net zero emission* pathway starts with reduced emissions of 48.9 Mt/a due to a compensation by the small photovoltaic feed-in. The *Renewable grid* pathway starts with the smallest amount of GHG emissions of 43.1 Mt/a, which is still not sufficient to reach a reduction of 80 % of the GHG emissions to the *Reference* scenario.

Based on those solutions as a starting point, the weighting of the GHG emissions is iteratively increased in the objective function. In consequence, the systems get more expensive since they are pulled out of the cost optimum towards a more GHG friendly solution. Noteworthy is that the resulting increase of the annual cost in Figure 5.24 is just related to the cost differences inside the systems and does not include the weighting factor of the GHG emissions themselves.

All three pathways are able to reach GHG neutral systems that are highlighted with gray circles, although different GHG weightings are required. For the *Renewable grid* pathway, only a weighting of 0.2 Euro/kg is required to reach GHG neutrality with a moderate cost increase to 68 billion Euro per year. The *Net zero emission* pathway slightly overshoots the GHG neutrality goal with a weighting of 0.4 Euro/kg and a cost increase to 73 billion Euro per year. It is the only pathway that is able to have negative GHG emissions by having a higher electricity grid feed-in than electricity demand. The most expensive pathway is the *Self-sufficiency* path that needs a GHG weighting of 2.0 Euro/kg to reach GHG neutrality and results in costs of 79 billion Euro per year.

The resulting annual cost compositions for the different pathways are illustrated in Figure 5.25. All pathways start with the same system design and take similar adaptions to reduce the GHG emissions until a GHG weighting of 0.2 Euro/kg: The amount of purchased fossil gas is reduced together with the capacities of fuel cells and gas boilers, and the capacities of heat pumps and photovoltaics increase. Additionally, pellet boilers are built that combust 7.5 to 10.2 TWh/a pellets.

Differences exist at 0.2 Euro/kg in the battery capacities: While they are extended in the *Self-sufficiency* and the *Net zero emission* pathways to 27.8 and 23.8 GWh, they are reduced to 7.76 GWh in the *Renewable grid* case. In the latter case, the increased weighting of the GHG emissions does not affect the electricity imported. In consequence, no increased incentive is given to self-consume the photovoltaic electricity. Instead, the flexibility provided by the increasing amount of heat pumps compensates for the demand for batteries in the *Renewable grid* path, reducing the economic value of batteries.

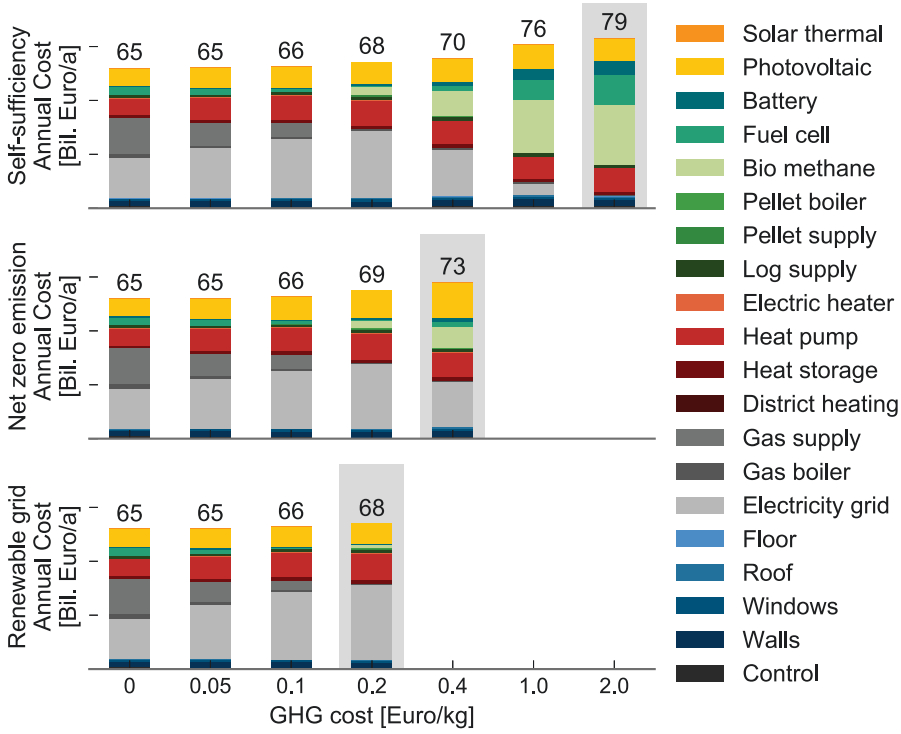

Figure 5.25: Composition of the annual cost of the three GHG reduction pathways of the *Min Cost* scenario with different GHG weighting costs.

Further, for a GHG weighting of 0.2 Euro/kg all three pathways include gas boilers that are operated with a bio-methane between 10.7 and 13.6 TWh/a. Those are primarily integrated in small efficient buildings where a heat pump investment would not be cost optimal. For the *Renewable grid* case, no self-supply with fuel cells remains since the energy costs of the fossil gas and bio-methane exceed the electricity import price. This is different for the *Self-sufficiency* and the *Net zero emission* scenario where the GHG footprint of the electricity purchased from the grid is avoided and small fuel cell capacities of 1.2 to 1.3 GW are built, which consume between 12.2 and 15.7 TWh/a bio-methane.

While the *Renewable grid* pathway has reached GHG neutrality for a weighting of 0.2 Euro/kg, it needs to be further increased for the other two scenarios: The *Net zero emission* pathway reaches GHG neutrality with 0.4 Euro/kg. Therefore, the

photovoltaic capacities increase further up to 295.2 GW and the renewable operated fuel cells reach an electric capacity of 7.7 GW. 116.7 TWh/a of electricity are fed-in to the grid by the photovoltaic, while only a residual demand of 83.8 TWh/a is purchased from the grid. 31.7 TWh/a are self-consumed from the fuel cell while 125.4 TWh/a are self-consumed from the photovoltaic. This highlights the accessible potential for photovoltaic self-consumption.

The *Self-sufficiency* pathway needs even higher incentives up to 2.0 Euro/kg to reach GHG neutrality. Then, the buildings do not purchase any fossil resources or electricity from the grid at all. Instead, high fuel cell capacities up to 34.5 GW are built that are operated with bio-methane to self-supply the buildings with 101.4 TWh/a of electricity. This goes along with a massive capacity of 145.1 GWh of batteries and 180.47 GW of photovoltaics. However, the overall cost of the system increases due to the expensive self-generation systems, and a further rollout of refurbishment measures in order to reduce the electricity demand of the heat pumps is not happening. The space heat demand still amounts to 297.7 TWh/a from which 243.9 TWh/a are provided by the heat pumps and the rest by the fuel cell, electric heater and fireplaces.

In all three GHG neutral cases, no major additional refurbishment measures are chosen, besides the ones that are already integrated in the *Min Cost* scenario. For the *Renewable grid* case the demand for space heating even increases from 309.8 TWh/a to 320.8 TWh/a. The increasing share of heat pumps reduces the heat reduction potential of the occupancy controllers wherefore less are implemented and a higher heat demand results, as explained in Section5.3.3. For the other two cases, the space heat demand is reduced to 303 TWh/a and 297 TWh/a. Nevertheless, the potential to reduce the space heat demand is by far not exploited, indicating that the majority of measures on the supply side are more cost effective. Furthermore, it shows that the supply side is highly sensitive to the requirements and regulation definitions, while the demand side is more or less robust to extrinsic conditions due to its high costs.

Grid impact of GHG neutrality

While the previous section introduced different pathways to GHG neutrality, the following section describes the different grid impact of the final GHG neutral cases.

The differences in the supply structure of the pathways also constitute the differences of the grid load, as visualized in Figure 5.26. The *Self-sufficiency* scenario has for most of the hours no grid load at all, and just feeds in photovoltaic electricity with a peak load up to 58.3 GW in the summer. The amount is slightly higher than

for the *Min Cost* case.

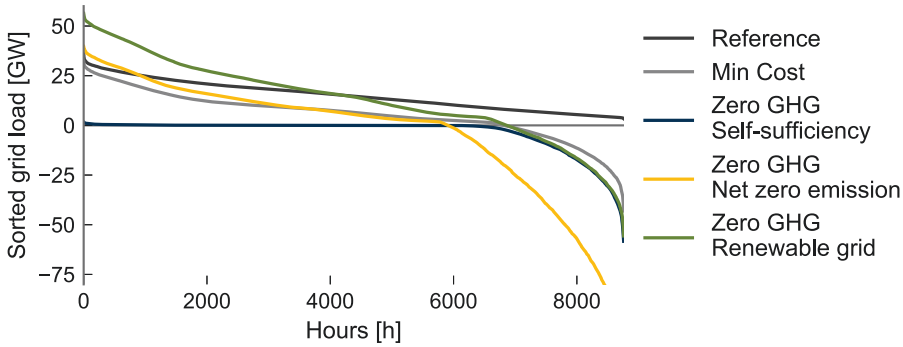

Figure 5.26: Sorted grid load of the aggregated residential building stock for the *Min Cost* scenario and the three GHG neutral cases.

The *Net zero emission* case has with 39.7 GW a higher peak load than the *Min Cost* scenario with 32.3 GW, due to a reduced fuel cell capacity and an increased heat pump capacity. Its peak load even exceeds the peak load of 36.4 GW of the *Reference* scenario. Nevertheless, its feed-in is order of magnitudes higher than the *Min Cost* scenario and peaks with 127.9 GW. Such a high capacity would expectantly exceed the grid limitations, although an integrated curtailment rate of 50% of the installed photovoltaic capacity is already included for each building. Further regulations or feed-in tariff designs designs would be required to flatten the profile and reduce the peak feed-in.

The highest peak load results from the *Renewable grid* scenario with 56.4 GW, which is 57% higher than the maximum *Reference* load. The only self-generation is given by the photovoltaic and is not able to reduce the peak demand of the heat pumps in the winter days. It indicates the impact of full electrification of the residential heat sector when no self-generation can compensate for the increasing demand.

Those changes of the peak load spatially vary between the different scenarios, as seen in Figure 5.27.

The figure shows the change of the three Zero GHG cases in comparison to the *Reference* scenario. While the peak load gets reduced by 100 % for the *Self-sufficiency* case for the rural regions as well as for the urban regions, differences occur for the two other scenarios: For the *Net zero emission* scenario an increase of the peak load in the Rural regions up to 100 % occurs, which is in a similar trend as

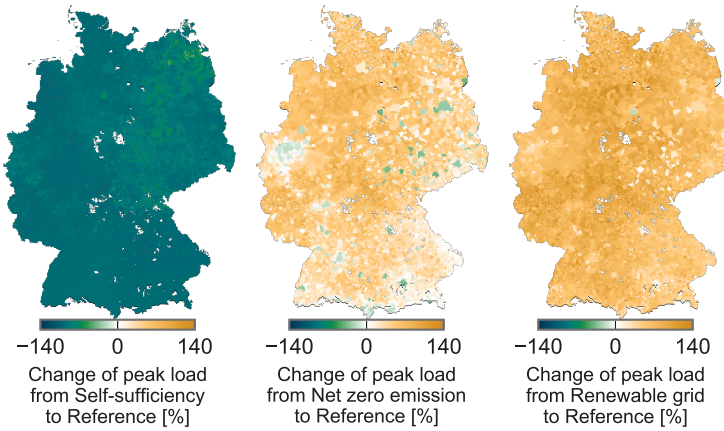

Figure 5.27: Change of the peak electricity demand from the different Zero GHG cases to the *Reference* scenario. 0 refers to no change, while positive values state an increase and negative values a reduction.

in the *Min Cost* scenario: The heat pumps demand electricity when no photovoltaic generation or other self-generation occurs and increase the total grid load. This effect is smaller in the urban regions since the small bio-methane operated fuel cell capacities reduce the heat pump load. For the case of the Renewable grid, the peak load even increases above 140 % of the *Reference* load. The difference between rural and urban regions is not that significant anymore, since no self-generation by fuel cells is built in the cities. Nevertheless, the increase of the electricity demand is still higher in the rural regions because there the specific demand for space heating is higher.

The change of the demand, basically the positive residual load, is visualized in Figure 5.28.

Again, the *Self-sufficiency* case obviously has no significant demand. For the other two cases, the change of the demands has a similar trend as the change of the peak demand. Nevertheless, the scales are different: The demand in the *Net zero emission* scenario reduces mainly in the urban areas, while in some rural areas an increase between 20 and 30 % is observed. The self-consumption of photovoltaics is not able to compensate for the increasing electricity demand of the heat pumps. This effect is enhanced in the *Renewable grid* scenario where the demand even doubles in some rural regions.

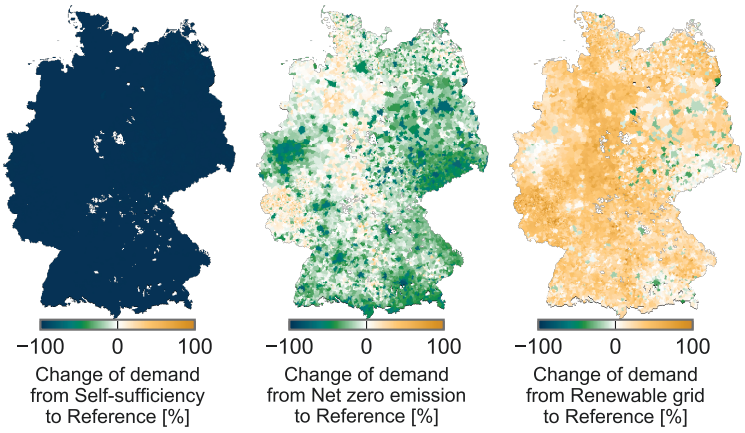

Figure 5.28: Change of the electricity demand from the different Zero GHG cases to the *Reference* scenario. 0 refers to no change, while positive values state an increase and negative values a reduction.

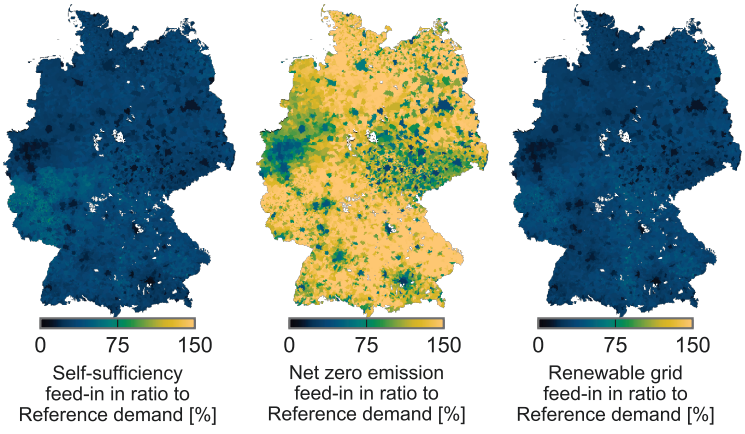

Figure 5.29: Feed-in of the different Zero GHG cases in ratio to the electricity demand of the *Reference* scenario. Above 100 percent refers to a higher cumulative feed-in of electricity than the region originally had as electricity demand.

Significant differences are observed for the comparison of the photovoltaic feed-in, shown in Figure 5.29.

The *Self-sufficiency* case and the *Renewable grid* case are similar: No feed-in exists in the urban areas where all photovoltaic generation is self-consumed. In the rural areas up to 50 % of the original electricity demands are fed-in to the grid, mainly constituted by the bigger roof areas with a higher potential of photovoltaic installations. This effect magnifies for the *Net zero emission* case: The rural areas are able to feed-in over 150 % of the *Reference* electricity load, indicating the huge photovoltaic potential that can be exploited. Nevertheless, for this case the urban areas are not self-consuming all photovoltaic generation anymore, wherefore they are able to feed-in around 30 % of the *Reference* electricity demand.

5.4 Discussion

While the previous sections introduced the results of the scenarios, they are compared and discussed with the related literature in the following section. First, Section 5.4.1 compares the absolute results between each other and evaluates them in terms of global feasibility. Afterwards, they are compared to the results reported in the literature in Section 5.4.2. Last, Section 5.4.3 analyzes the results in the context of the novel modeling approach.

5.4.1 Evaluation of the scenario results

A comparison of the resulting final energy demand of the considered scenarios is shown in Figure 5.30 and Table 5.12 summarizes the key results.

The *Min Cost* scenario is able to achieve a reduction of the final energy demand from 679.6 TWh/a to 355.3 TWh/a or 47.8 %, excluding the self-consumption with photovoltaics and the environmental heat. This reduction is on one hand achieved by saving 31.2 % of space heating in comparison to the *Reference* scenario. The other reductions result from a more efficient usage of the energy carriers in the supply system, e.g. the combination of fuel cells together with heat pumps can supply space heat with a much higher efficiency than the simple usage of combustion boilers. The second driver is the high self-consumption of photovoltaic electricity of 89.7 TWh/a, of which a significant amount is used for Power-to-Heat applications.

Similar efficiency potentials are used in the Zero GHG cases, nevertheless the energy carriers are changing.

The *Self-sufficiency* scenario switches completely to bio-methane with 202.4 TWh/a to operate fuel cells for self-consumption. It is the most expensive zero GHG case and also the most challenging to deploy, since the potential for biogas is limited. Although 505.3 TWh/a of domestic biomass potential are predicted in Germany for 2050 [FNR, 2016], this would further need to be fermented, purified and fed-in to the gas grid. Therefore, also the bio-methane potential that could be fed-in to the grid is just predicted to 109.2 TWh/a for 2030 [DVGW, 2014]. Additionally, cross-sectoral models [IWES, 2015] conclude that the usage of chemical energy carriers for space heating should be minimized since its usage is more crucial in the industry and mobility sectors. Also, the replacement of bio-methane with hydrogen is challenging since it would further increase the residential supply cost because the hydrogen price is expected to be with 16.5 ct/kWh [Robinius, 2015] above the 13.8 ct/kWh assumed for the bio-methane, even without tax. In summary,

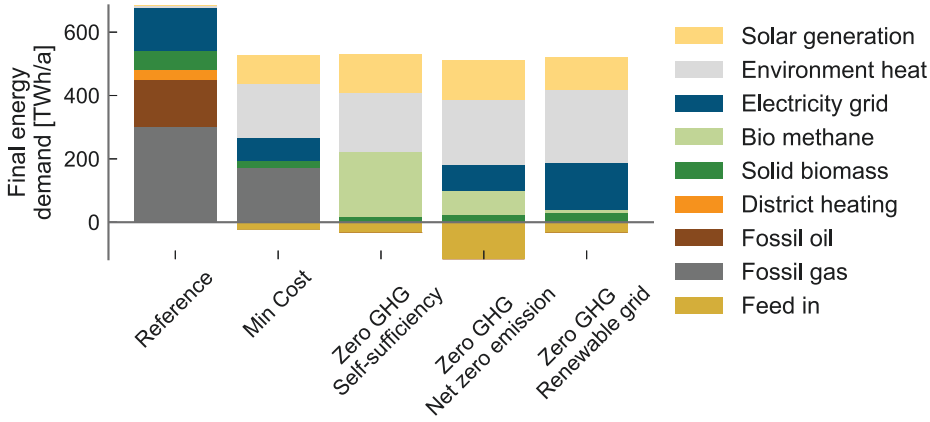

Figure 5.30: Comparison of the final energy demand of the different considered scenarios in this work.

the self-sufficient supply systems in this zero GHG case are only independent from the electricity grid but rely further on significant fuel consumption. Therefore, they have a limited value from a central systems perspective.

Instead an interaction with the grid should be encouraged, as in the *Net zero emission* case with a moderate cost increase to the *Min Cost* scenario. Thereby, a mixture of 83.7 TWh/a of electricity, 73.6 TWh/a of bio-methane and 25.1 TWh/a of solid biomass are imported while 116.7 TWh/a of electricity are fed-in to the grid. The bio-methane is also used in the fuel cells to generate electricity for self-consumption primarily in the winter hours. Therefore, they can compensate for the additional load of the heat pumps and no significant increase of the aggregated residential peak load results. Nevertheless, the 7.7 GW_{el} fuel cell co-generation units are mainly installed in the urban areas since they are too expensive for the low energy densities in the rural areas. In consequence, the peak load is increasing in the winter in the rural areas up by 140 % in comparison to the *Reference* load. Therefore, future analyses would need to consider the grid capabilities to balance the micro-generation in the urban areas and the increased demand in the rural areas.

The *Renewable grid* case switches almost completely to the sole import of electricity and results in a demand of 148 TWh/a, which is even above the demand of the *Reference* scenario. It has no incentive to self-generate electricity with co-generation in winter, wherefore the load is also increasing for the aggregated na-

Table 5.12: Comparison of the key results of the *Min Cost* scenario in 2050 and the three case studies to reach zero GHG emissions.

	Min Cost	Self sufficiency	Net zero emission	Renewable grid
Annual cost [Bil./a]	64.8	78.6	71.4	67.2
Peak-load [GW]	32.2	1.8	39.74	56.4
Space heat [TWh/a]	309.8	297.7	303.0	320.8
Grid demand [TWh/a]	71.9	0.5	83.7	148.2
Fuel demand [TWh/a]	193.6	221.5	98.6	40.1
Feed-in [TWh/a]	24.1	23.3	116.7	34.0
Batteries [GWh]	16.9	145.1	44.3	7.0
Fuel cells [GW_{el}]	12.7	34.5	7.7	0.0
Photovoltaic [GW_{el}]	133.4	180.5	295.5	160.9
Heat pumps [GW_{th}]	60.4	68.0	78.5	85.1

tionwide perspective due to a peak demand of the heat pumps by 26.1 GW_{el}. Although it is the most cost effective zero GHG case, it has the highest impact on the grid infrastructure and does not compensate for its high electricity demand by a feed-in.

5.4.2 Comparison of the scenario results to the literature

The following section discusses the scenario results for 2050 in comparison to the results in the literature. The validation of the model is found in Section 5.2.

Heat pumps

Significant for the change of the electricity peak load is the high diffusion of the heat pumps that constitute an additional load of 18 to 26 GW_{el} operated with above 3500 full load hours in winter.

For comparison, the *FORECAST* model predicts only a total electrical heat pump load of around 5 GW for all sectors in winter 2050 [Boßmann and Staffell, 2015] plus a significant reduction for other electric heating applications. Such low demands for electrically generated heat can only be achieved if the majority of the

residential heat is still supplied with chemical energy carriers, and if high refurbishment rates are already considered. Similarly, the study *Energieeffizienzstrategie Gebäude* [BMWi, 2015] assumes a limited potential for the heat pumps in 2050 with 58 to 100 TWh/a of environmental heat that can be used. This is exceeded by all scenarios in this work, which use between 170.4 TWh/a and 228.7 TWh/a of environmental heat. The limited potential in the *Energieeffizienzstrategie Gebäude* study [BMWi, 2015] is justified by the slow market development of heat pumps in recent years. Their share in new constructions has stagnated since 2010 [DESTATIS, 2014] while above 50 % of the new buildings are still built with gas boilers. Nevertheless, these limitations are not constituted by limited production capacities of the heat pumps, instead the current levy structure of the energy prices benefits gas boilers [Lindberg et al., 2016a; Schütz et al., 2017b].

The other extreme is defined by Fehrenbach et al. [2014]: They apply the *TIMES* model to estimate the future load management potential of the residential heating sector and result in 67 GW_{el} of heat pumps for 2050. Those over-capacities are not installed in this work, since the heat pumps are too expensive and other peak boiler technologies are installed to avoid too high costs. Further, no extrinsic incentive is considered to install higher capacities for additional flexibility. Nevertheless, the cross-sectoral optimization of Germany IWES [2015] also concludes that 39 GW of heat pumps are required in 2050 to reach an overall GHG reduction in Germany of 83% from 1990.

In summary, the resulting deployment of heat pumps aligns between the results' cross-sectoral optimization models as upper bound and the results of GHG reduction strategies for the sole building stock as lower bound. Nevertheless, the comparison also shows limitations of the model since replacement rates of the heating system are currently not considered in the model and should be extended. The technical lifetime of heating systems can be assumed on average to be 25 years [BMWi, 2018]. To reach sufficient deployment rates of heat pumps in 2050, e.g. Diefenbach et al. [2016] concluded that by 2025 at the latest, no new gas or oil boilers can be allowed to be installed. Therefore, either the gas price has to significantly increase, or the combustion of fossil fuels for space heating needs to be regulated and finally prohibited.

Solar energy

Most studies focusing only on the heat supply of buildings [BMWi, 2015; Diefenbach et al., 2016; Beuth, 2017; BMWi, 2018] consider a significant share of solar thermal collectors for the space heat supply and hot water supply in 2050.

In this work, no significant share of solar thermal rooftop collectors is installed. The reason is that solar thermal is not an economically competitive option from a single building perspective, which is already observed today [Evins, 2015; Lindberg et al., 2016a; Schütz et al., 2017b; Wu et al., 2017]. Nevertheless, rooftop solar thermal installations are also avoided from a cross-sectoral perspective in 2050 while only large-scale solar thermal for district heating is favored [IWES, 2015].

Instead, the rooftops are used for photovoltaic capacities between 133.4 and 295.2 GW, depending on the scenarios. The capacities are below the technical potential for residential rooftop photovoltaics in Germany of 641 GWp for 2050, which was concluded by Mainzer et al. [2014]. Excluding the *Net zero emission* scenario, the only motivation in the scenarios for photovoltaic deployment is self-consumption. Already the *Min Cost* scenario results in 89.7 TWh/a of photovoltaic electricity usage inside the building, which indicates the high potential that photovoltaic self-consumption can have to reduce the final energy demand. This self-consumption can be achieved by a combination of batteries, heat storage systems and the thermal storage capacities of the buildings. It illustrates further the advantage of photovoltaics in comparison to solar thermal: The electricity can be used in cheap electric heaters for high temperature hot water demand, with high efficiency in heat pumps for low temperature space heat, and for the supply of conventional electrical appliances. Although the self-consumption values seem high, Prognos [2016] concludes for single- and two-family buildings plus agriculture a potential of 38.7 TWh/a for photovoltaic self-consumption in 2035, where half of the energy is used for new heat applications. The value is in a similar magnitude as the predictions of the *Min Cost* scenario for 2050, where the single- and two-family house have 53.0 TWh/a of photovoltaic self-consumption. Nevertheless, this work additionally shows the high self-consumption potentials that could be achieved in urban areas with multi-family houses.

Fuel cells

In this work, the load increase by the heat pump is partially compensated with distributed fuel cell installations between 7 to 12 GW_{el} that are used for co-generation, exhibiting around 5000 full load hours. The values align well with Jungbluth [2007] who concludes a potential up to 12 GW_{el} for fuel cells in the year 2050 with the same amount of full load hours. The general installation of co-generation units in 2050 is supported by the majority of the reviewed studies [IWES, 2015; BMWi, 2015; Diefenbach et al., 2016; UBA, 2017b] since it states an efficient and flexible usage of the chemical energy carriers.

In the scenario of this work, fuel cells are more cost effective than internal combus-

tion engines, although the investment costs of the fuel cells are significantly higher for large scales. Nevertheless, the smaller electrical efficiency and the higher maintenance cost of the combustion CHP make them noncompetitive in the considered scenario for 2050.

The placement of fuel cells results in mainly multi-family houses wherefore they are only installed in urban areas. This is reasonable, since also spatially resolved energy system models conclude that flexible generation should be generally deployed close to demand centers [Zeyringer et al., 2018]. Nevertheless, the rural areas are in consequence critical to the grid, since they cannot compensate for the heat pump demand.

Energy savings

The used energy saving potential due to the construction of new buildings and refurbishment measures constituted a reduction of the space heat demand between 28.5 and 33.7 % in the *Reference* scenario. Although higher saving potentials of up to 53.5 % are illustrated in the sensitivity analysis and could have been achieved by higher refurbishment rates or higher refurbishment depth in this work, they are not exploited in the cost minimization due to their high costs.

The conclusion that the assessment of further energy savings is expensive is supported by the comparison of the scenarios in the *Energieeffizienzstrategie Gebäude* [BMWi, 2015]: Their *Energieffizienz* scenario results in final energy demand savings of 54 % and is above 30 % more expensive than the *EE-Szenario*, which has savings of 36 %. Also the unconstrained optimization of the cross-sectoral model by UBA [2017b] concludes that only the final energy demand savings of 24% from 2008 until 2050 are cost optimal.

Finally, the sensitivity analysis in Section 5.3.3 showed that higher refurbishment rates are not only expensive but do not necessarily have a significant impact on the GHG emissions: the resulting smaller heat demand can be supplied with cheap, yet inefficient heat generators, such as fossil fuel boilers, more cost effectively. Nevertheless, their high specific emissions deplete major parts of the GHG reduction potentials of the energy saving measures.

Summary

All in all, the deployed technology capacities and chosen efficiency measures align well with the results reported in the literature for the scenario in 2050. Therefore, also the spatial-temporal changes of the grid load can be concluded to be valid.

5.4.3 Discussion of the model approach

The *Reference* scenario shows that the model aligns with the final energy demand values reported by the AGEB [2017], provided that a sufficient number of archetype buildings is assumed. This is remarkable since a full bottom-up approach was taken that was not thoroughly fitted to the aggregated values. Nevertheless, minor deviations remain for rarely occurring building attributes, partially due to a lack of data and partially due to the aggregation to too few archetype buildings. Therefore, the demand for secondary energy carriers such as pellet boilers or solar thermal is underestimated in the *Reference* scenario, but also compensated for by the demand for other energy carriers. While this effect is on an aggregated national perspective small, it could be more significant on a disaggregated municipality perspective, although no sufficient data was found to validate it.

The analysis of the spatial impact of different weather years further shows the relevance of also modeling the nationwide energy performance based on spatially distributed weather time series. While it is common to include the impact of modeling different weather years, their spatial impact is neglected in energy performance models [Mata et al., 2014; McKenna et al., 2013; BMWi, 2015; IWES, 2015; UBA, 2017b]. Nevertheless, the example of the energy performance in the year 2010 illustrates their relevance: While 2010 was in general a cold year with a high nationwide energy demand, it impacted north-west Germany by an increase of the energy demand of up to 17 % above the average demand between 2010 and 2015, while for south-east Germany the increase amounted to only 11 %. Vice versa, an error above 6 % can be induced for an aggregated final energy demand prediction depending on the chosen location of the weather data. For temporally resolved results, even higher deviations are expected.

The optimization of the future residential supply structure reveals at the same time a strength and drawback of the approach: The sole financial agent decision making is known to perform well in rate of adoption and cumulative adoption but underestimates social and attitudinal components influencing the technology adoption [Robinson and Rai, 2015]. Therefore, only a few economically dominant technologies are chosen in the *Min Cost* case, although even a higher diversity would exist

in reality due to individually varying information levels. As a case in point, pellet boilers were down-selected, although those are considered in different scenarios in the literature [IWES, 2015; BMWi, 2015]. This dominance is related to the scenario, and a consideration of different biomass prices could change this. Nevertheless, in reality an adoption of pellets would also be expected without being economically competitive. Such non-cost optimal adoption behaviors are better included in simple adoption models such as *Invert* tool [Kranzl et al., 2013; Müller, 2015] that includes a statistical randomness in the adoption process, but neglects, e.g., the temporal operation. Nevertheless, the information basis for investment decisions is improving and wherefore the assumption of future cost optimal investment stays reasonable.

Still, a diversity of chosen supply technologies and refurbishment measures remains due to the diversity of building types. Different technologies are cost optimal for different building types, wherefore no single dominant system configuration exists in the scenarios. This makes the aggregated model robust to extrinsic changes, as shown in Section 5.3.3. E.g., the lack of the supply of an energy carrier can significantly impact a single building because it was previously supplied by it. On the other hand, a second building may have a completely different supply structure with the consequence that it is not affected at all. Further, this diversity of the building types also results in a spatial diversity of the supply technology adoption. This different adoption has a spatially varying impact on the grid load, confirming the assumption that the load will not change uniformly. This further justifies the spatially distributed approach of the bottom-up model that is able to predict those different changes.

Another advantage of the temporally resolved bottom-up approach is that capacities of the installed technologies can be predicted together with their related costs. Approaches relying on energy balances [BMWi, 2015; Diefenbach et al., 2016; BMWi, 2018] or on an aggregated central load [IWES, 2015; UBA, 2017b] are either not able to predict them, or underestimate them. The results of the bottom-up model in this work show that the installed technology capacities exceed the aggregated peak loads of the technologies, since the peak loads are occurring in different times in different buildings. Therefore, aggregated single node or single region models tend to underestimate the costs of the energy supply. Nevertheless, this effect applies mainly for cheap peak boiler technologies while expensive technologies are designed to have many full load hours.

The spatial disaggregated analysis also revealed limitations of the model: In the *Min Cost* scenario, the net load increase in the rural areas of Rhineland-Palatinate and the Saarland exceeds the load increase in the other rural areas, although no clear structural difference exists in comparison to the other regions. The reason for this deviation is that 200 archetype buildings are still not sufficient to model the

stochastic balancing effects of different building types and different optimal investment decisions on a municipality scale. If there is a single building significantly representing different municipalities, and this building is sensitive to the scenario, it overly impacts the change of the supply structure in the municipality, although a more diverse building stock would not be as sensitive. Higher numbers of archetype buildings can decrease this effect, as shown in Appendix B.3 and Appendix C.2.

Lastly, the good alignment with the reported final energy demand values of today makes the model further suitable to develop transformation paths of the building stock until the year 2050. E.g. additional projected supply years in 2020, 2030 and 2040 could be modeled. Such an approach could better consider the different lifetimes of the technologies and respect the inertia in the adoption process of the building owners. As seen in the discussion in Section 5.4.2, also adaptions of the current regulations could be better derived since their impact today can be extrapolated into the future.

5.5 Summary

This chapter introduced different scenarios for the residential energy supply, applied them to the models introduced in Chapter 3 and Chapter 4 and analyzed the resulting systems and their related grid impact.

Therefore, first all techno-economic parameters were introduced in Section 5.1 mainly based on the study *Energieeffizienzstrategie Gebäude* [BMWi, 2015] and technology specific analysis in Appendix A.3. Two scenario frames were derived: The year 2015 is used for validation and the year 2050 is defined for the future scenarios.

The first application was shown in Section 5.2 where the model is validated to the aggregated energy demand values provided by the AGEB [2017]. It was observed that a minimal number of archetype buildings is required to respect the diversity of the residential energy supply, while 200 archetype buildings were concluded to be sufficient for this work. The aggregated final energy demand could be met by the model with deviations below 2 %, depending on the weather year.

Afterwards, Section 5.3 introduced a cost minimal residential energy supply for the year 2050. It showed that the dominant supply technologies are photovoltaics, heat pumps and co-generation units in the form of fuel cells. Nevertheless, their deployment differs between rural and urban areas, significantly impacting the regional load. The co-generation units are mainly cost effective in urban areas, where they

are able to compensate for the increasing electricity demand of the heat pumps. This does not count for the rural areas where the photovoltaic generation and heat pump demand temporally disjoin, leading to an increased peak load. Since the sole cost minimization is not able to achieve sufficient GHG savings, three pathways to a GHG neutral residential building stock were introduced. Thereby, the pathway with net zero emissions was concluded to be the best compromise between grid impact and cost increase.

The chapter closed with a discussion in Section 5.4.1 and compared the scenario results to the results in the literature.

Chapter 6

Summary

The following chapter recapitulates the main methodological contributions of this thesis, summarizes the scenario results and outlines the central conclusions.

6.1 Scope and objective

Installation of distributed energy resources and electrification of the heat supply are promising options to reduce the greenhouse gas emissions of residential buildings. Nevertheless, the magnitude of their deployment and the resulting impact of their operation on the electricity grid infrastructure are uncertain.

Although many studies exist that determine technology and efficiency driven greenhouse gas reduction strategies for the residential building stock, these studies either rely on energy balances without a temporal resolution or do not consider single buildings. Therefore, they are not able to predict the resulting grid load or to derive the potential for self-sufficient energy supply of the residential building stock.

Consequently, this thesis closes this gap and introduces a new approach that predicts bottom-up the cost optimal technology adoption in residential buildings and derives the spatially and temporally resolved grid load.

6.2 Methodology and contributions

First, a **single building optimization model** is developed that determines the design and operation of the energy supply for single residential buildings. Thereby, a stochastic occupancy simulation based on a Markov chain defines the required demands for appliance electricity, hot water and thermal comfort with a high temporal resolution. It is able to respect the high fluctuation of single household profiles and their dampening for larger aggregations of households, which is significant for the prediction of self-consumption rates and the economic evaluation of supply technologies. Those demands need to be satisfied. Therefore, a generic optimization model is developed that designs and operates the residential energy supply system, e.g. photovoltaics, batteries, heat pumps etc., together with potential refurbishment measures of the building, e.g. additional roof insulations. It is implemented as a Mixed-Integer Linear Program that can be parametrized by all building types defined by the *EPISCOPE* database for the weather years 2010 until 2015 in the whole of Europe.

Nevertheless, the complexity of the model and the diversity of decision variables make it computationally challenging. Therefore, **time series aggregation** methods are introduced to reduce the temporal dimension of the model. They are promising, but novel state descriptions are required and developed in this thesis to sufficiently account for seasonal storage options. Further, a two-level optimization approach is proposed to separate the binary structural design decisions, and the continuous scale and operation related decisions. Such, it is possible to design energy supply systems with a high accuracy and a lean computational load, which is crucial since it is applied to a diversity of building types.

In order to determine the design of whole building stocks, a novel algorithm for the aggregation of **spatially distributed archetype buildings** based on Census data is developed. Thereby, the relevant attributes to describe an archetype building are discussed and introduced for Germany on the municipality level. Due to the structure of the data, no standard cluster approach is applicable to derive archetype buildings. Instead, a novel algorithm is proposed which divides the overall problem into two mathematical programs that are iteratively solved. It is applied to the German residential data for a varying number of archetype buildings, while the estimation errors to the different building statistics in the municipalities is reduced with an increasing number of archetype buildings. It is shown that already 25 buildings are enough to meet the aggregated building attribute distributions for Germany by a fit of 90.4 %. Nevertheless, 200 archetype buildings are concluded to sufficiently respect the diversity of the buildings in the municipalities while meeting the aggregated distributions by 98.2 %. Still, the number of archetypes can be flexibly adjusted depending on the required accuracy and the available computational re-

sources.

6.3 Scenario results

The single building model is applied to the spatially resolved archetype building stock of Germany. It is shown in the *Reference* scenario that the energy demand predictions of the bottom-up model **align with energy demand statistics** for Germany for the years 2010 until 2015 with 200 archetype buildings. Less archetype buildings are not able to represent the diversity of the residential energy supply structure in detail. Further, the variation of the weather years revealed that the extreme weather years are spatially differing: e.g., 2010 was in general a cold year with a high nationwide energy demand but it impacted the north-west by a total increase of 17 % above the average final energy demand, while for south-east Germany the increase amounted only to 11 %. This highlights the potential of the developed model to predict regional extreme scenarios that are essential for the design of a supply infrastructure.

To predict the change of the energy supply and its related grid load, the model is applied to a scenario frame for the year 2050. Thereby, refurbishment cycles and new constructions of buildings are integrated. All measures for energy savings or changes of the residential energy supply technologies, e.g. fuel cells or pellet boilers, are holistically optimized with the objective to **minimize the energy cost in 2050** from the perspective of the single residential building owner, referred to as *Min Cost* scenario.

The **dominant technologies** chosen for the residential energy supply in the *Min Cost* scenario are photovoltaics, heat pumps and co-generation units in the form of fuel cells. The peak heat loads are covered by additional technologies such as gas boilers, fireplaces or electric heaters. Sole gas boilers are cost optimal for small refurbished buildings due to their low investment costs and because the considered high energy prices are secondary for small heat demands. The flexible co-generation units are mainly cost effective in large multi-family houses where they can reach between 4000 to 5500 full load hours. Smaller buildings have too fluctuative electricity demand profiles and too low cumulative demands to reach a sufficient load that justifies the economy of scale of the co-generation units. Photovoltaics are chosen in all buildings such that almost 90 TWh of photovoltaic electricity is self-consumed per year. It is mainly used for hot water generation in summer, in small battery capacities for electrical appliance demand in the evening hours, or in the transient months to operate the heat pumps for space heating. The solar thermal collectors are not competitive in the scenario, especially since they do

not provide additional value besides the generation of hot water in comparison to the photovoltaics. Batteries are only minorly deployed with a total capacity of 16.9 GWh since the flexibility of the electric heat generators is already able to access large parts of the self-consumption potential.

The total annual electricity **grid load** is reduced by 56 % today due to the self-consumption while the aggregated peak load of the residential building sector just decreases by 11 %. Nevertheless, this differs regionally: Peak loads in the rural areas increase up to 100 % since photovoltaic generation and heat pump demand seasonal disjoin. The flexible co-generation units are mainly located in urban areas where they overcompensate for the increasing electricity demand of the heat pumps also in the winter days, such that a decrease of the peak load results. Photovoltaic feed-in is higher in the rural areas but does not exceed 45 % of the original peak demand. Nevertheless, higher feed-in peaks are uncritical since they can be curtailed without significant economic impact.

A **sensitivity analysis** of the scenario reveals enforcing economic effects between heat pumps and photovoltaics due to self-consumption. Also major parts of the fuel cells are not cost optimal for the case that the heat pumps are excluded from the solution space. The heat pumps increase the full load hours of the fuel cells and improve their profitability. Together, they state a cost effective supply system with large flexibility potentials that has a significant higher efficiency than a simple gas boiler. Further, an additional insulation of the envelope of the building is only chosen for the buildings that are in the refurbishment cycle, resulting in a reduction of the space heat demand of 31.2 % to the Reference scenario. Higher extrinsically enforced refurbishment rates significantly increase the cost without resulting in major GHG emission reductions. Instead an opposing effect is observed where the buildings change to cheap fossil boilers that are more cost effective for low energy demands than the investment intensive heat pumps. Nevertheless, the lower energy demands are not able to compensate for the higher carbon footprint of the gas boilers. Smart controllers that dynamically adapt the comfort temperature in the buildings are a cheap solution to reduce the space heat demand and are therefore installed in half of the archetype buildings. Nevertheless, their potential is reduced in case of high refurbishment rates since their absolute energy saving effect is reduced and does not further qualify their additional investment costs.

The sole cost minimization leads not to sufficient greenhouse gas emission savings. In consequence, three pathways to a **carbon neutral building stock** are introduced:

1. First, the technical feasibility of a building stock is shown that is completely independent from the electricity grid. Huge capacities of fuel cells and batteries are required to satisfy the electricity load of the buildings while the heat de-

mand is still mainly supplied by heat pumps. It states the most cost expensive zero emission pathway where an increased demand of other energy carriers such as bio-methane results, questioning the sense of such a transition from a cross-sectoral perspective.

2. The second pathway is inspired by the net Zero Energy Building definition of the European Union where the buildings can compensate for the carbon footprint of the energy demand by an energy export. Such a scenario results in a moderate aggregated cost increase of 10.1 % to the sole cost minimization scenario for the whole building stock. Significantly higher amounts of photovoltaics are deployed that feed 117 TWh/a of electricity to the grid. It illustrates the high potential that the residential building stock can have to an overall energy transition. The residual demand is covered by a mixture of 99 TWh/a of solid and gaseous biomass and 84 TWh/a of electricity. The grid load of the electricity demand is not significant changing to the sole cost minimization case, besides the higher photovoltaic feed-in.

3. The last scenario is based on a consideration of a 100 % renewable electricity grid supply. For this case all buildings switch to heat pumps to lower their carbon footprint while no fuel cells are deployed anymore. Only small peak boilers are operated in the winter with bio-methane. This leads to an increase of the total residential electricity demand to 148 TWh/a while the aggregated peak load of the residential sector increases by 54 % to the Reference scenario. It is the most cost effective zero GHG scenario but has the highest grid impact.

The deployed technologies of the carbon neutral building stock cases are similar to the *Min Cost* scenario with an electrification of the heat supply and high photovoltaic deployment rates. No significant increase of refurbishment measures is recognizable while the integration of the fuel cells is sensitive to the scenario but a shift from fossil to renewable energy carriers is observed.

6.4 Conclusions

All in all, the novel bottom-up model is able to respect the diverse demand of the building stock and to predict the cost optimal adoption and operation of the residential energy supply.

The following main conclusions can be drawn from its application to a supply scenario in 2050:

1. All pathways to a carbon neutral building stock are dominated by the deployment of photovoltaics and heat pumps, stating that their installation is robust in terms of economic and emission reduction objectives.
2. Self-consumption of electricity, especially for electrified heat applications, can significantly decrease the carbon footprint of residential buildings and is more cost effective than refurbishment measures.
3. The significant seasonal change of the residential electricity grid load can only be diminished by distributed flexible co-generation units, e.g. fuel cells within the scenario, that are either operated by a fossil or a renewable fuel.
4. Rural areas are more critical in terms of the peak electricity load than the urban areas since the balancing flexible co-generation units are not cost effective in small single-family buildings. Further, the specific heat demands are higher in the rural regions and constitute higher heat pump loads.

Lastly, the spatial and temporal resolution of the model makes it suitable for a future coupling with grid models to determine congestions and the flexibility potential of the residential buildings sector. The cost optimal adoption and operation approach allows thereby the analysis of the impact of political incentives on the residential grid load.

Appendix A

Optimal residential energy supply

The following Appendix clarifies the sub-models used in the single building optimization model, as introduced in Chapter 3. Section A.1 provides additional data for the electricity load model. The used building data is illustrated in Section A.2. The economic data of the considered supply technologies are discussed in Section A.3.

A.1 Electricity load model

The electricity load model relies on an open-source model from Richardson et al. [2010]. The majority of the data is introduced in their publication and the open-source model. This section further illustrates the relevant resident data in Section A.1.1. The fitting of the profiles to the seasonal variation of a German standard load profile is shown in Section A.1.2.

A.1.1 Resident data

The model is based on a Markov-Chain with transitional state probabilities. The states are discretely chosen in the model. Here, the relative transitional probabilities are multiplied with each other to get the overall probability of a certain activity at a certain time at the day. The resulting probabilities are shown in Figure A.1 for a two person household during week-end. These profiles are further available for one to six person households for week-days and weekend-days.

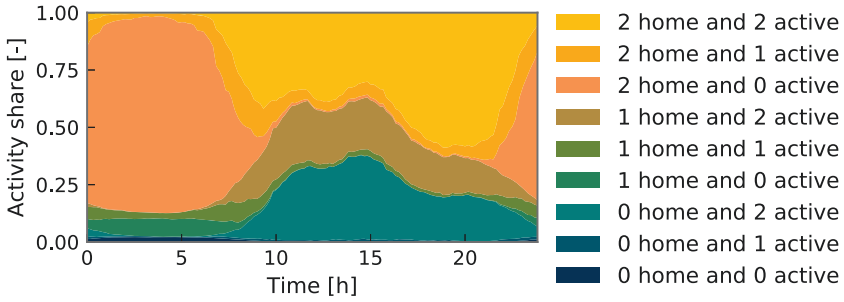

Figure A.1: Activity probability for a two person household during a weekend-day based on the four-state occupancy model of McKenna and Thomson [2016].

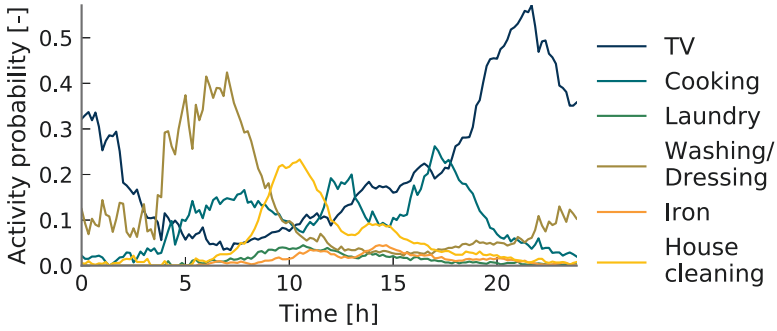

Figure A.2: Occupancy activity probability for a single person during a week-day in case that it is at home and active. The data is based on Richardson et al. [2010].

The visualization illustrates the day-night pattern of active and sleeping occupants. Further, the vacancy of the occupants during the day due to work and other activities is shown.

Different activities are performed for the case that the occupants are at home and active. The probability that an activity is triggered is shown in Figure A.2 for a single active person that is at home.

The used appliances are shown with their related power demand in Table A.1. The *Ownership* defines the probability that the appliance is belonging to the household. The *Activity use* refers to the previously introduced activities that triggers the usage

of the appliance.

While the data provides a good starting point, they should get adapted by national time of use-surveys and new appliance data in future. Further, their change could get predicted into the future in order to incorporate more efficient appliances or a changing occupancy behavior.

Table A.1: Considered appliance data of the electricity load model. It is derived from Richardson et al. [2010].

Name	Group	Activity use	Owner-ship [-]	Standby power [W]	Mean cycles power [W]	Mean cycles length [min]	Delay restart [min]	Calibration scalar [-]
Chest freezer	Cold	Level	0.163	0	190	14	56	0.062728
Fridge freezer	Cold	Level	0.651	0	190	22	44	0.050146
Fridge	Cold	Level	0.430	0	110	18	36	0.031307
Upright freezer	Cold	Level	0.291	0	155	20	40	0.038548
Answer machine	ICT	Active	0.900	1	0	0	0	0.000000
CD player	ICT	Active	0.900	2	15	60	0	0.007206
Clock	ICT	Level	0.900	2	0	0	0	0.000000
Phone	ICT	Active	0.900	1	0	0	0	0.000000
Hifi	ICT	Active	0.900	9	100	60	0	0.000467
Iron	ICT	Iron	0.900	0	1000	30	0	0.008002
Vacuum	ICT	House cleaning	0.937	0	2000	20	0	0.006952
Fax	ICT	Active	0.200	3	37	31	0	0.000839
PC	ICT	Active	0.708	5	140	300	0	0.004226
Printer	ICT	Active	0.665	4	335	4	0	0.002746
TV1	ICT	TV	0.977	3	124	73	0	0.032121
TV2	ICT	TV	0.580	3	124	73	0	0.032121
TV3	ICT	TV	0.180	2	124	73	0	0.034449
VCR/DVD	ICT	TV	0.896	2	33	73	0	0.032121
Receiver	ICT	TV	0.934	15	26	73	0	0.032121
Hob	Cooking	Cooking	0.463	1	2400	16	0	0.012360
Oven	Cooking	Cooking	0.616	3	2125	27	0	0.006480
Microwave	Cooking	Cooking	0.859	2	1250	30	0	0.002753
Kettle	Cooking	Active	0.975	1	2000	3	0	0.006426
Small cooking	Cooking	Cooking	1.000	2	1000	3	0	0.008437
Dish washer	Wet	Cooking	0.335	0	1130	60	0	0.007388
Tumble dryer	Wet	Laundry	0.416	1	2500	60	0	0.029510
Washing machine	Wet	Laundry	0.781	1	405	138	0	0.051719
Washer dryer	Wet	Laundry	0.153	1	792	198	0	0.054725
Elec. heater 1	Water heating	Active	0.170	0	3000	20	0	0.014330
Elec. heater 2	Water heating	Active	0.010	0	3000	5	0	0.035160
Elec. shower	Water heating	Washing/ dressing	0.670	0	9000	3	0	0.009661

A.1.2 Seasonal fitting of the electricity load model

Richardson et al. [2010] already show that the the original CREST-model does not cover the seasonal variation of its validation data set sufficiently. As seen in Figure A.3, this observation applies also for the comparison of the model results with the German Standard Load Profile (SLP) BDEW [2011] for the households (H0) or the measured data set from Tjaden et al. [2015].

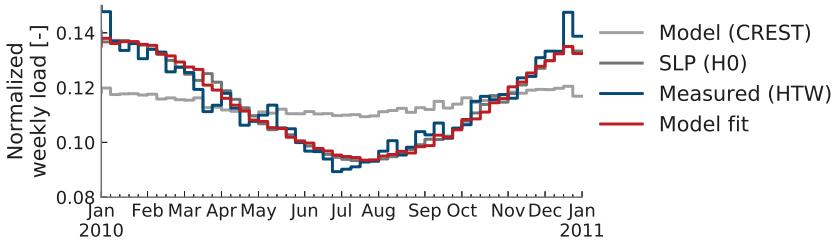

Figure A.3: Comparison of the average weekly load of 1000 normalized annual simulations of the CREST model before and after fitting to the Standard Load Profile and the average HTW profiles.

Therefore, a dynamic correction factor is introduced that strengthens the seasonal variation of the load profiles generated by the load model. The approach is similar to the methodology that is used to create a more dynamic sampling of the SLP BDEW [2011]. A correction factor for every day in the year d_{year} is introduced. It is described by a polynomial 4th order as follows:

$$r_{cor}(d_{year}) = p_0 + p_1 d_{year} + p_2 d_{year}^2 + p_2 d_{year}^3 + p_4 d_{year}^4 \tag{A.1}$$

The coefficients are determined by minimizing the squared error between the mean daily load of the original CREST model and the mean daily load of the SLP for all days in the year. The resulting coefficients are seen in Table A.2 and the fitted CREST model is shown in Figure A.3.

Table A.2: Polynomial coefficients for the seasonal variation of the electricity load model in comparison to the coefficients of the SLP.

	p_0	p_1	p_2	p_3	p_4
SLP	1.24	2.1e-3	-7.02e-5	3.2e-7	-3.92e-10
Model fit	1.14	1.99e-03	-4.91e-05	2.09e-07	-2.46e-10

With the integration of this daily changing coefficient, the updated model is able to describe seasonal variation of the residential electricity load sufficiently.

A.1.3 Deviation between the electricity load model and the two validation profiles

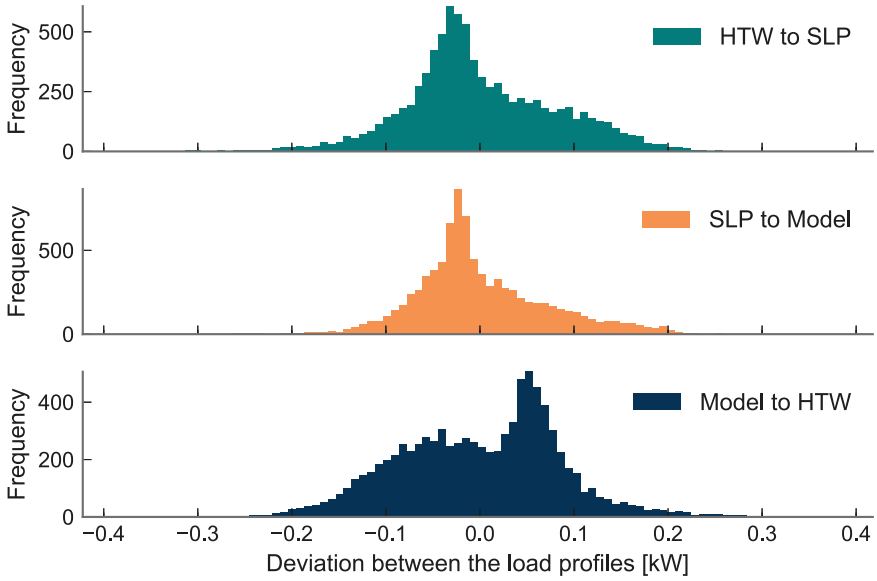

Figure A.4: Distribution of the deviation between the considered electricity load model for 1000 runs (Model) and the two validation profiles (SLP and HTW). The profiles are normalized to 3515 kWh/a.

A.2 Building parameters

Auxiliary to Section 3.2, this section introduces the configuration of the considered building types.

All building parameters are derived from the *Tabula*/*EPISCOPE* database. It has a large scale wherefore this section only illustrates the most relevant parameters for a limited set of building types.

It is shown for example Apartment Buildings (AB), Multi-Family Houses (MFH), Single-Family Houses (SFH), and Terraced Houses (TH).

Table A.3 illustrates the number of apartments and the number of storeys of a limited set of archetype buildings. All SFH and TH are single apartment buildings with one to two floors. The AB and MFH have higher floor and apartment numbers.

Table A.3: Number of apartments and storeys for different representative types of buildings in the different construction periods in Germany, based on the *Tabula* database [IWU, 2010].

Type	AB	MFH	SFH	TH	AB	MFH	SFH	TH
Year	Number apartments				Number storeys			
0	-	5	1	-	-	4	2	-
1860	11	4	1	1	5	4	2	2
1919	15	2	2	1	5	3	2	2
1949	20	9	1	1	5	3	1	2
1958	48	32	1	1	8	4	1	2
1969	48	8	1	1	8	4	1	2
1979	24	9	1	1	6	3	2	2
1984	24	10	1	1	6	3	1	2
1995	-	12	1	1	-	4	1	2
2002	-	19	1	1	-	3	2	2
2010	-	17	1	1	-	5	2	2
2016	-	17	1	1	-	5	2	2

The considered outer wall areas and their related thermal transmittance (U-Value) are listed in Table A.4. In general, the high reduction of U-values from around 2 W/(m^{2}K) in the early 20th century to 0.28 W/(m^{2}K) in 2010 is observed which is mainly related to the strict energy savings regulations. The wall area depends on the shape and size of the building.

Table A.4: Parameters of the main outside wall (Wall 1) for different types of buildings and different construction periods in Germany, based on the *Tabula* database [IWU, 2010].

Type	AB	MFH	SFH	TH	AB	MFH	SFH	TH
Year	U-Values [W/(m^{2}K)]				Wall Area [m^2]			
0	-	2	2	-	-	749.31	169.78	-
1860	1.7	2.2	1.7	1.7	305.4	146	194.04	74.47
1919	1.4	1.7	1.7	1.7	1244	323.54	235.3	64.14
1949	1.2	1.2	1.4	1.2	1376	462	117.8	134.66
1958	1.2	1.2	1.2	1.2	3247.79	2039	141.2	40.42
1969	1.1	1	1	1	2130	336	177.55	53.72
1979	0.9	0.8	0.8	0.8	1673.73	447.13	159.4	54.1
1984	0.6	0.6	0.5	0.6	1673.73	774.8	211.3	50.9
1995	-	0.4	0.3	0.6	-	695.8	126.6	45.2
2002	-	0.25	0.3	0.3	-	1698	188.86	140.7
2010	-	0.28	0.28	0.28	-	1193.16	227.6	137.8
2016	-	0.28	0.28	0.28	-	1193.16	227.6	137.8

Equivalently, the roof areas and their related thermal transmittance (U-Value) are listed in Table A.5. The U-values reduce from 1.3 W/(m^{2}K) in the early 20th century to 0.2 W/(m^{2}K) in 2010. They are below the U-Values of the walls. Here, only the areas for the first roof type are shown. Therefore, it does not imply that no roof exists at all, although the listed roof area is here sometimes zero.

Equivalent values exists for the windows, the floors and the doors. Additionally, the transmittance and the orientation of the windows is provided.

These buildings define the reference buildings and are adapted to the required building types in the model. Therefore, following modifications are made.

First, the *Tabula* building with the same surrounding type and the most similar reference area A_{ref}^{tab} is selected as basis for the shape of the building. This shape gets adapted to the reference area of the new archetype building A_{ref}^{new}.

The number of storeys n_{stor} and the height of the room h_{room} are kept constant wherefore also the height of the building is not changing. All floor areas $A_{floor,f}$ and all roof areas $A_{roof,f}$ are proportionally scaled with the size of the reference

Table A.5: Parameters of the main roof (Roof 1) for different types of buildings and different construction periods in Germany, based on the *Tabula* database [IWU, 2010].

	U-Values [W/(m^{2}K)] —				Wall Area [m^2]			
Type	AB	MFH	SFH	TH	AB	MFH	SFH	TH
Year								
0	-	2.6	2.6	-	-	284.1	134.19	-
1860	1.3	1.3	1.3	1.3	231.8	102.8	83.12	0
1919	1.4	1.4	1.4	1.4	0	158.5	213.99	0
1949	0.6	1.4	1.4	1.4	0	0	125.4	0
1958	0.8	0.8	0.8	0.6	0	0	168.9	0
1969	0.5	0.5	0.5	0.5	0	0	183.13	0
1979	0.5	0.5	0.5	0.5	0	0	100.8	97.63
1984	0.4	0.4	0.4	0.4	0	0	123.2	64.87
1995	-	0.35	0.35	0.35	-	0	115.5	77.4
2002	-	0.2	0.25	0.2	-	580	85.91	91.3
2010	-	0.2	0.2	0.2	-	321.05	131.9	75.7
2016	-	0.2	0.2	0.2	-	321.05	131.9	75.7

area as

$$A^{new}_{floor,f} = \frac{A^{new}_{ref}}{A^{tab}_{ref}} A^{tab}_{floor,f} \quad \forall \quad f \tag{A.2}$$

$$A^{new}_{roof,r} = \frac{A^{new}_{ref}}{A^{tab}_{ref}} A^{tab}_{roof,r} \quad \forall \quad r \tag{A.3}$$

.

The wall areas $A_{wall,w}$ and the window areas $A_{window,i}$ are scaled with the root of the ratio in order to keep a consistent overall shape as

$$A^{new}_{wall,w} = \sqrt{\frac{A^{new}_{ref}}{A^{tab}_{ref}}} A^{tab}_{wall,w} \quad \forall \quad w \tag{A.4}$$

$$A^{new}_{window,i} = \sqrt{\frac{A^{new}_{ref}}{A^{tab}_{ref}}} A^{tab}_{window,i} \quad \forall \quad i \tag{A.5}$$

.

Although the A/V-ratio is changing, such a scaling approach produces a further feasible overall shape of the building. Further, a similar aggregated A/V-ratio for the

nationwide perspective is expected since the buildings are sometimes down-scaled and sometimes up-scaled.

The *Tabula* database further provides data for the case that the roof is tilted or flat. For tilted roofs, the roof is divided into two areas with a tilt of 45° and opposing orientations from which 75% can be used for photovoltaic or solar thermal installations. For the case of a flat roof, an equivalent roof area of 28 % can be used for photovoltaic or solar thermal installations while the tilt is considered with 30° and a southern orientation. The utilization factors are slightly above the values of 58 % and 27 % considered by Mainzer et al. [2014].

The physical properties of the envelope, e.g. the thermal transmittance, are determined by the the construction year of the archetype building and the building type with the most similar reference area. For the case of refurbished buildings, the envelop standard of the buildings constructed thirty years later is considered. Nevertheless, the minimum envelope standard of a refurbished buildings is defined by the envelope standard of the construction year 1995.

The required supply temperatures are also determined by the building age. It is assumed that all buildings before 1990 have a design supply temperature T_{sup}^{des} of 70 °C. This reduces for buildings between 1990 to 2000 to 60 °C, 2000 to 2010 to 50 °C and for buildings constructed after 2010 to 40 °C. For all buildings that have more than six apartments, the supply temperature is increased by 5 °C since a bigger heat supply network is required. The supply temperatures assumed are in a similar range as the supply temperatures reported by Staffell et al. [2012] for different heating systems.

A.3 Techno-economic parameters

This section introduces all relevant economic and technical data to parametrize the introduced building and supply system optimization. For the case of photovoltaics (Section A.3.1), batteries (Section A.3.2) and fuel cells (Section A.3.3), today's and future techno-economic parameters are discussed in order to account for global experience rates sufficiently. Heat pumps (Section A.3.4), boilers (Section A.3.5) etc. are assumed to not change significantly wherefore only parameters for today are introduced. The considered supply system with all modeled supply technologies can be seen in Figure A.5. Energy and resource costs, like electricity tariff or biomass price, are values varying with the later scenarios and are therefore not discussed in this section. The energy and resource imports, like electricity grid or biomass supply, are modeled as *Source* objects with a flexible import. Therefore,

they only have economic parameters that vary with the later introduced scenarios. Therefore, they are not discussed in this section.

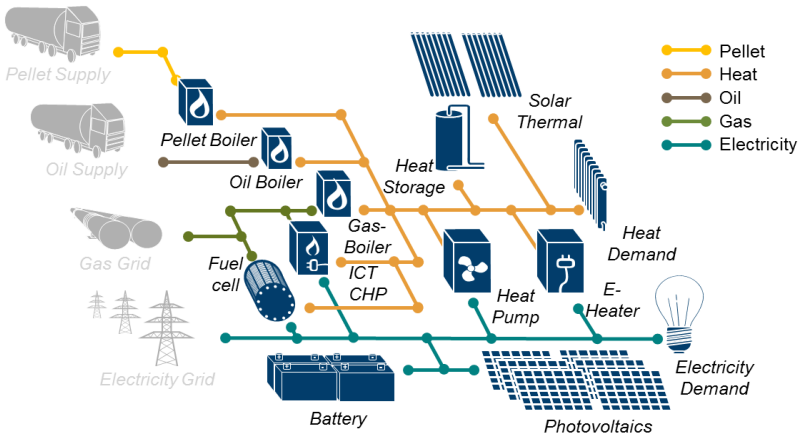

Figure A.5: Superstructure of the technology options for the supply system of a single building.

All literature values that consider a different currency than Euros are converted with the 2015 exchange rate.

Earlier versions of this work considered also technologies allowing for 100% self-sufficient supply systems, like a reversible Solide Oxide Cell [Nguyen et al., 2013] and Liquid Organic Hydrogen Carrier [Eypasch et al., 2017; Teichmann et al., 2012]. Nevertheless, they are discarded in this work since they further increase the model complexity. Additionally, their economic potential is seen as limited in a country with an existing electricity grid infrastructure [Kotzur et al., 2017; Röben, 2017].

A.3.1 Photovoltaic

The photovoltaic is modeled as a *Source* object. Its performance model is introduced in 3.3.4, wherefore this section mainly discusses the related investment cost. The section separates between cost for today and cost for the future.

Current status of photovoltaic

Figure A.6 introduces market data and literature values for photovoltaic investment from market analysis and different literature sources. The market data are full investment cost offers for roof-top photovoltaic in Germany in 2014, including the installation. They have a high spread, resulting in offers from 1000 to 2300 Euro/kW$_p$ for the same scale of photovoltaic. Although parts of the variation are related to the different matters of costs included in the different offers, the majority of the variance is explained by the high dynamics of the market. No significant economy of scale is recognizable. Nevertheless, the collector of the data set [Löhr, 2016] reports an average price of 1482 Euro/kW$_p$ for 0 to 5 kW$_p$, 1425 Euro/kW$_p$ for 5 to 10 kW$_p$ and 1415 Euro/kW$_p$ for 10 to 15 kW$_p$. The cheapest 25 % of all offers were 1327, 1299 and 1295 Euro/kW$_p$ regarding the same three capacity ranges. The second market data set [EuPD-Research, 2016] is from 2016 and shows a higher economy of scale from average prices of 1688 Euro/kW$_p$ for plants smaller than 3 kW$_p$ to 1228 Euro/kW$_p$ for plants bigger than 10 kW$_p$. The range from minimal until maximal price are in the same scale as the first market data set.

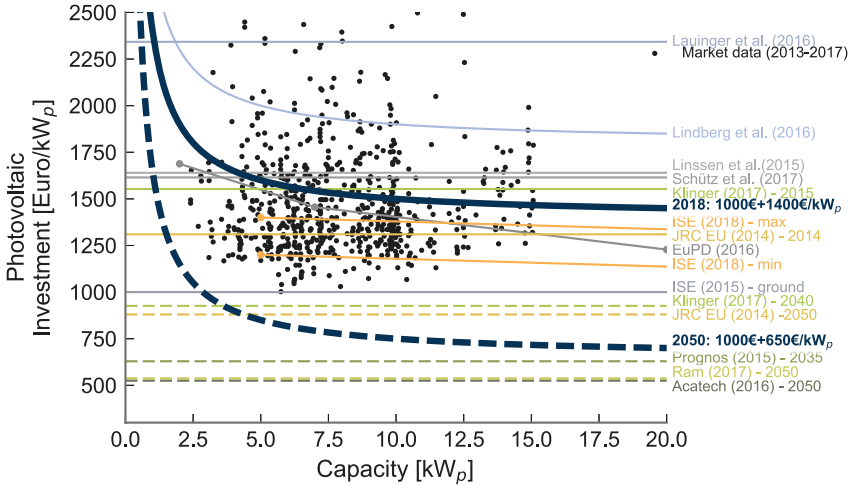

Figure A.6: Investment cost of photovoltaic for different capacities based on market and literature data, along with the considered cost of this work.

The considered cost values of the literature are more conservative with 1615 [Schütz et al., 2017a], 1640 [Linssen et al., 2015] and 2342 Euro/kW$_p$ [Lauinger et al., 2016]. The value from Lauinger et al. [2016] can be seen as an outlier be-

cause it is derived from the Swiss market. Lindberg et al. [2016a] consider a small scale-independent initial investment 1000 Euro for mounting and installation costs which causes high specific expenses for small photovoltaic units. The specific investment are additional 1800 Euro/kW$_p$ and derived from data of 2014. The bottom line is defined by the cost of utility scale ground-mounted photovoltaic in the year 2015 of 1000 Euro/kW$_p$ [ISE, 2015].

Although the photovoltaic had a price drop with a historical experience rate of 20.9% for every doubling of produced modules [ISE, 2015], it stagnated in Germany from 2015 to 2017 [ISE, 2017] because the local demand dwindled since the adaption of EEG-levy in 2014 [EEG, 2014]. Therefore, in this work only a moderate decrease of the cost is assumed for the last years and the photovoltaic is considered with 1000 Euro fix expenditures and 1400 Euro/kW$_p$. The resulting specific cost curve is seen in Figure A.6.

Future development of photovoltaic

Germany lead the international ranking of the total installed photovoltaic capacity until 2015 [IEA-PVPS, 2016] because it started at an early stage with high subsidized investments into the technology. In consequence, the majority of the photovoltaic were deployed when the module costs where still high, wherefore the required subsidies to fill the profit gap are still payed in form of the EEG-levy today. Nevertheless, a benefit is that production and technology improved and with it the overall experience curve proceeded.

The picture of a German dominated photovoltaic market has dramatically changed since the photovoltaic cost dropped to a level where it is becoming competitive with fossil electricity generation: While Germany had 1.5 GW of new photovoltaic installations in 2016, 14.7 GW were installed in the USA and 34.45 GW in China in the same time frame [IEA-PVPS, 2017]. This totaled in existing photovoltaic capacities around 300 GW worldwide in 2016 [ISE, 2017].

With these prospering markets also a further price drops of the photovoltaic modules are expected. Extrapolating the historical experience rate of 22.9 %, ISE [2015] expect a drop from 2015 around 500 Euro/kW$_p$ module price to a price between 175 and 315 Euro/kW$_p$ in 2050 at a cumulative installed capacity of 30749 GW or 4295 GW depending on the scenario. 100 to 200 Euro/kW$_p$ is seen as the line where fundamental material cost dominate the overall module price. IRENA [2016] assumes already for 2025 a module price between 280 to 460 \$/kW$_p$ for an extrapolation of a cumulative installed capacity of 1750 to 2500 GW until 2030. A bottom-up technology based approach supports this estimation [IRENA, 2016], concluding cost of

300 to 410 \$/kW$_p$.

The experience rate of the Balance of System (BoS) cost, including cabling, mounting, permitting, inverter etc., cannot keep up with the experience rate of the modules: Although, the BoS in Germany were 2015 with 500 \$/kW$_p$ together with China the cheapest worldwide, e.g. the BoS in the US were almost three times as expensive [IRENA, 2016], their share at the overall photovoltaic costs increased significantly from 29 % end of 2006 to 53 % end of 2016 for rooftop photovoltaic. Strupeit and Neij [2017] conclude that the historical experience rate for BoS in Germany is around 10-12 %.

A key driver to reduce the BoS cost further is an increase of the cell efficiency, leading to higher capacities for the same modules and smaller specific BoS. The challenge thereby is that the efficiency limit, e.g. for mono-crystalline photovoltaic, is seen by 25 % for industrial modules [ISE, 2015]. Alternative technologies, e.g. a Persovskite-Silicon tandem as dual-junction, could allow to achieve practical efficiencies of up to 35 % [ISE, 2015]. Still, they would require more complex production processes and additional materials, increasing the module cost. Therefore, a trade-off between module cost and BoS cost has to be made.

The second advantage of an increased cell efficiency would be a reduced coverage rate for the same peak power installed. Mainzer et al. [2014] illustrate it for the potential of residential roof-top photovoltaic in Germany: With state of the art modules they conclude a potential of 208 GW on residential rooftops in Germany which increases to 641 GW for their considered technology advancements in 2050.

Therefore, this work assumes a less aggressive experience rate of the overall system cost while assuming that high efficiency technologies will take over the market. Prognos [2016] considers an almost linear cost reduction of rooftop photovoltaic from 1252 Euro/kW$_p$ in 2015 to 629 Euro/kW$_p$ in 2035. Rech and Elsner [2016] suggest a price range of 650 to 400 Euro/kW$_p$ for rooftop photovoltaic in 2050 with an efficiency between 24 % and 35 %. In this work, the upper range is taken for the cost in 2050 with 650 Euro/kW$_p$, along with an efficiency of 30%.

A.3.2 Battery

Building integrated stationary battery systems can increase the self-consumption of distributed energy resources or offer a flexibility to the grid. They are modeled as electricity *Storage* object. All data and modeling refers to their net-capacity.

The charge- and discharge efficiencies of the battery systems are assumed to be

each 95 %, which is typical for today's Li-Ion batteries [Kairies et al., 2016]. No significant improvement of these values is expected for the future. The self-discharge rate is considered with 0.01 % per hour [Elsner and Sauer, 2015].

The lifetime of batteries available at the market is guaranteed with 5000 to 10000 cycles Tesla [2017]. Since a modeling of this as operation-depending lifetime would constitute a non-linear problem, a lifetime of 15 years is assumed which would allow for 333 to 666 cycles per year.

Current status of batteries

Figure A.7 introduces the different market data and literature values for battery cost today and predictions for the future. Similar to the photovoltaic, it exists a high variance in the real market data. A small economy of scale is recognizable which is probably related to the peripheral components of the batteries. While the majority of the costs are above a value of 1000 Euro/kWh, the Tesla Powerwall 2 [Tesla, 2017] constitutes an exception with an investment of 7150 Euro for a capacity of 13.5 kWh, resulting in specific investment of 5̃30 Euro/kWh. It is questionable whether this price represents the current real production cost or if it is strategic price to gain a higher market penetration.

The literature values for today's cost lay above this price: Linssen et al. [2015] assume 1000 Euro/kWh for the near future. Schmidt et al. [2017] report 1530 Euro/kWh in 2015 as average cost for Li-Ion batteries, which aligns with the market data. The study by *acatech* [Elsner and Sauer, 2015] respects this discrepancy of the market data by providing a range from 580 Euro/kWh to 2100 Euro/kWh for the current residential battery prices. All in all, it highlights the volatility of the market similar to the photovoltaic market.

Nykvist and Nilsson [2015] give an indication about the prices that car manufacturers pay for batteries, which were 300 $/kWh in 2015. They state that many publications take outdated prices for batteries. Although residential battery packs will stay more expensive than battery packs for electric vehicles, it shows a high potential for future price drops of stationary battery storage systems.

This work considers a value similar to Klingler [2017] (907 Euro/kWh) with a fix investment of 2000 Euro and a specific investment of 700 Euro/kWh.

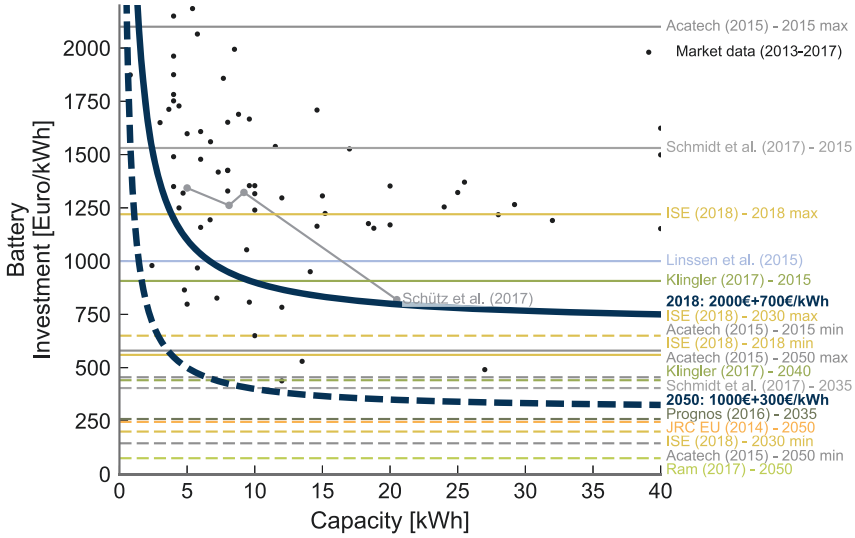

Figure A.7: Investment cost of batteries for different capacities based on market and literature data, along with the considered cost of this work.

Future development of batteries

The range of assumed future cost for stationary battery systems is vast: Klingler [2017] assume 441 Euro/kWh for 2040, while Prognos [2016] assumes already an investment of 442 Euro/kWh for the year 2020 and 259 Euro/kWh for the year 2035. Elsner and Sauer [2015] again give a range between 145 Euro/kWh and 455 Euro/kWh for the year 2050.

The market is even more difficult to predict than the photovoltaic market, since the costs of batteries are highly depending on to the roll out of battery electric vehicles. Additional, resource availability is more significant for batteries than for photovoltaic wherefore it is difficult to assume a rigorous learning rate. A competing resource demand will significantly influence the final cost of batteries at high penetration rates. Therefore, a conservative value is assumed for the futures cost of residential stationary energy storage systems with a fix investment of 1000 Euro and a specific investment of 300 Euro/kWh.

A.3.3 Fuel cell

Fuel cells allow for efficient heat and electricity co-generation, and are especially favored for small scale applications where the efficiency of combustion based technologies are dropping. They are modeled as *Transformer* unit.

Technical characteristics of fuel cells

Fuel cells available at the market available today can be divided into two types: Solide Oxide Fuel Cells (SOFC) or Polymer Electrolyte Fuel Cells (PEFC). The SOFC has higher conversion efficiencies than the PEFC because of the high operation temperatures above 700 °C, and its ceramics membrane allows for higher gas impurities and with it lower degradation rates than the polymer membrane of the PEFC. The drawback of the SOFC is that the combination of high operation temperature and ceramic membrane causes high thermo-mechanical tensions, e.g. in case of a cold-start of the system. Therefore, today's available systems such as the *BlueGEN* from *SolidPower* [SolidPower, 2018] are only shut down for maintenance in order the keep the number of thermal cycles small. This drawback does not exist for the PEFC which can be flexible operated.

Although these differences would require two independent models of the fuel cells, this work does not separate between them in order to keep the computational complexity of the overall system model low. Instead, just a single fuel cell type is considered in the system.

Available methane operated SOFC-systems can reach electrical efficiency up to 60% and the overall efficiency including heat extraction is given with 85% [SolidPower, 2018]. Similar efficiencies can be reached with hydrogen [Peters et al., 2016], although a different system design would be required. Napoli et al. [2015] consider for the PEMFC an electrical efficiency of 34%. The efficiency including the heat extraction was assumed for both systems SOFC and PEMFC with 90%.

Based on this, a mixed fuel cell system is considered with an electrical efficiency of 52%, and 33% heat efficiency with regard to the lower heating value of the fuel. No part load or ramp up constraints are considered.

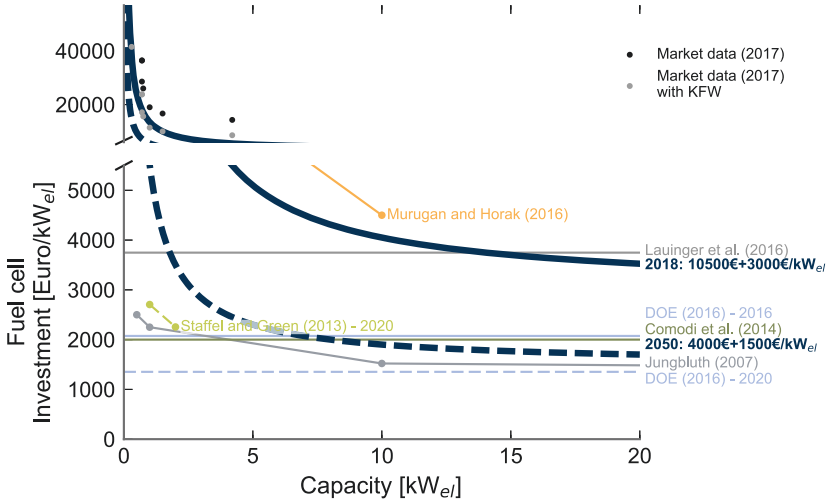

Figure A.8: Investment cost of fuel cells for different capacities based on market and literature data, along with the considered cost of this work.

Current status of fuel cells

Figure A.8 shows the different cost values for fuel cells assumed in the literature, and a rare selection of real market data in Germany [HZwei, 2016].

The DOE [2016] states that current prices for prime movers in the US are in the range of 20000 \$/kW$_{el}$ for small stationary fuel cell systems below 11 kW$_{el}$ and 4000 \$/kW$_{el}$ for larger systems, which would align with the German market data. Additional, the DOE assumes that today's production costs are at 2300 to 2800 \$/kW$_{el}$ at manufacturing volumes of 50000 units per year.

The prices considered by Comodi et al. [2015] of 2000 Euro/kW$_{el}$ are not reachable for today. Even the inclusion of subsidies is not sufficient to reach such prices, although they can amount up to 40 % of the total costs of the fuel cell system in Germany [Gleitmann, 2016; KfW, 2016]. Also the investment cost function of Jungbluth [2007], who assumes for small systems 2500 Euro/kW$_{el}$ can only be seen as a prediction for future cost but does not represent the effective prices today. Nevertheless, the cost function has the advantage that it includes an economy of scale derived from the prices of internal combustion CHPs.

Murugan and Horák [2016] estimate the prices for today's small scale systems between 1 and 3 kW_{el} to be around 15000 Euro. Based on this, this work assumes the investment costs with a fix investment of 10500 Euro and 3000 Euro/kW_{el} for the year 2018. Those prices lay above the production costs assumed by the DOE and align with today's German market prices including the subsidies. The assumed cost of Lauinger et al. [2016] could then be reached for large scale fuel cell systems.

Future development of fuel cells

The future costs of fuel cells have been historically underestimated. E.g. the *DOE* targeted 1200 \$/kW_{el} for the year 2015 and 1000 \$/kW_{el} for the year 2020 in 2012. Staffell and Green [2013] corrected this value to 3000 to 5000 \$ for 1 to 2 kW_{el} systems in 2020. They include further peripheral components like auxiliary heating units plus a heat storage systems, which are not integrated in the *DOE* target. The updated goal in 2016 of the *DOE* is to achieve investment costs of 1500 \$/kW_{el} for 2020 DOE [2016].

Still, all cost assumptions are too optimistic for 2020 if today's market prices are taken into account. Therefore, this work conservatively assumes that such fuel cell prices can only be reached in future for larger systems: The fix investment for the future 2050 case is considered with 4000 Euro and the specific investment is assumed with 1500 Euro/kW_{el}.

A.3.4 Heat pump

The heat pump is seen as key technology to provide efficiently low temperature space heat. It is modeled as a *Transformer* with a time-dependent efficiency which converts electricity and ambient heat into low temperature heat, as shown in Section 3.3.3. No major cost reductions are expected for the technology in the future because it is a Carnot-machine and its components are produced in large numbers since decades.

All following costs are related to the thermal capacity of the heat pump. The Coefficient Of Performance (COP) or rather the heating power is normally given for reference conditions, e.g., 2 °C to 35 °C (A2/W35) temperature difference, or 7 °C to 27 °C (A7/W27) temperature difference. Here, the heating power for the A2/W35 case is used to calculate the specific investment costs.

Figure A.9 shows the market prices for different heat pumps at different scales and

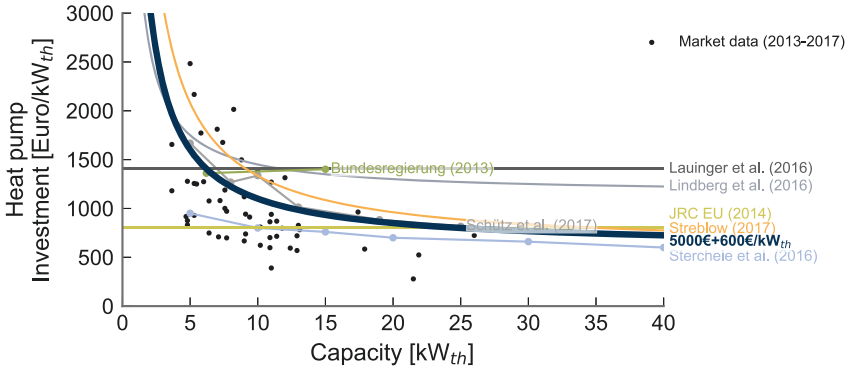

Figure A.9: Investment cost of heat pumps for different capacities based on market and literature data, along with the considered cost of this work.

the cost values assumed in the literature for heat pumps. Comparing the range of values to the range of prices reported for photovoltaics and the electrochemical technologies, a much more consistent cost database is noticeable. This indicates a more stable market and supports the assumption of no major future price drops.

A strong economy of scale is recognizable for the market data. This is also covered by the majority of the literature [Streblow and Ansorge, 2017; Sterchele et al., 2016; Schütz et al., 2017a]. Some of the data [BRD, 2013] originally included also an investment into a floor heating system. This part of investment is excluded, since the floor heating is just required for reducing the supply temperature of the heating system to gain a better heat pump efficiency. Nevertheless, the supply temperature is part of the model as introduced in section 3.3.3 and dynamically determined based on the heating system and the heat load itself.

Two cost functions deviate from the other literature and market data: [Lauinger et al., 2016] can not sufficiently model the economy of scale of the heating system since they just have a continuous linear cost model. Further, they consider the costs for a ground source heat pump, resulting in higher overall investment costs, while the other values are reported for air-source heat pumps. [Lindberg et al., 2016a] overestimates the cost for large heating systems. Nevertheless, they also state that their cost assumptions are just valid for scales between 5 kW$_th$ and 15 kW$_th$.

This work aligns with the other data and fit the heat pump prices with 5000 Euro of fix investment a 600 Euro/kW$_th$ specific investment related to the thermal capacity of the heat pump.

A.3.5 Oil and gas boiler

Although heat pumps have an increasing market share for the heat supply in new buildings [DESTATIS, 2014], the majority of today's energy supply is still combustion based: Conventional oil and gas boilers cover together 74.6 % of the residential heat in Germany in 2014 [BDEW, 2014]. Therefore, their technology can be seen as mature and as well no major cost reductions are expected in the future. They are modeled as *Transformer* with a constant efficiency. This simplification is made to keep the model linear despite the fact that a changing part load behavior exists in reality.

Market prices and cost functions assumed in the literature can be seen in Figure A.10 for boilers. Besides two outliers, again a consistent database for the market can be recognized which is similar to the heat pump data. An exception is Lindberg et al. [2016a] who overestimate the costs for large capacities due to their cost curve fitting to smaller technology scales.

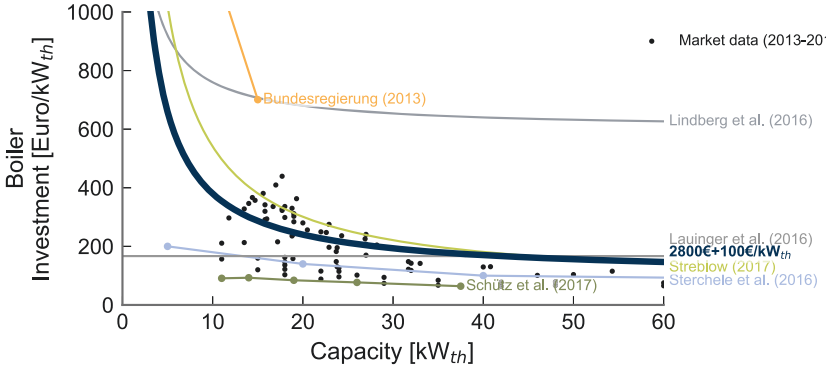

Figure A.10: Investment cost of boilers for different capacities based on market and literature data, along with the considered cost of this work.

Three observations can be made in comparison to the heat pump data:

1. The specific investment cost are almost 70 % smaller than the investment for the heat pumps.
2. A smaller economy of scale is recognizable.
3. The availability of boilers starts at capacities around 10 kW$_th$, while for the heat pumps also smaller devices, around 5 kW$_th$, are available.

The observations determine each other: The heat pump is a more complex and therefore more expensive technology than a conventional boiler. Therefore, their scale is optimized and they are often installed along with a electric or gas boiler covering the peak demands, resulting in scales smaller than the peak heat load of the building. This does not count for the conventional combustion based heat supply where a single technology normally covers the whole heat demand.

A.3.6 Internal combustion engine

The internal combustion engine is also a Combined Heat and Power plant (CHP) and can be seen as alternative to the fuel cell. It is also modeled as *Transformer* with two constant efficiencies for each heat and power generation that also results in a constant ratio of heat and power generation.

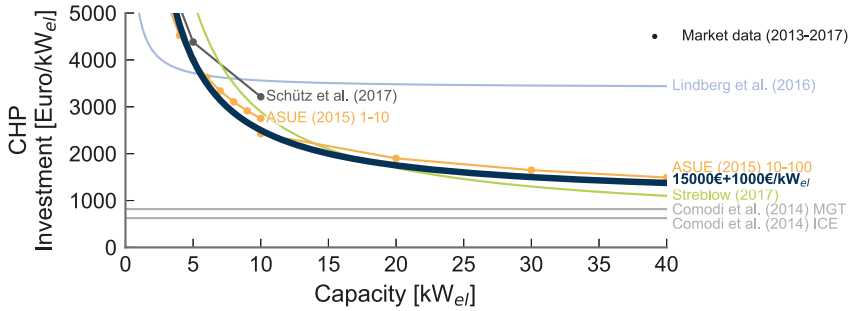

Figure A.11: Investment cost of internal combustion CHPs for different capacities based on market and literature data, along with the considered cost of this work.

ASUE [2015] frequently publishes techno-economic characteristics of the German CHP market, including a large set of real CHP units. They derive cost curves for different scaling ranges of CHP units, as shown in Figure A.11. The strong scaling effects cannot be captured for large ranges with the simple cost approach considered by Lindberg et al. [2016a], Streblow and Ansorge [2017] and this work. Lindberg et al. [2016a] adapt their cost curve for small CHP scales below 5 kW_{el}, while the cost curve of Streblow and Ansorge [2017] is probably influenced by large scale CHP units. Their scale-independent initial investment of 23942 Euro hampers the profitability of any small-scale CHP plant. The cost assumed by Comodi et al. [2014] for the Micro Gas Turbine (MGT) and the Internal Combustion Engine (ICE) could just be reached for scales which are not relevant for single residential building supply systems.

The costs in this work are assumed such that they align with the ASUE [2015] data for a wide range by assuming a fix investment of 15000 Euro and 1000 Euro/kW$_{el}$.

A.3.7 Heat storage

The heat storage is the second relevant *Storage* technology considered, besides the battery. It can be charged by all considered heat generators with the limitations introduced and explained in Section 3.3.3. A simple unpressurized hot water storage for sensitive heat is considered.

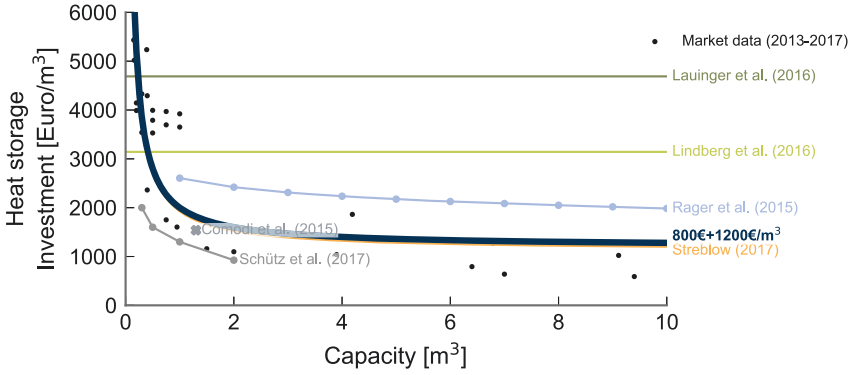

Figure A.12: Investment cost of solar thermal for different capacities based on market and literature data, along with the considered cost of this work.

The different costs in literature and for storage systems at the market are shown in Figure A.12 for different storage volumes. A description over the amount of heat that can be stored would be misleading since it is depending on the operation conditions.

Lauinger et al. [2016] and Lindberg et al. [2016a] both consider small scale storage systems and align with the market data in the range below 1.5 m^3 of 3000 to 5000 Euro/m^2. [Lindberg et al., 2016a] do not define the cost in Euro/m^3, instead assume 90 Euro/kWh for a storage operated at $\Delta T = 30°C$. Schütz et al. [2017a] define the lower bound of the costs for storage systems at the market but captures sufficiently the economy of scale with cost of around 1000 Euro/m^3 for a 2 m^3 storage. It is to be expected that they do not consider the storage installation costs. Rager [2015] introduces a cost function which applies for large scale seasonal storage applications in districts and overestimates therefore the cost of smaller storage

applications. Since Streblow and Ansorge [2017] align well with the market data, their cost data are rounded and considered for this work with a fix investment of 800 Euro and a specific investment 1200 Euro/m^3.

A.3.8 Solar thermal

Solar thermal is modeled as *Source/Sink* object with a time dependent heat generation, as introduced in Section 3.3.5. The different cost assumptions of the literature are shown in Figure A.13.

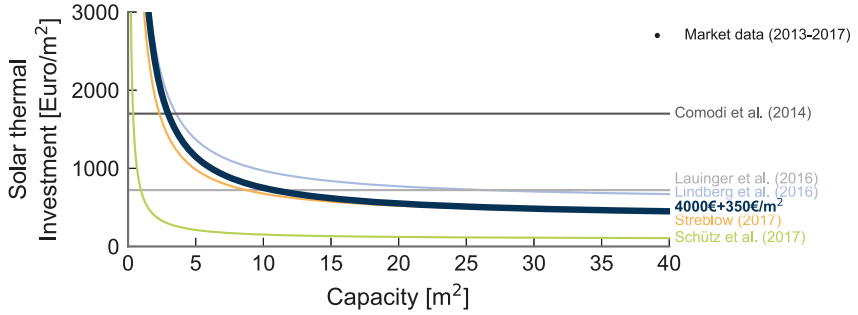

Figure A.13: Investment cost of solar thermal for different capacities based on literature data, along with the considered cost of this work.

Cost given in Euro/kW$_{th}$ are converted with energy density of 650 W/m^2 [Lauinger et al., 2016] to Euro/m^2. While the cost data of Lindberg et al. [2016a] and Streblow and Ansorge [2017] align well, the other cost data is inconsistent. The overestimation of Comodi et al. [2014] and Lauinger et al. [2016] is probably related to lack of an economy of scale since the values fit for small scales below 10 m^2. Schütz et al. [2017a] on the other hand underestimate the cost by far which is probably again related to a disregard of the installation costs. This work estimates the cost with 4000 Euro fix and 350 Euro/m^2 specific investment and does not consider significant reductions for the future.

A.3.9 Pellet boiler

The pellet boiler is modeled as *Transformer* with a constant efficiency, equivalent to the gas and oil boiler in Section A.3.5

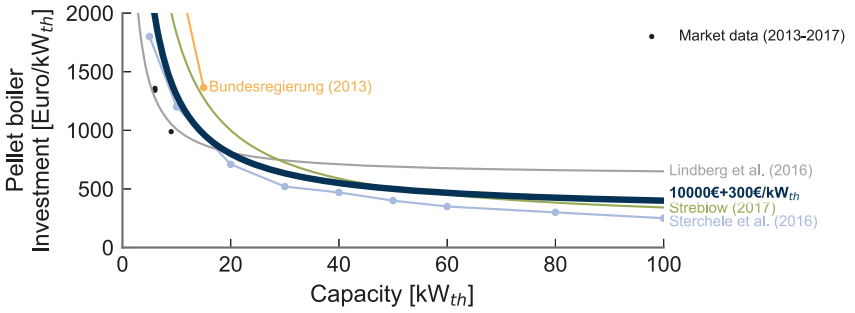

Figure A.14: Investment cost of the pellet boiler for different capacities based on literature data, along with the considered cost of this work.

The different cost assumptions in the literature are shown in Figure A.13. The data are relative consistent. This work aligns with the average and considers 10000 Euro fix investment and 300 Euro/kW$_{th}$ as specific investment.

Appendix B

Aggregation of an archetype building stock

Following chapter provides auxiliary information to Chapter 4. Section B.1 is clarifies the reasons for the exclusion of socio-structural changes in this work. Section B.2 gives additional data to the aggregation of the German building stock and Section B.3 explains further the representation of single municipalities by the archetype buildings.

B.1 Socio-structural changes

Some of the analyzed studies [Beuth, 2015; ISI, 2016] also consider socio-structural changes such as a population decrease or an increase of the specific demand for living area to derive the future demand for electricity and heat. Although the chosen methodology would allow an incorporation into the archetype aggregation by a spatial distribution of changing household sizes, it was decided to exclude those.

This simplification has two reason:

1. No good data is available, since the different data sources are not consistent: Many structural developments were not sufficiently predicted, as illustrated in Figure B.1. While most of the older studies consider a population decrease, an updated study by the *Institut für Wirtschaft* [IW, 2017] indicated a further population increase until 2035 due to migration and an increasing birth rate.

2. The results are more challenging to interpret with the inclusion of socio-structural changes, since the technological and the socio-structural impact have to be disaggregated again. The focus of this work is the impact of the changing energy supply structure.

Therefore, it was instead assumed that the population is in the year 2050 the same as in the Census year 2011 [Bundesamt, 2011].

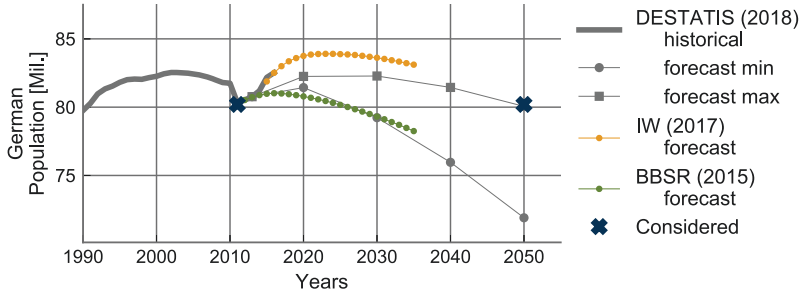

Figure B.1: Historical values and prediction of the population development in Germany based on different sources [DESTATIS, 2015; BBSR, 2015; IW, 2017; Bundesamt, 2011].

B.2 Aggregated attribute fitting

The weighting of the attributes in the aggregation influences the results, similar as in a clustering approach. The weighting chosen for this work is introduced in Table B.1.

Table B.1: Weighting of the attributes in the building aggregation.

Attribute	Construction year	Apartment size	Surrounding	Apartments	Persons per ap.	Orientation	Ownership	Rebuild	Photovoltaic	Supply technology	Longitude	Latitude
Weight	0.5	0.5	2	1	2	1	3	1	1	3	7	7

In general, attributes represented by the number of apartments and distributed over many expressions are smaller weighted than attributes with a few expressions

represented by the number of buildings. Otherwise, the attributes with many expressions would result in a high cumulative error and cause over-fitting of those, while attributes with less expressions are neglected. An exception is the number of persons or occupants per flat since their number is significant for the result. The latitude and longitude have a relative high weighting because they are the only continuous attributes in a range of 0 to 1. In consequence, their placement at 0.5 constitutes already at least an average fit of 0.5, although no spatial representation exists. Therefore, they are higher weighted in order to compete with the categorical attributes that have a distance evaluation of 1 in case that they are not met.

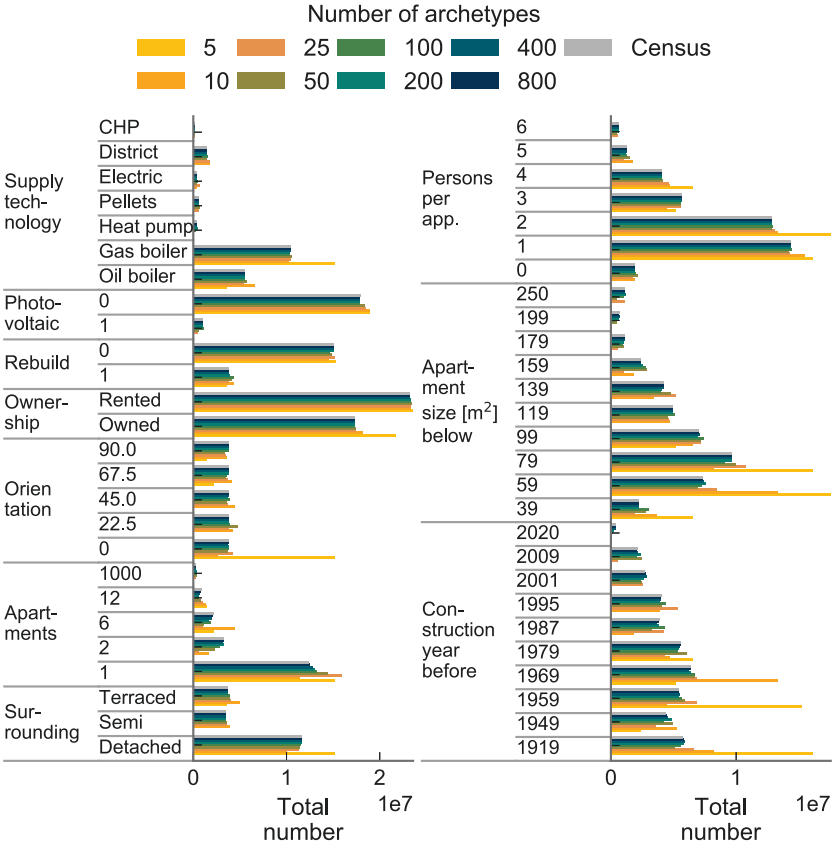

Figure B.2: Distribution of the considered building attributes in Germany and their fitting by the archetype aggregation algorithm on an aggregated nationwide scale.

Nevertheless, a further sensitivity analysis of the weighting factors could adjust them better in future. Also their impact on the final results could be evaluated.

Figure B.2 illustrates the attribute fitting from an aggregated perspective over all municipalities in Germany with the introduced weighting.

B.3 Number of archetypes representing a municipality

Figure B.3 illustrates the representation of the city *Köln* by archetype buildings for the case that in total 200 archetype buildings typify the building stock in the different municipalities in Germany. All in all, 37 different archetype buildings represent the 137725 real buildings in *Köln*. The characterization of the first eight building types is shown in Table B.2.

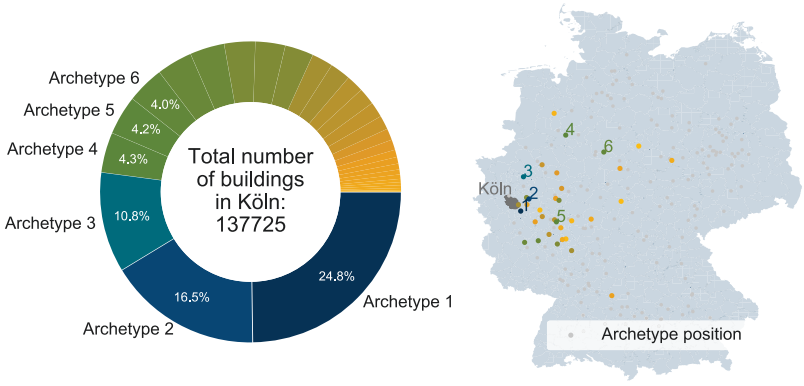

Figure B.3: Composition of archetype buildings representing *Köln* for the case of 200 archetype buildings and their related position in Germany.

Table B.2: Definition of the eight first archetype buildings that represent Köln for the case of 200 building aggregations.

	Construction year	Size [m²]	Surrounding	Persons per apart.	Orientation	Ownership	Rebuild	Photovoltaic	Supply technology	Longitude [°]	Latitude [°]	Apartments
Archetype 1	1919	99	Terraced	3	67.5	Rented	False	False	Gas boiler	7.208223	50.771462	1
Archetype 2	1949	79	Terraced	2	45.0	Rented	False	False	Oil boiler	7.437952	51.021117	2
Archetype 3	1969	139	Detached	2	0.0	Owned	False	False	Gas boiler	7.284898	51.479579	1
Archetype 4	1959	99	Semi	5	22.5	Owned	True	False	Gas boiler	8.461216	52.340127	1
Archetype 5	1959	59	Semi	1	0.0	Rented	False	False	Gas boiler	8.202385	50.548362	16
Archetype 6	1919	119	Terraced	2	22.5	Owned	False	False	Gas boiler	9.521178	51.990549	4
Archetype 7	1979	99	Detached	1	90.0	Owned	False	False	Gas boiler	7.696921	50.158805	1
Archetype 8	2020	179	Terraced	2	90.0	Owned	True	False	District heating	7.317294	50.124494	1

It is striking that archetype building 1 is representing almost one quarter of the building types in *Köln*. Therefore, the supply structure of this single building significantly impacts the aggregated results of the municipality.

This influence is reduced with a higher number of archetype buildings, as shown in Figure B.4 for the example of 800 archetype buildings. For this case, the most often occurring archetype building in *Köln* represents only 11.4 % of the overall building stock. In consequence, the result of a single building has a reduced impact on the overall results.

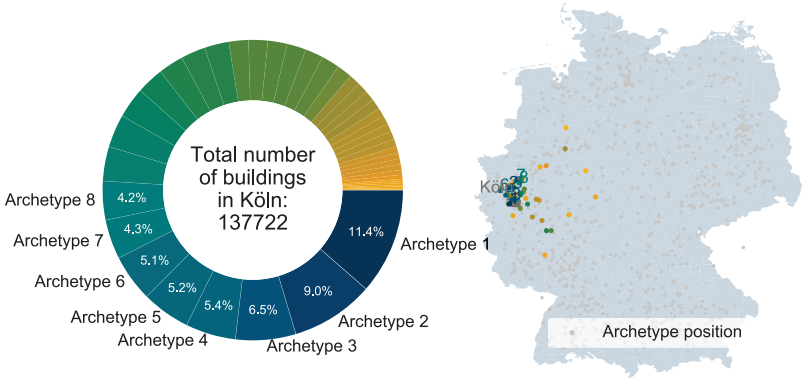

Figure B.4: Composition of archetype buildings representing *Köln* for the case of 800 archetype buildings and their related position in Germany.

Therefore, higher numbers of archetype buildings make the results on a municipality level more robust and stable since a higher diversity of building types constitutes the aggregated results. Nevertheless, the accuracy gain on for the aggregated nationwide perspective is limited, as shown in Section 5.2.

Appendix C

Scenario results for the German residential building stock

Following Section provides auxiliary plots and data to the scenario results. The detailed scenario descriptions and results are shown in Chapter 5. Section C.1 provides an aggregated flow chart for the *Reference* scenario. Section C.3 provides all aggregated data for the *Value Of* sensitivity analysis. Section C.4 shows the data for the sensitivity analysis of the gas price. The aggregated energy flows and capacities of the zero GHG cases are shown in Section C.5. The accuracy gain by using more archetype buildings to predict the regional load change is illustrated in Section C.2.

C.1 Reference scenario

Figure C.1 shows a Sankey-diagram of the nationwide energy flows for the Reference scenario. It is calculated with 200 archetype buildings for the Test Reference Year.

While most of the energy flows and demands align with the final energy demands by the AGEB [2017], solar thermal and photovoltaic are underestimated although their existence was forced into the solution space. Many solar thermal and photovoltaic instances are scaled to zero in the optimization since their specific cost are too high such that they cannot amortize themselves.

This is mainly constituted by the single cost, energy price and feed-in tariff as-

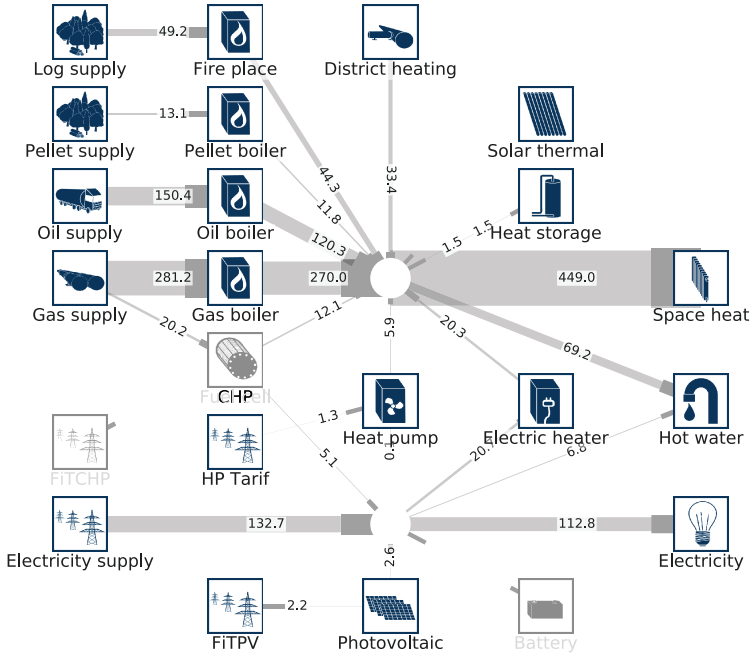

Figure C.1: Aggregated energy flows between the technologies for the *Reference* scenario.

sumptions considered in this work. In case that also historic market environments, including historic feed-in tariffs and historic technology prices, would be modeled, also past years with high residential photovoltaic deployment could be better respected in the model in future.

C.2 Load change predicted with different numbers of archetype buildings

The majority of the scenario cases in this work considered 200 archetype buildings since they provide a sufficient accuracy for an aggregated nationwide perspective, as shown in the validation in Section 5.2.1. Nevertheless, such a number results in an over-representation of single building types in a municipality, as shown in Section B.3. Therefore, regional obstacles occur regarding the predicted load change.

Figure C.2 shows the load change from the *Reference* to the *Min Cost* scenario in 2050, predicted with 200 archetype buildings. Figure C.3 shows the equivalent results predicted with 800 archetype buildings.

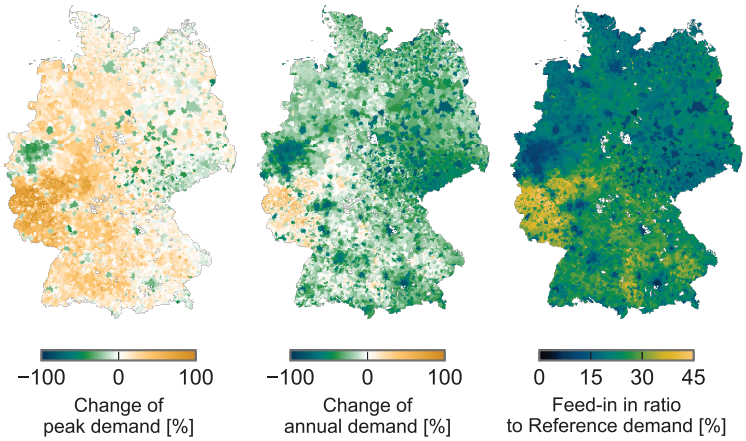

Figure C.2: Spatial change of the peak load, the cumulative positive demand, and the feed-in from the *Reference* scenario to the *Min Cost* scenario and predicted with **200** archetype buildings.

In general, the differences of the changing load between rural and urban areas are in a similar magnitude with 200 archetype buildings and 800 archetype buildings. Nevertheless, the load change in the rural regions Rhineland-Palatinate and Saarland stand out for the case of 200 archetype buildings, although no major structural differences exist in comparison to other regions. This is different for the case of 800 archetype buildings where an almost uniform load change in the rural regions results. Instead, a stronger difference for the feed-in between north and south Germany is recognizable due to the different solar irradiation. Therefore, the results

generated by 800 archetype buildings seem more plausible and indicate that more archetype buildings increase the accuracy of the overall load prediction on municipality level.

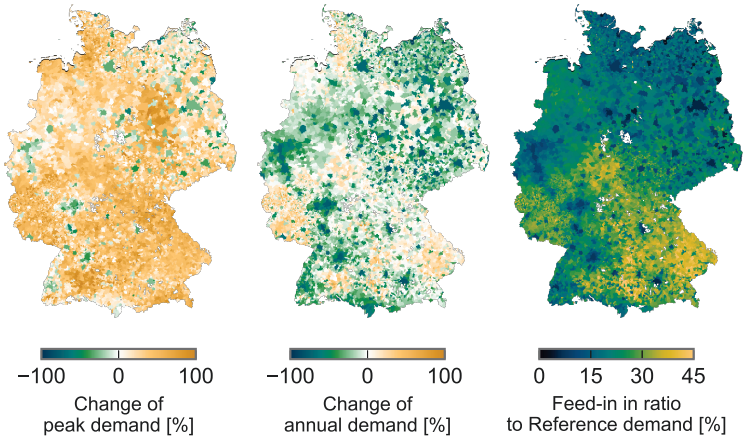

Figure C.3: Spatial change of the peak load, the cumulative positive demand, and the feed-in from the *Reference* scenario to the *Min Cost* scenario and predicted with **800** archetype buildings.

Thus, it is recommended to use at least 800 archetype buildings for a future coupling with grid models. Although this increases the computational load, the parallelized implementation of the model allows the usage of high performance computers. In consequence, even higher numbers of archetype buildings can be used in future in case of available computational resources.

C.3 Value of analysis

Following section provides additional information for the *Value of* analysis. It is described in detail in Section 5.3.3.

Figure C.4 shows the aggregated investment costs for the different cases.

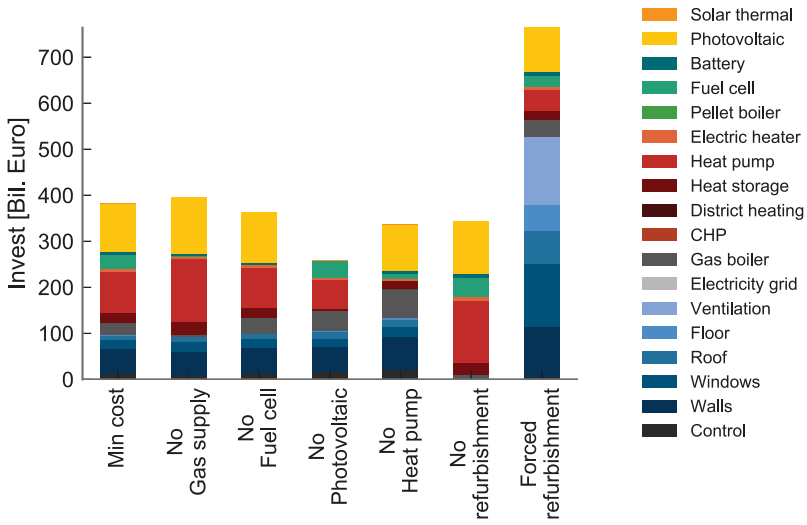

Figure C.4: Total investments of the *Min Cost* scenario and the resulting investments for the cases with a constrained solution space.

The resulting aggregated and sorted grid loads of the different cases are illustrated in Figure C.5.

Further, the aggregated annual energy flows between the different considered system components are listed in Table C.1.

Table C.2 shows the aggregated installed capacities for all residential buildings for the different sensitivity cases.

Table C.1: Aggregated energy flows [TWh/a] between the different technologies for *Value of* analysis.

	Min Cost	No Gas supply	No Fuel cell	No Photovoltaic	No Heat pump	No refurbishment	Forced refurbishment
AC Node to Battery	5.2	2.0	3.7	0.0	5.1	6.1	5.2
AC Node to Building	112.8	112.8	112.8	112.8	112.8	112.8	112.8
AC Node to Electric heater	40.8	56.1	43.3	4.6	48.1	45.0	40.0
AC Node to Heat pump	34.3	26.9	16.2	24.6	0.0	50.1	21.0
AC Node to Hot water	6.8	6.8	6.8	6.8	6.8	6.8	6.8
Battery to AC Node	4.7	1.8	3.3	0.0	4.6	5.5	4.7
CHP to AC Node	0.0	0.0	0.2	0.0	0.0	0.0	0.0
Cool supply to Building	19.8	21.4	19.6	19.0	18.5	29.0	31.6
Electricity supply to AC Node	51.5	100.5	84.7	63.5	57.7	47.3	52.7
Fuel cell to AC Node	53.9	0.0	0.0	85.3	20.1	69.1	45.7
Gas supply to CHP	0.0	0.0	0.7	0.0	0.0	0.0	0.0
Gas supply to Fuel cell	103.7	0.0	0.0	164.1	38.6	132.9	87.9
Gas supply to Gas boiler	68.7	0.0	91.2	121.6	226.6	26.8	65.7
HP Tarif to Heat pump	20.4	46.2	40.2	17.4	0.0	42.1	10.5
Log supply to Fire place	21.2	19.4	23.0	23.6	51.4	21.3	28.8
Pellet supply to Pellet boiler	0.0	10.3	0.0	0.0	3.1	0.0	0.0
Renewable gas to Gas boiler	0.0	8.7	0.0	0.0	0.0	0.0	0.0
Heat pump to Building	225.1	296.5	231.0	169.5	0.0	363.9	126.7
CHP to HNode	0.0	0.0	0.4	0.0	0.0	0.0	0.0
District heating to HNode	0.0	7.9	0.8	0.0	15.0	0.0	0.0
Electric heater to HNode	40.0	55.0	42.5	4.5	47.1	44.1	39.2
Fire place to HNode	17.6	16.1	19.1	19.6	42.7	17.7	23.9
Fuel cell to HNode	34.2	0.0	0.0	54.2	12.7	43.9	29.0
Gas boiler to HNode	66.0	8.3	87.6	116.7	217.5	25.7	63.1
HNode to Building	84.7	23.4	78.1	123.3	265.8	57.4	82.4
HNode to Hot water	69.2	69.2	69.2	69.2	69.2	69.2	69.2
Pellet boiler to HNode	0.0	9.3	0.0	0.0	2.8	0.0	0.0
HNode to Heat storage	54.5	41.8	38.3	77.2	52.2	59.6	52.9
Heat storage to HNode	50.5	37.8	35.2	74.5	49.2	54.8	49.3
Photovoltaic to AC Node	89.7	102.4	94.7	0.0	90.4	98.9	82.7
Photovoltaic to FiTPV	24.1	33.9	26.4	0.0	19.2	27.3	20.7
Solar thermal to HNode	0.1	0.0	0.0	0.1	0.1	0.0	0.0

Table C.2: Aggregated installed capacities of the different technologies for the *Value of* analysis.

	Min Cost	No Gas supply	No Fuel cell	No Photovoltaic	No Heat pump	No refurbishment	Forced refurbishment
Gas boiler [GW_{th}]	36.6	5.1	47.6	83.9	111.9	14.7	36.3
Oil boiler [GW_{th}]	0.0	0.0	0.0	0.0	0.0	0.0	0.0
CHP [GW_{el}]	0.0	0.0	0.0	0.0	0.0	0.0	0.0
District heating [GW_{th}]	0.0	7.5	0.9	0.0	13.1	0.0	0.0
Heat storage [GWh_{th}]	215.6	291.4	216.6	63.4	173.9	265.4	188.6
Heat pump [GW_{th}]	60.4	83.1	60.4	47.0	0.0	95.5	34.6
Electric heater [GW_{th}]	99.7	97.1	90.3	83.6	75.4	121.0	84.4
Solar thermal [GW_{th}]	0.2	0.0	0.0	0.2	0.2	0.0	0.0
Pellet boiler [GW_{th}]	0.0	2.4	0.0	0.0	0.8	0.0	0.0
Battery [GWh_{el}]	16.9	7.1	12.8	0.0	17.1	20.0	17.4
Fuel cell [GW_{el}]	12.7	0.0	0.0	14.5	5.1	16.9	10.7
Photovoltaic [GW_{el}]	133.4	160.3	142.3	0.0	127.8	147.6	121.0

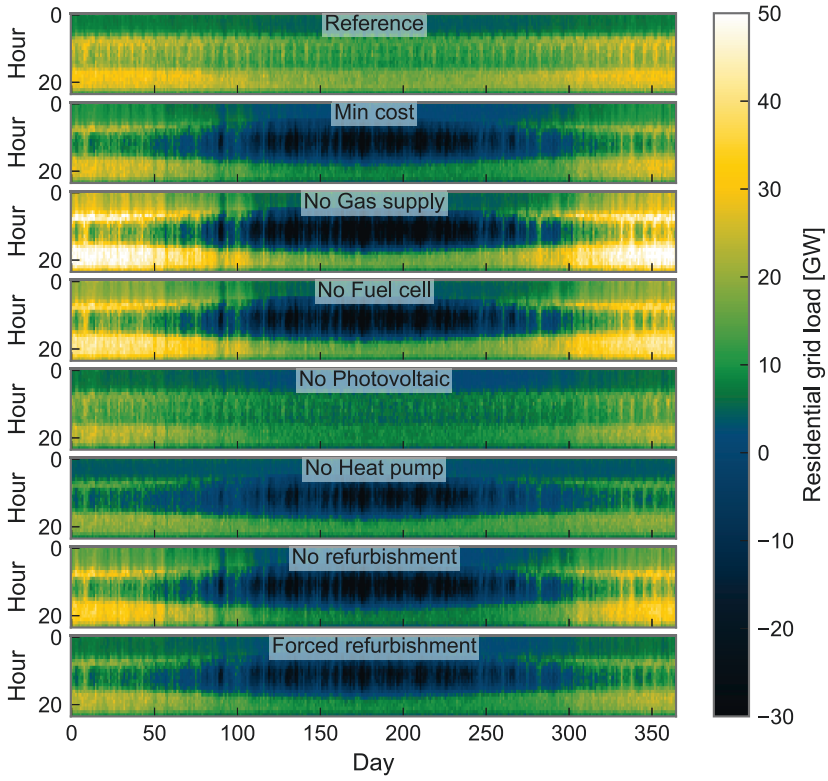

Figure C.5: Grid load of the *Min Cost* scenario and the grid loads for the cases with a constrained solution space.

C.4 Sensitivity to the gas price

Following section provides additional information to the sensitivity analysis of the gas price. It is described in detail in Section 5.3.3.

Figure C.6 shows the aggregated investment costs for the different gas prices.

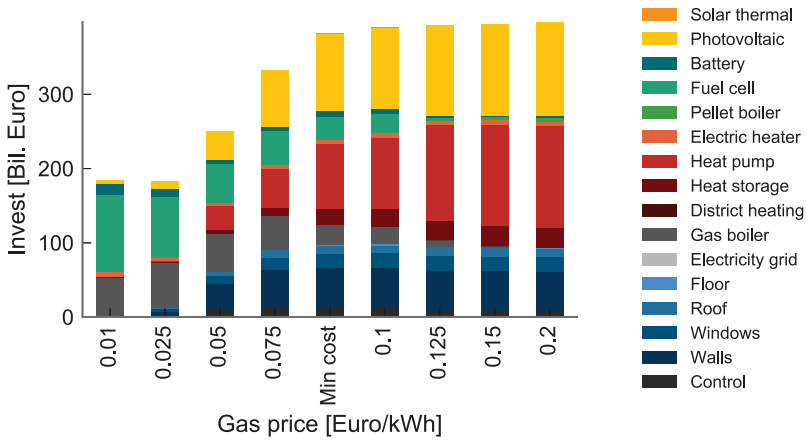

Figure C.6: Total investment cost of the *Min Cost* scenario and the total investment cost for different considered gas prices.

The resulting aggregated and sorted grid loads resulting for different gas prices are illustrated in Figure C.7.

Table C.3 shows the aggregated installed capacities for all residential buildings for the different sensitivity cases.

Further, the aggregated annual energy flows between the different considered system components are listed in Table C.4.

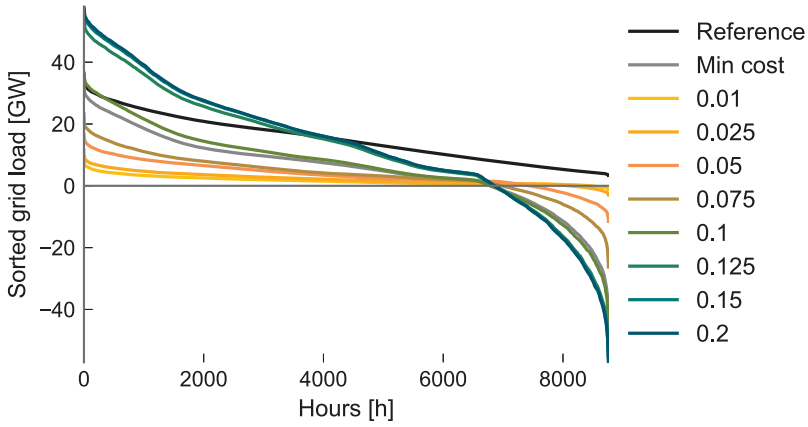

Figure C.7: Sorted electricity grid load for *Min Cost* scenario and the electricity grid load for the cases with different considered gas prices.

Table C.3: Aggregated installed capacities of the different technologies for the gas price variation.

Gas price [Euro/kWh]	0.01	0.025	0.05	0.075	*Min Cost*	0.1	0.125	0.15	0.2
Gas boiler [GW_{th}]	124.9	144.0	109.8	77.3	36.6	28.9	9.1	2.2	0.0
District heating [GW_{th}]	0.0	0.0	0.0	0.0	0.0	0.0	6.4	7.8	7.8
Heat storage [GWh_{th}]	10.3	10.0	49.0	103.8	215.6	233.2	282.7	297.5	298.4
Heat pump [GW_{th}]	0.0	1.0	27.8	42.0	60.4	65.9	80.5	83.5	83.4
Electric heater [GW_{th}]	111.7	87.5	78.8	87.8	99.7	100.3	97.7	98.6	99.0
Pellet boiler [GW_{th}]	0.0	0.0	0.0	0.0	0.0	0.0	1.5	3.0	3.8
Battery [GWh_{el}]	32.3	22.3	8.9	11.8	16.9	17.0	7.3	7.2	9.3
Fuel cell [GW_{el}]	33.1	25.1	21.3	18.4	12.7	10.7	0.9	0.0	0.0
Photovoltaic [GW_{el}]	3.7	9.2	41.8	92.7	133.4	140.6	159.2	161.6	163.4

Table C.4: Aggregated energy flows [TWh/a] between the different technologies for the gas price variation.

Gas price [Euro/kWh]	0.01	0.025	0.05	0.075	*Min Cost*	0.1	0.125	0.15	0.2
AC Node to Battery	5.2	8.4	5.6	2.2	3.8	5.2	2.0	2.0	2.6
AC Node to Building	112.8	112.8	112.8	112.8	112.8	112.8	112.8	112.8	112.8
AC Node to Electric heater	40.8	28.1	14.5	17.5	25.7	44.0	55.1	58.8	60.9
AC Node to Heat pump	34.3	0.0	1.1	26.2	34.0	31.3	26.1	26.6	26.4
AC Node to Hot water	6.8	6.8	6.8	6.8	6.8	6.8	6.8	6.8	6.8
Battery to AC Node	4.7	7.6	5.0	2.0	3.4	4.7	1.8	1.8	2.3
Cool supply to Building	19.8	28.8	26.4	22.9	20.6	19.9	20.9	21.3	21.4
Electricity supply to AC Node	51.5	15.6	21.9	37.7	41.0	54.3	94.2	102.4	103.5
Fuel cell to AC Node	53.9	130.7	107.6	96.9	73.6	47.6	4.9	0.0	0.0
Gas supply to Fuel cell	103.7	251.3	207.0	186.3	141.6	91.5	9.4	0.0	0.0
Gas supply to Gas boiler	68.7	388.7	382.9	215.8	147.1	53.5	15.8	4.0	0.0
HP Tarif to Heat pump	20.4	0.0	0.0	0.2	5.6	27.7	45.2	46.6	46.7
Log supply to Fire place	21.2	0.5	0.5	2.6	6.4	21.2	19.8	19.4	19.4
Pellet supply to Pellet boiler	0.0	0.0	0.0	0.0	0.0	0.0	6.4	12.0	14.2
Heat pump to Building	225.1	0.0	4.6	108.9	161.2	242.0	289.5	296.6	296.5
District heating to HNode	0.0	0.0	0.0	0.0	0.0	0.0	7.6	8.1	8.1
Electric heater to HNode	40.0	27.6	14.2	17.1	25.2	43.1	54.0	57.6	59.7
Fire place to HNode	17.6	0.4	0.4	2.2	5.3	17.6	16.5	16.1	16.1
Fuel cell to HNode	34.2	82.9	68.3	61.5	46.7	30.2	3.1	0.0	0.0
Gas boiler to HNode	66.0	373.1	367.5	207.2	141.3	51.4	15.2	3.8	0.0
HNode to Building	84.7	407.8	375.5	215.7	146.8	69.1	29.0	23.2	23.4
HNode to Hot water	69.2	69.2	69.2	69.2	69.2	69.2	69.2	69.2	69.2
Pellet boiler to HNode	0.0	0.0	0.0	0.0	0.0	0.0	5.8	10.8	12.7
HNode to Heat storage	54.5	354.4	282.9	107.6	45.3	55.1	42.6	42.0	41.6
Heat storage to HNode	50.5	347.3	277.1	104.5	42.7	50.9	38.5	37.8	37.4
Photovoltaic to AC Node	89.7	2.2	6.2	28.9	65.1	93.6	101.9	102.8	103.6
Photovoltaic to FiTPV	24.1	1.2	2.3	7.5	14.5	26.3	33.4	34.6	35.1
Solar thermal to HNode	0.1	0.0	0.0	0.0	0.0	0.1	0.0	0.0	0.0

C.5 Zero GHG

The aggregated installed capacities of the whole building stock for the three Zero GHG cases are listed in Table C.5

Table C.5: Aggregated installed capacities of the different technologies for the Zero GHG cases.

	Self-sufficiency	Net zero emission	Renewable grid
Gas boiler [GW_{th}]	7.9	7.4	6.1
Heat storage [GWh_{th}]	292.3	265.9	295.1
Heat pump [GW_{th}]	68.0	78.5	85.1
Electric heater [GW_{th}]	108.2	98.4	97.9
Solar thermal [GW_{th}]	0.3	0.3	0.0
Pellet boiler [GW_{th}]	0.0	0.4	2.4
Battery [GWh_{el}]	145.1	44.3	7.0
Fuel cell [GW_{el}]	34.5	7.7	0.0
Photovoltaic [GW_{el}]	180.5	295.2	160.9

Further, the aggregated annual energy flows between the different considered system components are listed in Table C.6.

Table C.6: Aggregated energy flows [TWh/a] between the different technologies for the Zero GHG cases.

	Self-sufficiency	Net zero emission	Renewable grid
AC Node to Battery	34.4	13.3	2.0
AC Node to Building	112.8	112.8	112.8
AC Node to Electric heater	41.5	54.6	56.2
AC Node to Heat pump	58.2	42.1	27.3
AC Node to Hot water	6.8	6.8	6.8
Battery to AC Node	31.0	12.0	1.8
Electricity supply to AC Node	0.3	60.5	100.6
Fuel cell to AC Node	101.4	31.7	0.0
HP Tarif to Heat pump	0.2	23.2	47.6
Log supply to Fire place	19.1	23.7	19.4
Pellet supply to Pellet boiler	0.0	1.3	10.2
Renewable gas to Fuel cell	195.0	60.9	0.0
Renewable gas to Gas boiler	7.4	12.7	10.5
Heat pump to Building	243.9	269.3	303.6
Electric heater to HNode	40.7	53.5	55.1
Fire place to HNode	15.8	19.7	16.1
Fuel cell to HNode	64.4	20.1	0.0
Gas boiler to HNode	7.1	12.2	10.0
HNode to Building	53.8	33.7	17.2
HNode to Hot water	69.2	69.2	69.2
Pellet boiler to HNode	0.0	1.2	9.2
HNode to Heat storage	66.0	47.2	42.5
Heat storage to HNode	60.8	43.2	38.4
Solar thermal to HNode	0.1	0.1	0.0
Photovoltaic to AC Node	120.9	125.4	102.8
Photovoltaic to FiTPV	32.3	116.7	34.0

Bibliography

Achtnicht, M. and Madlener, R. Factors influencing German house owners'preferences on energy retrofits. *Energy Policy*, 68:254–263, 2014. ISSN 03014215. doi: 10.1016/j.enpol.2014.01.006.

AGEB. Auswertungstabellen zur Energiebilanz Deutschland 1990 bis 2016, 2017.

Agnew, S. and Dargusch, P. Effect of residential solar and storage on centralized electricity supply systems. *Nature Climate Change*, 5(4):315–318, 2015. ISSN 1758-678X 1758-6798. doi: 10.1038/nclimate2523.

Ahmadi, S. and Abdi, S. Application of the Hybrid Big Bang–Big Crunch algorithm for optimal sizing of a stand-alone hybrid PV/wind/battery system. *Solar Energy*, 134:366–374, 2016. ISSN 0038092X. doi: 10.1016/j.solener.2016.05.019.

Andrews, R. W., Stein, J. S., Hansen, C., and Riley, D. Introduction to the Open Source PV-LIB for Python Photovoltaic System Modeling Package. 2014.

Appen, J. v., Braslavsky, J. H., Ward, J. K., and Braun, M. Sizing and grid impact of PV battery systems - a comparatative analysis for Australia and Germany, 2015.

Ashouri, A., Fux, S. S., Benz, M. J., and Guzzella, L. Optimal design and operation of building services using mixed-integer linear programming techniques. *Energy*, 59:365–376, 2013. ISSN 03605442. doi: 10.1016/j.energy.2013.06.053.

ASUE. BHKW-Kenndaten 2014/2015 - Module, Anbieter, Kosten, 2015.

Baeten, B., Rogiers, F., Patteeuw, D., and Helsen, L. Comparison of optimal control formulations for stratified sensible thermal energy storage in space heating applications, 2015. URL `https://lirias.kuleuven.be/bitstream/123456789/500689/1/Comparison+of+optimal+control+formulations+for+stratified+sensible+thermal+energy+storage+in+space+heating+applications.pdf`.

Bahl, B., Kümpel, A., Seele, H., Lampe, M., and Bardow, A. Time-series aggregation for synthesis problems by bounding error in the objective function. *Energy*, 135:900–912, 2017. ISSN 03605442. doi: 10.1016/j.energy.2017.06.082.

Balcombe, P., Rigby, D., and Azapagic, A. Investigating the importance of motivations and barriers related to microgeneration uptake in the UK. *Applied Energy*, 130:403–418, 2014. ISSN 03062619. doi: 10.1016/j.apenergy.2014.05.047.

Ballarini, I., Corgnati, S. P., and Corrado, V. Use of reference buildings to assess the energy saving potentials of the residential building stock: The experience of TABULA project. *Energy Policy*, 68:273–284, 2014. ISSN 03014215. doi: 10.1016/j.enpol.2014.01.027.

Baños, R., Manzano-Agugliaro, F., Montoya, F. G., Gil, C., Alcayde, A., and Gómez, J. Optimization methods applied to renewable and sustainable energy: A review. *Renewable and Sustainable Energy Reviews*, 15(4):1753–1766, 2011. ISSN 13640321. doi: 10.1016/j.rser.2010.12.008.

BBSR. Raumordnungsprognose 2035 nach dem Zensus. Bevölkerung, private Haushalte und Erwerbspersonen., 2015. URL http://www.bbsr.bund.de/BBSR/DE/Raumbeobachtung/UeberRaumbeobachtung/Komponenten/Raumordnungsprognose/Download_ROP2035/DL_ROP2035_uebersicht.html?nn=443262.

BDEW. Standardlastprofile (SLP), 2011.

BDEW. Stromverbrauch im Haushalt, 2013.

BDEW. Jährlicher Stromverbrauch eines privaten Haushaltes in Deutschland in den Jahren 1991 bis 2013 (in Kilowattstunden), 2014.

BDEW. Wie heizt Deutschland?, 2015.

Beck, T., Kondziella, H., Huard, G., and Bruckner, T. Assessing the influence of the temporal resolution of electrical load and PV generation profiles on self-consumption and sizing of PV-battery systems. *Applied Energy*, 173:331–342, 2016. ISSN 03062619. doi: 10.1016/j.apenergy.2016.04.050.

Becker, N. *Synthese von elektrischen Lastprofilen der Haushalte in Deutschland*. Thesis, 2016.

Bemporad, A. and Morari, M. Control of systems integrating logic, dynamics, and constraints. *Automatica*, 35(3):407–427, 1999. ISSN 0005-1098. doi: Doi10.1016/S0005-1098(98)00178-2. URL <GotoISI>://WOS:000079457800006.

Beuth. Dämmbarkeit des deutschen Gebäudebestands, 2015.

Beuth. Ableitung eines Korridors für den Ausbau der erneuerbaren Wärme im Gebäudebereich, 2017.

Bloess, A., Schill, W.-P., and Zerrahn, A. Power-to-heat for renewable energy integration: A review of technologies, modeling approaches, and flexibility potentials. *Applied Energy*, 212:1611–1626, 2018. ISSN 03062619. doi: 10.1016/j.apenergy.2017.12.073.

BMVBS. Kosten energierelevanter Bau- und Anlagenteile bei der energetischen Modernisierung von Wohngebäuden, 2012. URL http://www.bbsr.bund.de/BBSR/DE/Veroeffentlichungen/BMVBS/Online/2012/DL_ON072012.pdf?__blob=publicationFile&v=2.

BMWi. Energieeffizienzstrategie Gebäude, 2015.

BMWi. Zahlen und Fakten Energiedaten, 2016.

BMWi. Energiedaten - Tabelle 30: Internationaler Preisvergleich, 2018. URL https://www.bmwi.de/Redaktion/DE/Binaer/Energiedaten/Energiepreise-und-Energiekosten/energiedaten-energiepreise-5-xls.xls?__blob=publicationFile&v=17.

Bollmeyer, C., Keller, J. D., Ohlwein, C., Wahl, S., Crewell, S., Friederichs, P., Hense, A., Keune, J., Kneifel, S., Pscheidt, I., Redl, S., and Steinke, S. Towards a high-resolution regional reanalysis for the European CORDEX domain. *Quarterly Journal of the Royal Meteorological Society*, 141(686):1–15, 2015. ISSN 0035-9009. doi: 10.1002/qj.2486. URL <GotoISI>://WOS:000349663200001.

Boßmann, T. and Staffell, I. The shape of future electricity demand: Exploring load curves in 2050s Germany and Britain. *Energy*, 90:1317–1333, 2015. ISSN 03605442. doi: 10.1016/j.energy.2015.06.082.

Bracke, J., Tomaschek, J., Brodecki, L., and Fahl, U. Techno-ökonomische Bewertung von Energie-Autarkie für die Energieversorgung von Einfamilienhäusern. *Zeitung für Energiewirtschaft*, 40:127–137, 2016. doi: 10.007/s12398-016-0179-2.

BRD. Energiekonzept für eine umweltschonende, zuverlässige und bezahlbare Energieversorgung, 2010.

BRD. Bericht über die Berechnung des ,,Kostenoptimalen Niveaus von Mindestanforderungen an die Gesamtenergieeffizienz“, 2013.

Breyer, C. and Gerlach, A. Global overview on grid-parity. *Progress in Photovoltaics: Research and Applications*, 21(1):121–136, 2013. ISSN 10627995. doi: 10.1002/pip.1254.

Bundesamt, S. Zensus 2011, 2011. URL https://www.zensus2011.de/DE/Home/home_node.html.

Bundesnetzagentur. Biogas- Monitoringbericht 2014, 2014. URL https://www.bundesnetzagentur.de/SharedDocs/Downloads/DE/Sachgebiete/Energie/Unternehmen_Institutionen/ErneuerbareEnergien/Biogas/Biogas_Monitoring/Biogas_Monitoringbericht_2014.pdf?__blob=publicationFile&v=1.

Bundesnetzagentur. Monitoringbericht 2017, 2017. URL https://www.bundesnetzagentur.de/SharedDocs/Downloads/DE/Allgemeines/Bundesnetzagentur/Publikationen/Berichte/2017/Monitoringbericht_2017.pdf?__blob=publicationFile&v=4.

Capasso, A., Grattieri, W., Lamedica, R., and Prudenzi, A. A Bottom-up Approach to Residential Load Modeling. *Ieee Transactions on Power Systems*, 9(2):957–964, 1994. ISSN 0885-8950. doi: Doi10.1109/59.317650. URL <GotoISI>://WOS:A1994NV46600052.

Cerezo, C., Sokol, J., Reinhart, C., and Al-Mumin, A. Three Methods for Characterizing Building Archetypes in Urban Energy Simulation. A Case Study in Kuwait City. In *Proceedings of BS2015: 14th Conference of International Building Performance Simulation Association*, 2015. URL http://www.ibpsa.org/proceedings/BS2015/p2435.pdf.

Comodi, G., Cioccolanti, L., and Renzi, M. Modelling the Italian household sector at the municipal scale: Micro-CHP, renewables and energy efficiency. *Energy*, 68:92–103, 2014. ISSN 03605442. doi: 10.1016/j.energy.2014.02.055.

Comodi, G., Giantomassi, A., Severini, M., Squartini, S., Ferracuti, F., Fonti, A., Nardi Cesarini, D., Morodo, M., and Polonara, F. Multi-apartment residential microgrid with electrical and thermal storage devices: Experimental analysis and simulation of energy management strategies. *Applied Energy*, 137:854–866, 2015. ISSN 03062619. doi: 10.1016/j.apenergy.2014.07.068.

Controme. Controme - Fußbodenheizung Set-Funk, 2018. URL https://www.controme.com/produkt/fussbodenheizung-set-funk-2/.

Corgnati, S. P., Fabrizio, E., Filippi, M., and Monetti, V. Reference buildings for cost optimal analysis: Method of definition and application. *Applied Energy*, 102:983–993, 2013. ISSN 03062619. doi: 10.1016/j.apenergy.2012.06.001.

CREST. CREST Demand Model, 2017. URL http://www.lboro.ac.uk/research/crest/demand-model/.

De Rosa, M., Bianco, V., Scarpa, F., and Tagliafico, L. A. Heating and cooling building energy demand evaluation; a simplified model and a modified degree days approach. *Applied Energy*, 128:217–229, 2014. ISSN 03062619. doi: 10.1016/j.apenergy.2014.04.067.

Degefa, M. Z., Lehtonen, M., Nixon, K., and McCulloch, M. A high resolution model of residential internal heat gain — The subtle interdependencies among residential end uses. In *2015 IEEE Innovative Smart Grid Technologies - Asia (ISGT ASIA)*, pages 1–6, 2015. doi: 10.1109/ISGT-Asia.2015.7386990.

DESTATIS. Baugenehmigung / Baufertigstellung von Wohn- und Nichtwohngebäuden (Neubau) nach Art der Beheizung und Art der verwendenten Heizenergie, 2014.

DESTATIS. Bevölkerung Deutschlands bis 2060 - 13. koordinierte Bevölkerungsvorausberechnung, 2015. URL https://www.destatis.de/DE/Publikationen/Thematisch/Bevoelkerung/VorausberechnungBevoelkerung/BevoelkerungDeutschland2060Presse5124204159004.pdf?__blob=publicationFile.

DESTATIS. Umweltnutzung und Wirtschaft - Tabellen zu den Umweltökonomischen Gesamtrechnungen Teil 2: Energie, 2017. URL https://www.destatis.de/DE/Publikationen/Thematisch/UmweltoekonomischeGesamtrechnungen/Querschnitt/UmweltnutzungundWirtschaftTabellenband.html.

Deutsch, M. and Graichen, P. Was wäre, wenn ein flächendeckender Rollout von Solar-Speicher-Systemen stattfände? Eine erste Abschätzung für das Stromsystem und die Energiepolitik, 2015.

Diakaki, C., Grigoroudis, E., and Kolokotsa, D. Performance study of a multi-objective mathematical programming modelling approach for energy decision-making in buildings. *Energy*, 59:534–542, 2013. ISSN 03605442. doi: 10.1016/j.energy.2013.07.034.

Diefenbach, N., Loga, T., and Stein, B. Reaching the climate protection targets for the heat supply of the German residential building stock: How and how fast? *Energy and Buildings*, 132:53–73, 2016. ISSN 03787788. doi: 10.1016/j.enbuild.2016.06.095.

DIN. DIN EN 12831 - Heating systems and water based cooling systems in buildings –Method for calculation of the design heat load, 2014.

DIN. Energy efficiency of buildings –Calculation of the net, final and primary energy demand for heating, cooling, ventilation, domestic hot water and lighting, 2016.

DOE. Fuel Cell Technologies Office Multi-Year Research, Development, and Demonstration Plan, 2016.

Druckman, A. and Jackson, T. Household energy consumption in the UK: A highly geographically and socio-economically disaggregated model. *Energy Policy*, 36 (8):3177–3192, 2008. ISSN 0301-4215.

DVGW. Potenzialstudie zur nachhaltigen Erzeugung und Einspeisung gasförmiger, regenerativer Energieträger in Deutschland (Biogasatlas), 2014. URL https://www.dvgw.de/medien/dvgw/leistungen/forschung/berichte/gw2_01_10.pdf.

DWD. Testreferenzjahre (TRY). 2012.

EEG. Erneuerbare-Energien-Gesetz, 2014.

EEG. Gesetz für den Ausbau erneuerbarer Energien (Erneuerbare-Energien-Gesetz - EEG 2017), 2017. URL https://www.gesetze-im-internet.de/.

Elnakat, A., Gomez, J. D., and Booth, N. A zip code study of socioeconomic, demographic, and household gendered influence on the residential energy sector. *Energy Reports*, 2:21–27, 2016. ISSN 23524847. doi: 10.1016/j.egyr.2016.01.003.

Elsido, C., Bischi, A., Silva, P., and Martelli, E. Two-stage MINLP algorithm for the optimal synthesis and design of networks of CHP units. *Energy*, 121:403–426, 2017. ISSN 03605442. doi: 10.1016/j.energy.2017.01.014.

Elsland, R., Peksen, I., and Wietschel, M. Are Internal Heat Gains Underestimated in Thermal Performance Evaluation of Buildings? *Energy Procedia*, 62:32–41, 2014. ISSN 18766102. doi: 10.1016/j.egypro.2014.12.364.

Elsner, P. and Sauer, D. U. Energiespeicher - Technologiesteckbrief zur Analyse "Flexibilitätskonzepte für die Stromversorgung 2050", 2015.

EN ISO, D. Thermal performance and energy use in the build environment (ISO 13790:2008). 2008.

Energymap. Amtliche EEG-Anlagenregister bis 2015, 2015. URL http://www.energymap.info/download.html.

EnergyPlus. ¡http://www.energyplus.gov/¿, 2017.

EON. Google Sunroof, 2018. URL https://www.eon-solar.de/.

EPISCOPE. Energy Performance Indicator Tracking Schemes for the Continuous Optimisation of Refurbishment Processes in European Housing Stocks, 2016. URL http://episcope.eu/iee-project/episcope/.

EU. EC Regulation No. 244/2009 "Non-directional household lamps", 2009.

EU. Directive 2010/31/EU of the European Parliament and of the Council of 19 May 2010 on the energy performance of buildings, 2010. URL https://eur-lex.europa.eu/legal-content/en/TXT/?uri=CELEX:32010L0031.

EU. Directive 2012/27/EU of the European Parliament and of the Council of 25 October 2012 on energy efficiency, amending Directives 2009/125/EC and 2010/30/EU and repealing Directives 2004/8/EC and 2006/32/EC, 2012. URL http://eur-lex.europa.eu/legal-content/EN/TXT/PDF/?uri=CELEX:32012L0027&from=DE.

EuPD-Research. Photovoltaik-Preismonitor Deutschland, 2016. URL https://www.solarwirtschaft.de/fileadmin/user_upload/BSW_Preismonitor_Q1_2016.pdf.

Evins, R. Multi-level optimization of building design, energy system sizing and operation. *Energy*, 90:1775–1789, 2015. ISSN 03605442. doi: 10.1016/j.energy.2015.07.007.

EWI. Entwicklung der Energiemaerkte - Energiereferenzprognose, 2014.

Eypasch, M., Schimpe, M., Kanwar, A., Hartmann, T., Herzog, S., Frank, T., and Hamacher, T. Model-based techno-economic evaluation of an electricity storage system based on Liquid Organic Hydrogen Carriers. *Applied Energy*, 185:320–330, 2017. ISSN 03062619. doi: 10.1016/j.apenergy.2016.10.068.

Fabrizio, E., Filippi, M., and Virgone, J. An hourly modelling framework for the assessment of energy sources exploitation and energy converters selection and sizing in buildings. *Energy and Buildings*, 41(10):1037–1050, 2009. ISSN 03787788. doi: 10.1016/j.enbuild.2009.05.005.

Fazlollahi, S., Becker, G., and Maréchal, F. Multi-objectives, multi-period optimization of district energy systems: II-Daily thermal storage. *Computers & Chemical Engineering*, 71:648–662, 2014. ISSN 00981354. doi: 10.1016/j.compchemeng.2013.10.016.

Fehrenbach, D., Merkel, E., McKenna, R., Karl, U., and Fichtner, W. On the economic potential for electric load management in the German residential heating sector –An optimising energy system model approach. *Energy*, 71:263–276, 2014. ISSN 03605442. doi: 10.1016/j.energy.2014.04.061.

Fischer, D., Härtl, A., and Wille-Haussmann, B. Model for electric load profiles with high time resolution for German households. *Energy and Buildings*, 92:170–179, 2015. ISSN 03787788. doi: 10.1016/j.enbuild.2015.01.058.

FNR. Bioenergy in Germany - Facts and Figures 2016, 2016. URL https://www.biobasedeconomy.nl/wp-content/uploads/2017/03/Bioenergy_in_Germany_facts_and_figures_2016.pdf.

Fonseca, J. A. and Schlueter, A. Integrated model for characterization of spatiotemporal building energy consumption patterns in neighborhoods and city districts. *Applied Energy*, 142:247–265, 2015. ISSN 03062619. doi: 10.1016/j.apenergy.2014.12.068.

Frank, M., Deja, R., Peters, R., Blum, L., and Stolten, D. Bypassing renewable variability with a reversible solid oxide cell plant. *Applied Energy*, 217:101–112, 2018. ISSN 03062619. doi: 10.1016/j.apenergy.2018.02.115.

Fux, S. F., Ashouri, A., Benz, M. J., and Guzzella, L. EKF based self-adaptive thermal model for a passive house. *Energy and Buildings*, 68:811–817, 2014. ISSN 03787788. doi: 10.1016/j.enbuild.2012.06.016.

Gabrielli, P., Gazzani, M., Martelli, E., and Mazzotti, M. Optimal design of multi-energy systems with seasonal storage. *Applied Energy*, 2017. ISSN 03062619. doi: 10.1016/j.apenergy.2017.07.142.

Geidl, M. and Andersson, G. Optimal Power Flow of Multiple Energy Carriers. *IEEE Transactions on Power Systems*, 22(1):145–155, 2007. ISSN 0885-8950. doi: 10.1109/tpwrs.2006.888988.

GENESIS. Baufertigstellungen: Errichtung neuer Wohngebäude sowie Wohnungen in Wohngebäude - Jahressumme, 2018. URL `https://www.regionalstatistik.de/genesis/online/logon`.

Gleitmann, S. Förderung für effiziente Heizgeräte. *HZwei Das Magazin für Wasserstoff und Brennstoffzellen*, 10:10–11, 2016.

Goderbauer, S., Bahl, B., Voll, P., Lübbecke, M. E., Bardow, A., and Koster, A. M. C. A. An adaptive discretization MINLP algorithm for optimal synthesis of decentralized energy supply systems. *Computers & Chemical Engineering*, 95: 38–48, 2016. ISSN 00981354. doi: 10.1016/j.compchemeng.2016.09.008.

Haimes, Y. Y., Ladson, L. S., and Wismer, D. A. Bicriterion Formulation of Problems of Integrated System Identification and System Optimization. *Ieee Transactions on Systems Man and Cybernetics*, Smc1(3):296–&, 1971. ISSN 0018-9472. URL `<GotoISI>://WOS:A1971J744600012`.

Harb, H., Paprott, J.-N., Matthes, P., Schütz, T., Streblow, R., and Müller, D. Decentralized scheduling strategy of heating systems for balancing the residual load. *Building and Environment*, 86:132–140, 2015. ISSN 03601323. doi: 10.1016/j.buildenv.2014.12.015.

Hart, W. E., Laird, C., and Woodruff, D. L. Pyomo: modeling and solving mathematical programs in Python. *Mathematical Programming Computation*, 3(3): 219–260, 2011.

Hartmann, A., Meinel, G., Hecht, R., and Behnisch, M. A Workflow for Automatic Quantification of Structure and Dynamic of the German Building Stock Using Official Spatial Data. *ISPRS International Journal of Geo-Information*, 5(8), 2016. ISSN 2220-9964. doi: 10.3390/ijgi5080142.

Hendron, R. and Engebrecht, C. Building America Research Benchmark Definition, 2010. URL https://www.nrel.gov/docs/fy10osti/47246.pdf.

Henning, H.-M. and Palzer, A. A comprehensive model for the German electricity and heat sector in a future energy system with a dominant contribution from renewable energy technologies—Part I: Methodology. *Renewable and Sustainable Energy Reviews*, 30:1003–1018, 2014. ISSN 13640321. doi: 10.1016/j.rser.2013.09.012.

Heuberger, C. F., Rubin, E. S., Staffell, I., Shah, N., and Mac Dowell, N. Power capacity expansion planning considering endogenous technology cost learning. *Applied Energy*, 204:831–845, 2017. ISSN 03062619. doi: 10.1016/j.apenergy.2017.07.075.

Hosseinalizadeh, R., Shakouri G, H., Amalnick, M., and Taghipour, P. Economic sizing of a hybrid (PV–WT–FC) renewable energy system (HRES) for stand-alone usages by an optimization-simulation model: Case study of Iran. *Renewable and Sustainable Energy Reviews*, 54:139–150, 2016. ISSN 13640321. doi: 10.1016/j.rser.2015.09.046.

Huang, Z. Extensions to the k-Means Algorithm for Clustering Large Data Sets with Categorical Values, 1998.

Huchtemann, K. *Supply Temperature Control Concepts in Heat Pump Heating Systems*. Thesis, 2015.

HZwei. Ubersicht der im deutschsprachigen Raum erhältlichen BZ-Heizgeräte. *HZwei Das Magazin für Wasserstoff und Brennstoffzellen*, 10:12–13, 2016.

IEA. CO2 Emissions from Fuel Combustion - 2015 Edition, 2015.

IEA-PVPS. Trends 2016 in Photovoltaic Applications, 2016. URL http://www.iea-pvps.org/fileadmin/dam/public/report/national/Trends_2016_-_mr.pdf.

IEA-PVPS. Trends 2017 in Photovoltaic Applications, 2017. URL http://www.iea-pvps.org/fileadmin/dam/public/report/statistics/IEA-PVPS_Trends_2017_in_Photovoltaic_Applications.pdf.

IRENA. The Power to Change: Solar and Wind Cost Reduction Potential to 2025, 2016.

ISE, F. Wärmepumpen Effizienz –Messtechnische Untersuchung von Wärmepumpenanlagen zur Analyse und Bewertung der Effizienz im realen Betrieb, 2011. URL https://wp-monitoring.ise.fraunhofer.de/wp-effizienz/download/wp_effizienz_endbericht_kurzfassung.pdf.

ISE, F. Current and Future Cost of Photovoltaics. Long-term Scenarios for Market Development, System Prices and LCOE of Utility-Scale PV Systems, 2015.

ISE, F. Recent Facts about Photovoltaics in Germany, 2017. URL https://www.ise.fraunhofer.de/content/dam/ise/en/documents/publications/studies/recent-facts-about-photovoltaics-in-germany.pdf.

ISI. Netzentwicklungsplan Strom - Entwicklung der regionalen Stromnachfrage und Lastprofile, 2016.

ISI. FORECAST, 2018. URL https://www.forecast-model.eu/.

IW. Eigenerzeugung und Selbstverbrauch von Strom - Stand, Potentiale und Trends, 2014.

IW. Bevölkerungsentwicklung in den deutschen Bundesländern bis 2035, 2017. URL https://www.iwkoeln.de/fileadmin/publikationen/2017/357919/IW-Trends_2017-03-04_Deschermeier.pdf.

IWES. Interaktion EE-Strom, Wärme und Verkehr, 2015. URL https://www.iee.fraunhofer.de/content/dam/iwes-neu/energiesystemtechnik/de/Dokumente/Veroeffentlichungen/2015/Interaktion_EEStrom_Waerme_Verkehr_Endbericht.pdf.

IWU. Deutsche Gebaeudetypologie. Systematik und Datensaetze, 2005. URL http://www.iwu.de/fileadmin/user_upload/dateien/energie/klima_altbau/Gebaeudetypologie_Deutschland.pdf.

IWU. Datenbasis Gebäudebestand - Datenerhebung zur energetischen Qualität und zu den Modernisierungstrends im deutschen Wohngebäudebestand, 2010.

IWU. Datenerhebung Wohngebäudebestand 2016 - Datenerhebung zu den energetischen Merkmalen und Modernisierungsraten im deutschen und hessischen Wohngebäudebestand, 2018.

Jain, A. K. Data clustering: 50 years beyond K-means. *Pattern Recognition Letters*, 31(8):651–666, 2010. ISSN 01678655. doi: 10.1016/j.patrec.2009.09.011.

Jungbluth, C. H. Kraft-Wärme-Kopplung mit Brennstoffzellen in Wohngebäuden im zukünftigen Energiesystem, 2007.

Kairies, K., Haberschusz, D., Ouwerkerk, J. v., Strebel, J., Wessels, O., Magnor, D., Badeda, J., and Sauer, D. U. Wissenschaftliches Mess- und Evaluierungsprogramm Solarstromspeicher - Jahresbericht 2016, 2016.

KfW. KfW-Programm Erneuerbare Energien "Speicher", 2016.

Khalilpour, R. and Vassallo, A. Leaving the grid: An ambition or a real choice? *Energy Policy*, 82:207–221, 2015. ISSN 03014215. doi: 10.1016/j.enpol.2015.03.005.

King, B. H., Hansen, C. W., Riley, D., Robinson, C. D., and Pratt, L. Procedure to Determine Coefficients for the Sandia Array Performance Model, 2016.

King, D., Boyson, W., and Kratochvill, J. Sandia Photovoltaic Array Performance Model, 2004. URL `http://prod.sandia.gov/techlib/access-control.cgi/2004/043535.pdf`.

Klingler, A.-L. Self-consumption with PV + Battery systems: A market diffusion model considering individual consumer behaviour and preferences. *Applied Energy*, 205:1560–1570, 2017. ISSN 03062619. doi: 10.1016/j.apenergy.2017.08.159.

Kohlhepp, P. and Hagenmeyer, V. Technical Potential of Buildings in Germany as Flexible Power-to-Heat Storage for Smart-Grid Operation. *Energy Technology*, 2017. doi: 10.1002/ente.201600655.

Kossak, B. and Stadler, M. Adaptive thermal zone modeling including the storage mass of the building zone. *Energy and Buildings*, 109:407–417, 2015. ISSN 03787788. doi: 10.1016/j.enbuild.2015.10.016.

Kotak, Y., Gul, M. S., Muneer, T., and Ivanova, S. M. Impact of Ground Albedo on the Performance of PV Systems and its economic analysis, 2015.

Kotzur, L., Markewitz, P., Robinius, M., and Stolten, D. Kostenoptimale Versorgungssysteme für ein vollautarkes Einfamilienhaus, 2017.

Kotzur, L., Markewitz, P., Robinius, M., and Stolten, D. Impact of different time series aggregation methods on optimal energy system design. *Renewable Energy*, 117:474–487, 2018a. ISSN 09601481. doi: 10.1016/j.renene.2017.10.017.

Kotzur, L., Markewitz, P., Robinius, M., and Stolten, D. Time series aggregation for energy system design: Modeling seasonal storage. *Applied Energy*, 213:123–135, 2018b. ISSN 03062619. doi: 10.1016/j.apenergy.2018.01.023.

Kranzl, L., Hummel, M., Müller, A., and Steinbach, J. Renewable heating: Perspectives and the impact of policy instruments. *Energy Policy*, 59:44–58, 2013. ISSN 03014215. doi: 10.1016/j.enpol.2013.03.050.

KWKG. Gesetz für die Erhaltung, die Modernisierung und den Ausbau der Kraft-Wärme-Kopplung (Kraft-Wärme-Kopplungsgesetz - KWKG), 2016. URL `https://www.gesetze-im-internet.de/`.

Kwon, S., Won, W., and Kim, J. A superstructure model of an isolated power supply system using renewable energy: Development and application to Jeju Island, Korea. *Renewable Energy*, 97:177–188, 2016. ISSN 09601481. doi: 10.1016/j.renene.2016.05.074.

Lahnaoui, A., Stenzel, P., and Linssen, J. Techno-economic analysis of photovoltaic battery system configuration and location. *Applied Energy*, 2017. ISSN 03062619. doi: 10.1016/j.apenergy.2017.09.093.

Lauinger, D., Caliandro, P., Van herle, J., and Kuhn, D. A linear programming approach to the optimization of residential energy systems. *Journal of Energy Storage*, 7:24–37, 2016. ISSN 2352152X. doi: 10.1016/j.est.2016.04.009.

Leyffer, S., Linderoth, J., and Luedtke, J. The Leyffer-Linderoth-Luedtke (LLL) Measure of Complexity, 2016. URL `https://www.ima.umn.edu/materials/2015-2016/ND8.1-12.16/25419/Luedtke-minlp.pdf`.

Lindberg, K. B., Doorman, G., Fischer, D., Korpås, M., Ånestad, A., and Sartori, I. Methodology for optimal energy system design of Zero Energy Buildings using mixed-integer linear programming. *Energy and Buildings*, 127:194–205, 2016a. ISSN 03787788. doi: 10.1016/j.enbuild.2016.05.039.

Lindberg, K. B., Fischer, D., Doorman, G., Korpås, M., and Sartori, I. Cost-optimal energy system design in Zero Energy Buildings with resulting grid impact: A case study of a German multi-family house. *Energy and Buildings*, 127:830–845, 2016b. ISSN 03787788. doi: 10.1016/j.enbuild.2016.05.063.

Linssen, J., Stenzel, P., and Fleer, J. Techno-economic analysis of photovoltaic battery systems and the influence of different consumer load profiles. *Applied Energy*, 2015. ISSN 03062619. doi: 10.1016/j.apenergy.2015.11.088.

Lloyd, S. Least squares quantization in PCM. *IEEE Transactions on Information Theory*, 28(2):129–137, 1982. ISSN 0018-9448. doi: 10.1109/TIT.1982.1056489.

Löhr, M. Systempreise PV 2015 - Kurzauswertung der Angebotsdatenbank des Photovoltaikforum.com, 2016.

Lund, H., Andersen, A. N., Østergaard, P. A., Mathiesen, B. V., and Connolly, D. From electricity smart grids to smart energy systems –A market operation based approach and understanding. *Energy*, 42(1):96–102, 2012. ISSN 03605442. doi: 10.1016/j.energy.2012.04.003.

Luthander, R., Widén, J., Nilsson, D., and Palm, J. Photovoltaic self-consumption in buildings: A review. *Applied Energy*, 142:80–94, 2015. ISSN 03062619. doi: 10.1016/j.apenergy.2014.12.028.

Mainzer, K., Fath, K., McKenna, R., Stengel, J., Fichtner, W., and Schultmann, F. A high-resolution determination of the technical potential for residential-roof-mounted photovoltaic systems in Germany. *Solar Energy*, 105:715–731, 2014. ISSN 0038092X. doi: 10.1016/j.solener.2014.04.015.

Mainzer, K., Killinger, S., McKenna, R., and Fichtner, W. Assessment of rooftop photovoltaic potentials at the urban level using publicly available geodata and image recognition techniques. *Solar Energy*, 155:561–573, 2017. ISSN 0038092X. doi: 10.1016/j.solener.2017.06.065.

Mancarella, P. MES (multi-energy systems): An overview of concepts and evaluation models. *Energy*, 65:1–17, 2014. ISSN 03605442. doi: 10.1016/j.energy.2013.10.041.

Marshall, E., Steinberger, J. K., Dupont, V., and Foxon, T. J. Combining energy efficiency measure approaches and occupancy patterns in building modelling in the UK residential context. *Energy and Buildings*, 111:98–108, 2016. ISSN 03787788. doi: 10.1016/j.enbuild.2015.11.039.

Marszal, A. J., Heiselberg, P., Bourrelle, J. S., Musall, E., Voss, K., Sartori, I., and Napolitano, A. Zero Energy Building –A review of definitions and calculation methodologies. *Energy and Buildings*, 43(4):971–979, 2011. ISSN 03787788. doi: 10.1016/j.enbuild.2010.12.022.

Martinez Soto, A. and Jentsch, M. F. Comparison of prediction models for determining energy demand in the residential sector of a country. *Energy and Buildings*, 128:38–55, 2016. ISSN 03787788. doi: 10.1016/j.enbuild.2016.06.063.

Mashayekh, S., Stadler, M., Cardoso, G., and Heleno, M. A mixed integer linear programming approach for optimal DER portfolio, sizing, and placement in multi-energy microgrids. *Applied Energy*, 187:154–168, 2017. ISSN 03062619. doi: 10.1016/j.apenergy.2016.11.020.

Mata, É., Sasic Kalagasidis, A., and Johnsson, F. Building-stock aggregation through archetype buildings: France, Germany, Spain and the UK. *Building and Environment*, 81:270–282, 2014. ISSN 03601323. doi: 10.1016/j.buildenv.2014.06.013.

May, N. and Neuhoff, K. Eigenversorungs mit Solarstrom - ein Treiber der Energiewende?, 2016.

McKenna, E. and Thomson, M. High-resolution stochastic integrated thermal–electrical domestic demand model. *Applied Energy*, 165:445–461, 2016. ISSN 03062619. doi: 10.1016/j.apenergy.2015.12.089.

McKenna, E., Krawczynski, M., and Thomson, M. Four-state domestic building occupancy model for energy demand simulations. *Energy and Buildings*, 96:30–39, 2015. ISSN 03787788. doi: 10.1016/j.enbuild.2015.03.013.

McKenna, R., Merkel, E., Fehrenbach, D., Mehne, S., and Fichtner, W. Energy efficiency in the German residential sector: A bottom-up building-stock-model-based analysis in the context of energy-political targets. *Building and Environment*, 62: 77–88, 2013. ISSN 03601323. doi: 10.1016/j.buildenv.2013.01.002.

Meerts, N. *Development and Validation of a Geographically-Resolved Photovoltaic Performance Model for Feed-in Time Series*. Thesis, 2016.

Mehleri, E. D., Sarimveis, H., Markatos, N. C., and Papageorgiou, L. G. Optimal design and operation of distributed energy systems: Application to Greek residential sector. *Renewable Energy*, 51:331–342, 2013. ISSN 09601481. doi: 10.1016/j.renene.2012.09.009.

Merkel, E., McKenna, R., and Fichtner, W. Optimisation of the capacity and the dispatch of decentralised micro-CHP systems: A case study for the UK. *Applied Energy*, 140:120–134, 2015. ISSN 03062619. doi: 10.1016/j.apenergy.2014.11.036.

Milan, C., Stadler, M., Cardoso, G., and Mashayekh, S. Modeling of non-linear CHP efficiency curves in distributed energy systems. *Applied Energy*, 148:334–347, 2015. ISSN 03062619. doi: 10.1016/j.apenergy.2015.03.053.

Müller, A. *Energy Demand Assessment for Space Conditioning and Domestic Hot Water: A Case Study for the Austrian Building Stock*. Thesis, 2015. URL `http://www.invert.at/Dateien/Dissertation_AndreasM.pdf`.

Müller, D., Lauster, M., Constantin, A., Fuchs, M., and Remmen, P. AixLib - An Open-Source Modelica Library within the IEA-EBC Annex 60 Framework. *BauSIM 2016*, (September 2016):3–9, 2016. URL `http://www.iea-annex60.org/downloads/2016-bausim-aixlib.pdf`.

Murugan, S. and Horák, B. A review of micro combined heat and power systems for residential applications. *Renewable and Sustainable Energy Reviews*, 64: 144–162, 2016. ISSN 13640321. doi: 10.1016/j.rser.2016.04.064.

Napoli, R., Gandiglio, M., Lanzini, A., and Santarelli, M. Techno-economic analysis of PEMFC and SOFC micro-CHP fuel cell systems for the residential sector. *Energy and Buildings*, 103:131–146, 2015. ISSN 03787788. doi: 10.1016/j.enbuild.2015.06.052.

Nguyen, V. N., Fang, Q., Packbier, U., and Blum, L. Long-term tests of a Jülich planar short stack with reversible solid oxide cells in both fuel cell and electrolysis modes. *International Journal of Hydrogen Energy*, 38(11):4281–4290, 2013. ISSN 03603199. doi: 10.1016/j.ijhydene.2013.01.192.

Nykvist, B. and Nilsson, M. Rapidly falling costs of battery packs for electric vehicles. *Nature Climate Change*, 5(4):329–332, 2015. ISSN 1758-678X 1758-6798. doi: 10.1038/nclimate2564.

OCallaghan, J., Mezger, S., Coughlin, M., Isles, K., Welsh, A., and Lyttle, C. K. Utility of the future - A customer-led shift in the electricity sector, 2014.

Oldewurtel, F., Sturzenegger, D., and Morari, M. Importance of occupancy information for building climate control. *Applied Energy*, 101:521–532, 2013. ISSN 03062619. doi: 10.1016/j.apenergy.2012.06.014.

Olsberg. Produktdatenblatt Olsberg Palena Cmpact, 2018. URL `https://www.olsberg.com/578912-wee-de-wAssets/docs/kaminoefen/palena-compact/anleitungen-zertifikate-ersatzteillisten/Produktdatenblatt_Palena-Compact_23-575_ohne-OEC.pdf`.

Paatero, J. V. and Lund, P. D. A model for generating household electricity load profiles. *International Journal of Energy Research*, 30(5):273–290, 2006. ISSN 0363-907X 1099-114X. doi: 10.1002/er.1136.

Palzer, A. and Henning, H.-M. A comprehensive model for the German electricity and heat sector in a future energy system with a dominant contribution from renewable energy technologies –Part II: Results. *Renewable and Sustainable Energy Reviews*, 30:1019–1034, 2014. ISSN 13640321. doi: 10.1016/j.rser.2013.11.032.

Parag, Y. and Sovacool, B. K. Electricity market design for the prosumer era. *Nature Energy*, 1(4):16032, 2016. ISSN 2058-7546. doi: 10.1038/nenergy.2016.32.

Perez, R., Seals, R., Ineichen, P., Stewart, R., and Menicucci, D. A New Simplified Version of the Perez Diffuse Irradiance Model for Tilted Surfaces. *Solar Energy*, 39(3):221–231, 1987. ISSN 0038-092x. doi: Doi10.1016/S0038-092x(87)80031-2. URL `<GotoISI>://WOS:A1987J808200008`.

Peters, R., Deja, R., Engelbracht, M., Frank, M., Nguyen, V. N., Blum, L., and Stolten, D. Efficiency analysis of a hydrogen-fueled solid oxide fuel cell system with anode off-gas recirculation. *Journal of Power Sources*, 328:105–113, 2016. ISSN 03787753. doi: 10.1016/j.jpowsour.2016.08.002.

Petruschke, P., Gasparovic, G., Voll, P., Krajačić, G., Duić, N., and Bardow, A. A hybrid approach for the efficient synthesis of renewable energy systems. *Applied Energy*, 135:625–633, 2014. ISSN 03062619. doi: 10.1016/j.apenergy.2014.03.051.

Pfenninger, S. Dealing with multiple decades of hourly wind and PV time series in energy models: A comparison of methods to reduce time resolution and the planning implications of inter-annual variability. *Applied Energy*, 197:1–13, 2017. ISSN 03062619. doi: 10.1016/j.apenergy.2017.03.051.

Pflugradt, N. *Modellierung von Wasser und Energieverbräuchen in Haushalten*. Thesis, 2016. URL `http://nbn-resolving.de/urn:nbn:de:bsz:ch1-qucosa-209036`.

Poncelet, K., Delarue, E., Duerinck, J., Six, D., and D'haeseleer, W. The importance of integrating the variability of renewables in long-term energy planning models, 2014. URL https://www.mech.kuleuven.be/en/tme/research/energy_environment/Pdf/wp-importance.pdf.

prognos. Hintergrundpapier Energieeffizienzstrategie Gebäude, 2015.

Prognos. Eigenversorgung aus Solaranlagen. Das Potenzial für Photovoltaik-Speicher-Systeme in Ein- und Zweifamilienhäusern, Landwirtschaft sowie im Lebensmittelhandel., 2016.

Rager, J. M. F. *Urban Energy System Design from the Heat Perspective using mathematical Programming including thermal Storage*. Thesis, 2015. URL http://infoscience.epfl.ch/record/210788/files/EPFL_TH6731.pdf.

Ram, M., Dimitrii, B., Aghahosseini, A., Oyewo, S., Gulagi, A., Child, M., and Breyer, C. Global Energy System Based on 100% Renewable Energy - Power Sector, 2017.

Ratnam, E. L., Weller, S. R., and Kellett, C. M. An optimization-based approach to scheduling residential battery storage with solar PV: Assessing customer benefit. *Renewable Energy*, 75:123–134, 2015. ISSN 09601481. doi: 10.1016/j.renene.2014.09.008.

Rech, B. and Elsner, P. Photovoltaik - Technologiesteckbrief zur Analyse "Flexibilitätskonzepte für die Stromversorgung 2050", 2016.

REHVA. How to define nearly net zero energy buildings nZEB, 2011. URL https://www.rehva.eu/fileadmin/hvac-dictio/03-2011/How_to_define_nearly_net_zero_energy_buildings_nZEB.pdf.

Renaldi, R. and Friedrich, D. Multiple time grids in operational optimisation of energy systems with short- and long-term thermal energy storage. *Energy*, 133:784–795, 2017. ISSN 03605442. doi: 10.1016/j.energy.2017.05.120.

Richardson, I., Thomson, M., and Infield, D. A high-resolution domestic building occupancy model for energy demand simulations. *Energy and Buildings*, 40(8):1560–1566, 2008. ISSN 03787788. doi: 10.1016/j.enbuild.2008.02.006.

Richardson, I., Thomson, M., Infield, D., and Delahunty, A. Domestic lighting: A high-resolution energy demand model. *Energy and Buildings*, 41(7):781–789, 2009. ISSN 03787788. doi: 10.1016/j.enbuild.2009.02.010.

Richardson, I., Thomson, M., Infield, D., and Clifford, C. Domestic electricity use: A high-resolution energy demand model. *Energy and Buildings*, 42(10):1878–1887, 2010. ISSN 03787788. doi: 10.1016/j.enbuild.2010.05.023.

Rickerson, W., Couture, T., Barbose, G., Jacobs, D., Parkinson, G., Chessin, E., Belden, A., Wilson, H., and Barrett, H. Residential prosumers - Drivers and policy options, 2014.

Röben, F. *Techno-Economical Potential of Reversible Solid Oxide Cells for Autarkic Buildings and Districts*. Thesis, 2017.

Robinius, M. *Strom- und Gasmarktdesign zur Versorgung des deutschen Straßenverkehrs mit Wasserstoff*. Thesis, 2015.

Robinius, M., Otto, A., Heuser, P., Welder, L., Syranidis, K., Ryberg, D., Grube, T., Markewitz, P., Peters, R., and Stolten, D. Linking the Power and Transport Sectors—Part 1: The Principle of Sector Coupling. *Energies*, 10(7), 2017. ISSN 1996-1073. doi: 10.3390/en10070956.

Robinson, S. A. and Rai, V. Determinants of spatio-temporal patterns of energy technology adoption: An agent-based modeling approach. *Applied Energy*, 151: 273–284, 2015. ISSN 03062619. doi: 10.1016/j.apenergy.2015.04.071.

rwi. Erstellung der Anwendungsbilanzen 2015 und 2016 für den Sektor der Privaten Haushalte und den Verkehrssektor in Deutschland, 2017.

Samsatli, S. and Samsatli, N. J. A general spatio-temporal model of energy systems with a detailed account of transport and storage. *Computers & Chemical Engineering*, 80:155–176, 2015. ISSN 00981354. doi: 10.1016/j.compchemeng.2015.05.019.

Samsatli, S., Staffell, I., and Samsatli, N. J. Optimal design and operation of integrated wind-hydrogen-electricity networks for decarbonising the domestic transport sector in Great Britain. *International Journal of Hydrogen Energy*, 41(1): 447–475, 2016. ISSN 03603199. doi: 10.1016/j.ijhydene.2015.10.032.

Sandberg, N. H., Sartori, I., Heidrich, O., Dawson, R., Dascalaki, E., Dimitriou, S., Vimm-r, T., Filippidou, F., Stegnar, G., Šijanec Zavrl, M., and Brattebø, H. Dynamic building stock modelling: Application to 11 European countries to support the energy efficiency and retrofit ambitions of the EU. *Energy and Buildings*, 132: 26–38, 2016. ISSN 03787788. doi: 10.1016/j.enbuild.2016.05.100.

Schaller, R. R. Moore's law: past, present and future. *IEEE Spectrum*, 34(6):52–59, 1997. ISSN 0018-9235. doi: 10.1109/6.591665.

Schill, W.-P., Zerrahn, A., Kunz, F., and Kemfert, C. Decentralized solar prosumage with battery storage: system orientation required, 2017.

Schlachtberger, D. P., Brown, T., Schäfer, M., Schramm, S., and Greiner, M. Cost optimal scenarios of a future highly renewable European electricity system Exploring the influence of weather data, cost parameters and policy constraints. *arXiv*, 2018. doi: arXiv:1803.09711.

Schleich, J., Gassmann, X., Faure, C., and Meissner, T. Making the implicit explicit: A look inside the implicit discount rate. *Energy Policy*, 97:321–331, 2016. ISSN 03014215. doi: 10.1016/j.enpol.2016.07.044.

Schmidt, O., Hawkes, A., Gambhir, A., and Staffell, I. The future cost of electrical energy storage based on experience rates. *Nature Energy*, 6:17110, 2017. ISSN 2058-7546. doi: 10.1038/nenergy.2017.110.

Schütz, T., Streblow, R., and Müller, D. A comparison of thermal energy storage models for building energy system optimization. *Energy and Buildings*, 93:23–31, 2015. ISSN 03787788. doi: 10.1016/j.enbuild.2015.02.031.

Schütz, T., Schiffer, L., Harb, H., Fuchs, M., and Müller, D. Optimal design of energy conversion units and envelopes for residential building retrofits using a comprehensive MILP model. *Applied Energy*, 185:1–15, 2017a. ISSN 03062619. doi: 10.1016/j.apenergy.2016.10.049.

Schütz, T., Schraven, M. H., Remy, S., Granacher, J., Kemetmüller, D., Fuchs, M., and Müller, D. Optimal design of energy conversion units for residential buildings considering German market conditions. *Energy*, 139:895–915, 2017b. ISSN 03605442. doi: 10.1016/j.energy.2017.08.024.

Sokol, J., Cerezo Davila, C., and Reinhart, C. F. Validation of a Bayesian-based method for defining residential archetypes in urban building energy models. *Energy and Buildings*, 134:11–24, 2017. ISSN 03787788. doi: 10.1016/j.enbuild.2016.10.050.

SolidPower. Solid Power BlueGEN Brochure, 2018. URL `http://www.solidpower.com/fileadmin/user_upload/pages/Logos_materialien/SOLIDpower_BlueGEN_Brochure_UK_web.pdf`.

Solomon, S., Plattner, G.-K., Knutti, R., and Friedlingstein, P. Irreversible climate change due to carbon dioxide emissions. *Proceedings of the national academy of sciences*, 106(6):1704–1709, 2009. ISSN 0027-8424.

SPF. SPF Online Kollektorkatalog, 2017. URL `http://www.spf.ch/`.

Stadler, M., Groissböck, M., Cardoso, G., and Marnay, C. Optimizing Distributed Energy Resources and building retrofits with the strategic DER-CAModel. *Applied Energy*, 132:557–567, 2014. ISSN 03062619. doi: 10.1016/j.apenergy.2014.07.041.

Stadler, M., Kranzl, L., Huber, C., Haas, R., and Tsioliaridou, E. Policy strategies and paths to promote sustainable energy systems—The dynamic Invert simulation tool. *Energy Policy*, 35(1):597–608, 2007. ISSN 03014215. doi: 10.1016/j.enpol.2006.01.006.

Stadler, M., Cardoso, G., Mashayekh, S., Forget, T., DeForest, N., Agarwal, A., and Schönbein, A. Value streams in microgrids: A literature review. *Applied Energy*, 162:980–989, 2016. ISSN 03062619. doi: 10.1016/j.apenergy.2015.10.081.

Staffell, I. and Green, R. The cost of domestic fuel cell micro-CHP systems. *International Journal of Hydrogen Energy*, 38(2):1088–1102, 2013. ISSN 03603199. doi: 10.1016/j.ijhydene.2012.10.090.

Staffell, I., Brett, D., Brandon, N., and Hawkes, A. A review of domestic heat pumps. *Energy & Environmental Science*, 5(11):9291, 2012. ISSN 1754-5692 1754-5706. doi: 10.1039/c2ee22653g.

Steen, D., Stadler, M., Cardoso, G., Groissböck, M., DeForest, N., and Marnay, C. Modeling of thermal storage systems in MILP distributed energy resource models. *Applied Energy*, 137:782–792, 2015. ISSN 03062619. doi: 10.1016/j.apenergy.2014.07.036.

Stenzel, P., Linssen, J., Fleer, J., and Busch, F. Impact of temporal resolution of supply and demand profiles on the design of photovoltaic battery systems for increased self-consumption. In *IEEE Internationonal Energy Conference*, 2016.

Sterchele, P., Kalz, D., and Palzer, A. Technisch-ökonomische Analyse von Maßnahmen und Potentialen zur energetischen Sanierung im Wohngebäudesektor heute und für das Jahr 2050. *Bauphysik*, 38(4):193–211, 2016. ISSN 01715445. doi: 10.1002/bapi.201610022.

Stokes, M. *Removing barriers to embedded generation : a fine-grained load model to support low voltage network performance analysis*. Thesis, 2005. URL `http://hdl.handle.net/2086/4134`.

Streblow, R. and Ansorge, K. Genetischer Algorithmuszur kombinatorischen Optimierung von Gebäudehülle und Anlagentechnik, 2017.

Strupeit, L. and Neij, L. Cost dynamics in the deployment of photovoltaics: Insights from the German market for building-sited systems. *Renewable and Sustainable Energy Reviews*, 69:948–960, 2017. ISSN 13640321. doi: 10.1016/j.rser.2016.11.095.

Teichgräber, H., Brodrick, P. G., and Brandt, A. R. Optimal design and operations of a flexible oxyfuel natural gas plant. *Energy*, 141:506–518, 2017. ISSN 03605442. doi: 10.1016/j.energy.2017.09.087.

Teichmann, D., Stark, K., Müller, K., Zöttl, G., Wasserscheid, P., and Arlt, W. Energy storage in residential and commercial buildings via Liquid Organic Hydrogen Carriers (LOHC). *Energy & Environmental Science*, 5(10):9044, 2012. ISSN 1754-5692 1754-5706. doi: 10.1039/c2ee22070a.

Tesla. Tesla Powerwall, 2017. URL https://www.tesla.com/de_DE/powerwall.

Tjaden, T., Bergner, J., Weniger, J., and Quaschning, V. Repraesentative elektrische Lastprofile fuer Wohngebaeude in Deutschland auf 1-sekuendiger Datenbasis. 2015. doi: 10.13140/RG.2.1.5112.0080.

Torcellini, P., Deru, M., Griffith, B., and Benne, K. DOE commercial building benchmark models. In *ACEEE summer study on energy efficiency in buildings*, 2008.

TrnSys. http://www.trnsys.com/, 2018.

UBA. Datenbasis zur Bewertung von Energieeffizienzmaßnahmen in der Zeitreihe 2005 –2014, 2017a.

UBA. Klimaneutraler Gebäudebestand 2050 - Energieeffizienzpotentiale und die Auswirkungen des Klimawandels auf den Gebäudebestand, 2017b. URL https://www.umweltbundesamt.de/sites/default/files/medien/1410/publikationen/2017-11-06_climate-change_26-2017_klimaneutraler-gebaeudebestand-ii.pdf.

UN. Paris Agreement - COP21, 2015.

VDE. Der zellulare Ansatz, 2015. URL https://shop.vde.com/de/copy-of-vde-studie-der-zellulare-ansatz.

VDI. Reference load profiles of single-family and multi-family houses for the use of CHP systems, 2008.

VDI. Berechnung von Kühllast und Raumtemperaturen von Räumen und Gebäuden, 2012.

VDI. Statusreport Regenerative Energien in Deutschland 2015, 2015. URL https://www.vdi.de/fileadmin/vdi_de/redakteur_dateien/geu_dateien/Statusreport_Regenerative_Energien_-_WEB.pdf.

Vieira, F. M., Moura, P. S., and de Almeida, A. T. Energy storage system for self-consumption of photovoltaic energy in residential zero energy buildings. *Renewable Energy*, 103:308–320, 2017. ISSN 09601481. doi: 10.1016/j.renene.2016.11.048.

Voll, P., Klaffke, C., Hennen, M., and Bardow, A. Automated superstructure-based synthesis and optimization of distributed energy supply systems. *Energy*, 50: 374–388, 2013. ISSN 03605442. doi: 10.1016/j.energy.2012.10.045.

Wang, H., Yin, W., Abdollahi, E., Lahdelma, R., and Jiao, W. Modelling and optimization of CHP based district heating system with renewable energy production and energy storage. *Applied Energy*, 159:401–421, 2015. ISSN 03062619. doi: 10.1016/j.apenergy.2015.09.020.

Welder, L., Ryberg, D. S., Kotzur, L., Grube, T., Robinius, M., and Stolten, D. Spatio-temporal optimization of a future energy system for power-to-hydrogen applications in Germany, 2017.

Widén, J. and Wäckelgård, E. A high-resolution stochastic model of domestic activity patterns and electricity demand. *Applied Energy*, 87(6):1880–1892, 2010. ISSN 03062619. doi: 10.1016/j.apenergy.2009.11.006.

Willem, H., Lin, Y., and Lekov, A. Review of energy efficiency and system performance of residential heat pump water heaters. *Energy and Buildings*, 143: 191–201, 2017. ISSN 03787788. doi: 10.1016/j.enbuild.2017.02.023.

Wu, R., Mavromatidis, G., Orehounig, K., and Carmeliet, J. Multiobjective optimisation of energy systems and building envelope retrofit in a residential community. *Applied Energy*, 190:634–649, 2017. ISSN 03062619. doi: 10.1016/j.apenergy.2016.12.161.

Yoza, A., Yona, A., Senjyu, T., and Funabashi, T. Optimal capacity and expansion planning methodology of PV and battery in smart house. *Renewable Energy*, 69: 25–33, 2014. ISSN 09601481. doi: 10.1016/j.renene.2014.03.030.

Zerrahn, A. and Schill, W.-P. A Greenfield Model to Evaluate Long-Run Power Storage Requirements for High Shares of Renewables, 2015.

Zeyringer, M., Price, J., Fais, B., Li, P.-H., and Sharp, E. Designing low-carbon power systems for Great Britain in 2050 that are robust to the spatiotemporal and inter-annual variability of weather. *Nature Energy*, 3(5):395–403, 2018. ISSN 2058-7546. doi: 10.1038/s41560-018-0128-x.

Zogg, M. Wärmepumpen, 2009. URL `http://www.zogg-engineering.ch/Publi/WP_ETH_Zogg.pdf`.

Band / Volume 429
Characterization of spatial-temporal varying riverbed hydraulic conductivity and its role on the estimation of river-aquifer exchange fluxes with data assimilation
Q. Tang (2018), xv, 117 pp
ISBN: 978-3-95806-339-6

Band / Volume 430
Der Einfluss von Wasserdampf auf den Sauerstofftransport in keramischen Hochtemperaturmembranen
F. Thaler (2018), ii, 93, XXXI pp
ISBN: 978-3-95806-340-2

Band / Volume 431
Analysis & modeling of metastable photovoltaic technologies: towards dynamic photovoltaic performance models
M. Görig (2018), 246 pp
ISBN: 978-3-95806-342-6

Band / Volume 432
Laser Treatment of Silicon Thin-Films for Photovoltaic Applications
C. Maurer (2018), vii, 165 pp
ISBN: 978-3-95806-347-1

Band / Volume 433
Mentalitäten und Verhaltensmuster im Kontext der Energiewende in NRW
K. Schürmann & D. Schumann (Hrsg.) (2018), 236 pp
ISBN: 978-3-95806-349-5

Band / Volume 434
Adhäsionsverhalten von wässrigen Nafion-Lösungen an dispersen Phasengrenzen
A. Schulz (2018), xii, 129 pp
ISBN: 978-3-95806-354-9

Band / Volume 435
Alterungs- und fehlertolerante optimale Betriebsführung eines Direktmethanol-Brennstoffzellensystems
R. Keller (2018), XX, 175 pp
ISBN: 978-3-95806-355-6

Band / Volume 436
Chamber study of biogenic volatile organic compounds: plant emission, oxidation products and their OH reactivity
Y. Zhujun (2018), ix, 139 pp
ISBN: 978-3-95806-356-3

Band / Volume 437
Characterization of High Temperature Polymer Electrolyte Fuel Cells
Y. Rahim (2018), iii, 162 pp
ISBN: 978-3-95806-359-4

Band / Volume 438
Lattice Boltzmann Simulation in Components of Polymer Electrolyte Fuel Cell
J. Yu (2018), ii, 173 pp
ISBN: 978-3-95806-360-0

Band / Volume 439
Quantitative Luminescence Imaging of Solar Cells
V. Huhn (2018), 155 pp
ISBN: 978-3-95806-363-1

Band / Volume 440
Characterization of Phosphoric Acid Doped Polybenzimidazole Membranes
Y. Lin (2018), II, IV, 140 pp
ISBN: 978-3-95806-364-8

Band / Volume 441
Degradation Study of SOC Stacks with Impedance Spectroscopy
Y. Yan (2018), 135 pp
ISBN: 978-3-95806-367-9

Band / Volume 442
Future Grid Load of the Residential Building Sector
L. Kotzur (2018), xxi, 213 pp
ISBN: 978-3-95806-370-9

Energie & Umwelt / Energy & Environment
Band / Volume 442
ISBN 978-3-95806-370-9

Mitglied der Helmholtz-Gemeinschaft

JÜLICH
Forschungszentrum